Sec 2.3 Ref 13

WSRC-RP-98-5052

A

GROUNDWATER FLOW AND SOLUTE TRANSPORT MODELING REPORT
K-AREA BURNING/RUBBLE PIT AND RUBBLE PILE

Prepared for:

Westinghouse Savannah River Company
Environmental Restoration Department
Aiken, South Carolina 29808

Prepared by:

HSI GeoTrans, Inc.
1080 Holcomb Bridge Road
Building 200, Suite 305
Roswell, Georgia 30076

HSI GEOTRANS PROJECT NO. I014-000
JUNE 2, 1998

TABLE OF CONTENTS

Page

1 INTRODUCTION 1
1.1 UNIT DESCRIPTION 1
1.2 MODELING OBJECTIVE AND APPROACH 2

2 CONCEPTUAL HYDROGEOLOGIC MODEL 4
2.1 SRS GEOLOGY AND HYDROSTRATIGRAPHY 4
2.1.1 SRS GEOLOGY 4
2.1.2 SRS HYDROSTRATIGRAPHY 5
2.1.2.1 FLORIDAN AQUIFER SYSTEM 5
2.1.2.2 MEYERS BRANCH CONFINING SYSTEM 6
2.2 UNIT-SPECIFIC HYDROGEOLOGY 6
2.2.1 SURFACE FEATURES 9
2.2.2 UNIT-SPECIFIC HYDROSTRATIGRAPHIC UNITS 10
2.2.2.1 SHALLOW HYDROSTRATIGRAPHY 10
2.2.2.2 UPPER THREE RUNS AQUIFER 12
2.2.2.3 GORDON CONFINING UNIT 13
2.2.2.4 GORDON AQUIFER 13

3 CONSTITUENT CHARACTERIZATION 15
3.1 GROUNDWATER DATA SUMMARY 15
3.2 SOURCE AREAS 15
3.3 CONSTITUENTS OF CONCERN (COCs) 16
3.3.1 OBSERVED PCE DISTRIBUTION 17
3.3.2 OBSERVED TCE DISTRIBUTION 17
3.4 RELEVANT COC FATE AND TRANSPORT PROCESSES 18

4 MODEL CONSTRUCTION AND PARAMETER VALUES 19
4.1 MODEL DISCRETIZATION 19
4.2 INITIAL AND BOUNDARY CONDITIONS 20
4.3 GROUNDWATER FLOW MODEL PARAMETERS 22
4.4 TRANSPORT MODEL PARAMETERS 25

5 FLOW CALIBRATION AND TRANSPORT MODELING 27
5.1 GROUNDWATER FLOW MODEL CALIBRATION 27
5.1.1 FLOW CALIBRATION TARGETS 27
5.1.2 FLOW CALIBRATION PROCEDURE 28
5.2 GROUNDWATER FLOW MODELING RESULTS 29
5.2.1 SIMULATED HYDRAULIC HEADS 30

Page

5.2.2 Flow Model Calibration Residuals and Statistics 30
5.2.3 Flow Model Sensitivity Analysis 31
5.3 Groundwater Flow Model Analysis 32
5.3.1 Advective Particle Tracking Analysis 32
5.3.2 Flow Model Water Balance 33
5.4 Transport Modeling Results 34
5.4.1 Simulated Worst-Case Constituent Concentration Levels 34
5.4.2 Predicted PCE and TCE Concentration Levels 35
5.4.3 Other Constituents 37
5.4.4 Compliance Boundary Locations and Transport Model Sensitivity Analysis 38

6 SUMMARY AND RECOMMENDATIONS 40

REFERENCES 41

LIST OF FIGURES

Page

2-1. Site location map for K-Area Unit: Burning/rubble pit and rubble pile. 45
2-2. Hydrostratigraphic Units at the Savannah River Site. 46
2-3. Generalized schematic of hydrogeologic features near the K-Area burning rubble pit/rubble pile. 47
2-4. Water table surface of the Upper Three Runs Aquifer. 48
2-5. Potentiometric surface map of the Gordon Aquifer. 49
2-6. Site-specific water table surface for Upper Three Runs Aquifer, based on third quarter 1996 data 50
3-1. K-Area burning/rubble pit and rubble pile PCE concentration contour map in the upper zone of upper Three Runs Aquifer 51
3-2. Observed PCE concentration versus time at KRBP/KRP monitoring wells. 52
3-3. K-area burning/rubble pit and rubble pile TCE concentration contour map in the upper zone of upper Three Runs Aquifer 53
3-4. Observed TCE concentration versus time at KRBP/KRP monitoring wells. 54
4-1. Finite element mesh. 55
4-2. Initial condition values of PCE concentration in the model domain. 56
4-3. Initial condition values of TCE concentration in the model domain. 57
4-4. Flow boundary conditions for the Upper Three Runs Aquifer. 58
4-5. Flow boundary conditions for the Gordon Aquifer. 59
4-6. Generalized hydrostratigraphic column with corresponding model element layers, nodes, and calibrated parameter values. 60
4-7. Nodal recharge rate zonation. 61
4-8. Hydraulic conductivity of elements in the FACT Model. 62
4-9. Location of Pen Branch Fault in model domain 63
4-10. Top elevation of model element layer 10 ("A" Horizon). 64
4-11. Top elevation of model element layer 9 ("AA" Horizon). 65
4-12. Top elevation of model element layer 8 (Transmissive Zone). 66
4-13. Top elevation of model element layer 7 (Tan Clay Confining Unit). 67
4-14. Top elevation of model element layer 6 (Lower Zone of Upper Three Runs Aquifer) 68
4-15. Top elevation of model element layer 5 (Lower Zone of Upper Three Runs Aquifer) 69
4-16. Top elevation of model element layer 4 (Gordon Confining Unit). 70
4-17. Top elevation of model element layer 3 (Upper Zone of Gordon Aquifer). 71
4-18. Top elevation of model element layer 2 (Lower Zone of Gordon Aquifer). 72
4-19. Top elevation of model element layer 1 (Basal Confining Unit). 73
5-1. Map of groundwater flow model calibration targets. 74
5-2. Plot of simulated versus observed hydraulic heads at target locations. 75

Page

5-3. Model simulated water table surface of the Upper Three Runs Aquifer. 76
5-4. Model simulated hydraulic heads in the upper zone of the Gordon Aquifer. 77
5-5. Model simulated water table surface and residuals for the Upper Three Runs Aquifer at the K-Area 78
5-6. Areal map and cross-sectional area display of particle traces and travel times from constituent source area 79
5-7. Calibrated groundwater flow model budget. 80
5-8. Model simulated areal map of (steady-state/worst-case) concentration of hypothetical chlorinated compound based on use of a continuous source release. . . 81
5-9. Areal maps of model predicted future PCE concentrations after one year based on currently observed concentration levels and inactive source. 82
5-10. Areal maps of model predicted future PCE concentrations after five years based on currently observed concentration levels and inactive source. 83
5-11. Areal maps of model predicted future PCE concentrations after eight years based on currently observed concentration levels and inactive source. 84
5-12. Areal maps of model predicted future PCE concentrations after nine years based on currently observed concentration levels and inactive source. 85
5-13. Vertical cross-sectional view of model predicted future PCE concentrations based on currently observed concentration levels and inactive source. 86
5-14. Areal maps of model predicted future TCE concentrations after one year based on currently observed concentration levels and inactive source. 87
5-15. Areal maps of model predicted future TCE concentrations after three years based on currently observed concentration levels and inactive source. 88
5-16. Areal maps of model predicted future TCE concentrations after five years based on currently observed concentration levels and inactive source. 89
5-17. Areal maps of model predicted future TCE concentrations after six years based on currently observed concentration levels and inactive source. 90
5-18. Vertical cross-sectional view of model predicted future TCE concentrations based on currently observed concentration levels based on currently observed concentration levels and inactive source 91
5-19. Location of compliance boundary well locations based on transport modeling results. 92
5-20. Model simulated PCE concentrations versus time along the plume centerline at the compliance boundary. 93
5-21. Model simulated TCE concentrations versus time along the plume centerline at the compliance boundary. 94
5-22. Model simulated normalized concentrations versus time along the plume centerline at the compliance boundary. 95
5-23. Results of sensitivity analysis for PCE. 96

Page

6-1. Estimate of natural attenuation restoration time based on plots of maximum model predicted concentrations at various times for PCE and TCE. 97

6-2. Volume of water with a concentration of 5 ug/L or more of PCE and TCE. 98

LIST OF TABLES

Page

4-1. Calibrated groundwater flow model and transport parameter values. 100
5-1. Flow model calibration statistics. 101
5-2. Simulated versus observed volumetric flux (cfs) along stream gage target locations. 102
5-3. Results of flow model sensitivity analysis. 103
5-4. Summary of sensitivity simulations performed with the solute transport model. . . 104

1 INTRODUCTION

This report discusses the numerical groundwater flow model calibration and solute transport modeling that was performed to examine the fate and transport of dissolved Constituents of Concern (COCs) at the K-Area Burning/Rubble Pit (KRBP) and Rubble Pile (KRP) at the Savannah River Site (SRS) in Aiken, South Carolina. The three-dimensional, finite-element groundwater modeling code FACT (Flow and Contaminant Transport), which is described in detail in (Hamm et al., 1997), was used in this study. The model was first calibrated to both observed hydraulic head and stream gage data in the vicinity of the K-area. The fate and transport of the primary COCs were then simulated in order to evaluate the effectiveness of a natural attenuation remedy for groundwater at this operable unit. These numerical model simulations will be used to prepare and justify passive aquifer restoration using a Groundwater Mixing Zone (GWMZ) Application for impacted groundwater at this unit. The GWMZ will be developed in a manner consistent with South Carolina Department of Health and Environmental Control (SCDHEC) guidance.

1.1 UNIT DESCRIPTION

The KBRP and KRP are located within the SRS, a 300-square mile site near Aiken, South Carolina. The approximate SRS coordinates for the KBRP and KRP are N54415, E42628, and N54380, E42568, respectively. These units are approximately 9.5 km (5.9 mi) east of the nearest SRS site boundary and approximately 0.65 km (0.4 mi) east of the K-Area Reactor (see Figure 1-1). The KBRP is a shallow, unlined excavation measuring 73.2 m (240 ft) long by 2.7 m (9 ft) deep by 9.1 m (30 ft) wide, with a total pit volume of approximately 1798 m^3 (63,505 ft^3). The area of the pit is apparent in the field as a vegetated area of surface depression. The KRP arcs to the south and west of the KBRP and is located in wooded terrain. It is marked by several hummocks of soil-covered rubble that are between 1.2 and 1.8 m (4 to 6 ft) high.

1.2 MODELING OBJECTIVE AND APPROACH

The primary objective of this modeling analysis is to predict contaminant concentration levels at downgradient compliance boundaries and determine whether any downgradient receptors would be affected as a result of a natural attenuation remedy for groundwater. The modeling results will be used to create Mixing Zone Concentration Limits (MZCL) for relevant COCs, which were determined to be dissolved PCE and TCE in groundwater. The modeling will be used to examine the natural attenuation of PCE and TCE concentrations in groundwater based on current site conditions. Because the remedial measure will likely consist of source zone control by installation of a soil cap, groundwater concentration levels are expected to decrease at a greater rate in the future than is currently observed. The modeling will also be used to assess the potential for downward PCE/TCE migration into the Gordon Aquifer at levels above regulatory limits.

The modeling approach for the K-Area consisted of using the WSRC FACT code to simulate three-dimensional transport of dissolved PCE and TCE in groundwater. The model developed using the FACT code was calibrated to the mean of groundwater elevation data collected from approximately 1985 to 1997 (personal communication, R. A. Hiergesell) at target well locations in the model domain. Recently collected stream gage data (personal communication, R.A. Hiergesell) along Pen Branch and Indian Grave Branch were also used to calibrate the flow model.

Model simulations were initially performed using a continuous source in order to show that the model can produce plumes that are consistent with observed COC plume distributions. This increases the confidence in the model's capability of predicting future COC migration pathways. Because the observed concentrations of PCE and TCE are decreasing and the source area concentrations are low, additional releases to groundwater from the unsaturated zone are unlikely. Therefore, the modeling will focus on the future fate and transport of currently observed PCE and TCE concentration levels in the saturated zone assuming no additional releases from the source area. For this approach, calibration of the transport model to observed conditions is unnecessary, and actual observed COC values are

initialized in the model. The model simulations will focus on simulating future concentration levels for shallow impacted groundwater at the KBRP/KRP.

2 CONCEPTUAL HYDROGEOLOGIC MODEL

A conceptual hydrogeologic model succinctly describes the principal hydrogeologic components of a groundwater flow system and is developed from regional, local, and site-specific data. The primary components of groundwater flow systems include: (1) areal extent, configuration, and type of aquifers and aquitards; (2) hydraulic properties of aquifers and aquitards; (3) natural groundwater recharge and discharge zones; (4) anthropogenic groundwater sources and sinks; and (5) areal and vertical distribution of groundwater hydraulic head potential. These aquifer system components serve as a hydrogeologic framework for the construction of a numerical groundwater flow model.

2.1 SRS GEOLOGY AND HYDROSTRATIGRAPHY

2.1.1 SRS GEOLOGY

The SRS is underlain by Atlantic Coastal Plain sediments that unconformably overlie crystalline and sedimentary basement rock. The Atlantic Coastal Plain consists of a southeast-dipping wedge of unconsolidated and semi-consolidated sediment that extends from its contact with the Piedmont province at the Fall Line to the edge of the continental shelf. The sediment ranges from Late Cretaceous to Miocene in age and comprises layers of sand, muddy sand, and mud with subordinate calcareous sediment. The most prominent structural feature in the northern part of the study area is the generally east-west trending Pen Branch Fault (see Figure 2.1). Detailed descriptions of the geology of the SRS can be found in several reports (Colquhoun and others, 1983; Fallaw and others, 1990; Aadland and others, 1991; Dennehy and others, 1989; Logan and Euler, 1989; and Fallaw and Price, 1995).

2.1.2 SRS HYDROSTRATIGRAPHY

The hydrostratigraphy of the SRS has been subject to several different classifications. This report incorporates the hydrostratigraphic nomenclature currently established for the SRS vicinity by Aadland and others (1995). The nomenclature has been correlated with the local lithostratigraphy as shown in Figure 2-2. A detailed review of the hydrostratigraphy of the SRS region is provided in Aadland and others (1995).

2.1.2.1 FLORIDAN AQUIFER SYSTEM

The Upper Three Runs Aquifer (UTRA), Gordon Confining Unit, and the Gordon Aquifer (see Figure 2-3) are the local members of the regional Floridan Aquifer system. The UTRA is recharged primarily by precipitation. Groundwater also has a downward component of flow from the UTRA into the Gordon Aquifer. The Floridan Aquifer system is underlain by the low permeability sediments of the Meyers Branch confining system.

UPPER THREE RUNS AQUIFER

The Water Table Aquifer includes all saturated material from the water table to the top of the Gordon Confining Unit, and is equivalent to the Upper Three Runs Aquifer of Aadland and others (1995). The Water Table Aquifer incorporates the "upland" unit, the Tobacco Road Sand, Dry Branch Formation, and Santee Limestone (Figure 2-2). The Water Table Aquifer is locally divided into informal, yet distinct, "lower" and "upper" aquifer zones separated by the "tan clay" semi-confining zone. Based on available water level data, a water table map (personal communication, R.A. Hiergesell) of the area of interest is shown in Figure 2-4.

GORDON CONFINING UNIT

Below the Upper Three Runs Aquifer are clays that form the Gordon Confining Unit. This unit is commonly referred to as the "green clay" in previous SRS literature and includes sediment of the Warley Hill Formation (Figure 2-2). This unit consists of interbedded silty

and clayey sand, sandy clay, and clay. The clay is stiff to hard and is often fissile. Glauconite is a common constituent and imparts a distinctive greenish cast to the sediment, hence the informal name "green clay" for this unit. The Gordon Confining Unit includes some calcareous sediment and limestone, primarily calcarenaceous sand and clayey sand with subordinate calcarenaceous and micritic clay, and sandy micrite and limestone.

GORDON AQUIFER

The lowermost aquifer of interest in this report is the Gordon Aquifer. The Gordon Aquifer is the basal unit of the Floridan Aquifer system in the K-Area vicinity. The Gordon Aquifer is made up of the loose sand and clayey sand of the Congaree Formation and, where present, the sandy parts of the underlying Fishburne and Williamsburg Formations (Figure 2-2) (Harris and others, 1990; Aadland and others, 1991, 1995). The sand within the Gordon Aquifer is yellowish to grayish orange in color and is sub-to well-rounded, moderately to poorly sorted, and medium to coarse-grained. Pebbly zones of iron and silica cement are common. Thin layers (less than 6 inches) of clay are often found near the base of this unit. Figure 2-5 presents a potentiometric surface map of the Gordon Aquifer.

2.1.2.2 MEYERS BRANCH CONFINING SYSTEM

The Meyers Branch Confining System defines the base of the Floridan aquifer system in the study area. The top of the Meyers Branch Confining System is delineated by the laterally continuous, dense, gray to black, clay and sandy clay of the Lang Syne Formation of the Blank Mingo Group (Figure 2-2) (Aadland and others, 1991, 1995). The thickness of this unit is approximately 120 ft based on data collected at the P-25 well cluster (see Figure 5-1).

2.2 UNIT-SPECIFIC HYDROGEOLOGY

Figure 2-3 shows a generalized cross section of the hydrostratigraphic units of the Floridan Aquifer system at the K-Area based on site-specific data. The UTRA is recharged primarily by precipitation events. Indian Grave Branch and Pen Branch serve as local

discharge zones for shallow groundwater in the UTRA. Groundwater also has a downward component of flow from the UTRA into the Gordon Aquifer. Groundwater flows, in the Gordon Aquifer, is generally toward the southwest in the K-Area. The Floridan Aquifer system is underlain by the low permeability Crouch Branch basal confining unit.

Specific field information collected during previous investigations in the study area included core data, lithologic and stratigraphic data, water level data, geophysical logs, cone penetrometer data, and permeability data. Composite lithology/CPT logs were used to develop structural contour maps of relevant hydrostratigraphic units. The lithologic data were then used to define the stratigraphy of the Floridan Aquifer system for incorporation into the groundwater flow and transport model.

As discussed above, the Water Table Aquifer extends to the top of the Gordon Confining Unit as the Upper Three Runs Aquifer (UTRA) (see Figure 2-3). The Water Table Aquifer is divided into upper and lower sections to correspond with the saturated zone above and below the "tan clay," respectively. The saturated zone from the water table to the top of the "tan clay" interval is identified as the UUTR Aquifer and the zone between the "tan clay" and the Gordon Confining Unit is identified as the LUTR Aquifer. A brief discussion of these units follows.

"Upper" Upper Three Runs (UUTR) Aquifer Zone

The UUTR Aquifer consists of all sediment from the ground surface to the top of the "tan clay" confining zone. It includes the "upland" unit, Tobacco Road Sand, and part of the Dry Branch Formation (see Figure 2-2). This unit is characterized by sand and clayey sand with minor intercalated clay layers. The sediment within the "upland" unit is commonly very dense and clayey and contains some gravelly sand.

The UUTR Aquifer is approximately 50 ft thick in the K-area, and includes the "A" horizon, the "AA" horizon, and the undifferentiated materials, which are commonly known as the "transmissive zone" above the "tan clay." This zone is the primary zone of interest because no impacted groundwater has been detected below the "tan clay" at KRBP\KRP. A

majority of the historical water level monitoring data and data collected for this investigation are from the UUTR Aquifer, and typically from wells screened in the "A" and "AA" horizons. Water level data from the lower section of the UUTR Aquifer is limited, and the hydrology of this portion of the aquifer in the vicinity of the unit is poorly understood.

"TAN CLAY" SEMI-CONFINING ZONE

The "tan clay" semi-confining zone is equivalent to the "tan clay" zone referred to in previous SRS reports. The "tan clay" confining zone includes sediment of the Dry Branch Formation (see Figure 2-2). The zone contains light-yellowish tan to orange clay and sandy clay interbedded with clayey sand and sand. The lithology of the clay is similar to that of the Twiggs Clay Member, but is dispersed vertically and horizontally and is not continuous over long distances (Harris and others, 1990; Aadland and others, 1991). However, the "tan clay" confining zone is considered to be continuous in this study within the vicinity of the K-Area Burning Rubble Pit (personal communication, Dennis Jackson).

"LOWER" UPPER THREE RUNS (LUTR) AQUIFER ZONE

The LUTR Aquifer consists of the dominantly fine-grained, well-sorted sand and clayey sand of the Santee Limestone and parts of the Dry Branch Formation beneath the "tan clay" confining zone (see Figure 2-2). Descriptions of drill core indicate that the carbonate sediment in the area has a dominant siliciclastic component, and consists of calcarenaceous sand, micritic sand, shelly sand and some sandy calcarenite and shelly limestone. The LUTR Aquifer is approximately 50 ft thick in the vicinity of the KBRP\KRP. The available monitoring data in this portion of the LUTR Aquifer is limited. The hydrogeologic interpretation of this unit is the study area vicinity is therefore limited.

2.2.1 SURFACE FEATURES

The KBRP and KRP are located in the southwest-central portion of the SRS, approximately 0.65 km (0.4 mi) east of the K-Area Reactor and 9.5 km (5.9 mi) east of the nearest SRS site boundary (see Figure 2-1). This unit is generally located in an area of higher topography. A runoff swale is located 61 m (200 ft) east and downslope from the units. The swale is drained by an unnamed tributary of Pen Branch, located 1529 m (5016 ft) southeast of the units. This swale is the nearest surface water relative to the KBRP and KRP. Water is collected in the swale due to runoff through a breach in a nearby roadway drainage ditch.

METEOROLOGY

The regional climate at the SRS is characterized by warm, humid summers and mild winters (WSRC, 1996a). The average annual temperature is 17.2 °C (63 °F), with daily temperatures ranging from 21° to 33 °C (70° to 92 °F) in the summer, and 3.9° to 15 °C (39° to 59 °F) in the winter. Average annual precipitation is approximately 44 inches, predominantly in the form of rainfall with an occasional snowfall. The average annual wind speed is approximately 7 mph, generally to the southeast or northwest.

SURFACE WATER HYDROLOGY

The KBRP and KRP are located within the Pen Branch Watershed (see Figure 2-1). Surface drainage in the area is southeast at a gradient of approximately 2.2 percent toward an unnamed tributary of Pen Branch, which is located 5000 ft southeast of the units (see Figure 2-1). At the KBRP and KRP, groundwater flows to the west and discharges to Indian Grave Branch, which is located approximately 5500 ft east of the units (see Figure 2-1). The KBRP and KRP are approximately 100 ft above the elevation of both Pen Branch and Indian Grave Branch. The stream gradient along the tributary of Indian Grave Branch is moderate (approximately 100 ft/mile), and the stream gradient of Pen Branch is low (8.6 ft/mile). The stream gradient along Indian Grave Branch is low to moderate (24 ft/mile). Surface water

from Pen Branch and Indian Grave Branch ultimately flows south and discharges into the Savannah River, which is approximately 7 miles from the units.

2.2.2 UNIT-SPECIFIC HYDROSTRATIGRAPHIC UNITS

Based on the lithologic data collected during a recent investigation, the hydrostratigraphy above the "tan clay" (the vadose zone and UUTR Aquifer) has been subdivided into five distinct horizons that are correlatable in the vicinity of the KRBP/KRP. The vadose zone and the UUTR Aquifer are presented in greater detail because they are the primary pathway of observed impacted groundwater. The horizons consist of clay and clayey sand which may affect groundwater infiltration and flow within the uppermost saturated zone. Their horizons are termed, from shallowest to deepest: (1) undifferentiated surface soil; (2) the "A" horizon; (3) "AA" horizon; (4) undefined high permeability "transmissive zone"; and, (5) "tan clay" interval. The occurrence and nature of these horizons in the vicinity of the KRP/KRBP are summarized below. All of these data were incorporated into the groundwater flow model, and are the primary focus of the solute transport modeling.

2.2.2.1 SHALLOW HYDROSTRATIGRAPHY

UNDIFFERENTIATED SURFACE SOILS

The shallow surface soil in the vicinity of the KBRP and KRP consists of interbedded sands, silts, and clays that overlie the "A" horizon. These strata are unsaturated and range in thickness from approximately 0 to 30 ft across the study area. These strata are correlatable to the Upland Unit that is of fluvial origin (Aadland et al., 1995).

"A" HORIZON

The "A" horizon is the shallowest of the identified hydrostratigraphic units and is generally unsaturated in the study area. It consists of a clayey sand, sandy clay, and sand. The upper surface of the "A" horizon occurs at a depth of approximately 0 to 30 ft across the site. The color is described as reddish brown, reddish yellow and brownish yellow near the

upper contact of the unit with increasing depth the color grades to gray, grayish purple, and medium purple. Clay balls are common, especially at the middle and basal zones of the unit.

The boundaries of the "A" horizon were selected based on lithologic and CPT data. The "A" horizon has a characteristic signature of low tip pressure and a high friction ratio throughout the unit. These characteristic signatures are typical of a fine-grained matrix with some clay. Although the horizon includes sands, very coarse-grained material is almost nonexistent in the section. Sleeve pressures throughout the CPT holes were relatively consistent within the "A" horizon.

"AA" Horizon

Underlying the "A" horizon is a more sandy interval that has been termed the "AA" horizon. The upper surface of the "AA" horizon occurs at a depth of approximately 30 to 70 ft across the site. From CPT data, it is distinguished by the relatively high tip resistance as compared to the overlying "A" horizon. This condition indicates the appearance of a more coarse grained material than what occurs in the overlying "A" horizon. In addition, the gamma signature within the "AA" horizon is highly variable, indicating interbedded and interlayered sands, silts and clays.

The "AA" horizon is described as clayey sand and sand that is poorly to very poorly sorted, very fine grained to pebble sized, and subangular to surrounded. The color is light red, medium red and light purple at the upper contact of the horizon.

Undifferentiated High Permeability (Transmissive) Zone

Underlying the "AA" horizon is a sandy, high-permeability interval. Based on its hydraulic properties, this interval has been designated as the Transmissive Zone. Strata within this interval are predominantly sand to silty sands with interbedded clay and pebble layers. The thickness of the Transmissive Zone ranges from approximately 25 to 50 ft.

"TAN CLAY" INTERVAL

In the study area, the "tan clay" represents a semi-confining zone. The clay occurs as lenses and is interbedded with sands, silty sands, clayey sands, and sandy clays. For hydrostratigraphic purposes in this report, the "tan clay" zone is referred to as an interval. The upper surface of the "tan clay" interval ranges in elevation between 130 and 180 ft msl. The "tan clay" is relatively uniform in thickness and ranges from approximately 10 to 15 ft across the site. The upper and lower boundaries of the "tan clay" interval were selected from lithologic and CPT data. The contact can be distinguished by the relatively low tip stress relative to the overlying "AA" horizon. This characteristic signature indicates a finer grained matrix than in the overlying "AA" horizon. Although the "tan clay" includes variable lithology, the unit contacts also correspond to a very high positive deflection in measured pore pressures. Relatively low pore pressures are encountered in the overlying units. In addition, the upper contact of the "tan clay" interval corresponds to a positive deflection on gamma logs.

2.2.2.2 UPPER THREE RUNS AQUIFER

In the KBRP/KRP area, the Upper Three Runs Aquifer (UTRA) consists of sediments from the Tobacco Road, Dry Branch, and Tinker/Santee Formations. Observations of split spoon samples and permeability tests indicate that the UTRA permeability is highly heterogeneous and anisotropic. As previously indicated, the "tan clay" semi-confining zone separates the UTRA into the UUTR Aquifer and the LUTR Aquifer. Based on an estimated horizontal hydraulic conductivity of 5 ft/day from the range of compiled hydraulic conductivity data (personal communication, M.K. Harris), a hydraulic gradient of 0.006 (WSRC, 1996), and an effective porosity of 0.20 based on lithology (de Marsily, 1986), the average linear horizontal groundwater velocity in the UTRA is calculated to be 55 ft/yr.

Figure 2-4 shows a water table map of the UTRA. This figure shows that the site is located west of the groundwater divide in the UTRA. To the west of the divide, groundwater in the vicinity of the KBRP and KRP flows west-southwest towards Indian Grave Branch.

To the east and southeast of the divide, groundwater most likely flows to the east and south toward Pen Branch. Based on water level data at P-25C and P-25D (see Figure 5-1 for location of P-25 well cluster), the downward hydraulic gradient in the UTRA is approximately 0.13 ft/ft. Groundwater levels (third quarter 1996 data) in the immediate KRBP and KRP vicinity indicate that groundwater flows to the west toward Indian Grave Branch (Figure 2-6).

2.2.2.3 GORDON CONFINING UNIT

Based on data collected at the P-25 well cluster approximately 800 ft southeast of the KBRP and KRP, the Gordon confining unit consists of orange gray to dark gray, glauconitic, sandy clay from the Warley Hill Formation. The Gordon Confining Unit is approximately 4 ft thick at this cluster. Laboratory tests of undisturbed soil samples from this location indicate that the vertical hydraulic conductivity of the Gordon Confining Unit is 0.002 ft/day (WSRC, 1996). Using an observed downward hydraulic gradient of 1.15 ft/ft (WSRC, 1996) and an estimated effective porosity of 0.1 based on lithology (de Marsily, 1986), the downward average linear velocity through this unit is approximately 8.4 ft/yr.

2.2.2.4 GORDON AQUIFER

Regional and site-specific data indicate that sediments primarily from the Congaree Formation form the Gordon Aquifer beneath the study area (Aadland et al., 1995; WSRC, 1996). The Gordon Aquifer is approximately 75 feet thick and is recharged primarily by downward leakage from the UTRA. Based on aquifer tests, the hydraulic conductivity of the Gordon Aquifer is estimated to be 50 ft/day (WSRC, 1996). Potentiometric surface maps show that groundwater flow is generally to the west in the study area. Based on an estimated hydraulic gradient of 0.0015 (WSRC, 1996), a hydraulic conductivity of 50 ft/day (WSRC, 1996), and an estimated effective porosity of 0.2 based on lithology (de Marsily, 1986), the average horizontal linear velocity in the Gordon Aquifer is estimated to be 137 ft/yr. The

Gordon Aquifer is underlain by relatively thick, low permeability clays that form the Crouch Branch Confining Unit for the Floridan Aquifer system.

3 CONSTITUENT CHARACTERIZATION

3.1 GROUNDWATER DATA SUMMARY

Quarterly sampling of the first four monitoring wells (KRP-1, KRP-2, KRP-3, and KRP4) at the KRP/KRBP began in October 1983. These wells monitor the UUTR Aquifer. The sampling parameters included Target Compound List (TCL) organics, Target Analyte List (TAL) inorganics, radionuclide parameters, and radionuclides. Background concentration levels were estimated based on sampling results at the two upgradient wells (KRP-2 and KRP-3). Shallow hydrocone samples were collected and analyzed for VOCs in order to delineate the horizontal extent of contamination. This sampling was also used to determine appropriate locations for KRP-5, KRP-6, and KRP-7. Results of a later round of deeper hydrocone sampling showed that impacted areas were limited to the vadose zone and UUTR Aquifer. Two additional rounds of groundwater sampling events were performed during the second and third quarters of 1996. Results from these sampling events (WSRC, 1997) indicated that the primary constituents of concern (COCs) were tetrachloroethylene (PCE) and trichloroethylene (TCE).

3.2 SOURCE AREAS

The source areas of concern in this MZ analysis are the K-Area Burning/Rubble Pit (KBRP) and the K-Area Rubble Pile (KRP). The KBRP was constructed in 1951 for use as a burning pit. It is a shallow, unlined pit 9.1 m (30 ft) wide by 73 m (240 ft) long by 2.7 m (9 ft) deep. Combustible wastes such as organic liquids of unknown source, paper, plastics and rubber were burned in the pit. After 1973, the pit was used for "inert rubble" disposal with all burning operations discontinued. The facility was abandoned by backfilling in 1981. The KRP is semi-circular in shape, 91.4 m (300 ft) long by 15.2 to 41.2 m (50 to 135 ft) wide. The KRP was used for disposal of tree stumps, empty cans and drums, scrap metal, asphalt,

concrete, glass, used batteries, and transite. Rubble and debris were collected and disposed of at the SRS Sanitary Landfill. No operational records are available for either facility.

Source characterization data collection activities were performed between March 2 1996 and June 20, 1997 at the KBRP and KRP. As discussed in detail in the RFI\RI\BRA report (WSRC, 1997b), these investigations included both trench investigations and the collection of soil samples, groundwater samples, and headspace analyses of soil samples at numerous sampling locations in and near the source areas in order to characterize the source of contamination. Based on these extensive investigations, the primary source of contamination was determined to be the debris in the trench and rubble pile. Secondary sources of contamination include surface and subsurface soil in the vicinity of the KBRP and KRP. The most important mechanism for the observed impacts to groundwater was determined to be infiltration/percolation of rainwater through contaminated areas in the subsurface soil and debris at both the KBRP and KRP (WSRC, 1997b).

3.3 CONSTITUENTS OF CONCERN (COCs)

As stated above, the primary COCs were determined to be PCE and TCE because they are present in groundwater at concentrations above their MCL in the vicinity of the waste units. These were the only compounds which showed spatial trends consistent with contaminant plumes at KRBP/KRP. All other compounds were within their expected range of background concentrations with no evidence of plume-like behavior. It should also be noted that soil screening analyses in the RFI/RI/BRA (WSRC, 1997b) indicate that none of the constituents are at concentration levels in the source area soils that would lead to future groundwater contamination above MCLs. Using site-specific data and observed levels of dissolved PCE and TCE in groundwater, simple one-dimensional advection-dispersion equation calculations indicate that these compounds are likely to naturally attenuate to levels below MCLs prior to discharge to surface water. Three-dimensional calibrated flow and solute transport modeling was then performed to more accurately assess the potential for natural attenuation.

3.3.1 OBSERVED PCE DISTRIBUTION

Figure 3-1 (WSRC, 1997b) shows isocontours based on interpretation of dissolved PCE data in 1996 using both groundwater sampling analysis results from monitoring wells and hydrocone sampling. Based on these results, the PCE plume extends (at levels above 5 ppb) downgradient a distance of approximately 500 ft from the source area. This figure also shows that higher concentration levels are present at downgradient locations (~30 ppb at HC-10) in comparison to lower levels at the source. This indicates that the PCE plume center of mass has migrated away from the source area, which suggests that source area releases are diminishing. The observed rapid decrease in PCE concentrations over the last seven years at KRP-4, which is located in the source area, is consistent with this interpretation as shown in Figure 3-2. This figure also shows that PCE concentration levels in the other monitoring wells have been historically very low.

3.3.2 OBSERVED TCE DISTRIBUTION

Figure 3-3 (WSRC, 1997b) shows isocontours of dissolved TCE based on interpretation of TCE data in 1996 as a result of both groundwater sampling analysis results from monitoring wells and hydrocone sampling. This figure shows that the TCE plume extends (at levels above 5 ppb) a smaller downgradient distance of approximately 350 ft from the source area in comparison to PCE. Maximum dissolved TCE concentrations levels are approximately twice (~60 ppb) as high as PCE at hydrocone location HC-10. These higher downgradient TCE concentration levels are again consistent with the interpretation that the source area releases are diminishing. In support of this interpretation, Figure 3-4 shows that the observed concentration levels of TCE at KRP-4 have decreased significantly since 1990. In addition, observed TCE concentration levels have been historically low at the other monitoring wells at the KBRP/KRP.

3.4 RELEVANT COC FATE AND TRANSPORT PROCESSES

The most important physical and chemical processes affecting the fate and transport of dissolved constituents in groundwater are advection, hydrodynamic dispersion, sorption, and biodegradation. These processes cause changes in both the mass and distribution of dissolved constituents in groundwater. Advection is the most important solute transport process. Because of this, it is important to have a well-calibrated groundwater flow model that matches variations in both groundwater flow rates and directions at the site.

Dispersion is a secondary physical process (Domenico and Schwartz, 1990) in which dissolved constituents spread both horizontally and vertically away from the center of mass of the plume. Dispersion is scale dependent and occurs as a result of small-scale variations in the groundwater velocity caused by differences in soil pore sizes and shapes.

Sorption is the chemical process by which dissolved organic constituents adhere to organic carbon present in the soils at a site. Laboratory studies have shown that the mass of organic constituents adsorbed to soils is proportional to the amount of organic carbon in the soils (Karickhoff et al., 1979). The process of sorption causes the constituent plume center of mass to migrate at a fraction of the rate that groundwater moves.

Biodegradation occurs as a result of microbial activity in the subsurface. Whereas many aromatic hydrocarbons degrade (as evidences by relatively small plumes associated with gasoline spills), chlorinated aliphatic hydrocarbons (chlorinated solvents) are more resistant to degradation. Recent evidence demonstrates that intrinsic remediation of chlorinated solvents is occurring at some sites (Semprini et al., 1995). This generally occurs under anaerobic conditions where terminal electron acceptors, other than oxygen, are used.

4 MODEL CONSTRUCTION AND PARAMETER VALUES

The primary phases in the development of a numerical groundwater flow and transport model include: (1) development of a conceptual hydrogeologic model; (2) the construction of a finite-element grid for the model area; (3) specification of model layer top and bottom elevations; (4) assignment of initial and boundary conditions; (5) specification of hydraulic and transport parameter values; and (6) selection of appropriate targets for calibration of the model. This information forms the basis for subsequent calibration of the numerical model to observed groundwater flow conditions and transport modeling of COCs at the site.

4.1 MODEL DISCRETIZATION

The three-dimensional model grid developed for the simulating dissolved COC transport at the KRP and KRBP covers approximately 6 square miles (Figure 4-1). The model domain is approximately 2.25 miles along the east-west boundary and 2.7 miles along the north-south boundary. The finite-element grid was composed of 100 east-west nodes by 125 north-south nodes with 10 vertical nodes for a total number of 125,000 nodes. Of this total, 86, 597 are in the active area of the model. Figures 4-2 and 4-3 present the initial conditions for PCE and TCE concentrations in model element layer 9 (AA Horizon), respectively, used in the model. The flow boundary conditions for the UTRA (Figure 4-4) were specified to coincide with natural hydrogeologic boundaries when possible in order to minimize the influence of model boundaries on simulation results at the site. For the Gordon Aquifer, the flow boundary conditions are shown in Figure 4-5.

Figure 4-6 presents a generalized hydrostratigraphic column with corresponding element layers and nodes for this modeling effort. Based on the hydrostratigraphy at the site, nine layers of vertical discretization were used to simulate flow in the Floridan Aquifer system, which is consistent with the vertical discretization in the regional reactor model that

is currently under development (personal communication, D. Jackson). The Upper Three Runs Aquifer was represented using five model element layers. The Gordon Aquifer was represented using two model element layers in order to improve the numerical accuracy for the simulation of any downward solute transport into the Gordon Aquifer. The "tan clay" and Gordon Confining Unit were each represented by one model element layer.

The model also represents Pen Branch fault (see Figure 4-9), located at the northern part of the model domain, as a continuous linear shift of the hydrostratigraphic units over a short interval. The fault offset is assumed constant at a given elevation. The offsets were estimated from Aadland, et al., (1995).

WSRC has collected an extensive amount of site-specific hydrogeologic data and has constructed structural contour elevation maps of relevant hydrostratigraphic units over the model domain. Figures 4-10 through 4-19 present the top elevations of each of the model element layers in the numerical model. These contour maps were digitized with interpolated values being specified for each corresponding element in the model grid in order to define the vertical discretization of model layers.

A variable grid spacing was used for computational efficiency. The mesh spacing was more coarse in areas away from the zone of COC transport. A finer grid node spacing of 50 feet was used in the zone of COC transport in order to minimize the effects of numerical overshoot and dispersion. This grid spacing near the K-Area also allowed a sufficiently detailed simulation of hydraulic heads to match water levels and groundwater flow directions measured in this area.

4.2 INITIAL AND BOUNDARY CONDITIONS

The initial conditions for this modeling effort consist of hydraulic head and concentration values of PCE and TCE at each node. The initial head values consisted of the simulated hydraulic heads values resulting from the steady-state flow model calibration. As stated previously, the primary source areas in this MZ application are the burning/rubble pit and the rubble pile waste units in the K-Area. Because these source areas are inactive, they

will not be represented in this modeling predictive analysis because future releases to groundwater are highly unlikely. Instead, the observed COC concentration levels will be initialized in the model in order to simulate future concentration levels. Therefore, the initial concentration values will consist of the observed concentration values based on the data presented in Figures 3-1 and 3-3 for PCE and TCE, respectively. The initial conditions for PCE and TCE are shown on Figures 4-2 and 4-3, respectively. The concentrations values at every other node were set to zero.

External model boundaries were chosen to coincide with the hydrogeologic boundaries of the UTRA. The groundwater flow model boundary conditions for each model layer are discussed below. These boundary conditions were specified according to hydraulic conditions encountered in each layer.

At the edge of the model domain, both constant head and no-flow boundary conditions in the Gordon Aquifer were assigned in order to match observed groundwater flow directions. The constant head values were assigned using the best available potentiometric surface map of the Gordon Aquifer (see Figure 2-5). Since groundwater flow in the "tan clay" and Gordon Confining Unit is primarily vertical, no-flow boundary conditions were specified on each model boundary for these units. The Crouch Branch confining unit was also effectively represented using no-flow boundary conditions through its location at the bottom of the model domain.

No-flow boundary conditions were specified for the area both northeast and west of Indian Grave Branch and south of Pen Branch. Head-dependent flux type conditions were specified in appropriate upper model layers to represent Indian Grave and Pen Branch along with their tributaries (see Figure 4-4). The stream elevation for these elements were assigned based on estimated elevations from site topographic maps. The stream stage elevations were estimated between these points using linear interpolation. The effective conductance of surface water bottom sediments in each stream element was calculated based on the length of reach in each element, the width of each surface water feature, a bottom sediment thickness of one foot, and a bottom sediment hydraulic conductivity value that was consistent with the

observed aquifer vertical hydraulic conductivity along each reach. The effective bottom conductance of surface water bodies in the model ranges from 75 to 30,000 ft^2/d, with the range being most reflective of varying reach lengths caused by variable grid spacing.

4.3 GROUNDWATER FLOW MODEL PARAMETERS

In constructing the model for the K-Area, representative values for flow model parameters were initially chosen based on site-specific data, and are shown in Table 3-1. These model parameters include aquifer recharge rate, and both horizontal and vertical hydraulic conductivity of the aquifers and aquitards. Site-specific data for these parameters and their calibrated values are discussed below.

The recharge rate was initially assigned a uniform value of 15 in/yr in the model, which is consistent with the value used at the Old F-Area Seepage Basin. However, model calibration required different zoned values of recharge rates in order to match observed heads (see Figure 4-7). These recharge rate zones were defined based on observed topography and land development in the model domain. In other words, the simulated recharge rate is higher (17 in/yr) in relatively flat, upland areas where runoff is less and is lower (10 in/yr) in areas of steeper topography and paved areas where runoff is greater.

The model calibration was initiated with uniform initial values of hydraulic conductivity for each of the relevant hydrostratigraphic units based site-specific data and results of modeling studies at SRS. During the calibration of the model, the values of these parameter zones were adjusted to minimize the error between observed and simulated groundwater elevations at target locations. Near Pen Branch and Indian Grave Branch, the separate zones of hydraulic conductivity are consistent with the hydrostratigraphic units that are present in these areas of lower topography (see Figure 4-8).

HORIZONTAL HYDRAULIC CONDUCTIVITY OF UPPER THREE RUNS AND GORDON AQUIFER

Slug, infiltrometer, and cone penetrometer tests (CPT) in the UTRA indicate that the hydraulic conductivity of the UTRA is highly heterogeneous at the K Area. This data provides an estimate of the relative difference in hydraulic conductivity across the model domain. Additional hydraulic conductivity has been collected at other areas of SRS using pumping tests, which estimate average hydraulic conductivity values over a greater area. Results of previous flow model calibrations are also useful in defining the range of hydraulic conductivity of hydrostratigraphic units.

Based on a compilation of available hydraulic conductivity collected in the K Area (M.K. Harris, personal communication), infiltrometer, slug, and laboratory tests of field samples were used to guide the flow calibration. For the A Horizon, the horizontal hydraulic conductivity of the A Horizon varied from 0.02 to 3.1 ft/day and the vertical hydraulic conductivity ranged from 0.00028 ft/day to 8 ft/day. The higher values of vertical hydraulic conductivity may not be representative of actual subsurface conditions as a result of rearrangement of pore space during sample collection. For the AA Horizon, slug tests at the KBRP/KRP indicate that the horizontal hydraulic conductivity ranged from approximately 0.27 to 5.3 ft/day. Laboratory tests in the K Area indicate that the vertical hydraulic conductivity ranged from approximately 0.034 to 4.5 ft/day in the AA Horizon. Because limited data is available for hydraulic properties of the transmissive zone, lower part of the UTRA, and the Gordon Aquifer in the K Area, results of previous modeling studies (GeoTrans, 1992; Aadland et al., 1995; Flach and Harris, 1997; and others) were used to determine initial parameter values for these zones.

The calibrated hydraulic conductivity values for each aquifer zone are shown in Figure 4-8. For the A Horizon, the calibrated horizontal and vertical hydraulic conductivity values were 1 and 0.1 ft/day, respectively. For the AA Horizon, the calibrated horizontal and vertical hydraulic conductivitity were 6 and 0.6 ft/day, respectively. These calibrated values of hydraulic conductivity were consistent with site-specific data available in the K Area. For

the other aquifer zones, the calibrated values were consistent with values estimated from other modeling studies (GeoTrans, 1992; Aadland et al., 1995; Flach and M.K. Harris, 1997; and others). As stated previously, the different zonations of hydraulic conductivity in model layers 8 and 9 (Figure 4-8) were required in order to represent the actual hydrogeologic units that were present.

VERTICAL HYDRAULIC CONDUCTIVITY OF THE "TAN CLAY" SEMI-CONFINING UNIT AND GORDON CONFINING UNIT

Groundwater flow is primarily vertical through low permeability aquitards such as the "tan clay" semi-confining unit and the Gordon confining unit. Therefore, the vertical hydraulic conductivity is the most important hydraulic parameter for an aquitard. The vertical hydraulic conductivity of the "tan clay" semi-confining unit has been estimated to be approximately 0.0005 to 0.05 ft/day based results of previous flow model calibrations (Flach and Harris, 1997; D. Jackson, 1998). Laboratory tests of undisturbed soil samples from the P-25 cluster (see Figure 5-1) indicate that the vertical hydraulic conductivity of the Gordon Confining Unit is 0.002 ft/day (WSRC, 1996). Analyses by Aadland et al. (1995) indicate that the vertical hydraulic conductivity of the Gordon Confining Unit may be as low as 0.00001 ft/day.

The calibrated model parameter values for these aquitards are provided in Table 4-1. For the "tan clay" semi-confining unit, the calibrated value for the vertical hydraulic conductivity was 0.001 ft/day. This value is consistent with the estimated range of 0.0005 to 0.05 ft/day based results of previous flow model calibrations (Flach and Harris, 1997; D. Jackson, 1998) performed at SRS. For the Gordon Confining Unit, the calibrated value for the vertical hydraulic conductivity was 0.0007 ft/day, which is also within the range of values (Aadland et al., 1995; WSRC, 1996) that have been determined for this unit.

4.4 TRANSPORT MODEL PARAMETERS

The transport model parameters are summarized in Table 4-1. Uniform values of each component of dispersivity were used in this model based on data in Looney et al. (1987). These values are consistent with the values used in the transport modeling performed for the MZ application at the Old F-Area Seepage Basin. Site-specific values were used for the soil-water partition coefficient based on data provided in Looney et al. (1987). Although PCE and TCE are known to biodegrade given appropriate geochemical conditions, it is assumed that biodegradation does not occur in the transport modeling in order to provide conservative estimates of the future extent of these compounds.

The finite element solution to the advective-dispersive transport equation may be affected by numerical errors, including a phenomenon known as "numerical dispersion," which refers to artificial dispersion caused by errors associated with the discretization of the model domain (Anderson and Woessner, 1992). The Peclet number is defined as:

$$P_e = \frac{\Delta L}{\alpha_L} \tag{4-1}$$

Where ΔL is the characteristic nodal mesh spacing and α_L is the longitudinal dispersivity. Huyakorn and Pinder (1983) suggest that the local P_e be less than or equal to 2 for stable solutions. In the immediate vicinity of the KBRP/KRP, and in the area of expected plume migration, the mesh spacing is 50 ft. A uniform longitudinal dispersivity value of 30 ft is used throughout the model domain, resulting in an appropriate Peclet number of 1.67.

In addition to grid spacing, care should be taken when discretizing time steps such that the Courant number (C_r) is less than or equal to one (Anderson and Woessner, 1992), meaning the solute should not move any further than one element per time step. The Courant number is defined as:

$$C_r = \frac{V_t \Delta t}{\Delta L} \tag{4-2}$$

Where V_t is the average interstitial velocity between any two mesh nodes, ΔL is the characteristic nodal mesh spacing, and Δt is the time step length. A uniform time step of 91.25 days was used for all transport simulations, and the average interstitial velocity (V_t) in the upper UTRA is approximately 0.08 ft/d. This results in an appropriate Courant number equal to 0.15, which is less than 1.0.

5 FLOW CALIBRATION AND TRANSPORT MODELING

This report section first describes the methodology and results of the groundwater flow model calibration for the K area. Based on the calibrated steady-state groundwater velocity field, groundwater flow directions and travel times are examined using particle tracking analyses. This section concludes with an examination of the future fate of dissolved PCE and TCE based on the solute transport modeling results.

5.1 GROUNDWATER FLOW MODEL CALIBRATION

Calibration of a groundwater flow model refers to the process of adjusting model parameters and boundary conditions to obtain a reasonable match between observed and simulated water levels. In general, model calibration is an iterative procedure that involves variation of hydraulic properties and\or boundary conditions to achieve the best match between observed and simulated water levels. During model calibration, site-specific data were used as the primary constraints for the calibrated parameter values. Based on site-specific data, model parameters were varied manually to calibrate the flow model.

5.1.1 FLOW CALIBRATION TARGETS

Calibration targets are a set of field measurements, typically groundwater elevations, which are used to test the ability of a model to reproduce actual conditions within a groundwater flow system. For the calibration of a steady-state (time-invariant) flow model, the goal in selecting calibration targets is to define a set of water-level measurements that gage data and stream at locations throughout the model domain. Based on both stream gage and water data provided by WSRC, approximately 45 monitoring wells and six stream gage measurement locations within the model domain were used to calibrate the flow model. Most of these wells are screened in the UTRA. Several deeper wells such as the P-25 well cluster (see Figure 5-1) provide important data for matching vertical hydraulic gradients in

the model domain. A number of observations of water levels through time were made at monitoring wells in the vicinity of the K-Area, and some wells had more water level measurements taken than others. The mean value of water level from 1985 to 1997 (personal communication, R.A. Hiergesell) for each of these monitoring wells was used as head target values. Stream gage data was also used to guide the calibration. Locations of stream gages are shown in Figure 5-1. The amount of groundwater discharge to surface water on the K-Area side of both Indian Grave Branch and Pen Branch was compared with observed stream gage data, and the contribution from the model domain was estimated to be 30% of the total measured value (personal communication, R.A. Hiergesell). This data was useful in matching site-specific groundwater flow rates in the Upper Three Runs Aquifer.

5.1.2 FLOW CALIBRATION PROCEDURE

For best calibration results, calibration of a model should rely on discrete measurements to produce answers free of contouring interpretations and artifacts. In the calibration of a groundwater flow model, use of point data eliminates the potential for interpretive bias that may result from attempting to match a contoured potentiometric surface (Konikow, 1978). In calibrating the groundwater flow model for the K-Area, the water-level calibration targets measured in monitor wells distributed in the model domain were used.

The primary criterion for evaluating the calibration of the groundwater flow model was examining the difference between simulated and observed water levels at the calibration targets. A residual or model error, e_i, is defined as the difference between the observed and simulated hydraulic head measured at target location:

$$e_i = h_i - \hat{h}_i \tag{5-1}$$

where h_i is the measured value of hydraulic head and $\hat{h}_i$ is the simulated value at the i target location. A residual with a negative sign indicates over-prediction by the model (i.e., the simulated head is higher than the measured value). Conversely, a positive residual indicates

under-prediction. The calibration will also seek to minimize the residual sum of squares (RSS):

$$RSS = \sum_{i=1}^{n} \left(h_i - \hat{h}_i\right)^2 \tag{5-2}$$

where n is the total number of calibration targets. The RSS is the primary measure of model fit. The residual standard deviation (RSTD), which normalizes the RSS by the number of calibration targets (n) and number of estimated parameters (p), is defined as follows:

$$RSTD = \sqrt{\frac{RSS}{n-p}} \tag{5-3}$$

The RSTD is useful for comparing model calibrations with different numbers of calibration targets and estimated parameters. Another calibration measure is the mean of all residuals. A mean residual significantly different from zero indicates model bias. The objective of this model calibration is to achieve a mean residual error equal to or very close to zero, and to have the RSTD fall within the standard deviation of observed water level measurements.

5.2 GROUNDWATER FLOW MODELING RESULTS

The FACT code was used to simulate unsaturated-saturated flow with the finite-element option and Newton-Raphson method with three backtracks. The "pseudo-soil" relative permeability and water retention curves were used to simulate flow in the unsaturated zone. For the saturated zone, Figure 5-1 shows the location of the 45 water-level targets selected for model calibration. The results of the groundwater flow model calibration results are discussed below.

The groundwater flow model calibration required approximately 50 individual computer simulations in order to achieve an appropriate match to observed water level data. Figure 5-2 shows the good match between simulated and observed groundwater elevation

values at each target location throughout the model domain. The accuracy of the flow model calibration in the area of interest (KBRP/KRP) was improved by: 1) more closely matching targets near the KBRP/KRP; 2) matching of observed discharge fluxes into Indian Grave Branch, which is the discharge point for the area of interest; and 3) matching observed transport pathways and bounding the maximum extent of both dissolved PCE and TCE during transport modeling. The calibrated values of hydraulic parameters are also within the observed range of site-specific data.

5.2.1 SIMULATED HYDRAULIC HEADS

As a part of evaluating the calibration of the numerical model, simulated potentiometric surface maps were prepared for each of the aquifers to show groundwater flow conditions over the entire model domain. Figure 5-3 shows the simulated water table surface for the entire model domain. As expected, this figure shows that shallow groundwater discharges to Pen Branch, Indian Graves Branch, and their tributaries. At the KBRP/KRP, which is located west of the divide in the UTRA, the simulated groundwater flow is to the west towards Indian Graves Branch. This result is consistent with flow directions shown in Figures 2-4 and 2-6. Figures 5-4 shows the simulated water levels in the upper part of the Gordon Aquifer. Groundwater flow in this aquifer is also primarily to the southwest. The contours indicate an good match with observed flow directions and water-level elevations (see Figure 2-5).

5.2.2 FLOW MODEL CALIBRATION RESIDUALS AND STATISTICS

Residual statistics for the calibrated groundwater flow model also indicate good agreement between simulated and observed groundwater elevations. The residuals were generally one foot or less in the area of interest (see Figure 5-5). Besides the close match to observed steady-state water levels, simulated groundwater flow directions are consistent with observed flow directions. Outside the area of interest, the largest residuals are found south of

the KRBP\KRP at wells (KSS-1 D, KSS-2D, and KSS-3D) near Pen Branch, and at a cluster of wells (KAC- 1 through KAC-8) located approximately 1000 ft south of the area of interest.

Table 5-1 also shows the residual mean, residual standard deviation, and residual sum of squares for the calibrated model. The mean is close to zero, residual sum of squares is 274 ft^2, and the residual standard deviation (2.50 ft) is less than 5 percent of the range of simulated water-level elevations for the entire model domain, which indicates a very good calibration. In addition, the residual standard deviation falls within the range of standard deviations computed for observed water level measurements.

Table 5-2 shows the observed versus simulated volumetric flux along the reaches of the stream gage targets. The modeled volumetric flux to Indian Grave Branch is 0.99 cfs, as compared to the estimated flux of 1.53 cfs (30% of total flow of 5.1 cfs). As discussed previously, the value of 30% of total stream flow was chosen based on discussions with SRS (Hiergesell, 1998). For Pen Branch, the modeled volumetric flux is 0.53 cfs, as compared to the estimated flux of 0.29 cfs (30% of total flow of 0.96 cfs). The model wide flux to the streams is 1.52 cfs, while the estimated flows equal 1.82 cfs, representing a difference of only 17%. This difference is within the range of uncertainty of the actual volumetric flux into both Indian Grave Branch and Pen Branch for the model domain.

5.2.3 FLOW MODEL SENSITIVITY ANALYSIS

A sensitivity analysis was performed to examine the effects of uncertainties in each of the key model calibration parameters. Table 5-3 shows the results of this sensitivity analysis. The response of the calibrated flow model to changes in horizontal hydraulic conductivity of the upper UTRA, vertical hydraulic conductivity of the Tan Clay Confining Unit, model-wide recharge rate, and stream conductance was evaluated through a discrete sensitivity analysis. In this analysis, one parameter at a time was adjusted while all other parameters were held constant. No significant improvement was achieved in the model calibration by these parameter changes.

The most sensitive model parameters were the vertical hydraulic conductivity of the Tan Clay Confining Unit, horizontal hydraulic conductivity of the Transmissive Zone, and recharge rate. Groundwater heads were also sensitive to changes in horizontal hydraulic conductivity in the other layers of the upper UTRA, but to a much lesser degree than the response to changes in vertical hydraulic conductivity. Decreasing stream conductances one order of magnitude had a marginal impact on groundwater heads; however, an increase of one order of magnitude made the calibration much worse. The conductance values used in the calibrated model are reasonable, and fall within the expected range based on the hydraulic connection between the streams and the upper UTRA.

5.3 GROUNDWATER FLOW MODEL ANALYSIS

Based on the calibrated three-dimensional model developed for the KBRP\KRP site and vicinity, analyses of both the groundwater flow budget for the entire model domain and site-specific groundwater velocity were performed. The groundwater flow budget for the model, in addition to showing conservation of mass in the calibrated model, indicates the major groundwater sources and sinks in the model and large-scale exchange of groundwater flow between aquifers over the domain of the model. Particle-tracking analyses, performed to evaluate groundwater flow rates and directions from specific locations at the KBRP\KRP site, provide a more detailed assessment of groundwater flow rates and direction from the source area in the upper part of the Upper Three Runs Aquifer.

5.3.1 ADVECTIVE PARTICLE TRACKING ANALYSIS

Particle-tracking techniques are useful tools for evaluating groundwater flow directions and constituent migration pathways. Particle tracking is a simple form of contaminant transport analysis which neglects the effects of dispersion, retardation, and chemical reactions. Using an initial starting point, particle tracking simulates the movement of a particle through a groundwater velocity field over time. Particle tracking also acts as a

check on model calibration by allowing comparison of simulated and observed migration pathways and travel times.

Figure 5-6 shows both area and vertical cross sectional views of particle tracking results in the vicinity of the KBRP/KRP. The particles were initially placed at various points at land surface along the downgradient part of the KBRP. For the plan view, the pathlines near the source are consistent with the observed distribution of the dissolved PCE and TCE plumes as shown in Figures 3-1 and 3-3, respectively. For the elevation view, this figure shows that groundwater particle particles travel primarily downward in the A and AA horizons with a more horizontal component in the Transmissive Zone in the area of interest located near the source area. The particle tracking also shows that groundwater particles reach the Gordon Aquifer after approximately 25 years. Although groundwater flow may have a strong downward component of flow, the low amounts of dissolved COC mass in this area prevents impacted groundwater at levels above MCLs from reaching the Gordon aquifer. In other words, the impacted groundwater is diluted as a result of dispersive natural attenuation mechanisms prior to impacting the Gordon Aquifer.

5.3.2 FLOW MODEL WATER BALANCE

A requirement of groundwater flow simulations with models such as FACT is the conservation of flow over the entire model domain. In other words, for a steady-state flow simulation, the sum of all sources of groundwater (flow entering the model domain) should balance the total of all groundwater sinks (flow leaving the model domain). In addition to checking the accuracy of a model simulation, an analysis of a groundwater flow model budget also provides useful insight into the major directions and rates of groundwater flow within the domain of a model.

An analysis of the major groundwater sources and sinks within the K Area groundwater flow model has the components shown in Figure 5-7. This figure summarizes the principal pathways for water entering and leaving the model domain under steady-state flow conditions. The highest volumetric flux (325,1 50 ft^3/day) into the model domain is

from precipitation recharge. Stream gains or losses refer to flow entering or leaving surface water bodies represented in the model by head dependent flux boundary conditions. The model budget shows that stream gain is approximately 254, 633 ft^3/day, which represents discharge to both Indian Grave Branch, Pen Branch, and associated tributaries and wetlands. The stream loss (25,924 ft^3/day) is a result of vertically downward leakage from these surface water bodies into the lower part of the UTRA. This model budget shows that the Gordon Aquifer receives a significant amount (97,407 ft^3/day) of water as a result of downward flow from the UTRA. This amount is the difference between the amount leaving (124,998 ft^3/day) and the amount entering (27,59 1 ft^3/day) the constant head boundary conditions in the Gordon Aquifer.

5.4 TRANSPORT MODELING RESULTS

Solute transport modeling was performed in order to predict the future fate of elevated dissolved COCs in groundwater at the KBRP/KRP. The modeling focused on PCE and TCE because they were only COCs that exhibited a plume-like behavior. However, this analysis is also applicable for other COCs because their concentration levels are lower and they are less mobile than PCE. In this section, the modeling results first examine the maximum lateral extent of a hypothetical chlorinated compound based on a continuous source release. Transport modeling is then applied to both predict future concentration levels of PCE and TCE and determine compliance monitoring well locations based on the initialization of present concentration levels into the model. This section concludes with a discussion of transport model uncertainty based on sensitivity analyses.

5.4.1 SIMULATED WORST-CASE CONSTITUENT CONCENTRATION LEVELS

Figure 5-8 shows the simulated steady-state concentrations for a hypothetical chlorinated compound based on a continuous source release from the KRP. The results are presented in both the AA horizon and the Transmissive Zone. The source release was represented as infiltration of 17 in/yr (same as precipitation recharge) with a constant

concentration that produces concentration levels that are greater than twice the maximum observed concentration of PCE, which had the highest observed historical concentrations for chlorinated compounds at the site. The maximum observed PCE concentration was 140 ug/L at KRP-4, which is located in the source area, and is based on groundwater sampling performed on November 26, 1990. Steady state conditions were reached in 25 years.

This simulation shows that a steady-state or equilibrium plume configuration similar to the one observed in the field will be attained with a constant source of contamination entering the system. The equilibrium condition is attained because the mass being added to the system is being diluted by uncontaminated residual groundwater and recharge which enters the system. Although low concentrations of contaminants are continuously moving downgradient, the plume has the appearance of not moving because the input mass is constantly being swept away before concentrations can go higher. Note that this plume configuration represents the furthest downgradient extent of the plume based on the indicated source concentration. Removal of the input source concentration will cause concentrations within the plume to decline as no more mass is added to the system.

5.4.2 PREDICTED PCE AND TCE CONCENTRATION LEVELS

The simulated future PCE concentrations levels for 1, 5, 8, and 9 years after present conditions are shown in Figures 5-9 through 5-12, respectively. These simulated concentration levels are based on the assumption that the source area is inactive, which is consistent with the low levels of observed PCE in groundwater beneath the source area. The initial concentration levels (see Figure 4-2) in the AA horizon (model element layer 9) were chosen based on the observed 1996 data shown in Figures 3-1. This representation most likely overestimates the amount of PCE mass in groundwater because the initial model concentration is assumed to be uniform throughout the AA horizon. Hydrocone sampling at locations HC-3, HC-10, and HC-10 actually show that PCE levels are below detection limits in the bottom part of the AA horizon. In addition, this model simulation does not include effects of biodegradation and is therefore conservative. Based on this representation, these

simulations are expected to predict the maximum lateral and vertical extent of impacted groundwater.

An examination of these plots shows that the currently observed low levels of PCE will decrease to below their MCL (5 μg/L) within nine years. The plots also show that the plume spreads both laterally and vertically. Figure 5-13 shows more clearly the vertical extent of future PCE concentrations in cross sectional view along the plume centerline. This figure shows that the simulated plume center of mass migrates downward into the transmissive zone and lower UTRA with concentrations being reduced over time by hydrodynamic dispersion. Although these transport modeling results may overpredict the maximum vertical and horizontal extent, they still show that regulatory limits will not be exceeded downgradient of the current location of the plume or in the Gordon Aquifer.

Figures 5-14 through 5-17 show, respectively, simulated future TCE concentrations levels for 1, 3, 5, and 6 years after present conditions. These simulated concentration levels are based on the assumption that the source area is inactive. The plume initialization most likely overestimates the amount of dissolved TCE mass in groundwater because the initial model concentration is assumed to be uniform throughout the AA horizon. As was the case for PCE, hydrocone sampling at locations HC-3, HC-10, and HC-10 actually show that TCE levels are below detection limits in the bottom part of the AA horizon. This model simulation also does not include effects of biodegradation of TCE. Based on this conservative representation, these simulations are expected to predict the maximum lateral and vertical extent of impacted TCE in groundwater.

These simulation plots show that the currently observed low levels of TCE will decrease to below their MCL (5 μg/L) within six years. As expected, the plume spreads both laterally in the upper part of the UTRA and vertically into the lower part of the UTRA. The vertical extent of future TCE concentrations in cross sectional view along the plume centerline is shown in Figure 5-18. This figure also shows that the simulated plume center of mass migrates downward into the transmissive zone with concentrations being reduced over

time by hydrodynamic dispersion. The model results show that that regulatory limits will not be exceeded at both downgradient receptors in the UTRA and Gordon Aquifer.

5.4.3 OTHER CONSTITUENTS

Other constituents (Dichloromethane, Lead, Thallium) have been proposed as COCs because they have been sporadically observed in groundwater. However, their presence or distribution is not consistent enough from which to conceptualize a plume. Therefore, it is reasonable to assume that the mass of these constituents is considerably less than that of PCE or TCE, which have enough mass in the system to indicate a plume. Based on their limited amount of retardation, the PCE and TCE concentration plumes can be used as templates for computing worst case dilution factors for other constituents. Based on the continuous source PCE simulation, a dilution factor of approximately 20 to 1 is present between the source area and the proposed compliance wells. This factor is based on the 100 μg/L concentration in the source area divided by the 5 μg/L concentration at the proposed compliance wells. Application of the this dilution factor to the highest observed concentrations of lead, thallium, and DCM in groundwater reduces their concentrations significantly below MCLs at the proposed compliance wells.

Daughter products in the TCE chain are generally not present in detectable quantities in the monitoring well data base. These constituents, if present, will behave in a similar manner as their parent compounds. As such, dilution and dispersion will reduce their concentrations at the same rate of reduction as the parent concentrations. In addition, any daughter products, that are present, will exist in concentrations significantly lower than those of their parents. Because the parent concentrations are already low, and decline rather quickly, daughter products will not constitute an exceedance of MCLs at downgradient locations.

5.4.4 COMPLIANCE BOUNDARY LOCATIONS AND TRANSPORT MODEL SENSITIVITY ANALYSIS

The location of the compliance wells used in the transport sensitivity analysis are shown in Figure 5-19 . The locations were based on the results of the future predicted concentrations of PCE and TCE. Compliance well cluster location # 1 (CP 1), located approximately 800 ft downgradient of the source area, lies along the predicted PCE/TCE plume centerline. Compliance well cluster locations #2 and #3 (CP2 and CP3) lie approximately 100 ft northwest and southeast, respectively, of CP 1 and are located such to bracket the expected maximum lateral width of the predicted PCE/TCE plumes. Based on the potential for vertically downward transport as shown in the transport modeling, the compliance well screen depths should be placed to monitor three zones: (1) approximately 15 ft saturated thickness of the AA Horizon; (2) lowermost 10 ft of the Transmissive Zone; and (3) uppermost 10 ft of the Gordon Aquifer.

Figures 5-20 and 5-21 display the simulated concentrations of PCE and TCE, respectively, versus time at the compliance well CP 1. The simulation breakthrough curves at CP1 show maximum concentrations of approximately 3 and 4 μg/L, respectively, for TCE and PCE. The model results show that neither constituent exceeds the MCL of 5 μg/L at CP1. In order to examine other potential COCs, Figure 5-22 shows a plot of normalized concentration versus time for a conservative compound that does not adsorb or decay. By multiplying this plot by the maximum observed concentration of any compound, one can estimate the worst case concentration at the compliance point.

A series of sensitivity runs were performed to analyze the effects on future predicted concentrations at the compliance well. The following runs were performed: 1) reduce recharge globally by 30%; 2) increase dispersivities by a factor of 3; 3) reduce dispersivities by a factor of 3; 4) increase effective porosities by 50%; and, 5) decrease effective porosities by 50%. For each run, PCE was used as the simulated constituent as it has a higher maximum concentration at the downgradient compliance well compared to TCE. Table 5.4 summarizes the sensitivity simulations that were performed with the transport model.

Figure 5-23 displays the results of the sensitivity analyses for PCE at the compliance well CP 1. In each sensitivity run, the maximum predicted concentration remains below the MCL. The analyses indicate that predicted concentrations are most sensitive to changes in dispersivity. However, the change in predicted maximum concentration with changes in dispersivity is approximately 25%. The predicted maximum concentration is fairly insensitive to changes in recharge or effective porosity. In either case, the predicted maximum concentration was not significantly higher than the base case; only the time for the center of mass to pass through the system was changed.

6 SUMMARY AND RECOMMENDATIONS

This groundwater flow and solute transport modeling report summarizes the relevant site-specific hydrogeology, geochemical data, and modeling results for the simulation of future concentration levels of dissolved PCE and TCE in groundwater at the KBRP and KRP. The numerical model simulations will be used to prepare and justify passive aquifer restoration using a GWMZ application for impacted groundwater at this unit. The MZ will be developed in a manner consistent with South Carolina Department of Health and Environmental Control (SCDHEC) guidance.

The numerical model was first calibrated to average observed water level and stream gage data in the vicinity of the K area. A detailed examination of the flow calibration results of the flow model indicates that a very good match to observed conditions has been achieved. The flow calibration from this work will also facilitate the development of the regional reactor model that is currently under development.

The transport modeling results were applied to simulate both a worst-case continuous source release and the more realistic simulation of an inactive source. Field data supports the conceptual model of an inactive source area that is no longer contributing contaminants to the groundwater system. As displayed in Figure 6-1, the transport modeling results indicate that concentration levels of both PCE and TCE will decrease to levels below their corresponding MCLs in six and nine years, respectively, based on an inactive source. Plumes of lower, but detectable, concentration will persist in the aquifer for at least an additional ten years. Figure 6.2 shows that the volume of water with concentrations of 5 ug/L or more of PCE and TCE declines rapidly with time. The modeling results show that there will be no future discharge to surface water of impacted groundwater as a result of releases from the Burning/Rubble Pit and Rubble Pile. Furthermore, the transport modeling results show that the PCE and TCE plumes will not reach the Gordon Aquifer at levels above MCLs. These modeling results therefore show that use of a GWMZ alternative is a viable groundwater remedy for impacted groundwater at the KRP and KRBP waste units.

REFERENCES

Aadland, R. K., J.A. Gellici, and P.A. Thayer, 1995. Hydrogeologic Framework of West Central South Carolina. Report 5, South Carolina Department of Natural Resources, Water Resources Division.

Aadland, R. K., M.K. Harris, C.M. Lewis, T.F. Gaughan, and T.M. Westbrook, 1991. Hydrostratigraphy of the General Separations Area, Savannah River Site (SRS), South Carolina, USDOE Report WSRC-RP-91-13, Westinghouse Savannah River Company, Aiken, SC 29808, 114 p.

Anderson, M.P. and W.W. Woessner, 1992. Applied Groundwater Modeling: Simulation of Flow and Advective Transport, Academic Press, Inc., New York, pp. 326-327.

Buck, J. W., G. Whelan, J.G. Droppo, Jr., D.L. Strenge, K.J. Castleton, J.P. McDonald, C. Sato, and G.P. Streile, 1995. Multimedia Environmental Pollutant Assessment (MEPAS) Application Guidance; Guidelines for Evaluating MEPAS Input Parameters for Version 3.1. Battelle Memorial Institute, Pacific Northwest Laboratory, Richland, WA. USDOE contract no. DE-AC0-76RLO 1830.

Colquhoun, D.J., I.D. Wollen, D.S. Van Nieuwenhuise, G.G. Padgett, R.W. Oldham, D.C. Boylan, J.W. Bishop, and P.D. Howell, 1983. Surface and Subsurface Stratigraphy, Structure and Aquifers of the South Carolina Coastal Plain, SCDHEC Report ISBN 0-9613154-0-7, 78 p.

de Marsily, G., 1986. Quantitative Hydrogeology, San Diego: Academic Press.

Dennehy, K. F., D.C. Prowell, and P.B. McMahon, 1989. Reconnaissance Hydrogeologic Investigation of the Defense Waste Processing Facility and Vicinity, Savannah River Plant, South Carolina, U.S. Geological Survey Water Resources Investigations, Report 88-4221, 68 p.

Domenico, P., and F. Schwartz, 1990. Physical and Chemical Hydrogeology, John Wiley & Sons, New York.

Fallaw, W. C., and V. Price, 1995. Stratigraphy of the Savannah River Site and vicinity, Southeastern Geology, 35: 21-58.

Fallaw, W. C., V. Price, and P. Thayer, 1990. Stratigraphy of the Savannah River Site, South Carolina, in Zullo, V. A., W.B. Harris, and V. Price, eds., 1990, Savannah River Region: Transition Between the Gulf and Atlantic Coastal Plains. Proceedings of the Second Bald Heal Island Conference on Coastal Plains Geology, University of North Carolina at Wilmington, Wilmington, NC.

GeoTrans, Inc., 1992. Groundwater flow model for the General Separations Area, Savannah River Site, report prepared for Westinghouse Savannah River Company, GeoTrans project no. 3017-003, May 15.

Flach, G.P. and M.K. Harris, 1997. Integrated hydrogeological model of the General Separations Area (U); Volume 2: Groundwater flow model (U), WSRC-TR-96-0399.

Hamm, L. L., S. E. Aleman, W. F. Jones, G. P. Flach, J. S. Haselow, P. S. Huyakorn, S. Panday, and T. Birdie, 1997. FACT: Subsurface Flow and Contaminant Transport Documentation and User's Guide, Version 1.0, WSRCTR-95-223.

Harris, M. K., R.K. Aadland, and T.M. Westrbook, 1990. Lithological and Hydrological Characteristics of the Tertiary Hydrostratigraphic Systems of the General Separations Area, Savannah River Site, South Carolina, in Zullo, V.A., W.B. Harris, and V. Price, eds., 1990, Savannah River Region: Transition Between the Gulf and Atlantic Coastal Plains. Proceedings of the Second Bald Heal Island Conference on Coastal Plains Geology, University of North Carolina at Wilmington, Wilmington, NC, pp. 68-73.

Harris, M. K., April 1998. Personal communication.

Hiergesell, R.A., March 1998. Personal communication.

Howard, P. H., 1991. Handbook of Environmental Degradation Rates: Lewis Publishers.

Huyakorn, P.S. and G.F. Pinder, 1983. Computational Methods in Subsurface Flow, Academic Press, New York, pp. 206-207.

Jackson, D., April 1998. Personal communication.

Karickhoff, S. W., D.S. Brown, and T.A. Scott, 1979. Sorption of Hydrophobic Pollutants on Natural Sediments. Water Research, Vol. 13, p. 241-248.

Konikow, L., 1978. Calibration of Groundwater Models. Proceedings of the Specialty Conferences on Verification of Mathematical and Physical Models in Hydraulic Engineering, College Park, Maryland, August 9-11, 1978.

Logan, W. R., and G.M. Euler, 1989. Geology and groundwater resources of Allendale, Bamberg, and Barnwell counties and part of Aiken County, SC, South Carolina Water Resources Commission Report, 155, 113 pp.

Looney, B. B., M. W. Grant, and C. M. King, 1987. Estimation of Geochemical Parameters for Assessing Subsurface Transport at the Savannah River Plant. DPST-85-903.

Pekkala, R. O., C.E. Jewell, V. Price, and H. W. Bledsoe, 1987. Environmental Information Document: L-Area Oil and Chemical Basin, DPST-85-700, E.I. du Pont de Nemours and Company, Savannah River Plant, Aiken, SC.

SCDHEC (South Carolina Department of Health and Environmental Control) 1994. Groundwater Mixing Zone Guidance Document, March 1994.

Semprini, L., P.K. Kitanidis, D.H. Kampbell, and J.T. Wilson, 1995. Anaerobic transformation of chlorinated aliphatic hydrocarbons in a sand aquifer based on spatial chemical distributions, Water Resources Research, 31(4): 1051-1062.

WSRC (Westinghouse Savannah River Company), 1996. Phase II RCRA Facility Investigation/Remedial Work Plan for the K-Area Burning/Rubble Pit and Rubble Pile (U), Rev. 1.1. Westinghouse Savannah River Company, Savannah River site, Aiken, SC. August 1996. WSRC-RP-94-1200.

WSRC (Westinghouse Savannah River Company), 1997a. Integrated Hydrogeological Model of the General Separation Area (U), Volume 2: Groundwater Flow Model, WSRC-TR-96-0399, Westinghouse Savannah River Company, Aiken, SC.

WSRC (Westinghouse Savannah River Company), 1997b. Final: RCRA Facility Investigation/Remedial Investigation Report With the Baseline Risk Assessment for the K-Area Burning Rubble Pit (131-K) and Rubble Pile (631-20G) (U). Westinghouse Savannah River Company, Savannah River site, Aiken, SC.

WSRC (Westinghouse Savannah River Company), 1997c. Evaluation of cone penetrometer data for permeability correlation at Savannah River Site, WSRC-RP-97-63, Westinghouse Savannah River Company, Aiken, SC.

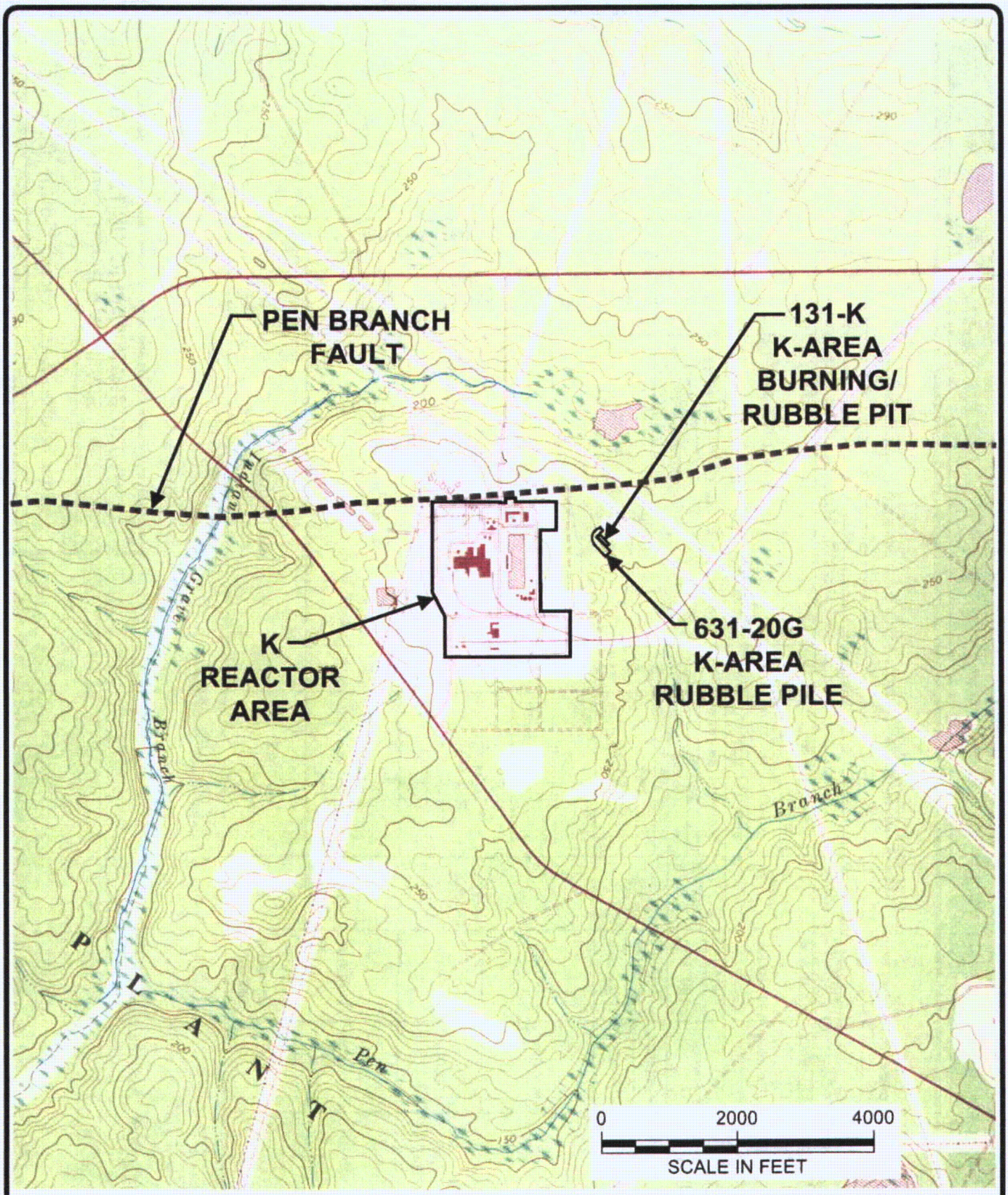

TITLE: SITE LOCATION MAP FOR K-AREA UNIT: BURNING/RUBBLE PIT AND RUBBLE PILE

LOCATION: Savannah River Site, Aiken, South Carolina

HSI GEOTRANS
A TETRA TECH COMPANY

CHECKED:	JJB	FIGURE:
DRAFTED:	CMP	2-1
FILE:	I014001A.DSF	
DATE:	5-19-98	

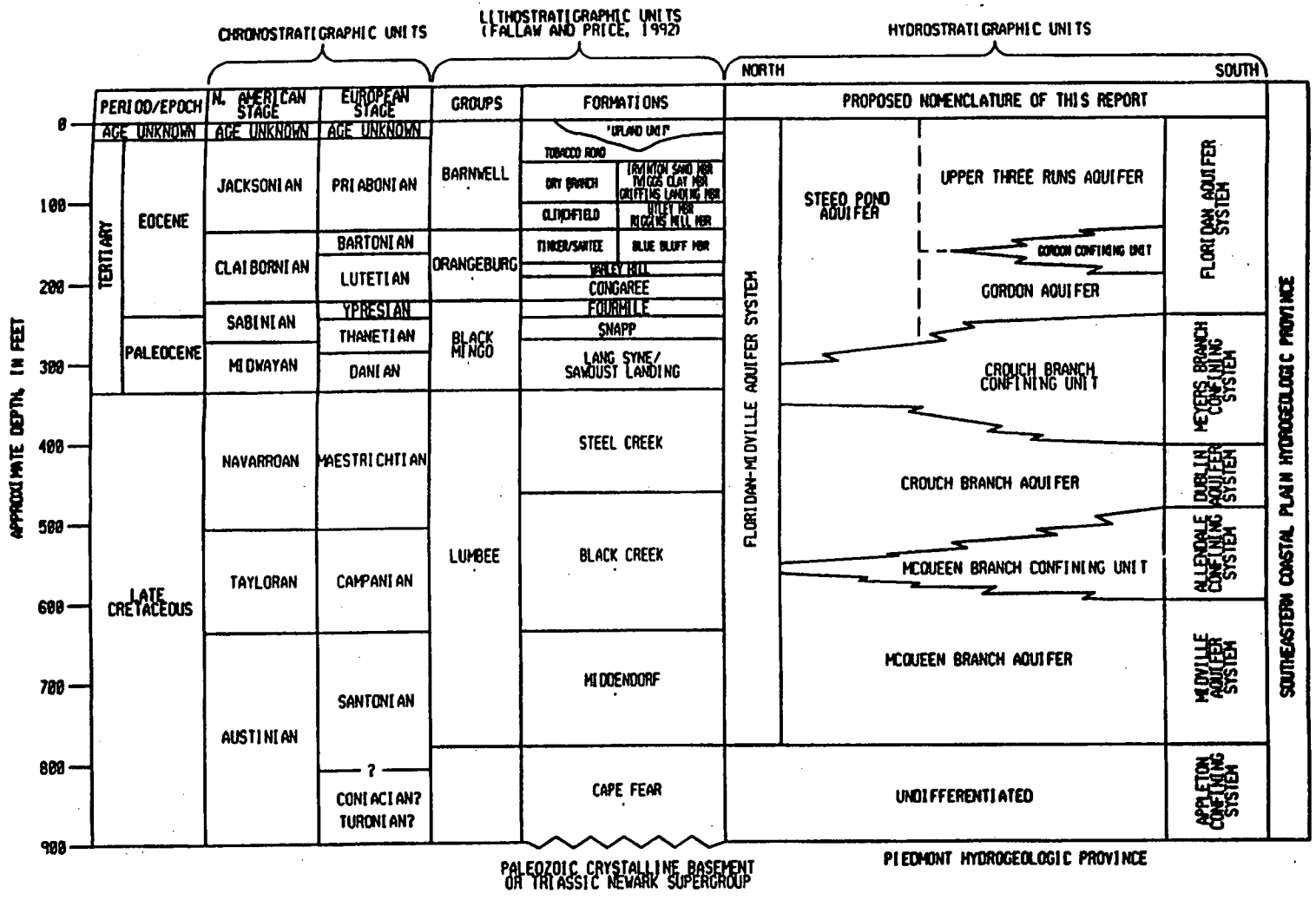

(Source: Aadland et al. 1995)

TITLE:	HYDROSTRATIGRAPHIC UNITS AT THE SAVANNAH RIVER SITE
LOCATION:	Savannah River, Aiken, South Carolina
HSI GEOTRANS A TETRA TECH COMPANY	CHECKED: JJB; DRAFTED: SDL; FILE: N/A; DATE: 4-10-9
FIGURE:	2-2

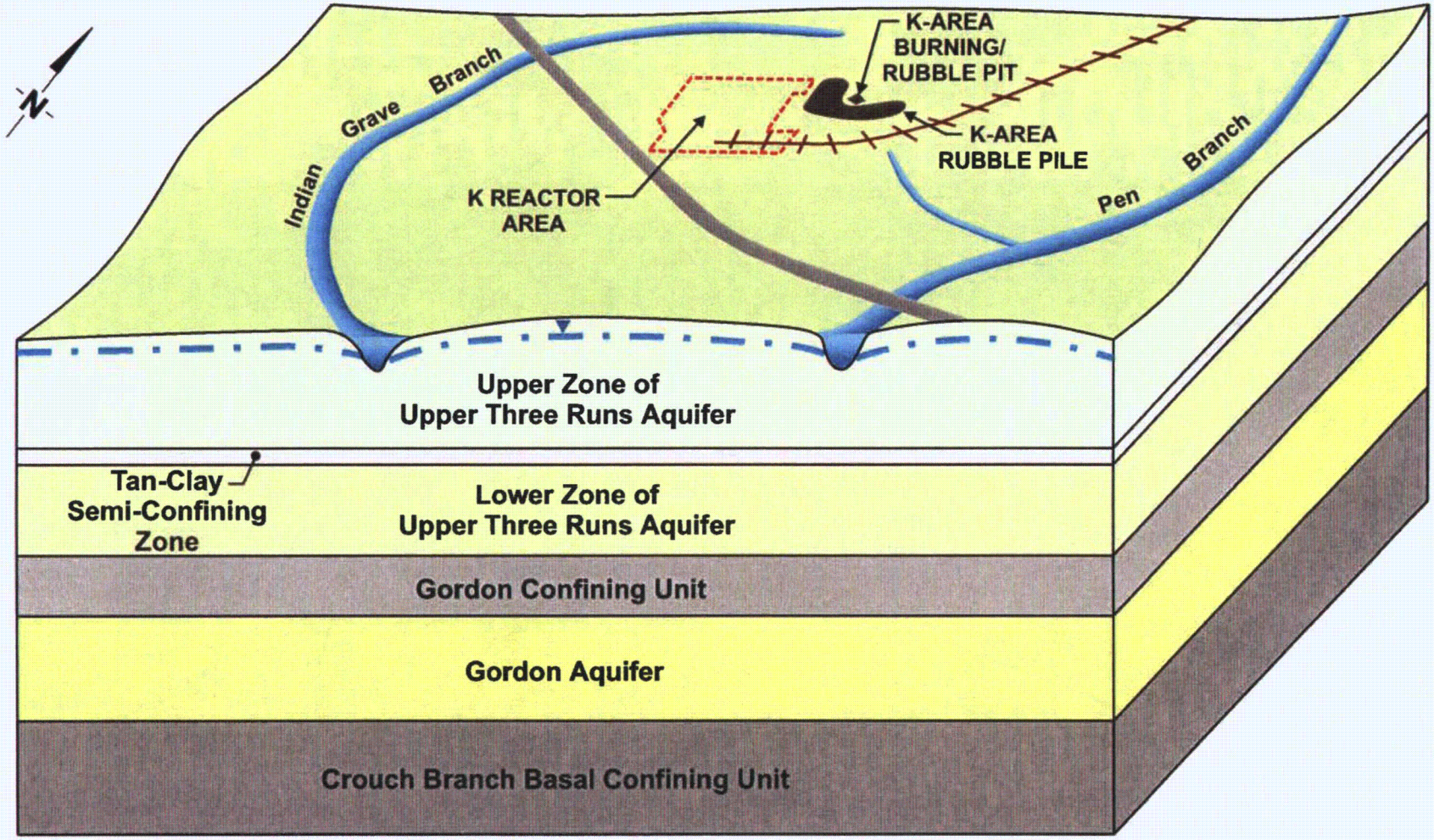

NOTE: NOT DRAWN TO SCALE

TITLE:
GENERALIZED SCHEMATIC OF HYDROGEOLOGIC FEATURES NEAR THE K-AREA BURNING RUBBLE PIT/RUBBLE PILE

LOCATION:
Savannah River Site, Aiken, South Carolina

HSI GEOTRANS
A TETRA TECH COMPANY

CHECKED:	DB
DRAFTED:	CP
FILE:	IO14001A.CDR
DATE:	5-6-98

FIGURE:
2-3

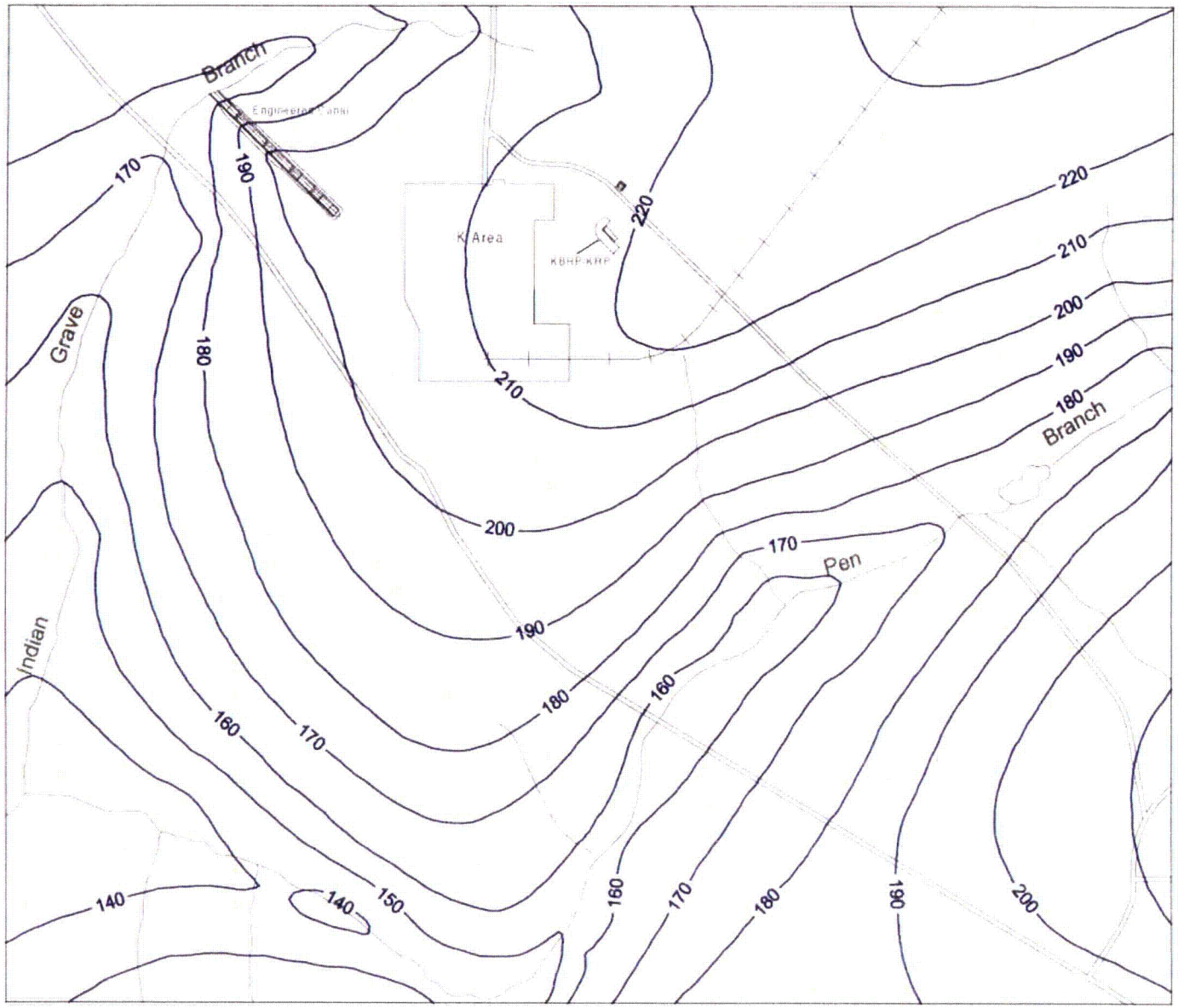

N

Legend

Water Level Elevation (ft. MSL)

0 2000 4000
Feet

Water table surface of the Upper Three Runs Aquifer

HSI GEOTRANS A TETRA TECH COMPANY	CHECKED:	JJB	FIGURE: 2-4
	DRAFTED:		
	FILE:	fig2-4 SRF	
	DATE:		

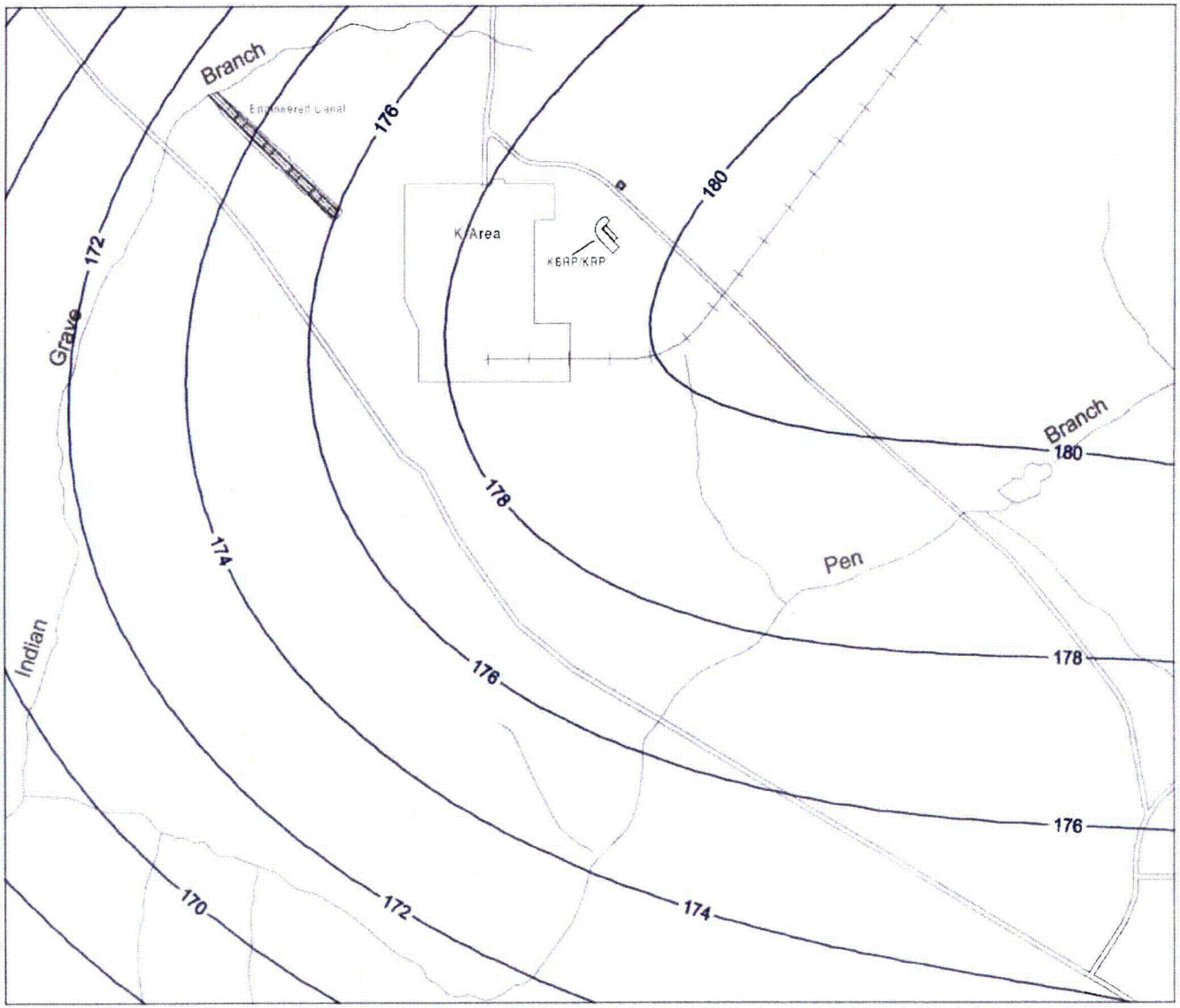

N

Legend

Water Level Elevation (ft. MSL)

0 2000 4000
Feet

Potentiometric surface map of the Gordon Aquifer

HSI GEOTRANS A TETRA TECH COMPANY	CHECKED:	JJB	FIGURE:
	DRAFTED:		2-5
	FILE	fig2-5 SRF	
	DATE:		

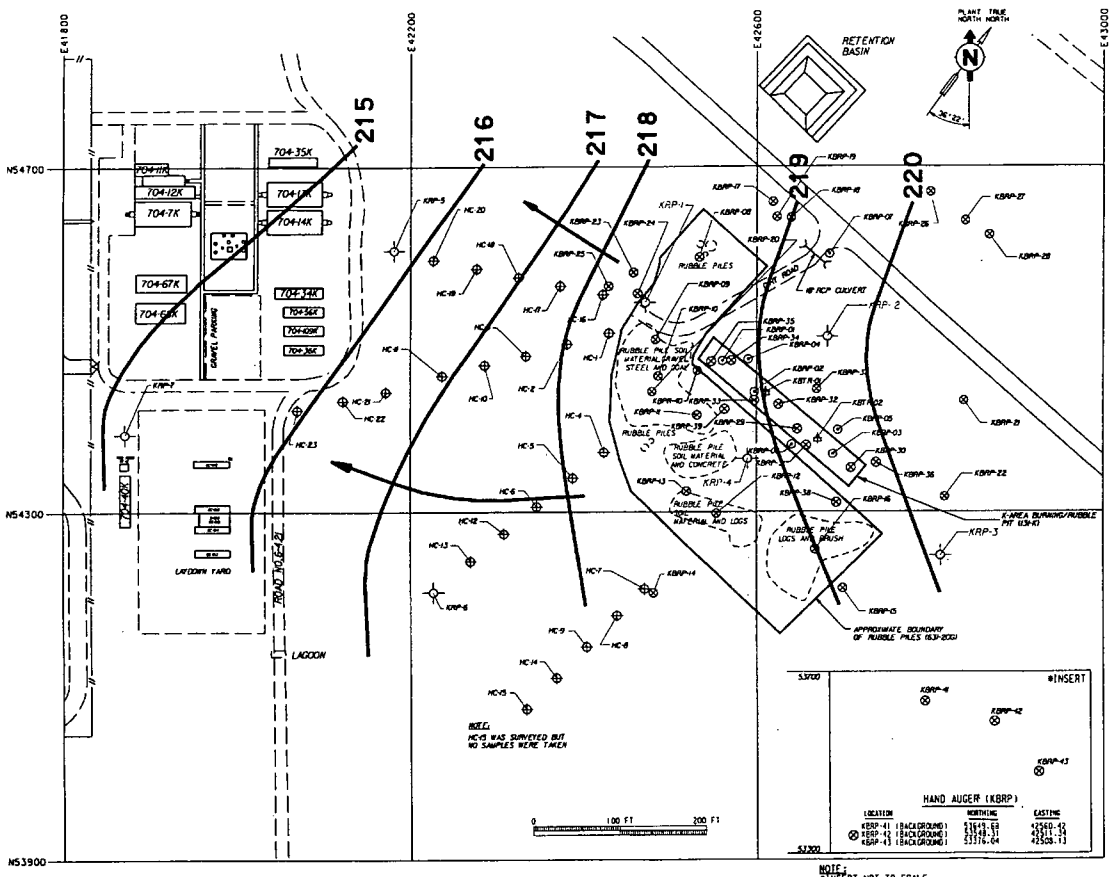

WELLS (KRP)

SYMBOL	LOCATION	NORTHING	EASTING
	KRP-1	54544.00	42471.20
	KRP-2	54503.60	42681.60
	KRP-3	54248.70	42814.30
	KRP-4	54367.90	42590.30
	KRP-5	54606.64	42181.79
	KRP-6	54206.68	42226.85
	KRP-7	54390.33	41871.70

HYDROCONE (HC)

LOCATION	NORTHING	EASTING
HC-1	54528.22	42433.09
HC-2	54435.52	42491.65
HC-3	54481.48	42533.62
HC-4	54369.13	42424.25
HC-5	54339.19	42388.35
HC-6	54305.69	42346.36
HC-7	54210.51	42470.11
HC-8	54175.31	42438.30
HC-9	54143.45	42404.22
HC-10	54470.80	42285.25
HC-11	54458.33	42236.84
HC-12	54274.47	42107.58
HC-13	54242.75	42268.74
HC-14	54107.88	42369.15
HC-15	54107.32	42333.93
HC-16	54552.90	42422.93
HC-17	54655.42	42418.11
HC-18	54572.80	42324.92
HC-19	54582.51	42275.88
HC-20	54532.93	42226.86
HC-21	54439.54	42170.87
HC-22	54421.89	42122.01
HC-23	54416.40	42069.05

SOIL BORINGS (KBRP)

LOCATION	NORTHING	EASTING
KBRP-01	54475.75	42561.39
KBRP-02	54440.98	42598.64
KBRP-03	54366.69	42687.56
KBRP-04	54477.52	42590.97
KBRP-05	54394.81	42693.83
KBRP-06	54377.96	42640.46
KBRP-07 (BACKGROUND)	54599.19	42683.13

HAND AUGER (KBRP)

LOCATION	NORTHING	EASTING
KBRP-08	54535.67	42524.32
KBRP-09	54500.64	42483.13
KBRP-10	54458.22	42486.24
KBRP-11	54412.56	42531.39
KBRP-12	54297.90	42532.92
KBRP-13	54324.40	42518.83
KBRP-14	54205.34	42475.98
KBRP-15	54210.72	42638.71
KBRP-16	54255.74	42666.89
KBRP-17 (BACKGROUND)	54659.42	42618.11
KBRP-18 (BACKGROUND)	54641.20	42619.18
KBRP-19 (BACKGROUND)	54649.06	42622.02
KBRP-20	54440.06	42478.92
KBRP-21	54438.88	42440.57
KBRP-22	54317.06	42819.18
KBRP-23	54578.57	42457.83
KBRP-24	54534.49	42427.50
KBRP-25	54582.73	42423.31
KBRP-26 (BACKGROUND)	54670.94	42802.61
KBRP-27 (BACKGROUND)	54637.51	42842.50
KBRP-28 (BACKGROUND)	54621.34	42870.06
KBRP-29	54356.26	42645.56
KBRP-30	54350.66	42706.17
KBRP-31	54376.96	42656.98
KBRP-32	54424.80	42674.88
KBRP-33	54429.40	42597.21
KBRP-34	54476.07	42571.21
KBRP-35	54475.12	42547.86
KBRP-36	54356.70	42738.52
KBRP-37	54442.37	42669.07
KBRP-38	54310.54	42631.81
KBRP-39	54419.56	42582.22
KBRP-40	54466.44	42531.44

TRENCH (KBTR)

LOCATION	NORTHING	EASTING
KBTR-01	54439.18	42610.22
KBTR-02	54385.11	42670.22

LEGEND:

WATER TABLE ELEVATION (FEET ABOVE MEAN SEA LEVEL)

GROUNDWATER FLOW DIRECTION

FROM: WSRC (1997b)

TITLE: SITE-SPECIFIC WATER TABLE SURFACE FOR UPPER THREE RUNS AQUIFER, BASED ON THIRD QUARTER 1996 DATA.

LOCATION: Savannah River Site, Aiken, South Carolina

HSI GEOTRANS
A TETRA TECH COMPANY

CHECKED:	JJB
DRAFTED:	SDL
FILE:	N/A
DATE:	4-10-98

FIGURE: 2-6

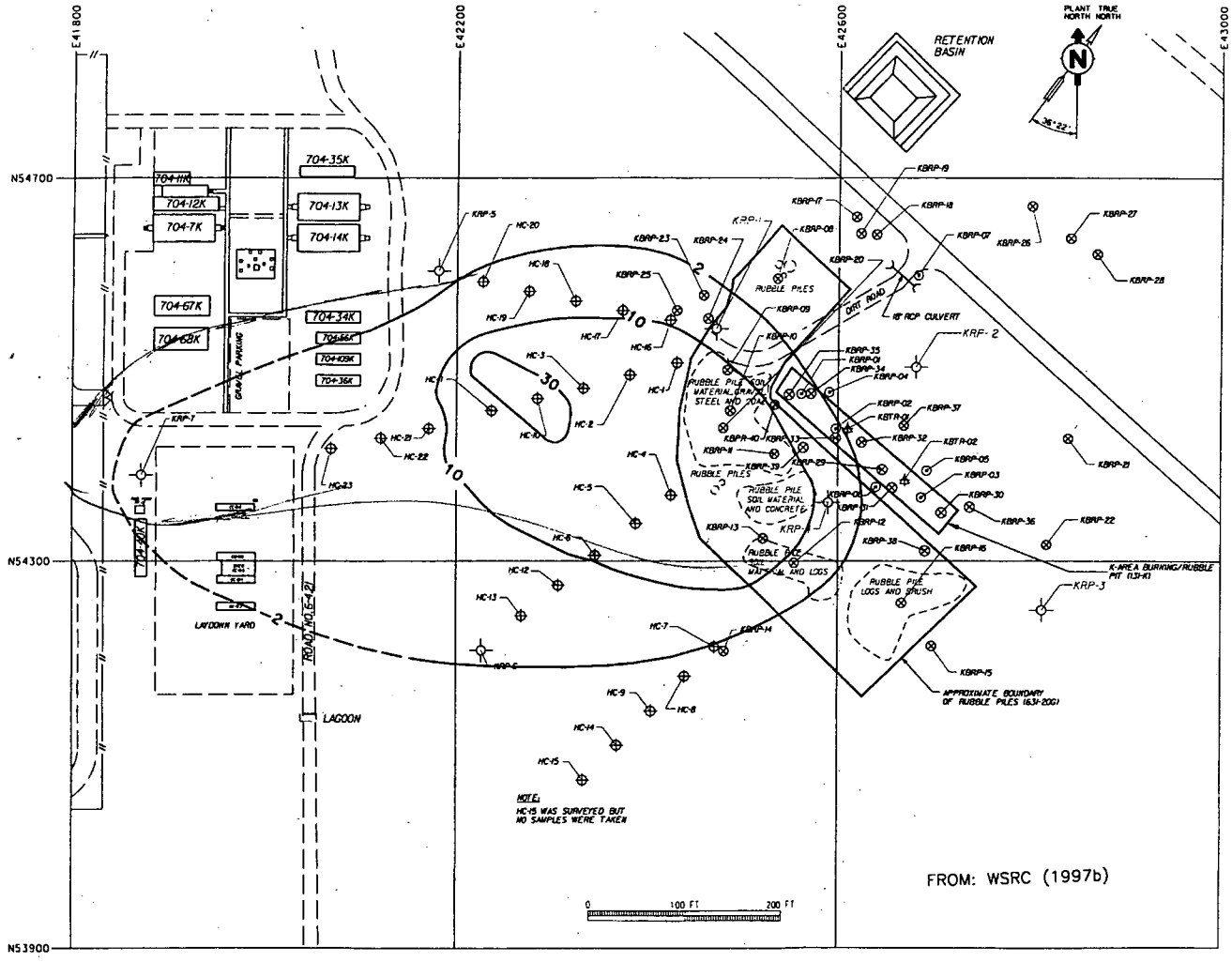

LEGEND

- SOIL BORINGS (KBRP)
- HAND AUGER (KBRP)
- TRENCH (KBTR)
- HYDROCONE (HC)
- INTERPRETATED CONCENTRATION CONTOUR (ug/L)
- ESTIMATED CONCENTRATION CONTOUR (ug/L)

NOTE:
ALL CONCENTRATIONS ARE IN MICROGRAMS PER LITER (ug/L).

CONTOURS WERE DRAWN BASED ON A COMBINATION OF CPT AND MONITORING WELL DATA

TITLE: K-AREA BURNING/RUBBLE PIT AND RUBBLE PILE PCE CONCENTRATION CONTOUR MAP IN THE UPPER ZONE OF UPPER THREE RUNS AQUIFER

LOCATION: Savannah River Site, Aiken, South Carolina

HSI GEOTRANS A TETRA TECH COMPANY

CHECKED:	JJB
DRAFTED:	SDL
FILE:	N/A
DATE:	5-5-98

FIGURE: 3-1

Figure 3-2. Observed PCE concentration versus time at KRBP/KRP monitoring wells.

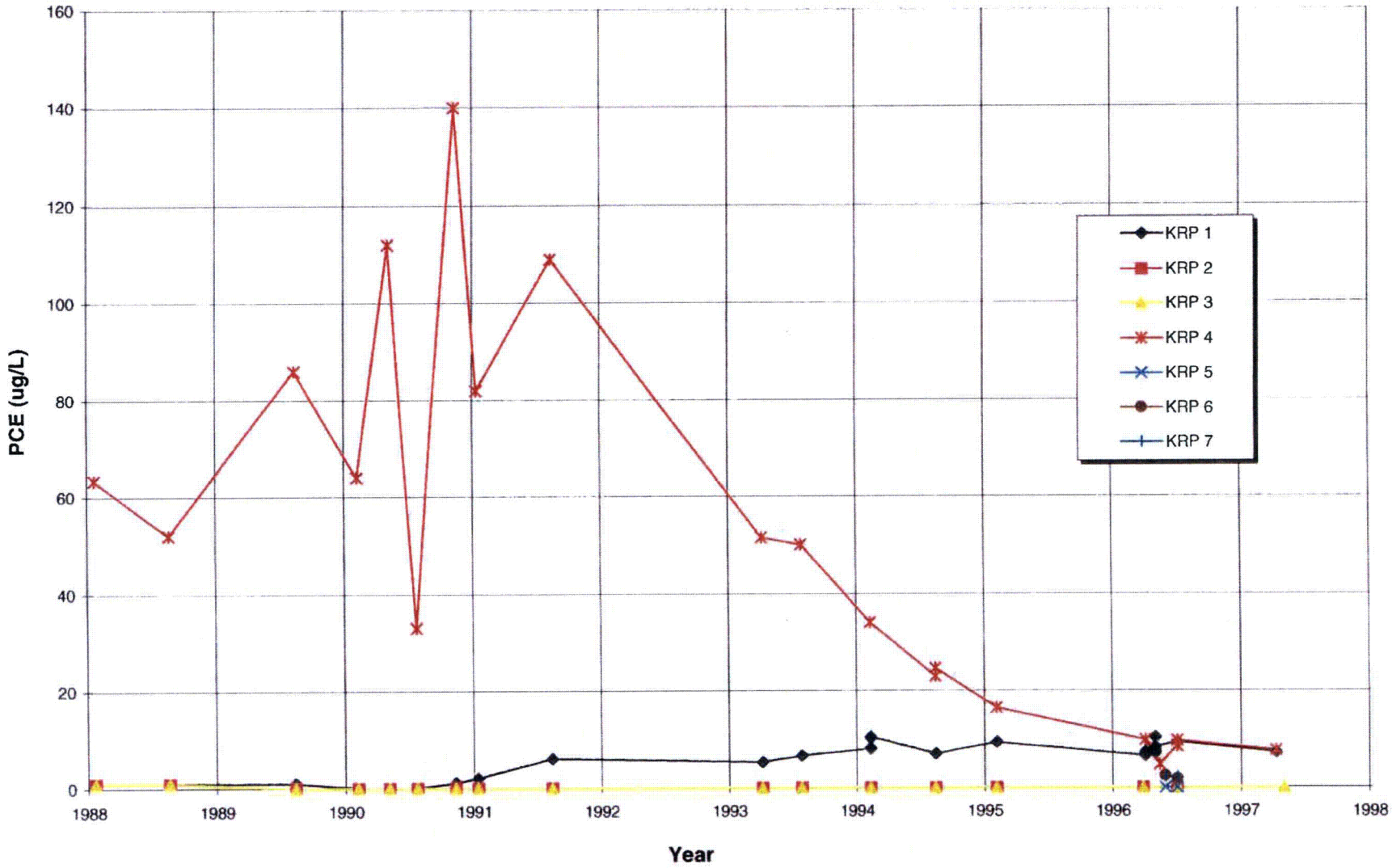

p:\srs\K_area\welldata\krp_pce.xls

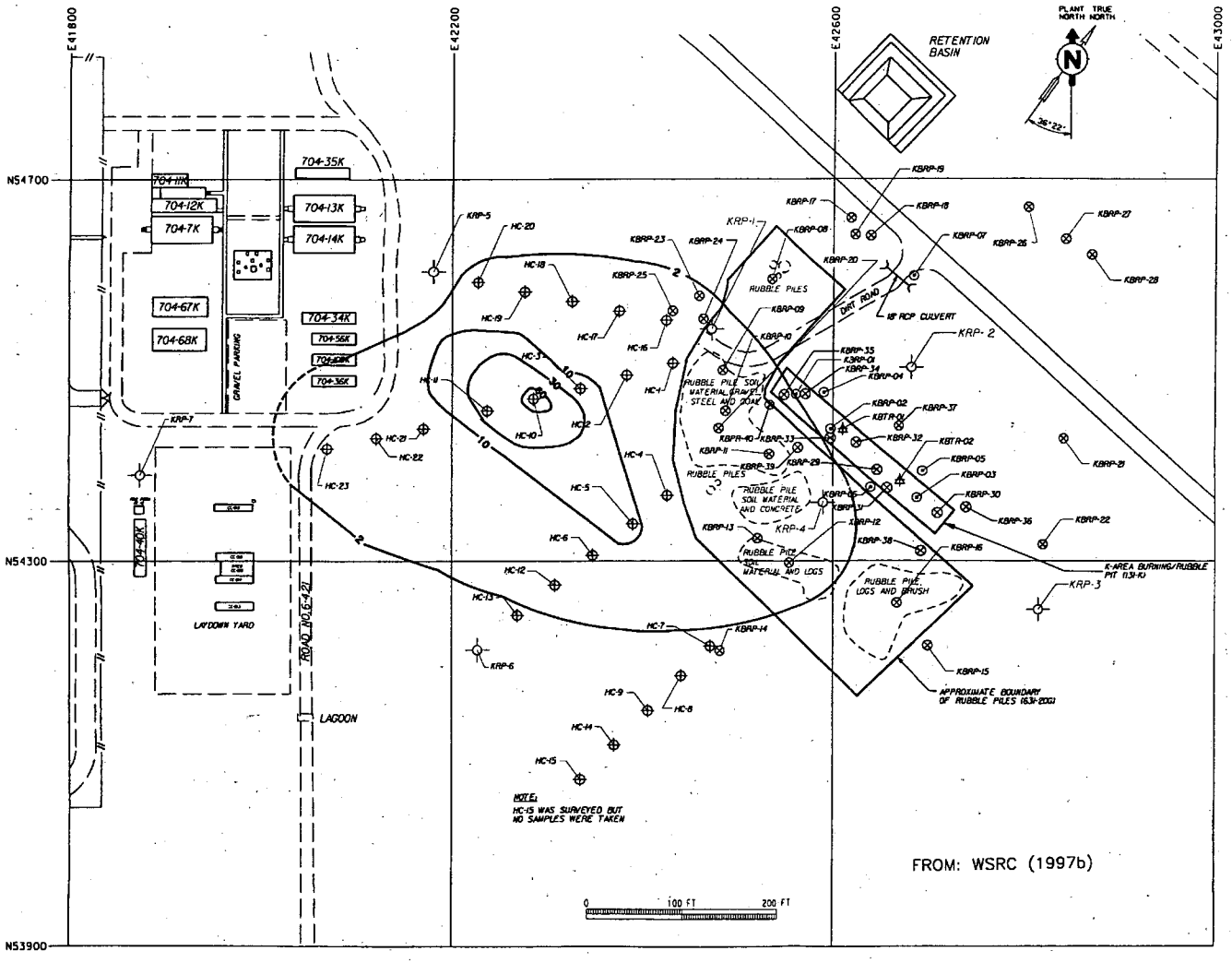

NOTE:
HC-15 WAS SURVEYED BUT NO SAMPLES WERE TAKEN

FROM: WSRC (1997b)

LEGEND

- SOIL BORINGS (KBRP)
- HAND AUGER (KBRP)
- TRENCH (KBTR)
- HYDROCONE (HC)
- INTERPRETATED CONCENTRATION CONTOUR (ug/L)
- ESTIMATED CONCENTRATION CONTOUR (ug/L)

NOTE:
ALL CONCENTRATIONS ARE IN MICROGRAMS PER LITER (ug/L).

CONTOURS WERE DRAWN BASED ON A COMBINATION OF CPT AND MONITORING WELL DATA

TITLE: K-AREA BURNING/RUBBLE PIT AND RUBBLE PILE TCE CONCENTRATION CONTOUR MAP IN THE UPPER ZONE OF UPPER THREE RUNS AQUIFER

LOCATION: Savannah River Site, Aiken, South Carolina

HSI GEOTRANS A TETRA TECH COMPANY

CHECKED:	JJB
DRAFTED:	SDL
FILE:	N/A
DATE:	5-5-98

FIGURE: 3-3

Figure 3-4. Observed TCE concentration versus time at KRBP/KRP monitoring wells.

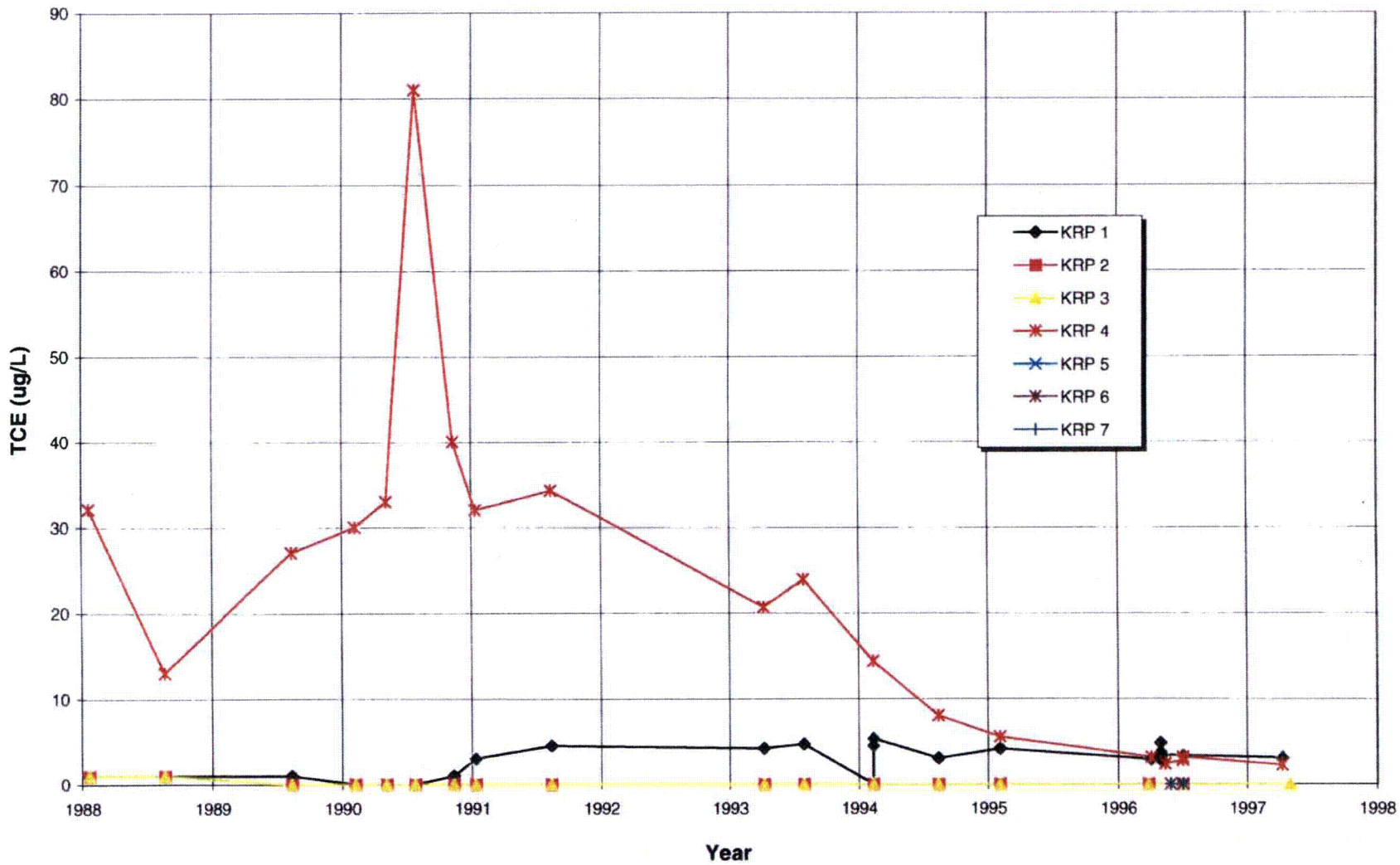

p:\srs\k_area\welldata\krp_tce2.xls

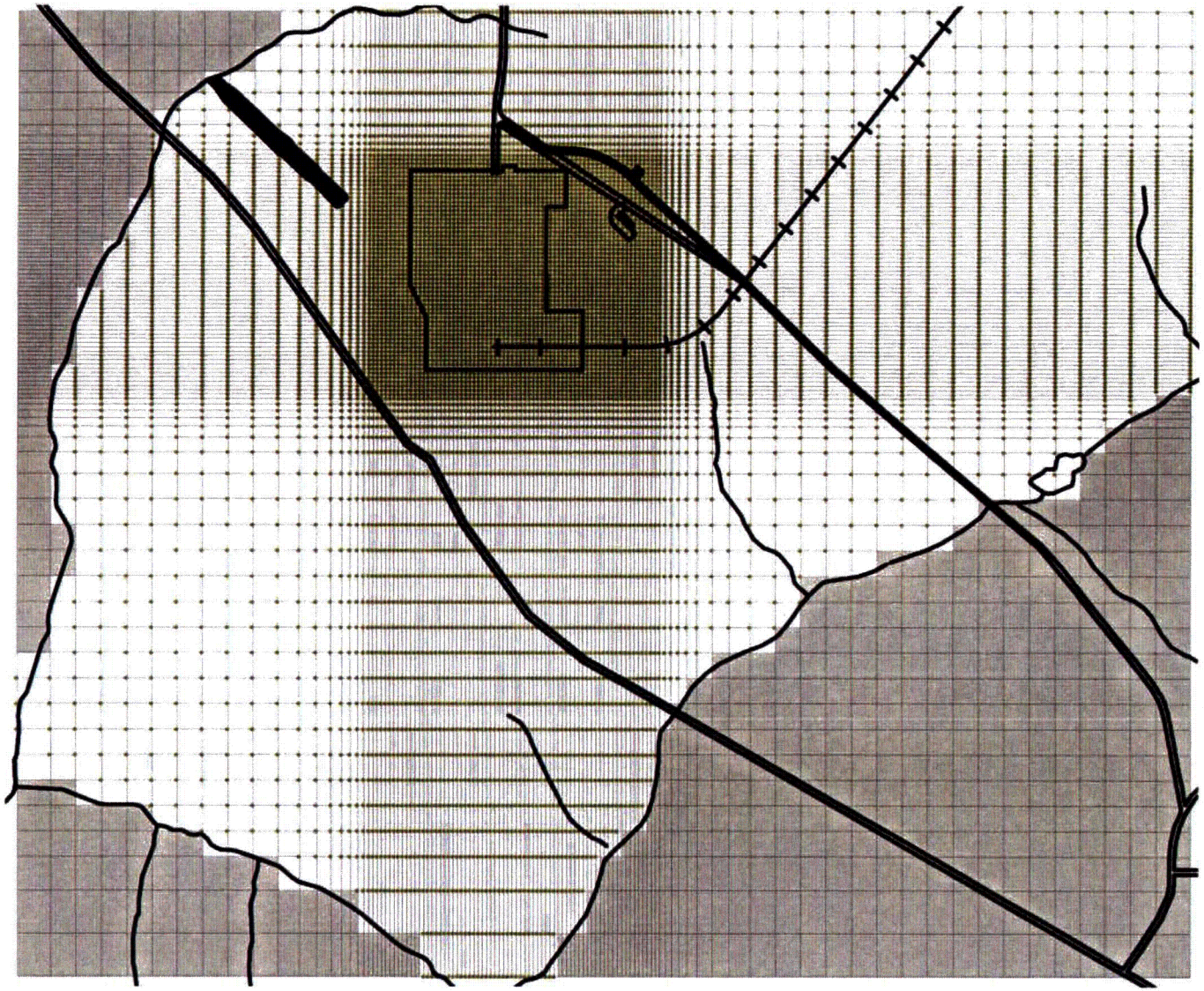

0 2000 4000

Scale in Feet

Legend

· Active Node

Inactive cells

Finite Element Mesh

Savannah River Site, Aiken, South Carolina

HSI GEOTRANS
A TETRA TECH COMPANY

Checked:	DKB
Drafted:	GWC
File:	Mesh.wor
Date:	May 1998

FIGURE: 4-1

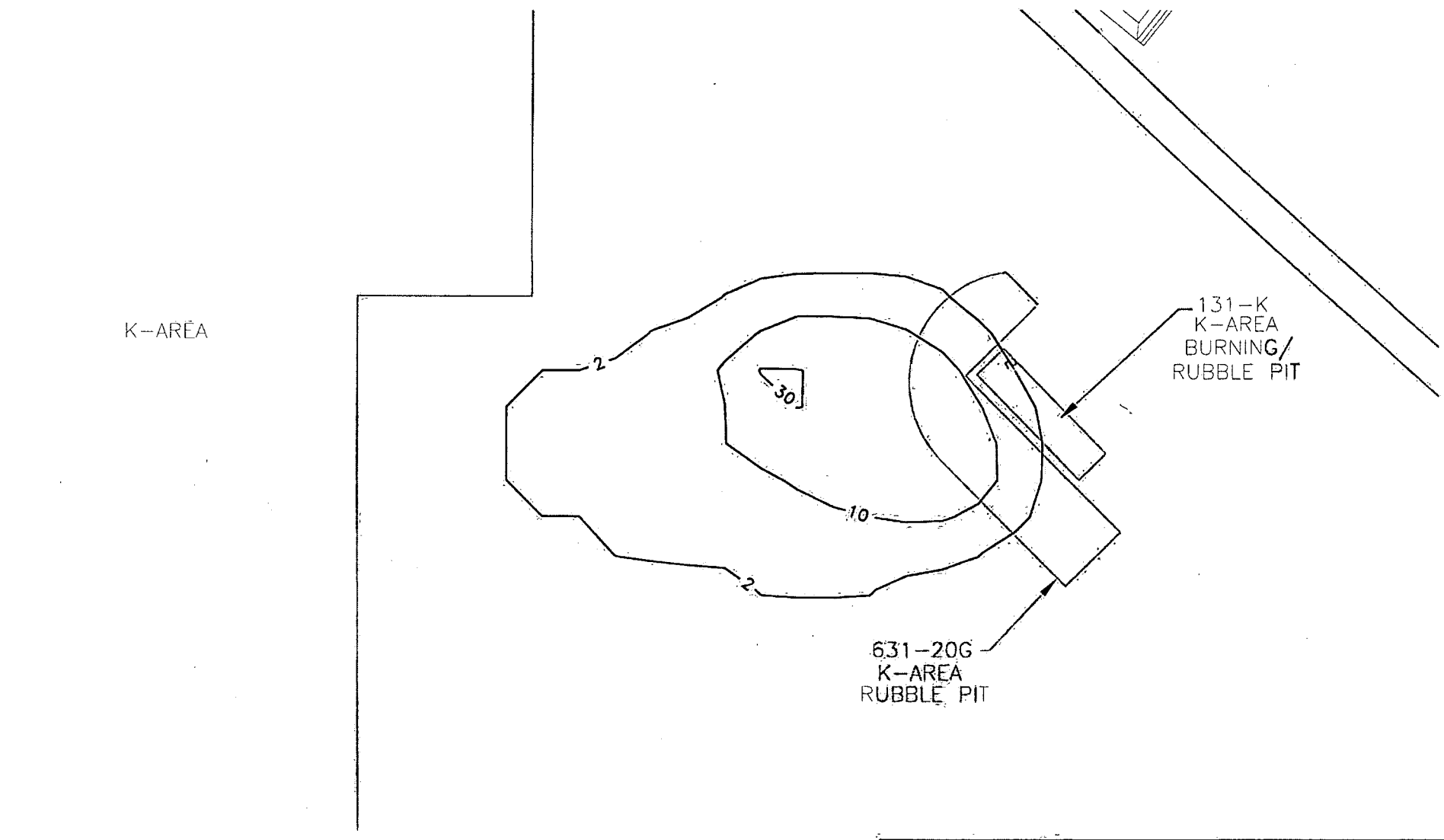

LEGEND

— 2 — CONCENTRATION CONTOUR (ug/L)

N

0 200 400

SCALE IN FEET

TITLE: INITIAL CONDITION VALUES OF PCE CONCENTRATION IN THE MODEL DOMAIN

LOCATION: Savannah River Site, Aiken, South Carolina

HSI GEOTRANS A TETRA TECH COMPANY

CHECKED:	DKB
DRAFTED:	CMP
FILE:	1014012A.DWG
DATE:	5-5-98

FIGURE: 4-2

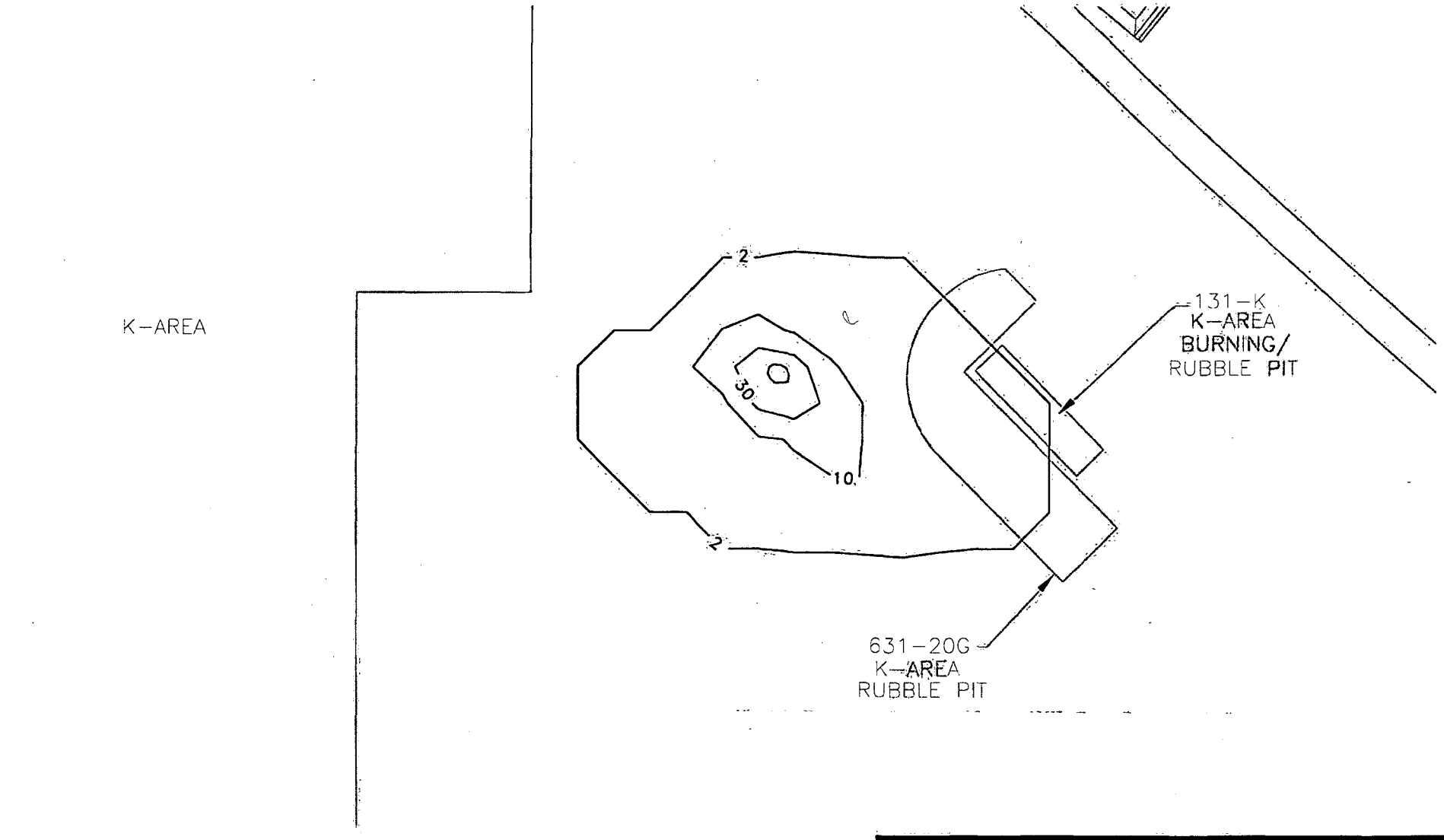

LEGEND

— 2 — CONCENTRATION CONTOUR (ug/L)

0 200 400
SCALE IN FEET

TITLE: INITIAL CONDITION VALUES OF TCE CONCENTRATION IN THE MODEL DOMAIN

LOCATION: Savannah River Site, Aiken, South Carolina

HSI GEOTRANS
A TETRA TECH COMPANY

CHECKED:	DKB
DRAFTED:	CMP
FILE:	1014013A.DWG
DATE:	5-5-98

FIGURE: 4-3

0 2000 4000

Scale in Feet

Legend

- Head-Dependent Flux (River) Node

Inactive Cells

Flow Boundary Conditions for the Upper Three Runs Aquifer
(Model layers 8,9 and 10)

Savannah River Site, Aiken, South Carolina

HSI GEOTRANS
A TETRA TECH COMPANY

Checked:	DKB
Drafted:	GWC
File:	RivNode.wor
Date:	May 1998

FIGURE: 4-4

0 2000 4000

Scale in Feet

Legend

- Fixed Head Node
- Inactive Cells

Flow Boundary Conditions for the Gordon Aquifer
(Model layers 2 and 3)

Savannah River Site, Aiken, South Carolina

HSI GEOTRANS
A TETRA TECH COMPANY

Checked:	DKB
Drafted:	GWC
File:	FixHead.wor
Date:	May 1998

FIGURE: 4-5

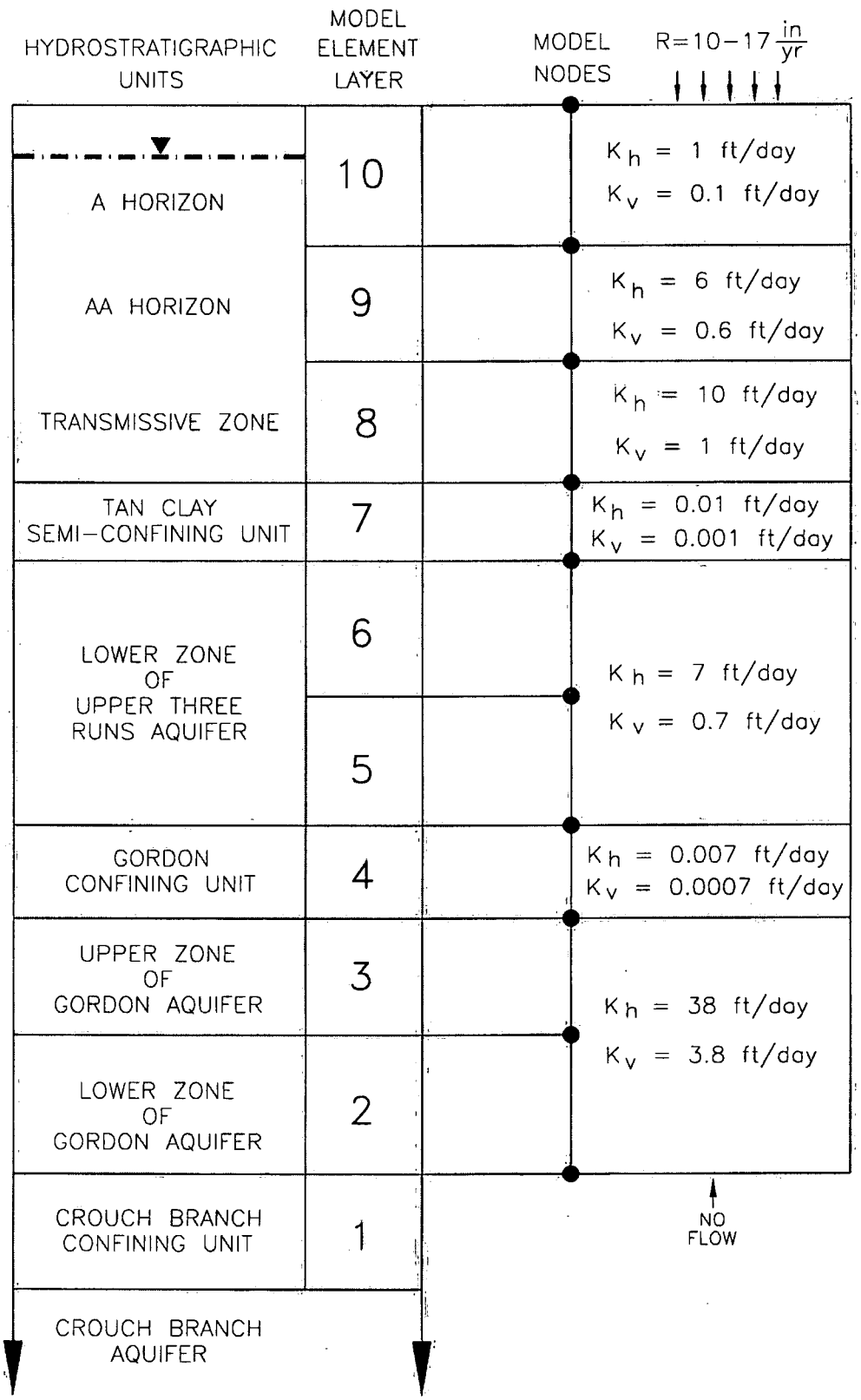

TITLE: GENERALIZED HYDROSTRATIGRAPHIC COLUMN WITH CORRESPONDING MODEL ELEMENT LAYERS, NODES, AND CALIBRATED PARAMETER VALUES

LOCATION: Savannah River Site, Aiken, South Carolina

HSI GEOTRANS
A TETRA TECH COMPANY

CHECKED:	DB	FIGURE: 4−6
DRAFTED:	CP	
FILE:	1014002A.DWG	
DATE:	5−19−98	

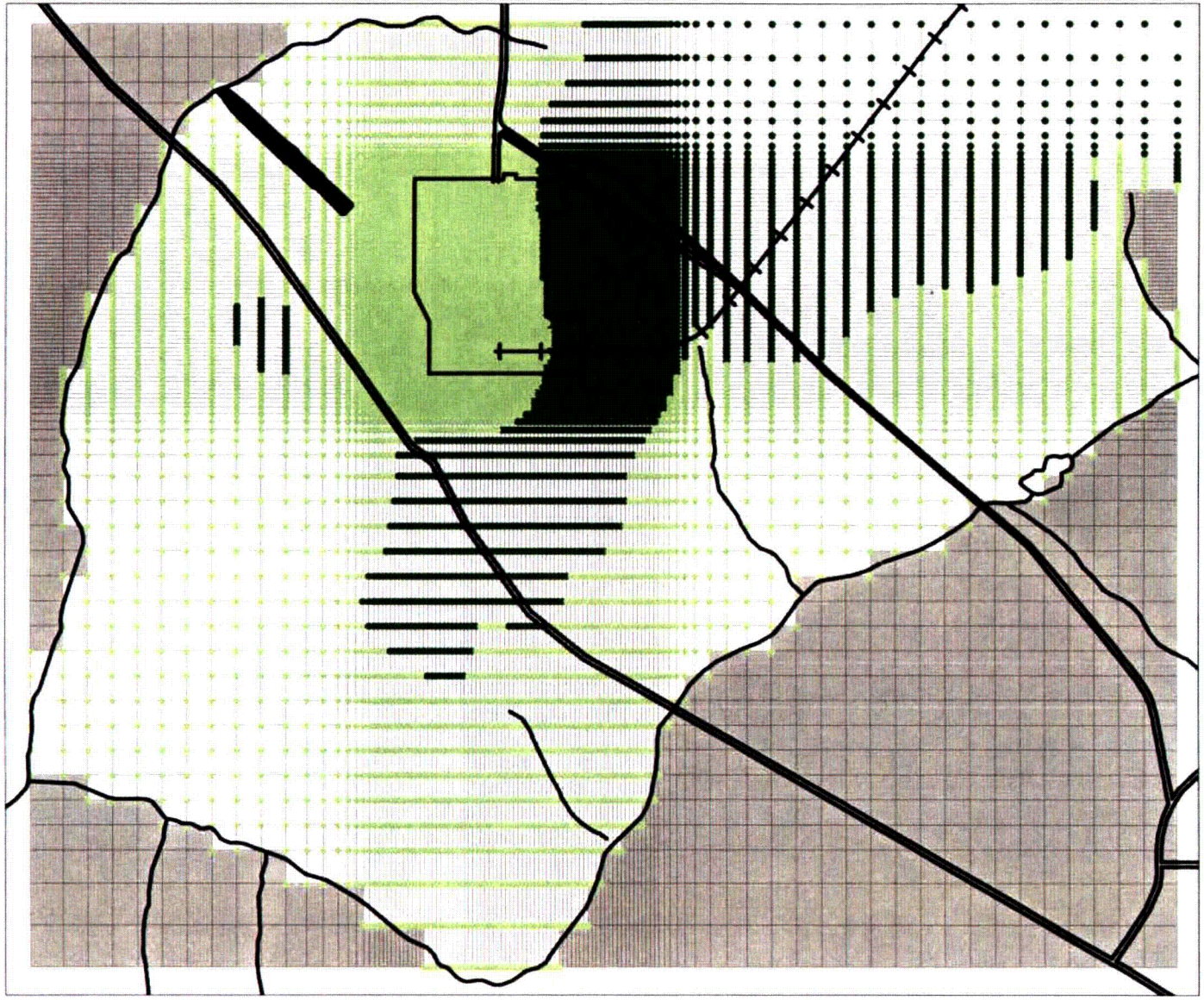

0 2000 4000

Scale in Feet

Legend

10 in./year

17 in./year

Nodal Recharge Rate Zonation

Savannah River Site, Aiken, South Carolina

HSI GEOTRANS
A TETRA TECH COMPANY

Checked:	DKB
Drafted:	GWC
File:	RchNode.wor
Date:	May 1998

FIGURE: 4-7

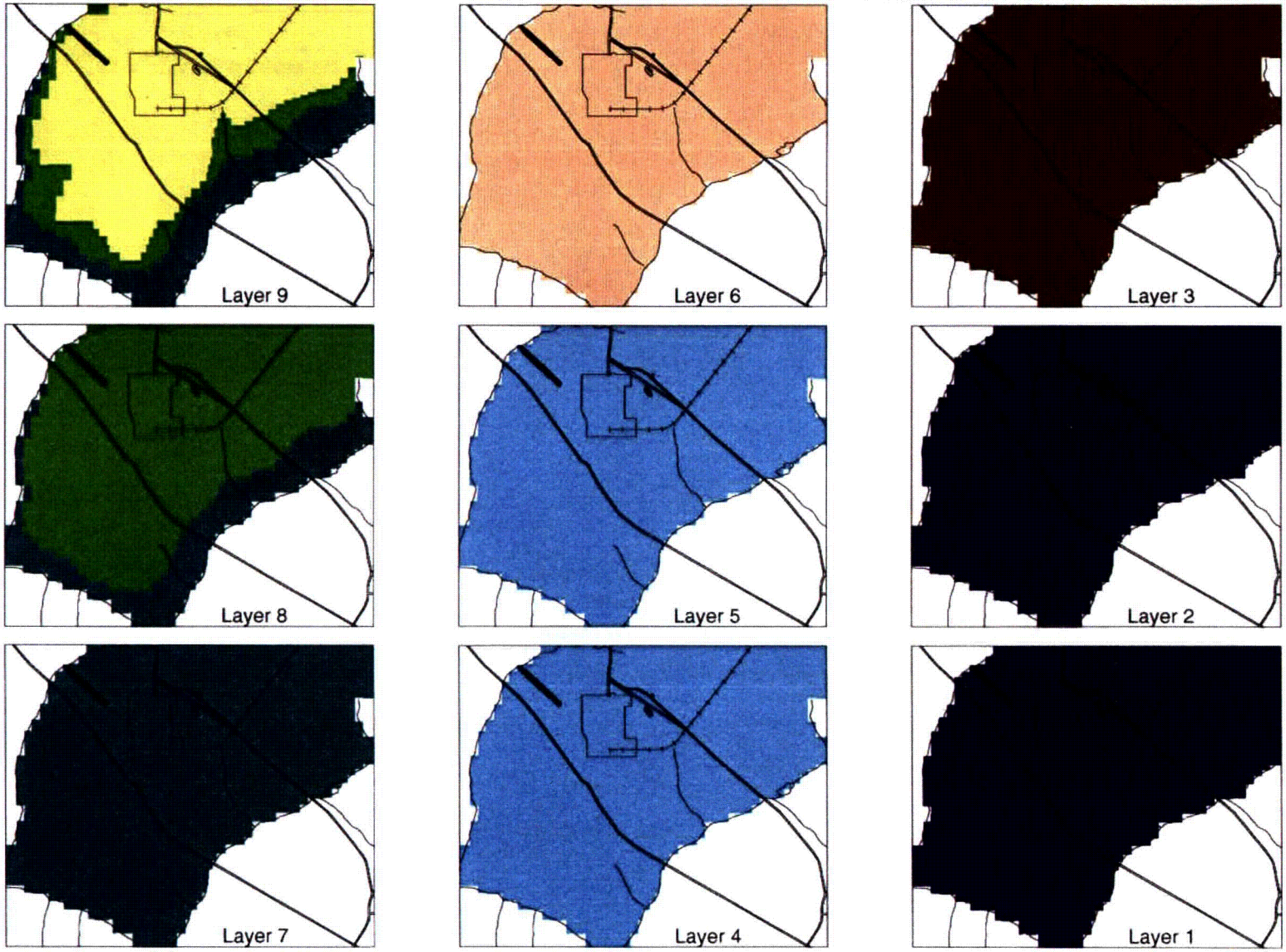

Hydraulic Conductivity

- K_h = 0.01 ft/day, K_v = 0.001 ft/day
- K_h = 0.007 ft/day, K_v = 0.0007 ft/day
- K_h = 1 ft/day, K_v = 0.1 ft/day
- K_h = 6 ft/day, K_v = 0.6 ft/day
- K_h = 7 ft/day, K_v = 0.7 ft/day
- K_h = 10 ft/day, K_v = 1 ft/day
- K_h = 38 ft/day, K_v = 3.8 ft/day

NOTE:

K_h = Horizontal Hydraulic Conductivity

K_v = Vertical Hydraulic Conductivity

0 6000 12,000

Scale in Feet

Hydraulic Conductivity of Elements in the FACT Model

HSI GEOTRANS
A TETRA TECH COMPANY

Checked:	DKB
Drafted:	GWC
File:	Property.wor
Date:	May 1988

FIGURE: 4-8

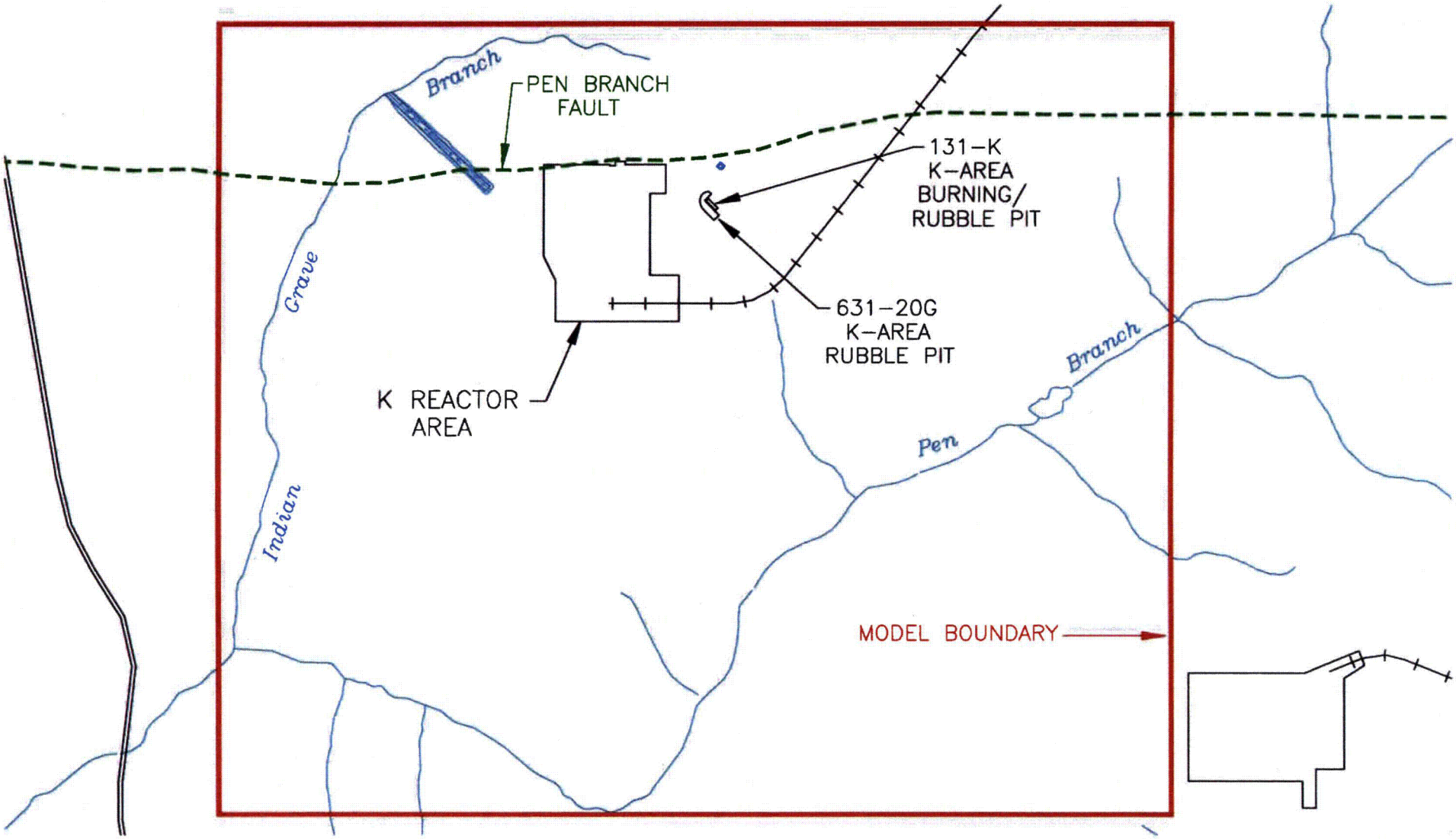

0 2200 4400
SCALE IN FEET

N

TITLE: LOCATION OF PEN BRANCH FAULT IN MODEL DOMAIN

LOCATION: Savannah River Site, Aiken, South Carolina

HSI GEOTRANS
A TETRA TECH COMPANY

CHECKED:	JJB
DRAFTED:	CMP
FILE:	1014009A.DWG
DATE:	5-5-98

FIGURE: 4-9

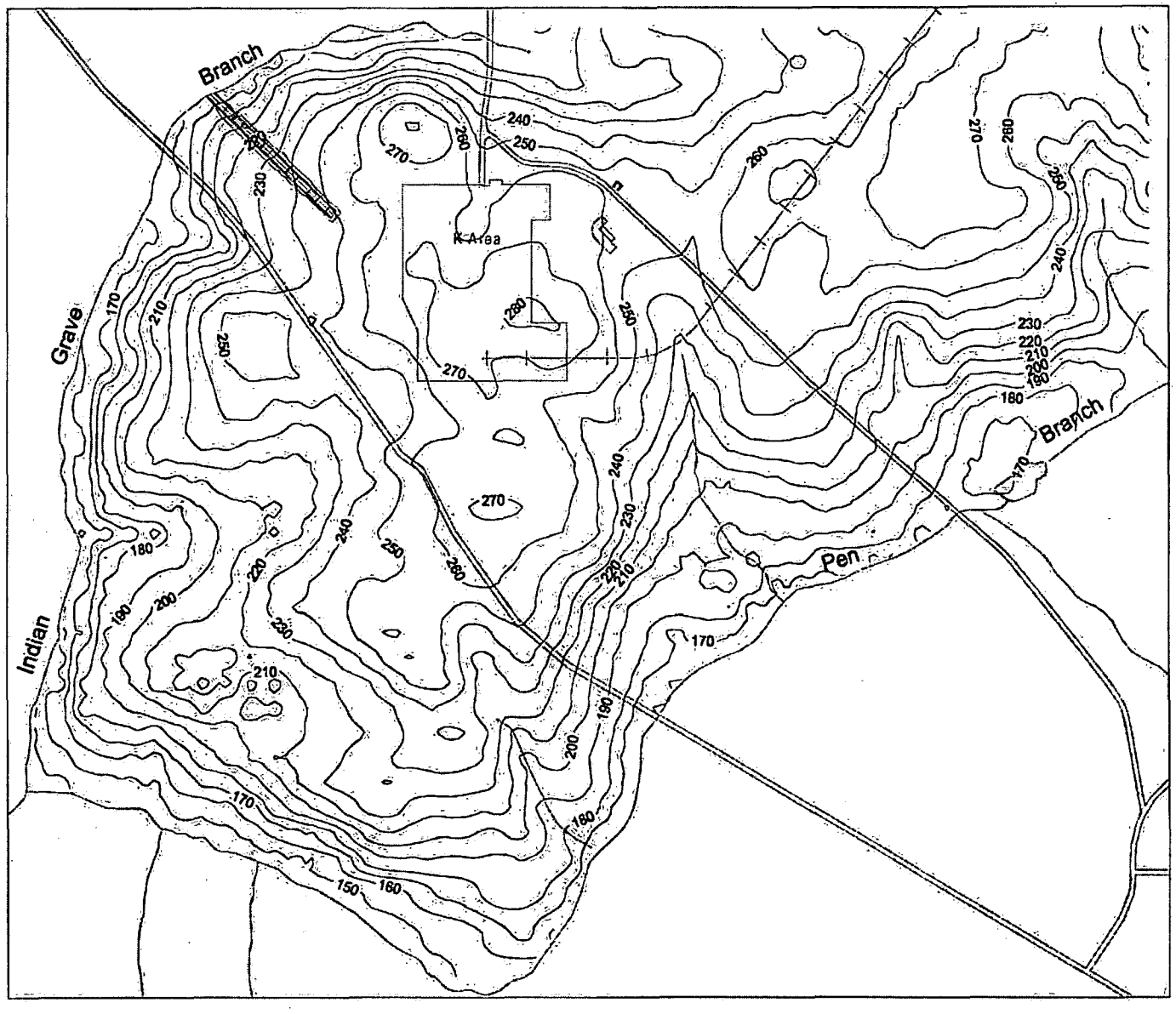

Legend

Layer Elevation (ft. MSL)

0 2000 4000
Feet

Top elevation of model element layer 10 ("A" Horizon)

HSI GEOTRANS
A TETRA TECH COMPANY

CHECKED:	JJB	FIGURE:
DRAFTED:		4-10
FILE:	fig4-10.SRF	
DATE:		

p:/srs/k_area/figures/fig

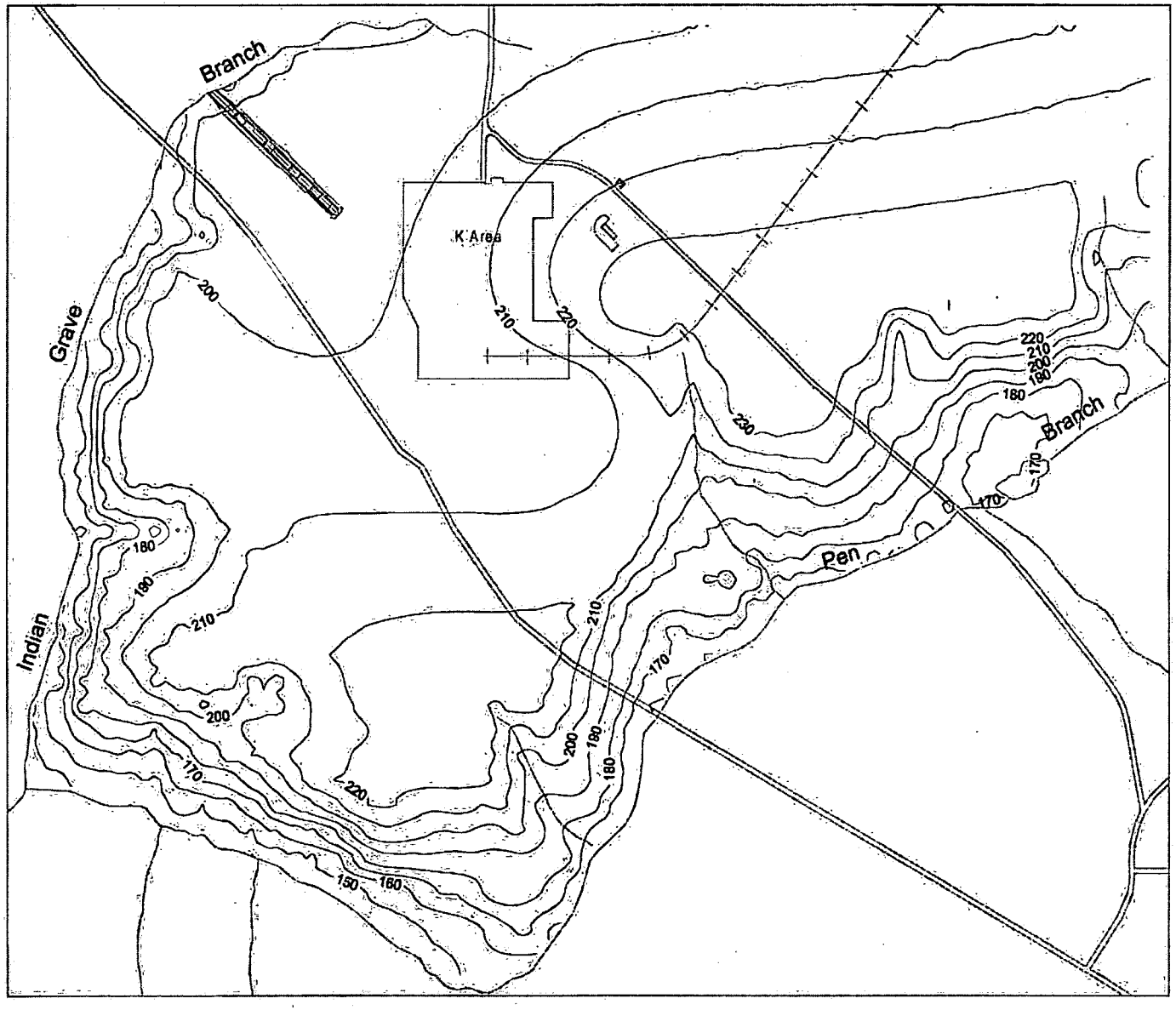

N

Legend

Layer Elevation (ft. MSL)

0 2000 4000
Feet

Top elevation of model element layer 9 ("AA" Horizon)

HSI GEOTRANS
A TETRA TECH COMPANY

CHECKED:	JJB	FIGURE:
DRAFTED:		4-11
FILE:	fig4-11.SRF	
DATE:		

p:\srs\k_area\figures\fig4-11.srf

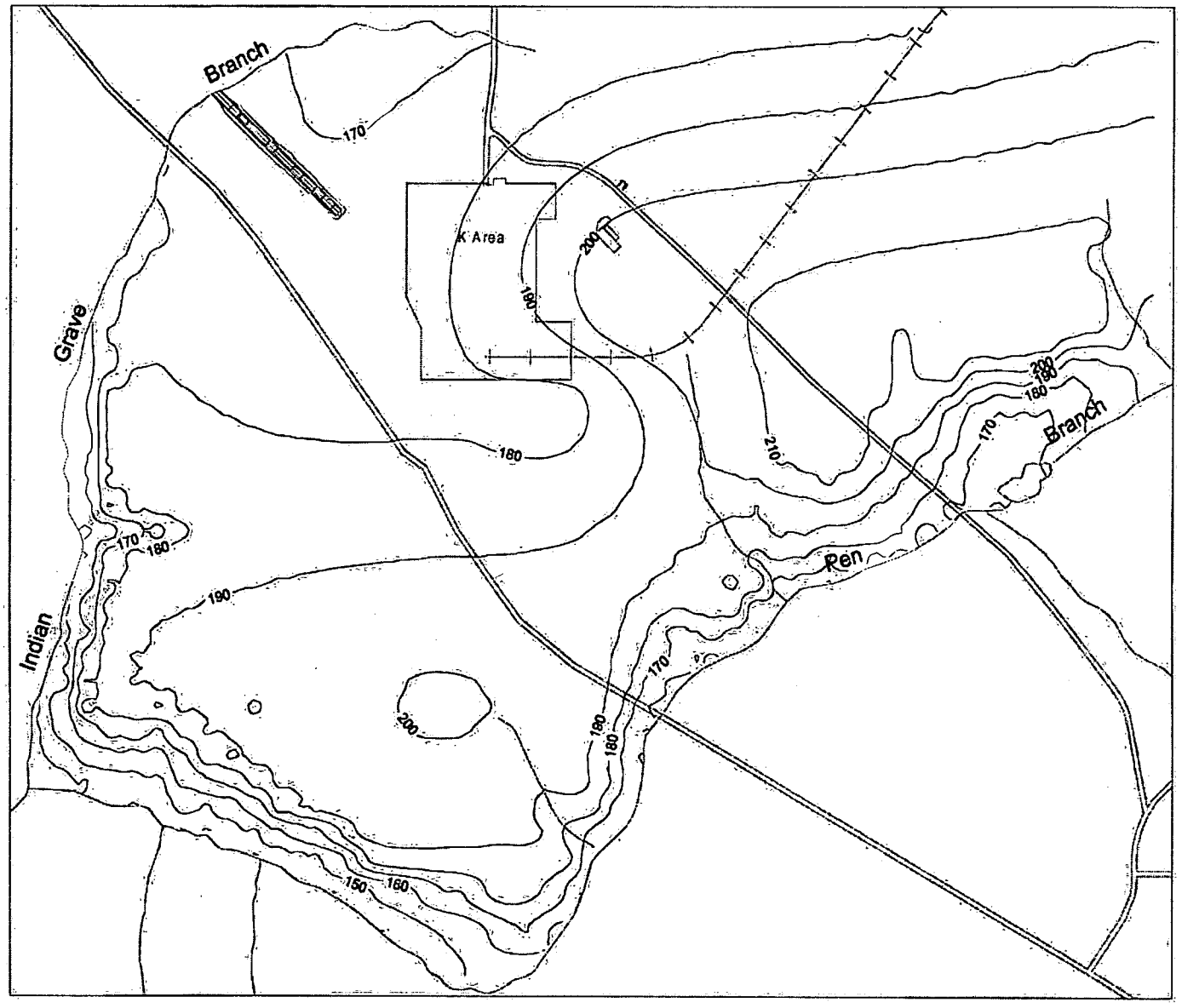

N

Legend

Layer Elevation (ft. MSL)

0 2000 4000
Feet

Top elevation of model element layer 8
(Transmissive Zone)

HSI GEOTRANS
A TETRA TECH COMPANY

CHECKED:	JJB	FIGURE:
DRAFTED:		4-12
FILE:	fig4-12.SRF	
DATE:		

p:/ers/k_area/figures/fig4-

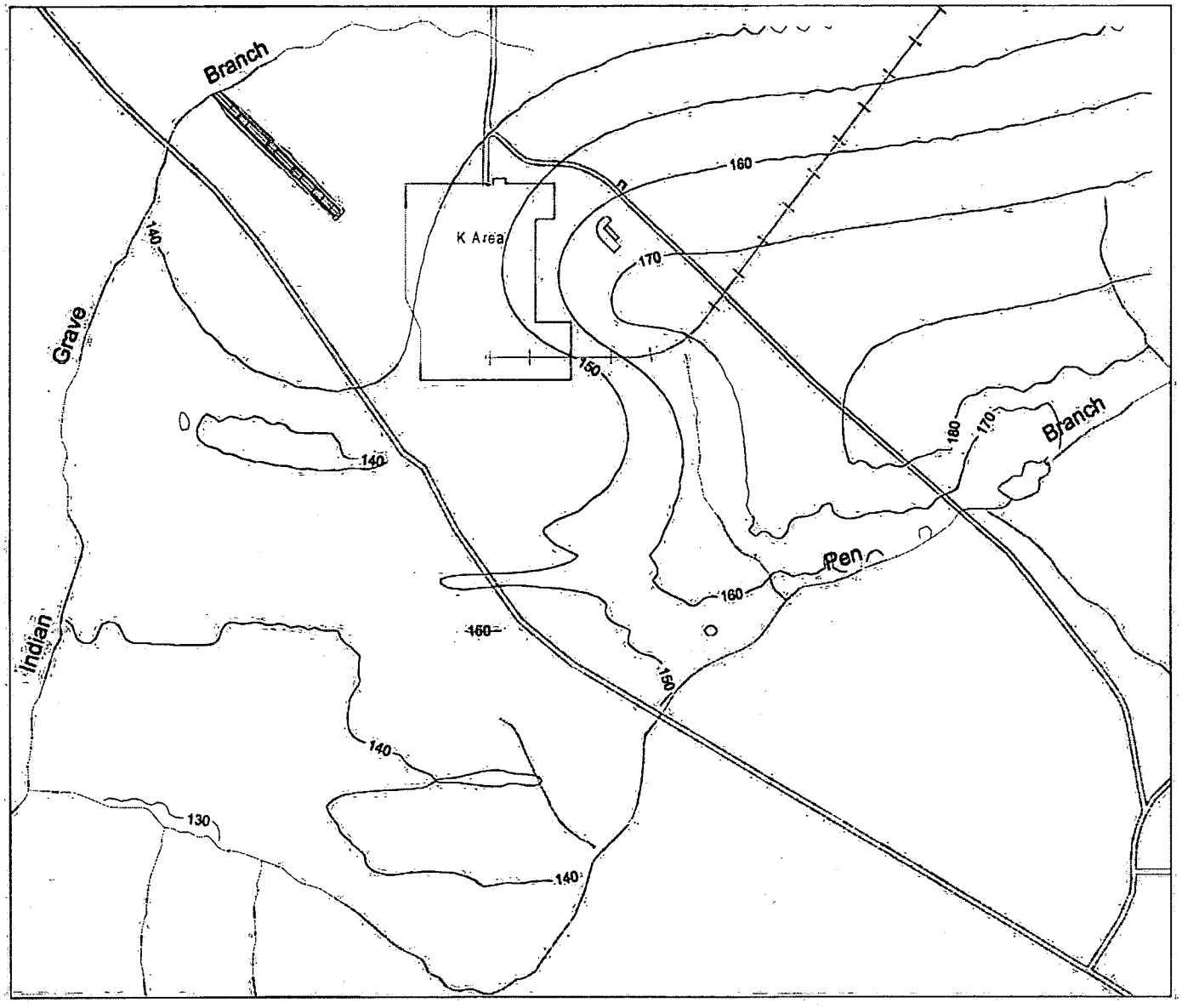

Legend

Layer Elevation (ft. MSL)

0 2000 4000
Feet

Top elevation of model element layer 7
(Tan Clay Confining Unit)

HSI GEOTRANS
A TETRA TECH COMPANY

CHECKED:	JJB	FIGURE:
DRAFTED:		4-13
FILE:	fig4-13.SRF	
DATE:		

p:\srs\k_area\figures\fig4-13.srf

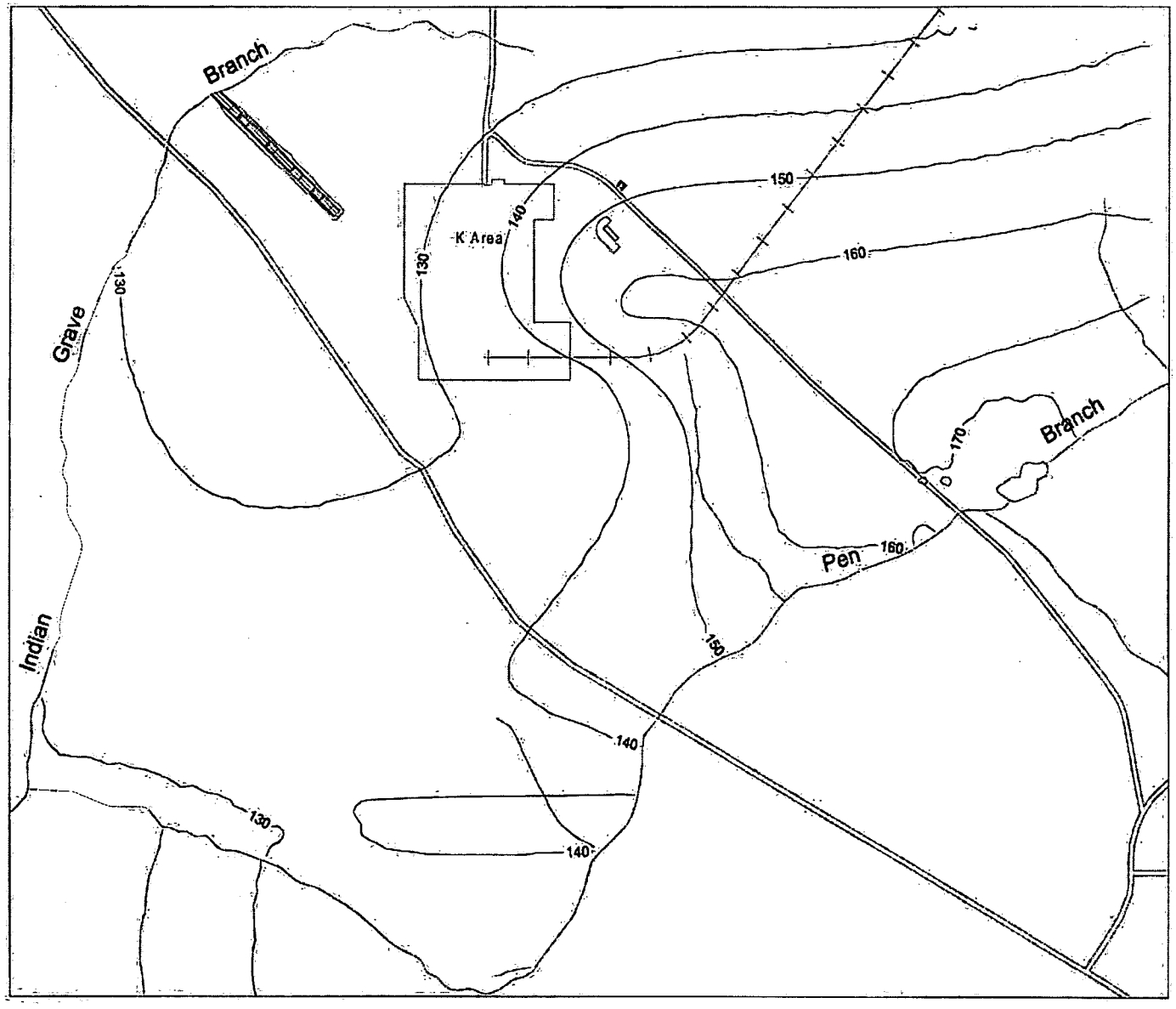

Legend

Layer Elevation (ft. MSL)

0 2000 4000
Feet

Top elevation of model element layer 6
(Lower zone of Upper Three Runs Aquifer)

HSI GEOTRANS
A TETRA TECH COMPANY

CHECKED:	JJB	FIGURE:
DRAFTED:		4-14
FILE:	fig4-14.SRF	
DATE:		

p:/srs/k_area/figures/fig

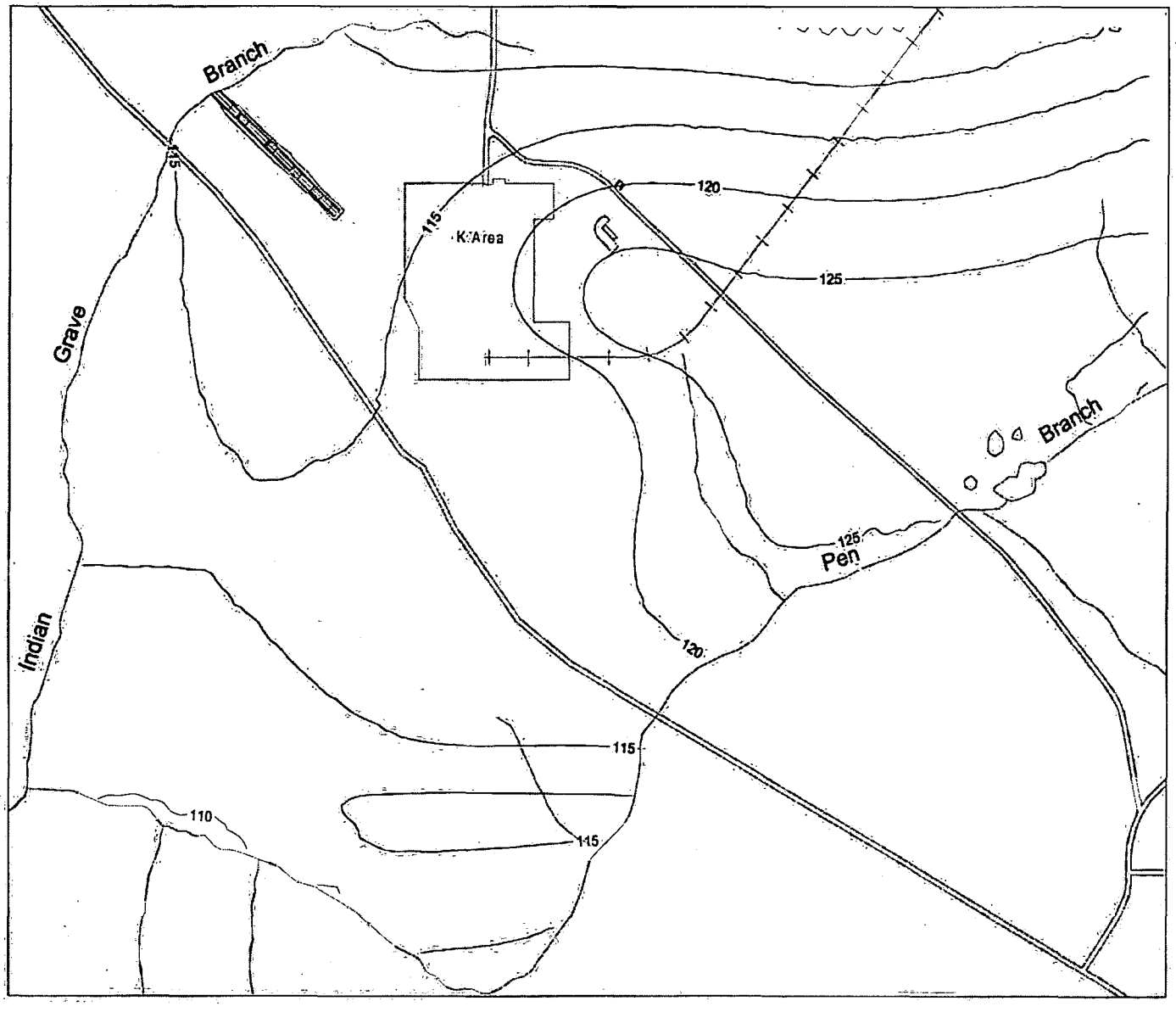

N

Legend

Layer Elevation (ft. MSL)

0 2000 4000
Feet

Top elevation of model element layer 5
(Lower zone of Upper Three Runs Aquifer)

HSI GEOTRANS
A TETRA TECH COMPANY

CHECKED:	JJB	FIGURE:
DRAFTED:		4-15
FILE:	fig4-15.SRF	
DATE:		

p:/srs/k_area/figures/fig4-15.srf

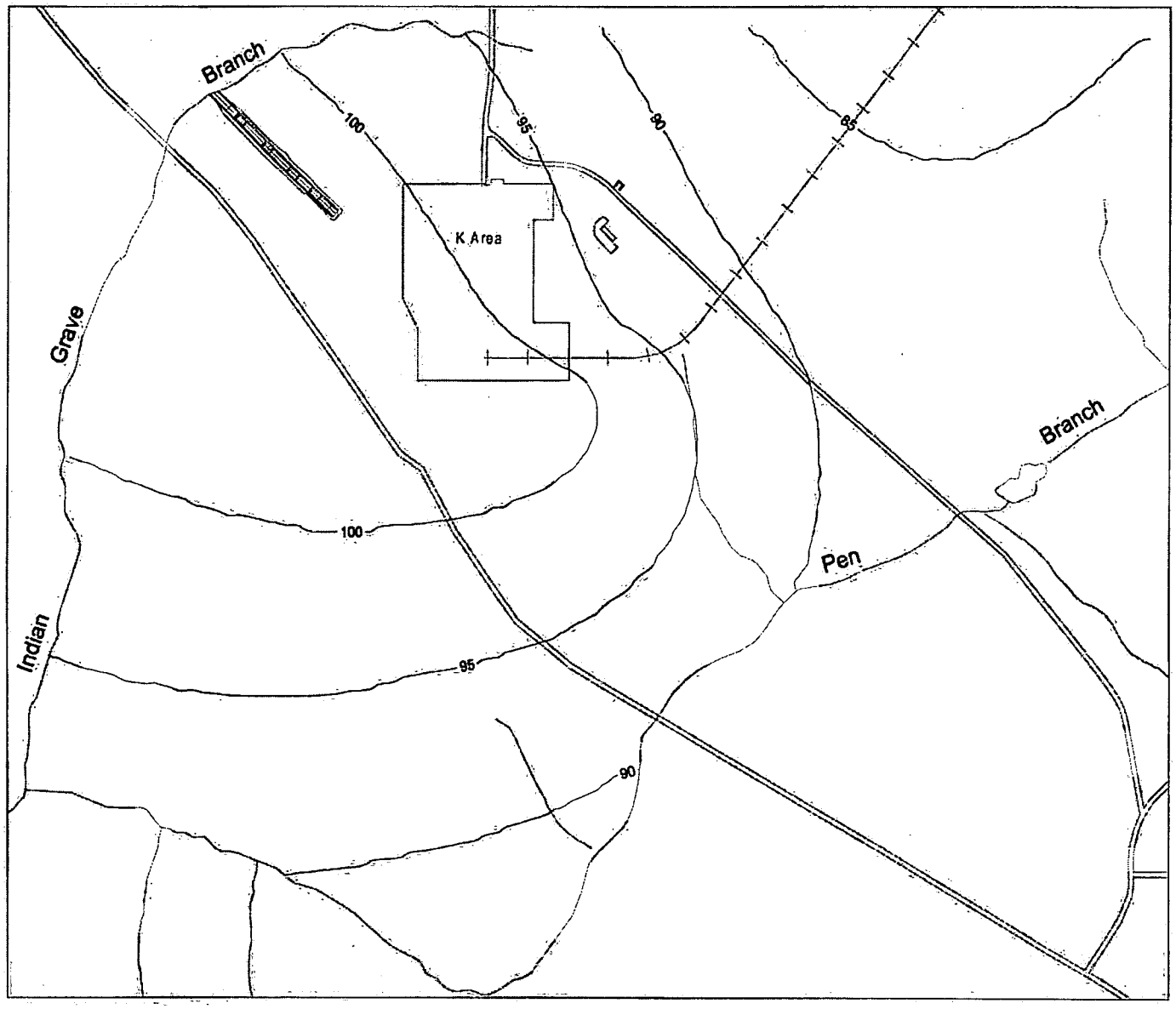

Legend

Layer Elevation (ft. MSL)

0 2000 4000
Feet

Top elevation of model element layer 4
(Gordon Confining Unit)

HSI GEOTRANS
A TETRA TECH COMPANY

CHECKED:	JJB	FIGURE:
DRAFTED:		4-16
FILE:	fig4-16.SRF	
DATE:		

p:/srs/k_area/figures/fig4-

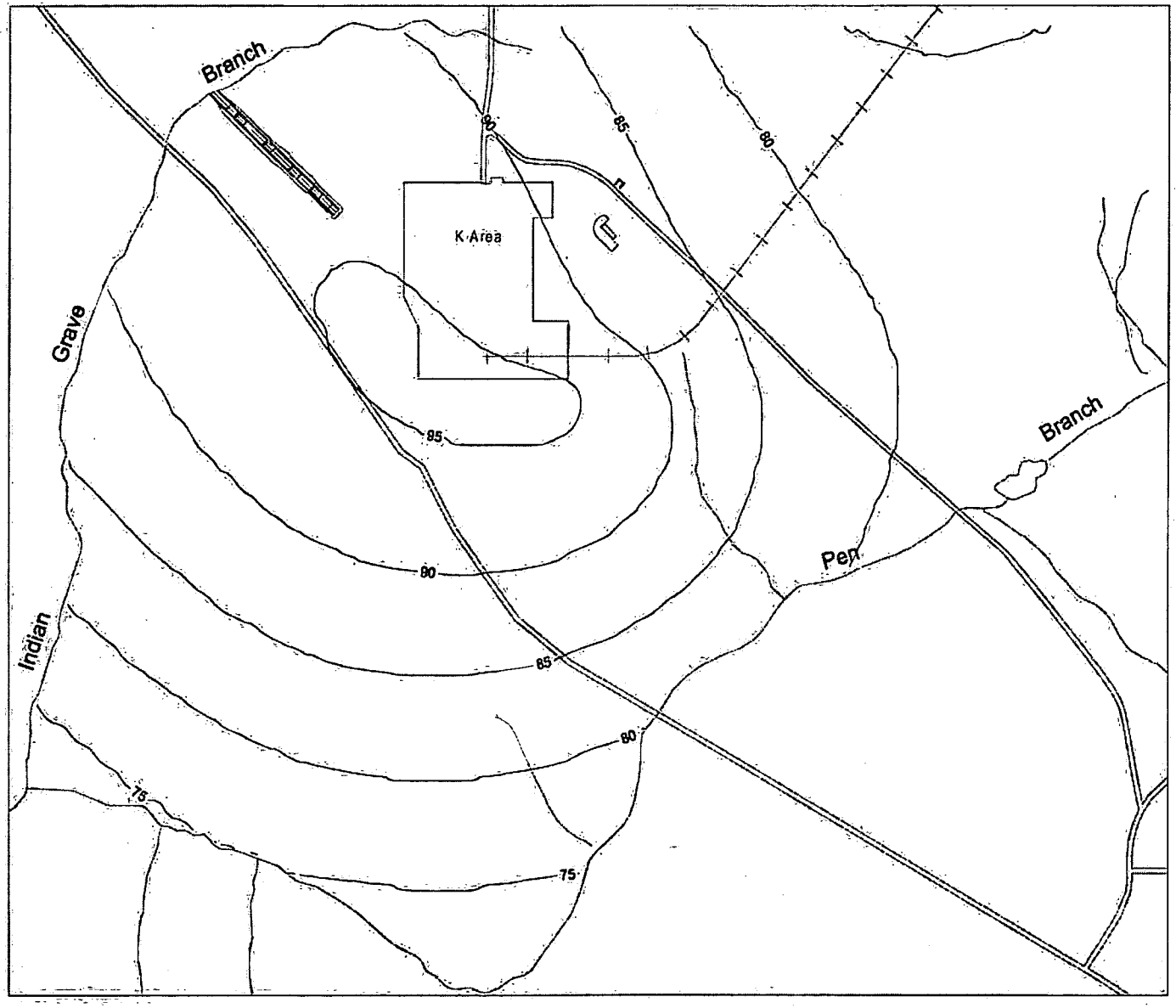

Legend

Layer Elevation (ft. MSL)

0 2000 4000
Feet

Top elevation of model element layer 3
(Upper zone of Gordon Aquifer)

HSI GEOTRANS
A TETRA TECH COMPANY

CHECKED:	JJB	FIGURE:
DRAFTED:		4-17
FILE:	fig4-17.SRF	
DATE:		

p:\srs\k_area\figures\fig4-17.srf

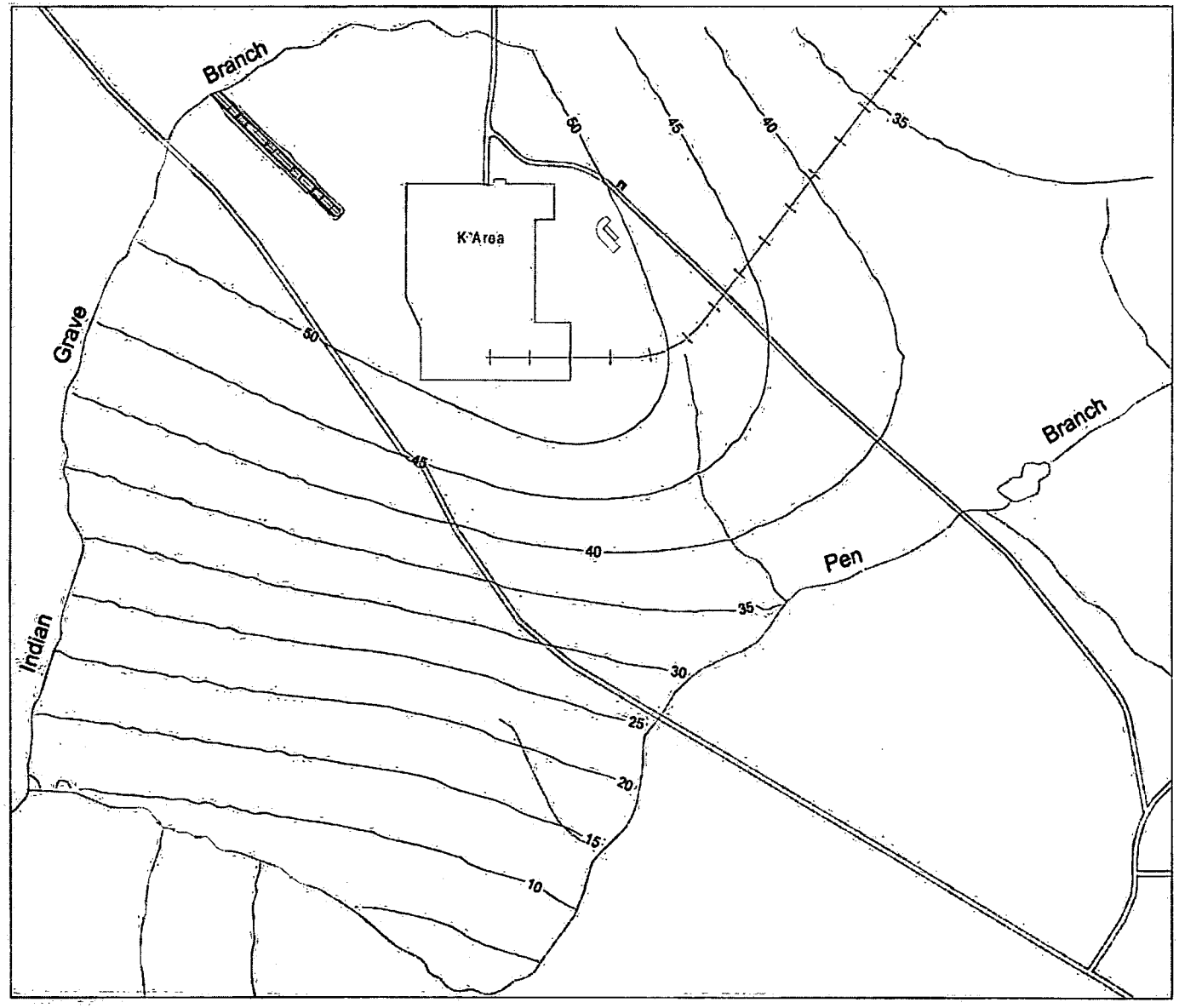

Legend

Layer Elevation (ft. MSL)

0 2000 4000
Feet

Top elevation of model element layer 2
(Lower zone of Gordon Aquifer)

HSI GEOTRANS
A TETRA TECH COMPANY

CHECKED:	JJB	FIGURE:
DRAFTED:		4-18
FILE:	fig4-18.SRF	
DATE:		

p:/srs/k_area/figures/fig4

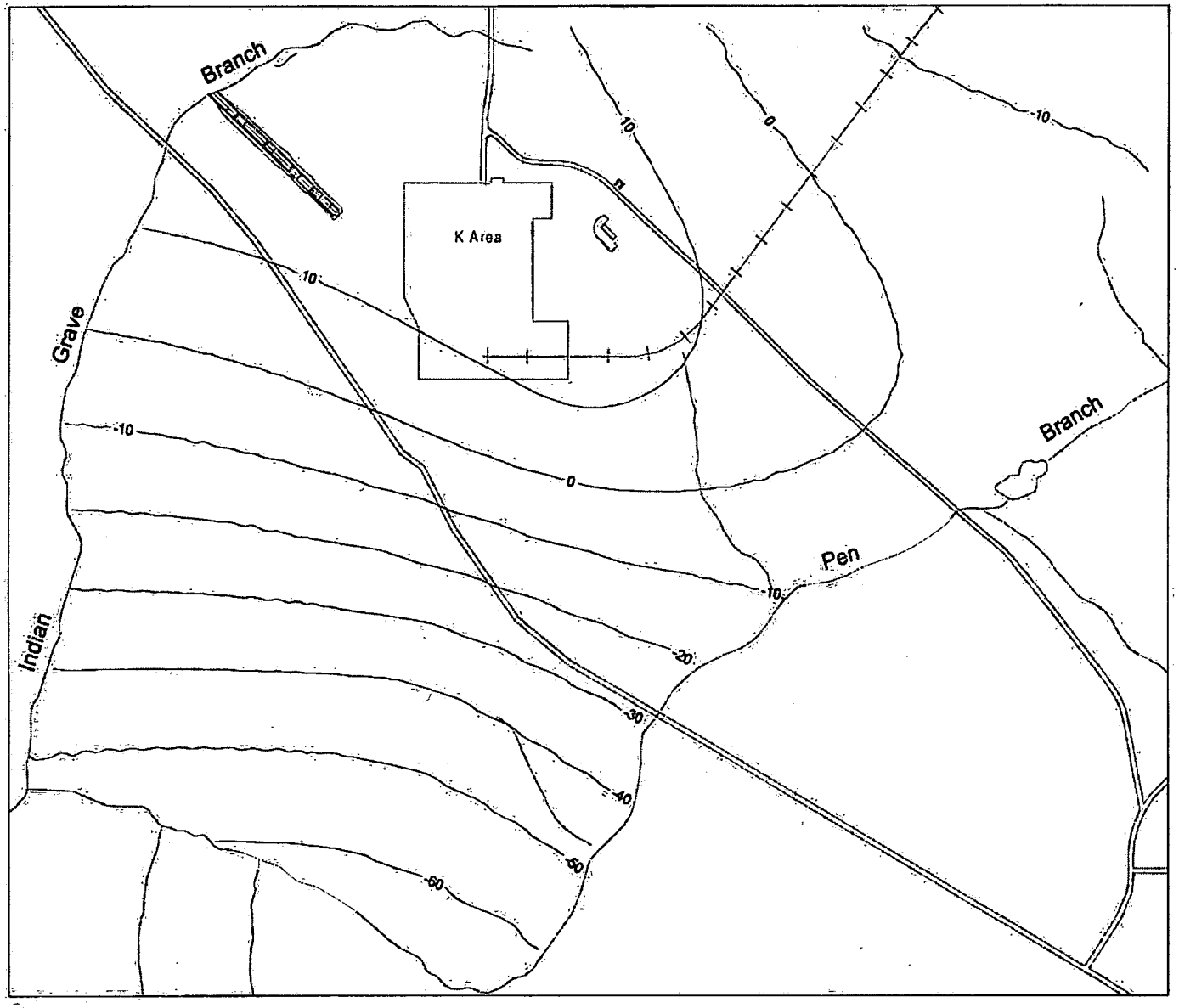

N

Legend

Layer Elevation (ft. MSL)

0 2000 4000
Feet

Top elevation of model element layer 1
(Basal Confining Unit)

HSI GEOTRANS
A PETROTECH COMPANY

CHECKED:	JJB	FIGURE:
DRAFTED:		4-19
FILE:	fig4-19.SRF	
DATE:		

p:\srs\k_area\figures\fig4-19.srf

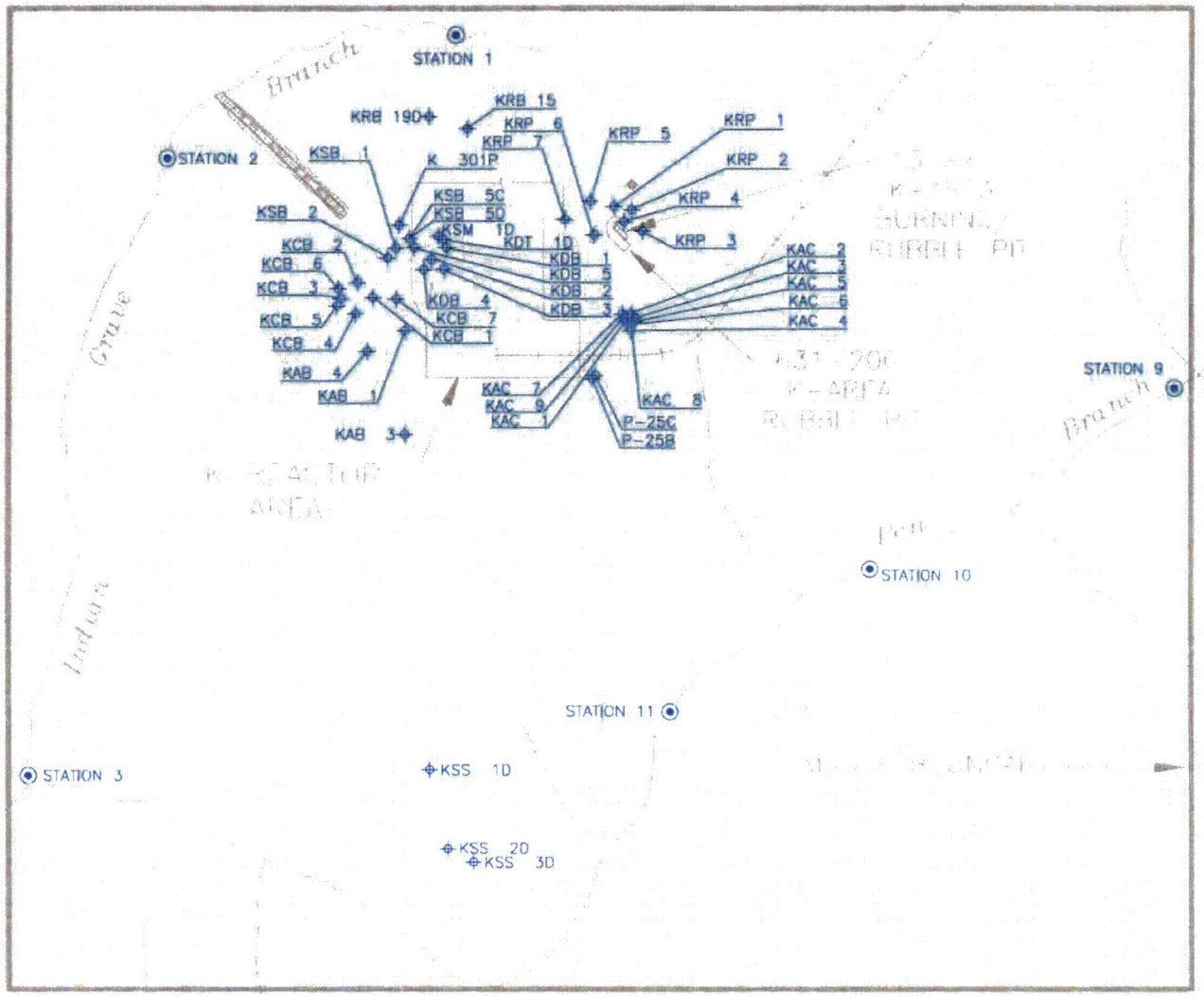

LEGEND

- MONITORING WELL CALIBRATION TARGET
- STREAM GAUGE CALIBRATION TARGET AND VALUE (CFS)

0 2200 4400

SCALE IN FEET

N

TITLE: MAP OF GROUNDWATER FLOW MODEL CALIBRATION TARGETS

LOCATION: Savannah River Site, Aiken, South Carolina

HSI GEOTRANS
A TETRA TECH COMPANY

CHECKED:	JJB
DRAFTED:	CMP
FILE:	1014010A.DWG
DATE:	6-1-98

FIGURE: 5-1

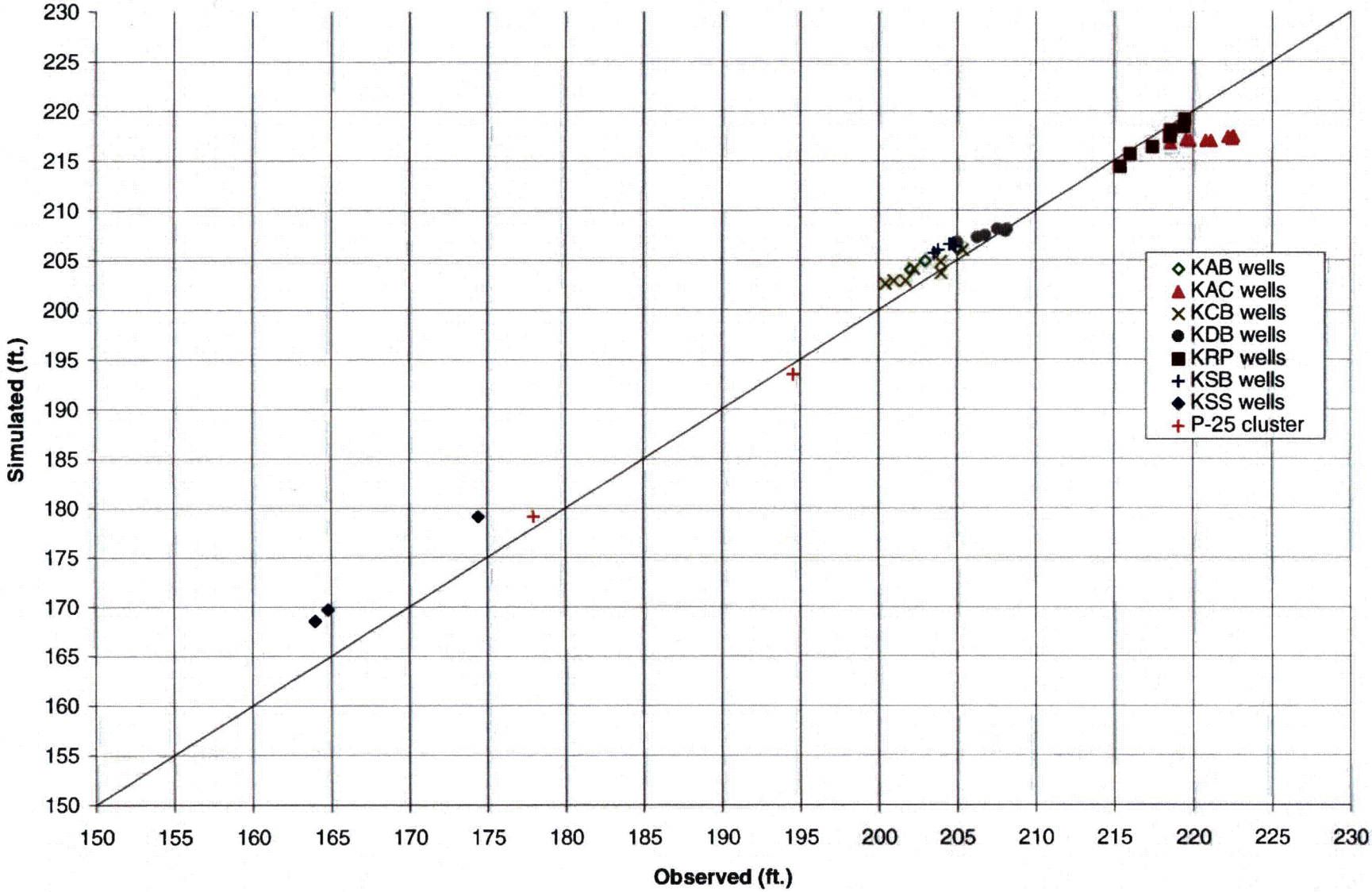

Figure 5-2. Plot of simulated versus observed hydraulic heads at target locations.

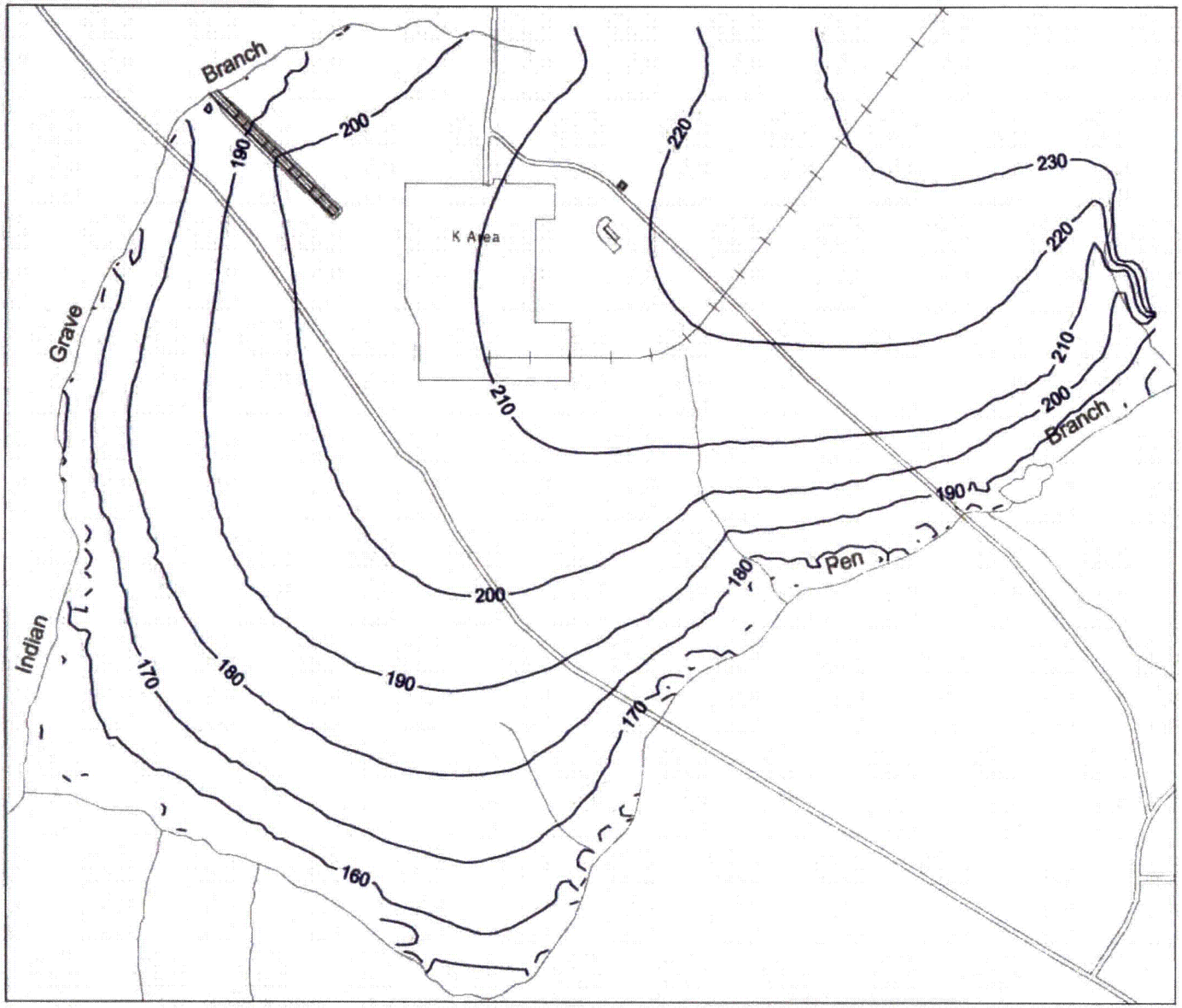

N

Legend

Simulated Water Level Elevation (ft. MSL)

0 2000 4000
Feet

Model simulated water table surface of the Upper Three Runs Aquifer

HSI GEOTRANS
A TETRA TECH COMPANY

CHECKED:	JJB	FIGURE:
DRAFTED:		5-3
FILE:	fig5-3.SRF	
DATE:	4/29/98	

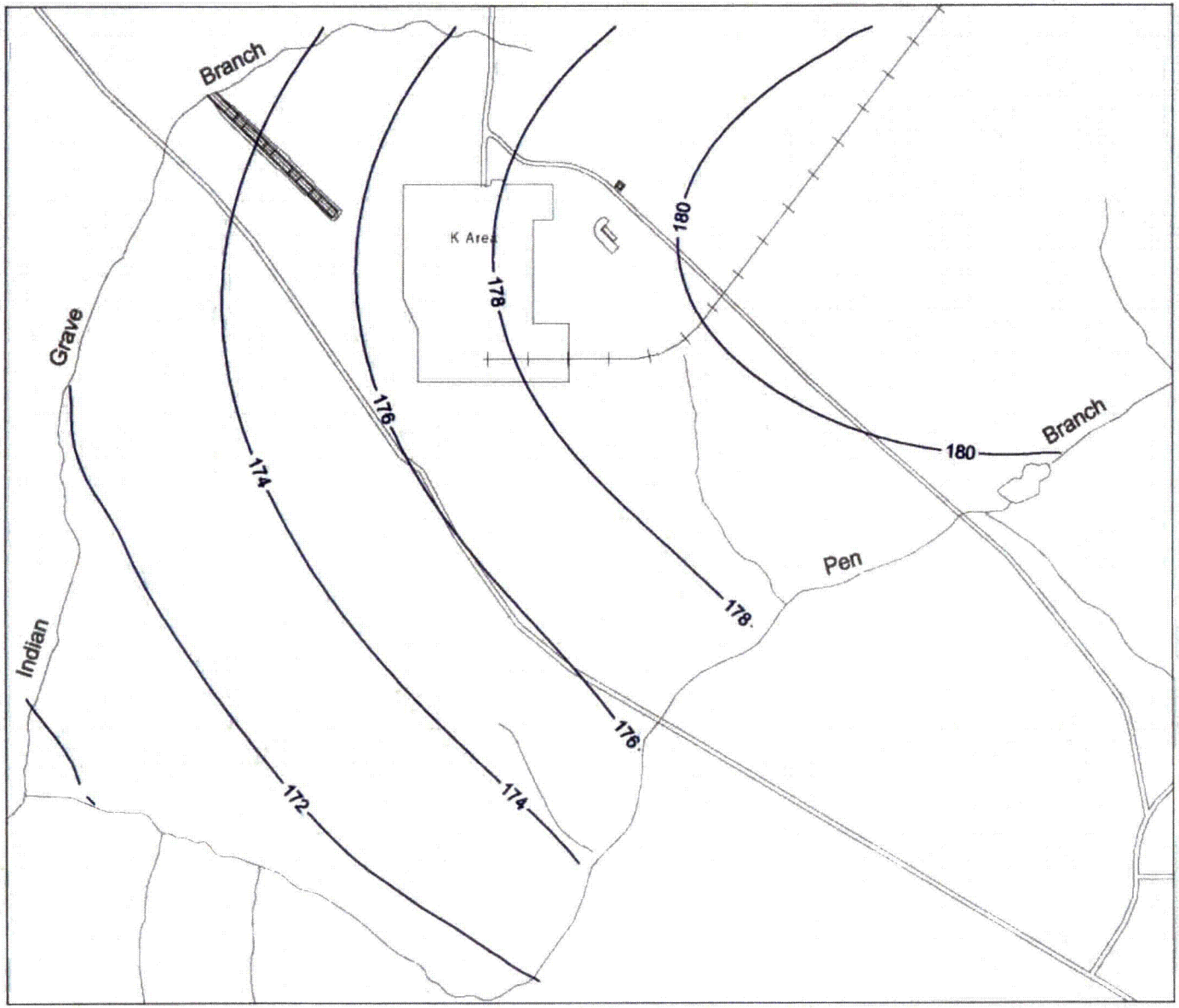

Legend

Simulated Water Level Elevation (ft. MSL)

0 2000 4000
Feet

Model simulated hydraulic heads in the upper zone of the Gordon Aquifer

HSI GEOTRANS
A TETRA TECH COMPANY

CHECKED:	JJB
DRAFTED:	
FILE:	fig5-4.SRF
DATE:	4/29/98

FIGURE: 5-4

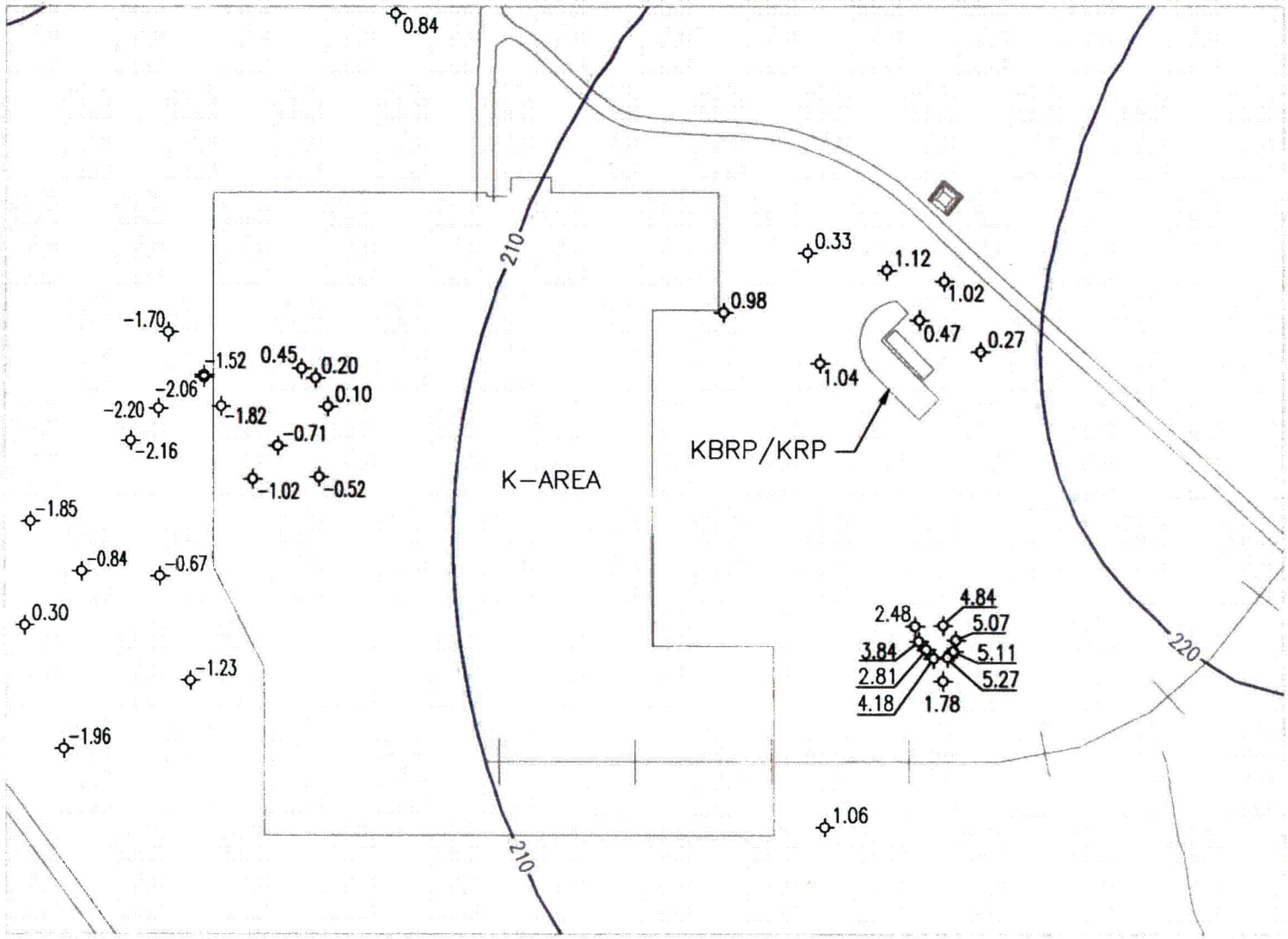

LEGEND

Simulated Water Level Elevation (ft. MSL)

0.58 Residual (Observed – Predicted water level)

0 600 1200

SCALE IN FEET

TITLE: Model simulated water table surface and residuals for the Upper Three Runs Aquifer at the K-Area

LOCATION: Savannah River Site, Aiken, South Carolina

HSI GEOTRANS A TETRA TECH COMPANY

CHECKED:	JJB	FIGURE:
DRAFTED:	CMP	5-5
FILE:	1014015A.DWG	
DATE:	5-21-98	

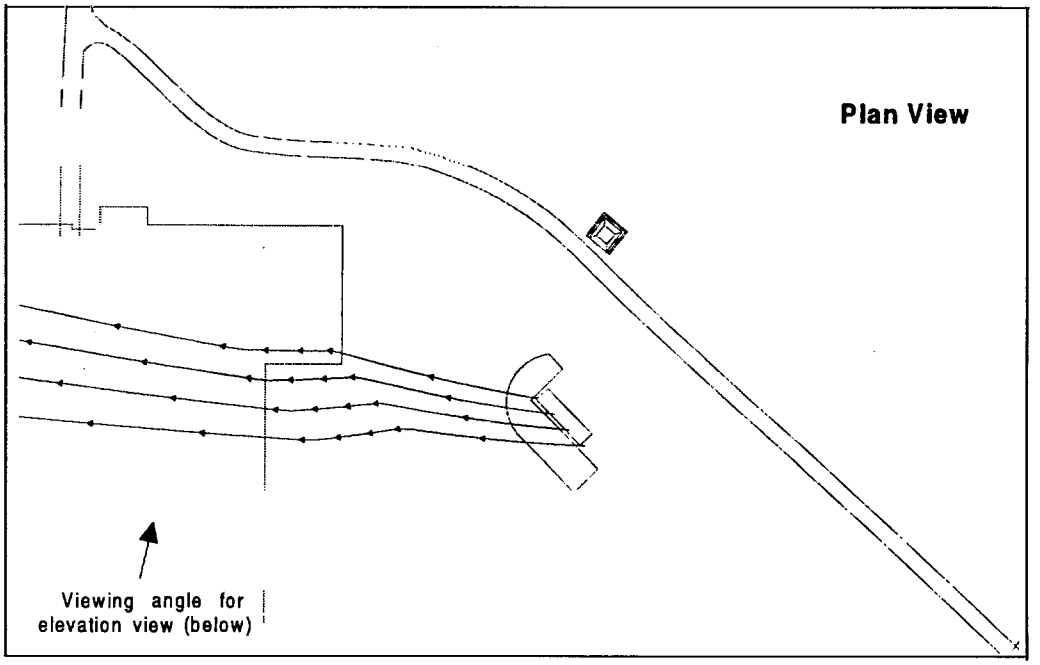

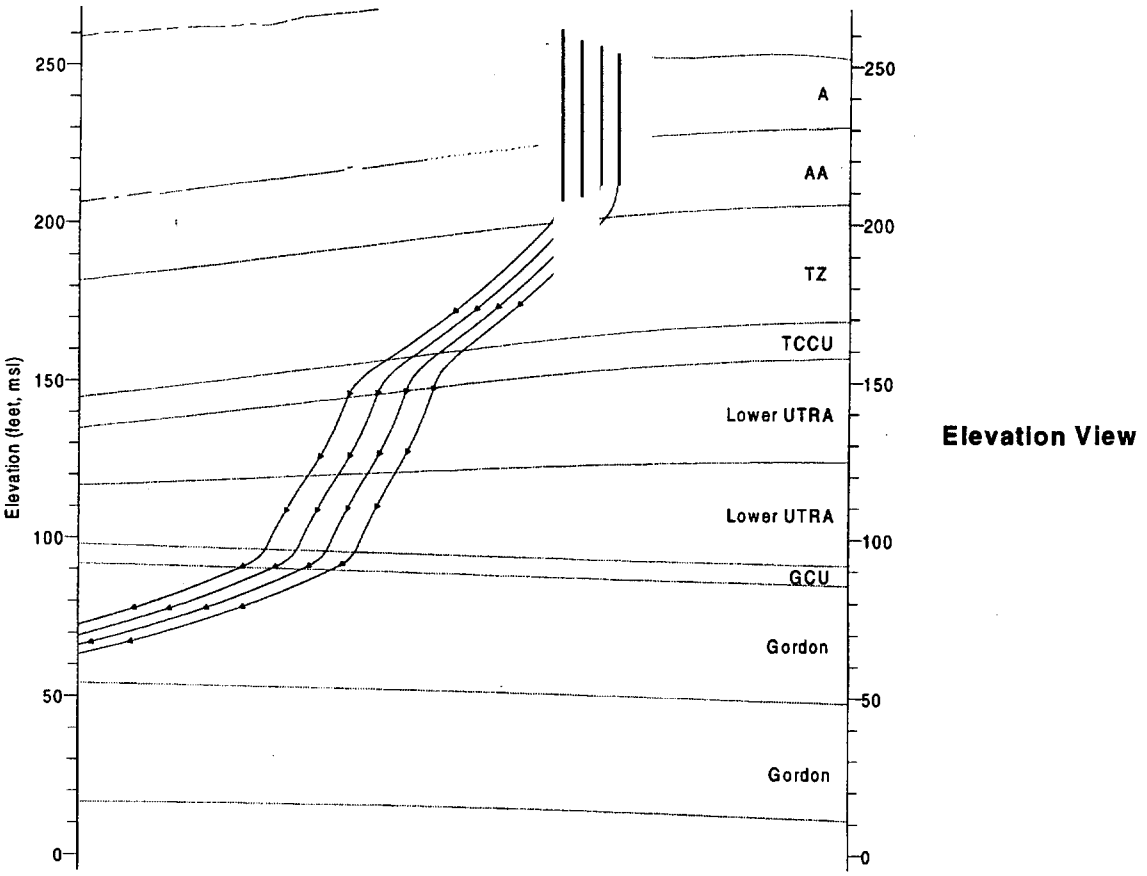

0 600 1200
Horizontal Scale in Feet
(Vertical Exaggeration x10)

Legend

Simulated particle path
(arrow shown every 5 years)

Figure 5-6. Areal map and cross-sectional display of particle traces and travel times from constituent source area.

HSI GEOTRANS
A TETRA TECH COMPANY

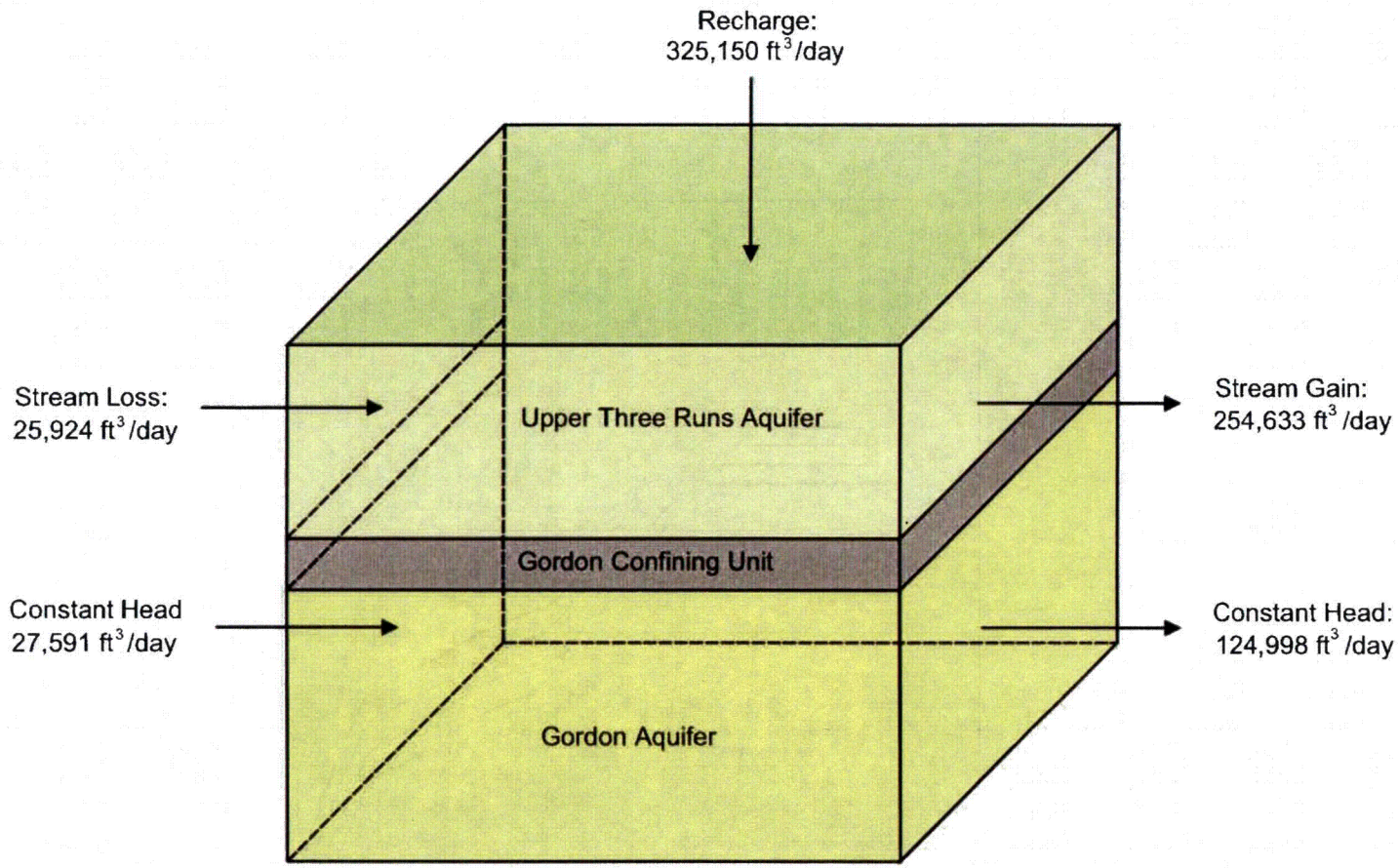

Total In: 378,665 ft^3/day
Total Out: 371,631 ft^3/day

$$\text{Mass Balance Error} = \frac{\text{Total In - Total Out}}{\text{Total Out}} = -0.25\%$$

TITLE: CALIBRATED GROUNDWATER FLOW MODEL BUDGET

LOCATION: Savannah River Site, Aiken, South Carolina

HSI GEOTRANS
A TETRA TECH COMPANY

CHECKED:	DKB
DRAFTED:	SDL
FILE:	IO14003A.CDR
DATE:	5-6-98

FIGURE: 5-7

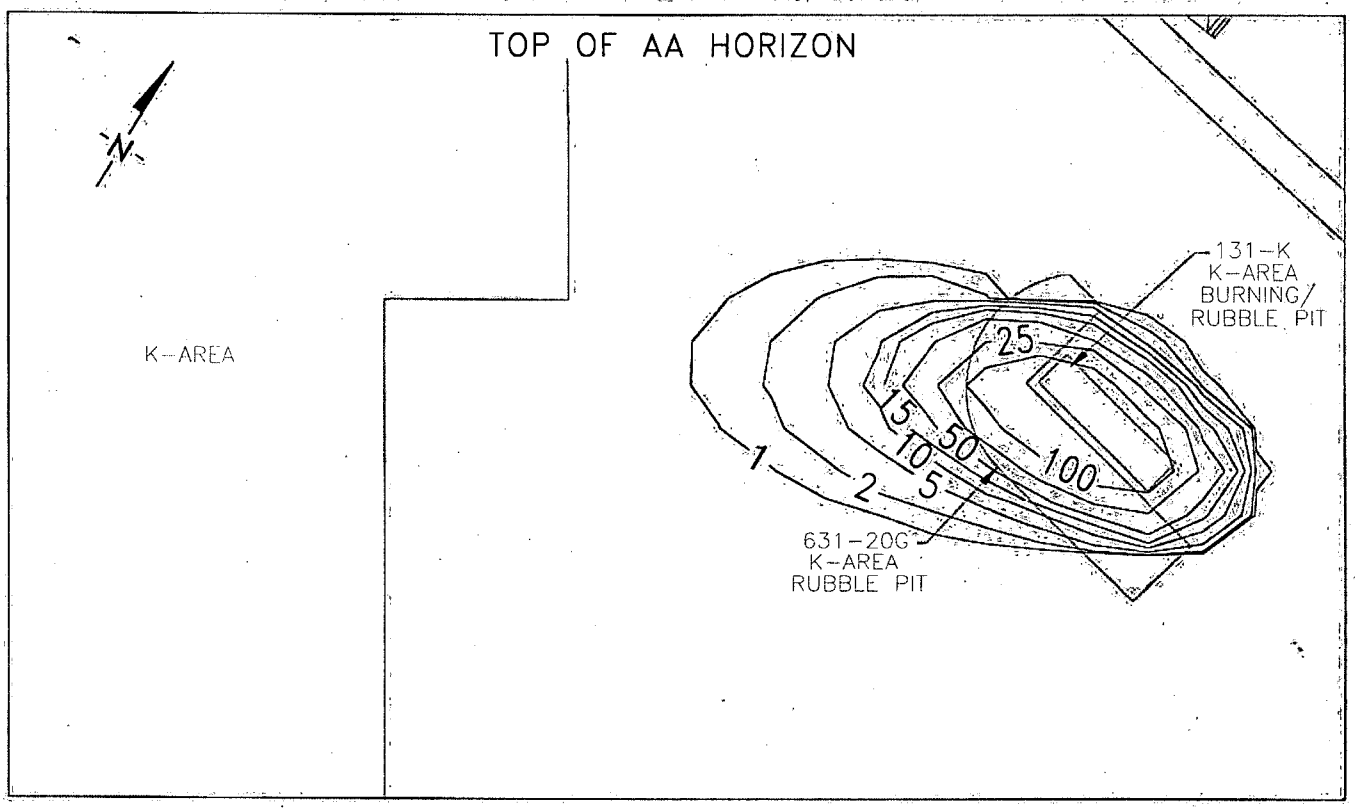

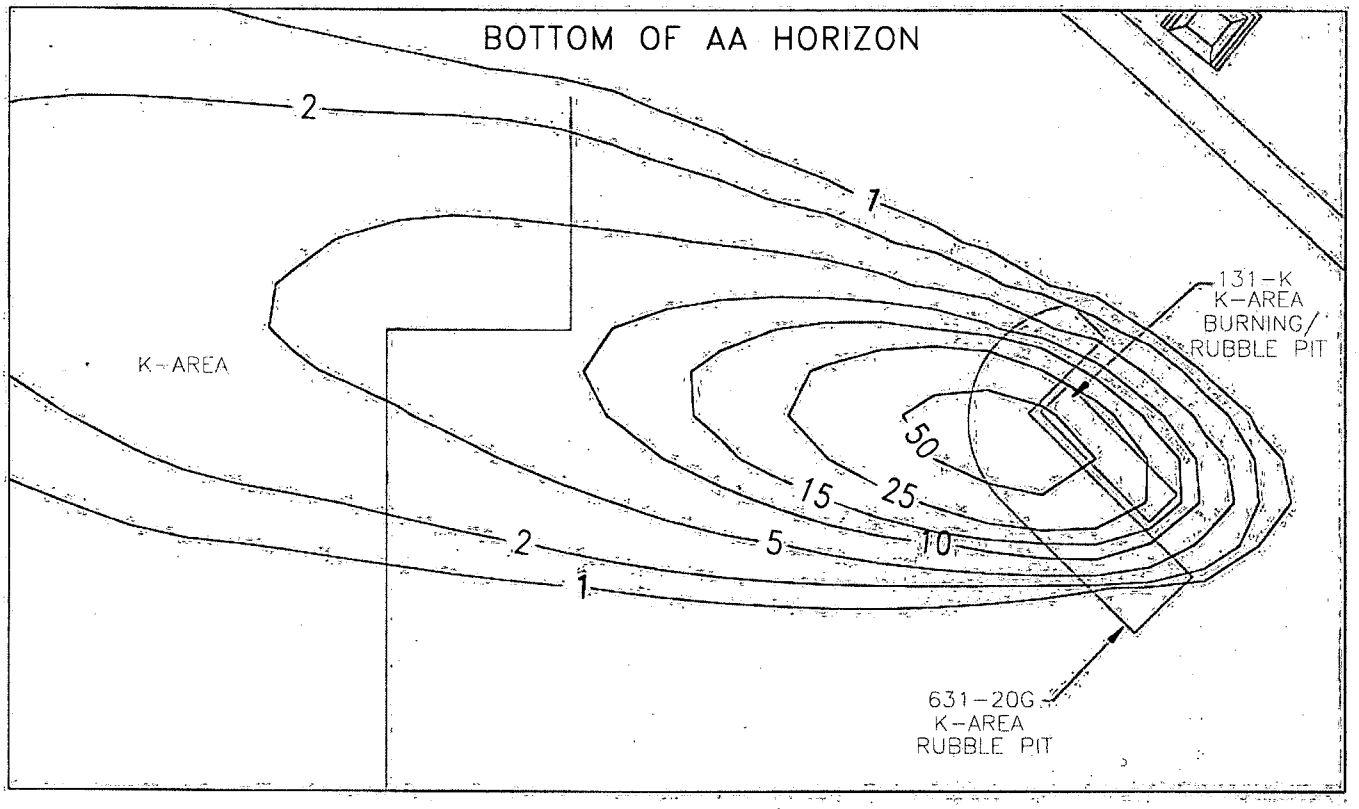

LEGEND

— 5 — CONCENTRATION CONTOUR (ug/L)

0 250 500

SCALE IN FEET

TITLE:
MODEL SIMULATED AREAL MAP OF STEADY-STATE (WORST-CASE) CONCENTRATION OF HYPOTHETICAL CHLORINATED COMPOUND BASED ON USE OF A CONTINUOUS SOURCE RELEASE

LOCATION:
Savannah River Site, Aiken, South Carolina

HSI GEOTRANS
A TETRA TECH COMPANY

CHECKED:	DKB
DRAFTED:	CMP
FILE:	1014011A.DWG
DATE:	5-19-98

FIGURE: 5-8

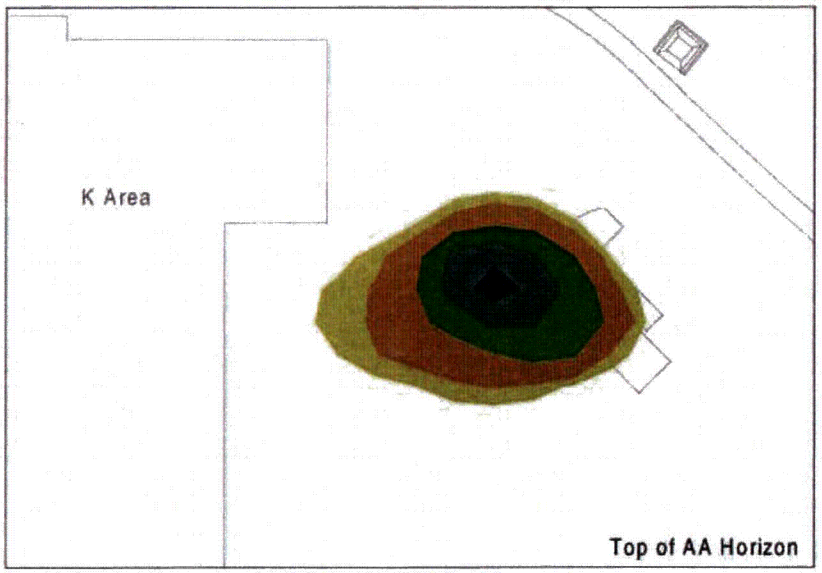

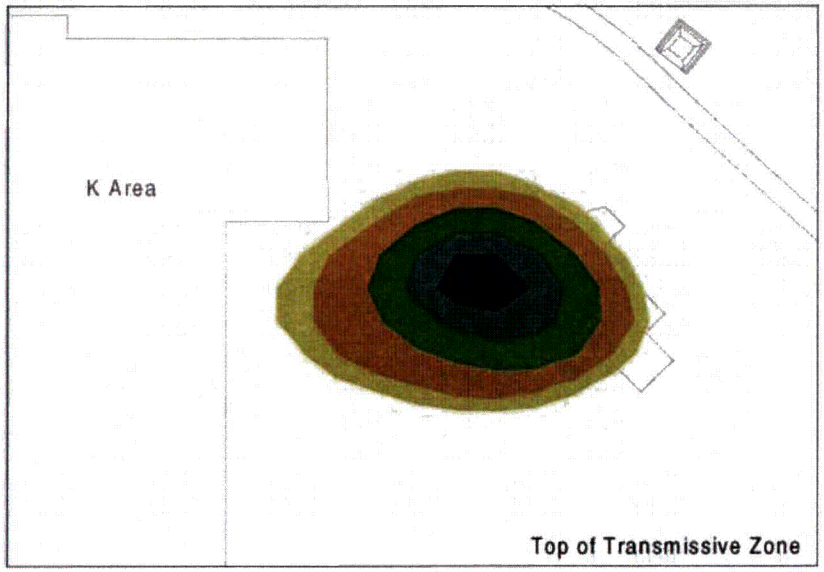

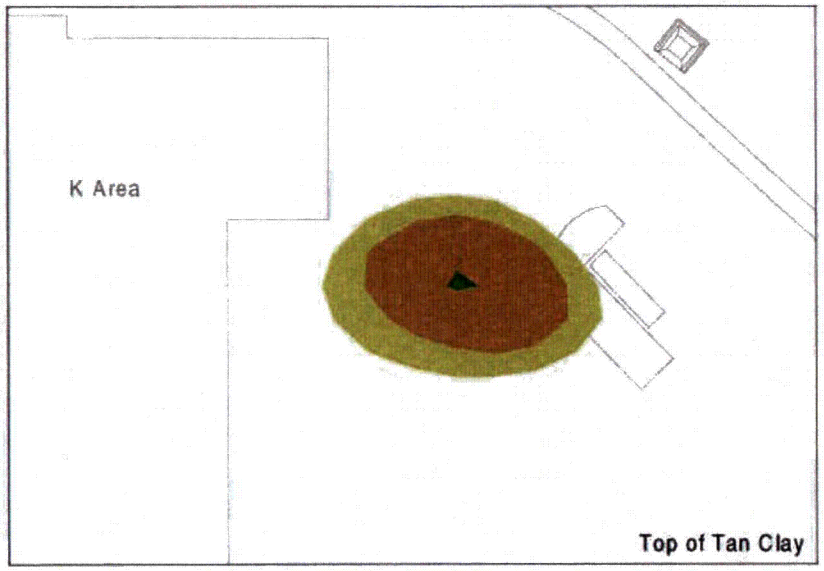

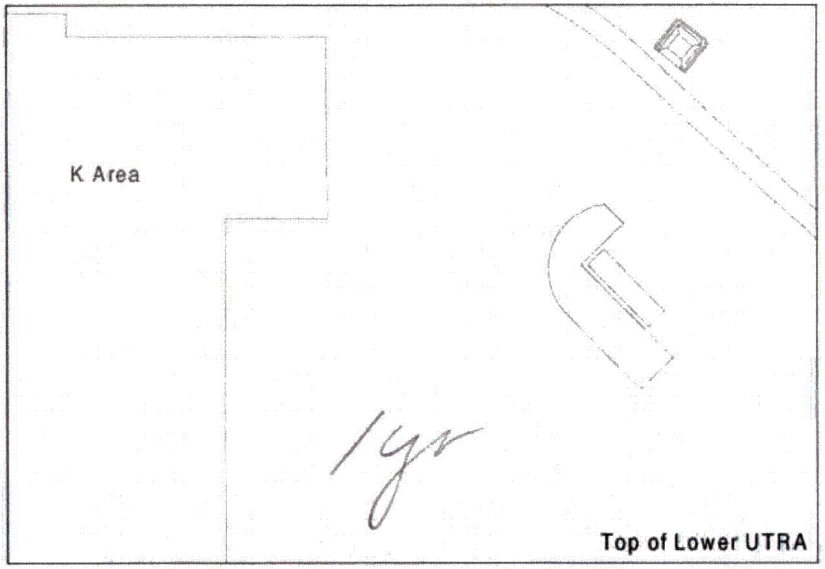

N

Legend

Concentration contour (ug/L)

1 ug/L
2 ug/L
5 ug/L
10 ug/L
>15 ug/L

0 450 900
Feet

Areal maps of model predicted future PCE concentrations after one year based on currently observed concentration levels and inactive source

HSI GEOTRANS
A TETRA TECH COMPANY

CHECKED:	JJB	FIGURE:
DRAFTED:		5-9
FILE:	fig5-9.SRF	
DATE:		

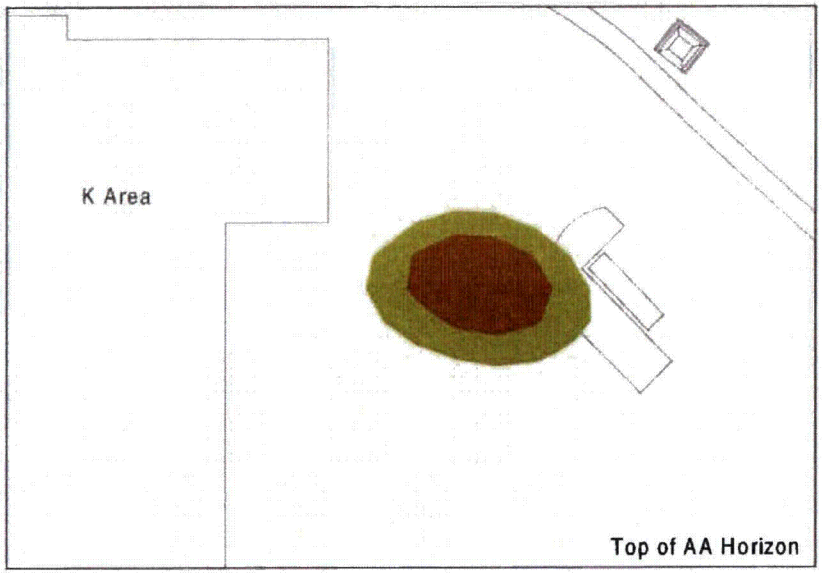

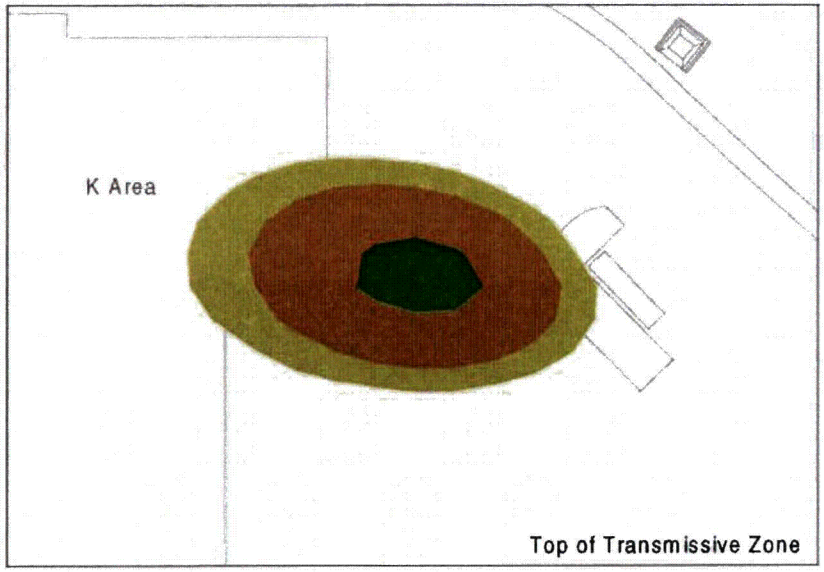

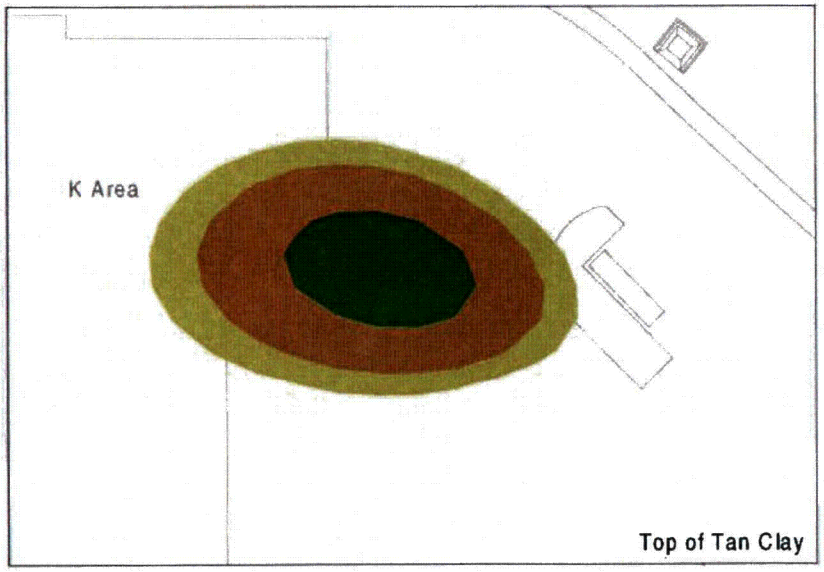

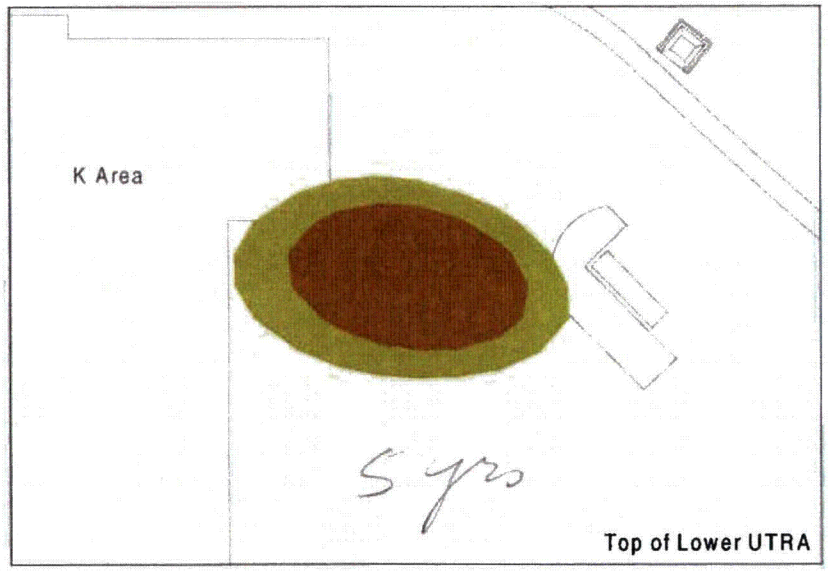

N

Legend

Concentration contour (ug/L)

1 ug/L
2 ug/L
5 ug/L
10 ug/L
>15 ug/L

0 450 900
Feet

Areal maps of model predicted future PCE concentrations after five years based on currently observed concentration levels and inactive source

HSI GEOTRANS
A TETRA TECH COMPANY

CHECKED:	JJB	FIGURE:
DRAFTED:		5-10
FILE:	fig5-10.SRF	
DATE:		

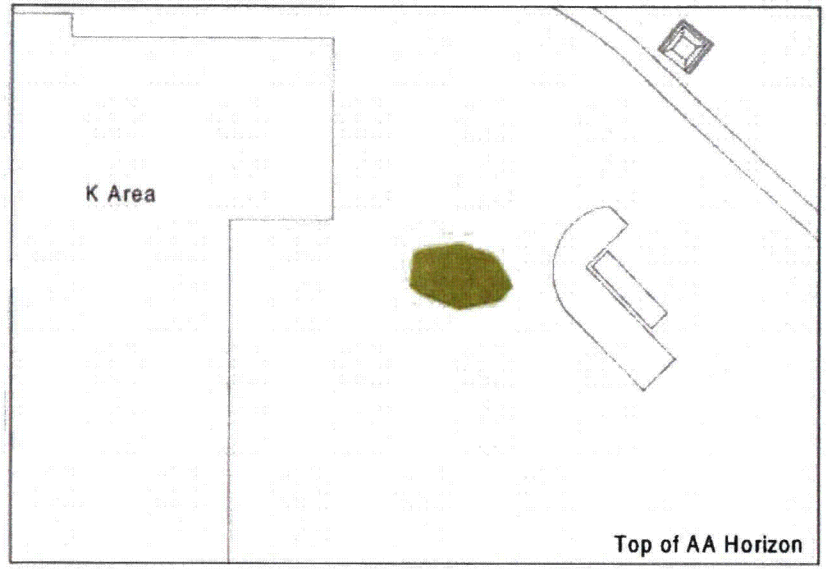

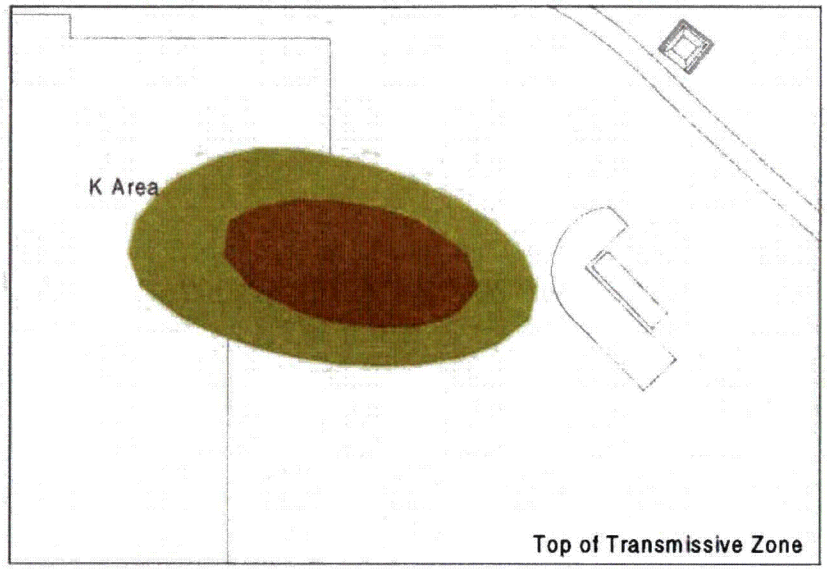

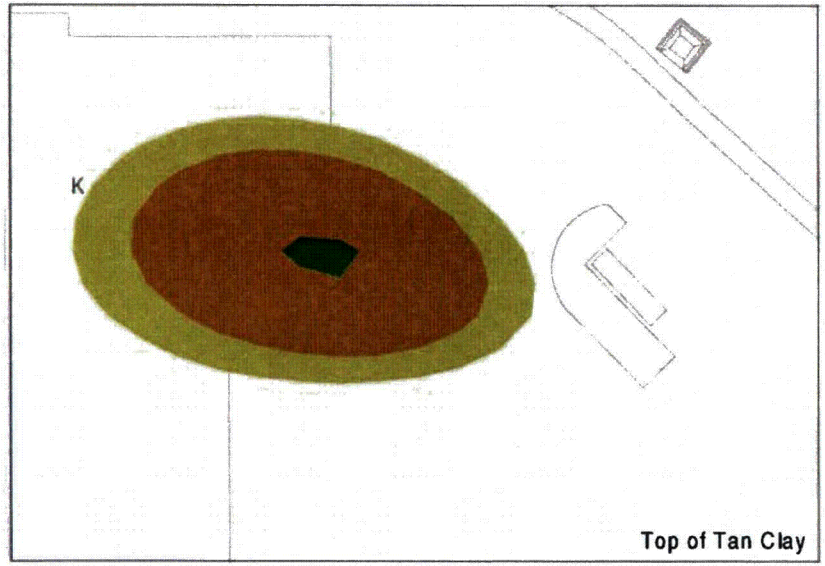

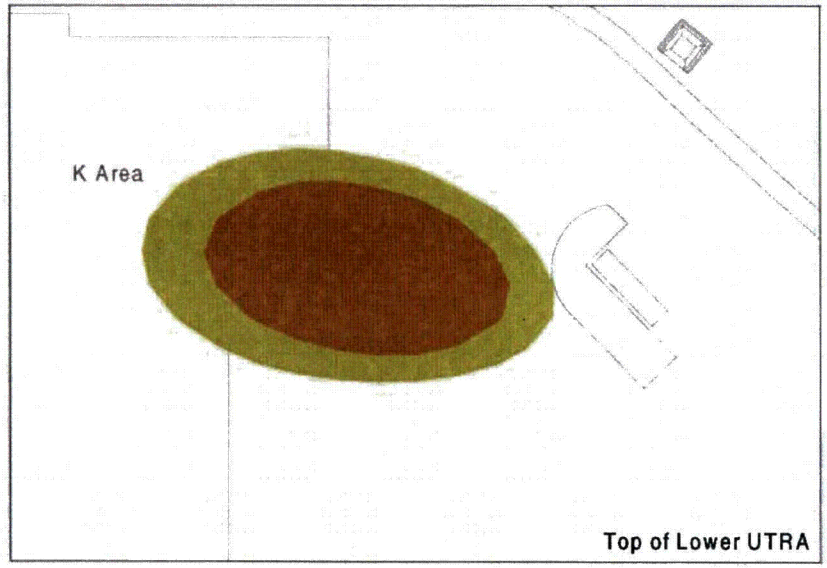

N

Legend

Concentration contour (ug/L)

1 ug/L
2 ug/L
5 ug/L
10 ug/L
>15 ug/L

0 450 900
Feet

Areal maps of model predicted future PCE concentrations after eight years based on currently observed concentration levels and inactive source

HSI GEOTRANS
A TETRA TECH COMPANY

CHECKED:	JJB	FIGURE:
DRAFTED:		5-11
FILE:	fig5-11.SRF	
DATE:		

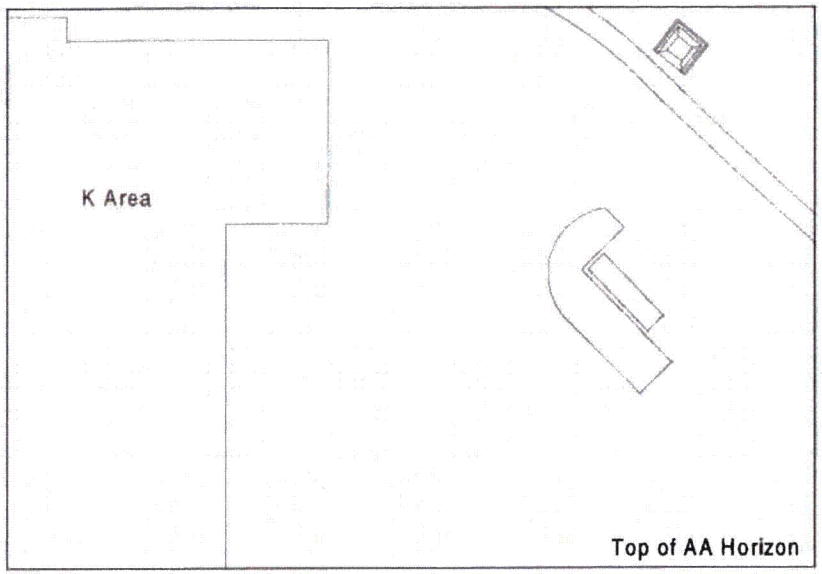

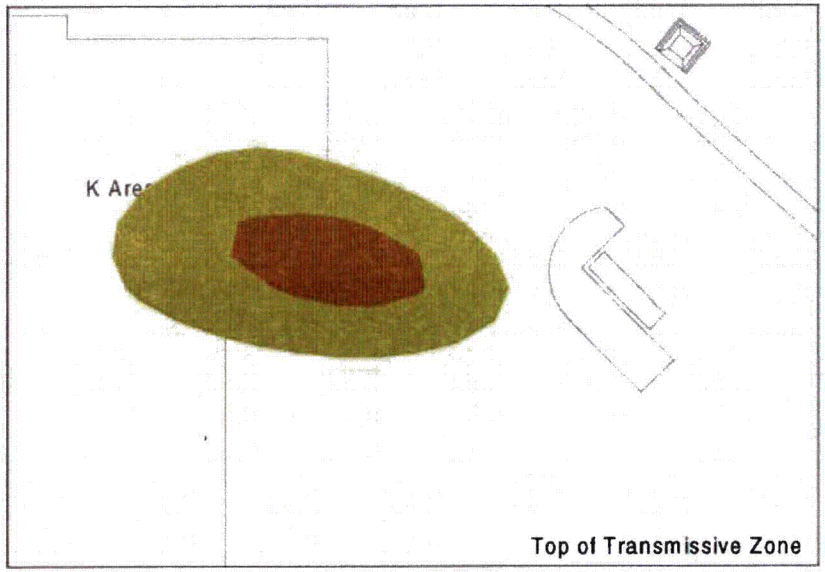

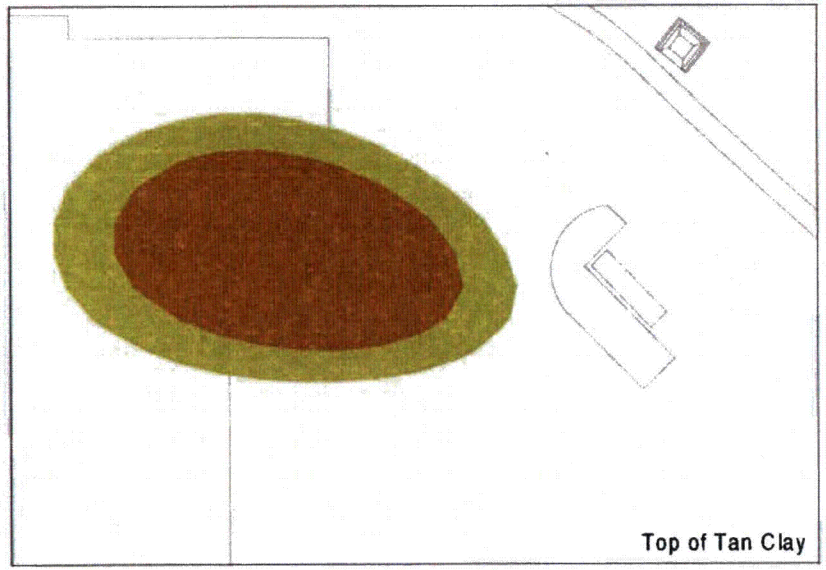

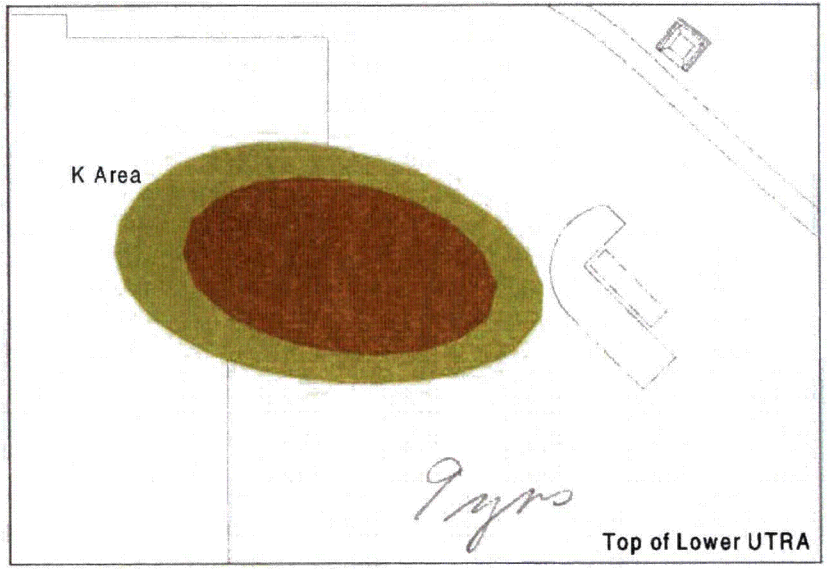

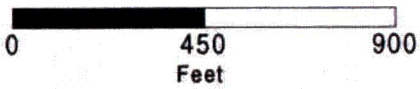

Legend

Concentration contour (ug/L)

1 ug/L
2 ug/L
5 ug/L
10 ug/L
>15 ug/L

Areal maps of model predicted future PCE concentrations after nine years based on currently observed concentration levels and inactive source

HSI GEOTRANS
A TETRA TECH COMPANY

CHECKED:	JJB	FIGURE:
DRAFTED:		5-12
FILE:	fig5-12.SRF	
DATE:		

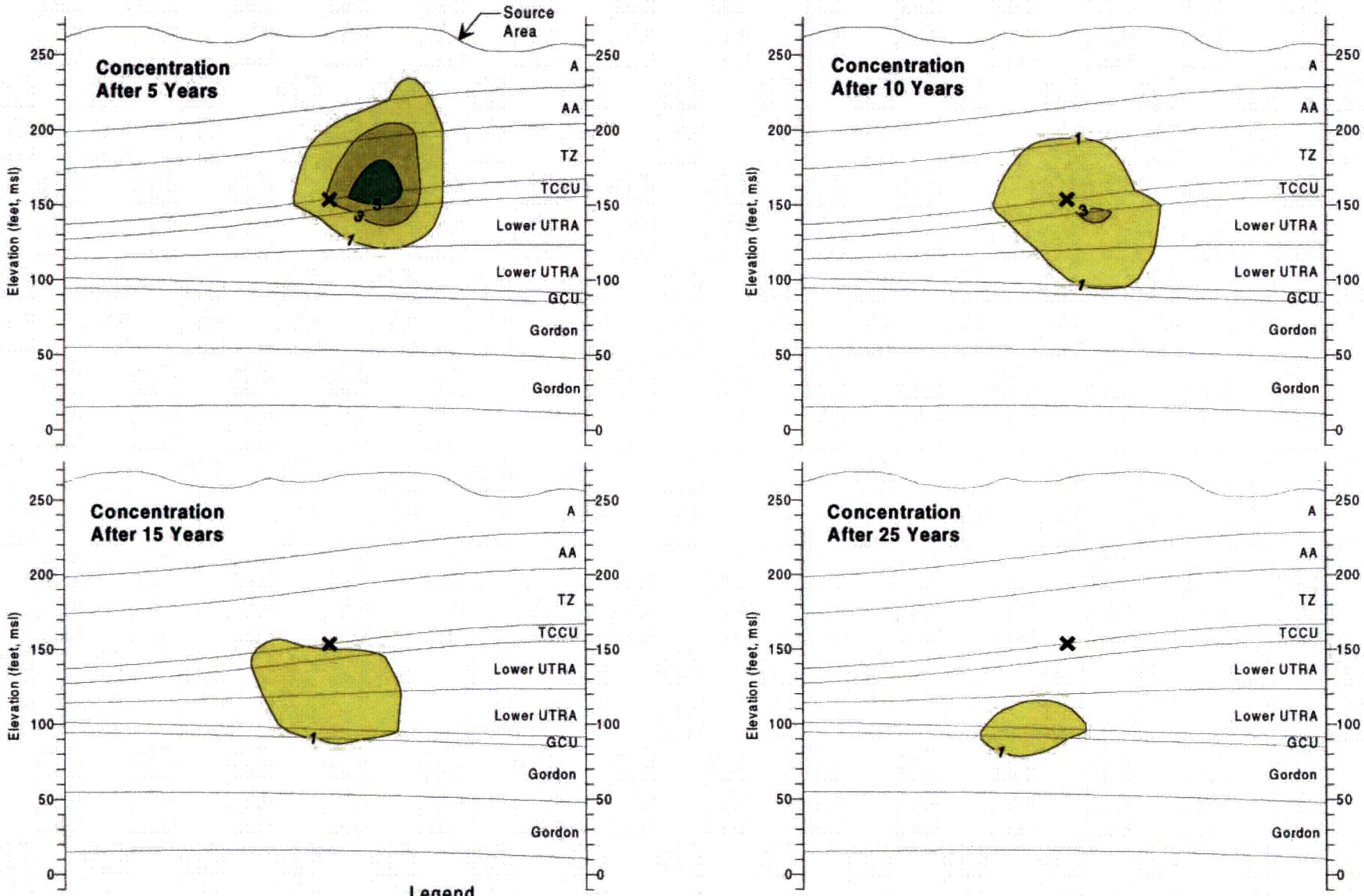

Legend

- 1-3 ppb
- 3-5 ppb
- 5-10 ppb
- >10 ppb
- ✖ Proposed Compliance Location

0 1000 2000

Horizontal Scale in Feet
(Vertical Exaggeration x10)

Note:
Section shown along the 69th row of nodes.

Vertical cross-sectional view of model predicted future PCE concentrations based on currently observed concentration levels and inactive source

HSI GEOTRANS
A TETRA TECH COMPANY

CHECKED:	
DRAFTED:	GWC
FILE:	fig5-13.srf
DATE:	May 1998

FIGURE: 5-13

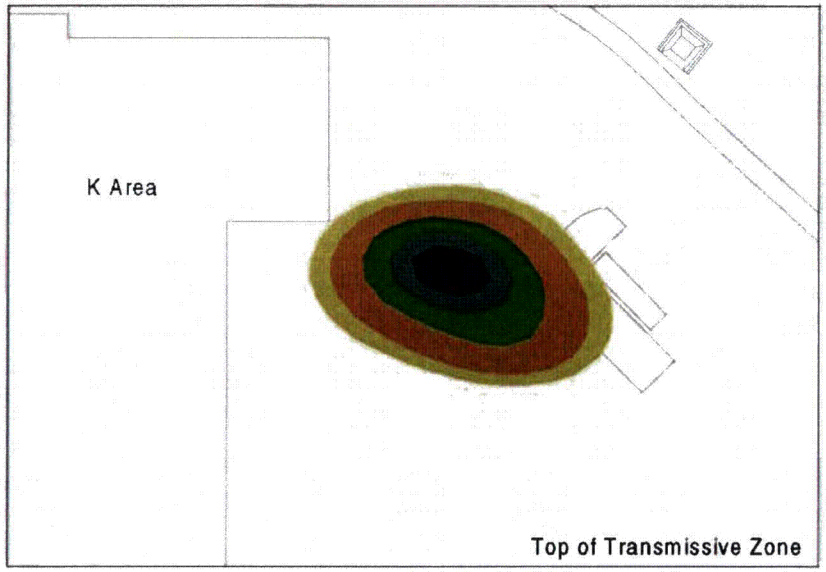

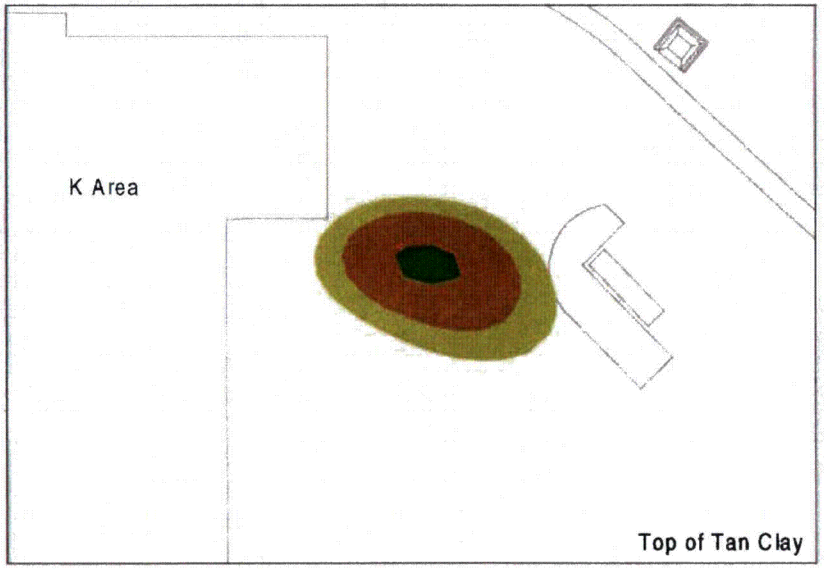

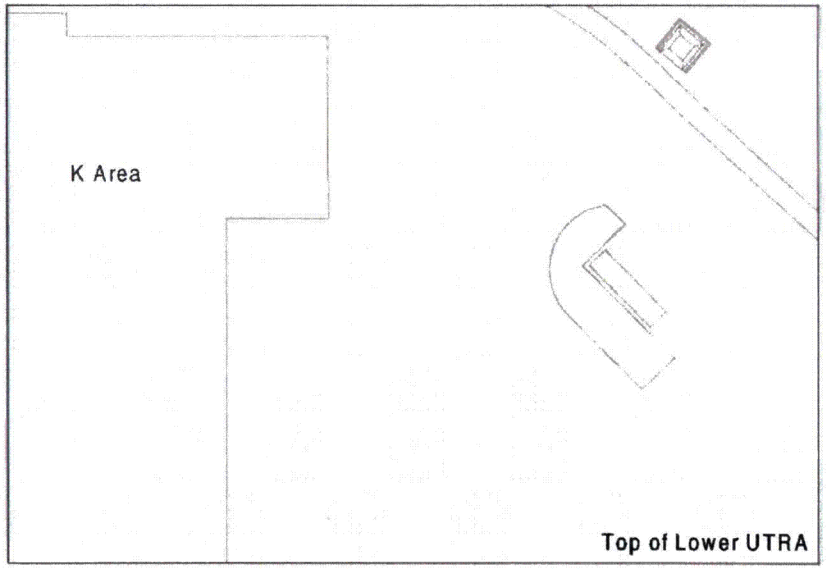

N

Legend

Concentration contour (ug/L)

1 ug/L
2 ug/L
5 ug/L
10 ug/L
>15 ug/L

0 450 900
Feet

Areal maps of model predicted future TCE concentrations after one year based on currently observed concentration levels and inactive source

HSI GEOTRANS
A TETRA TECH COMPANY

CHECKED:	JJB
DRAFTED:	
FILE:	fig5-14 SRF
DATE:	

FIGURE: 5-14

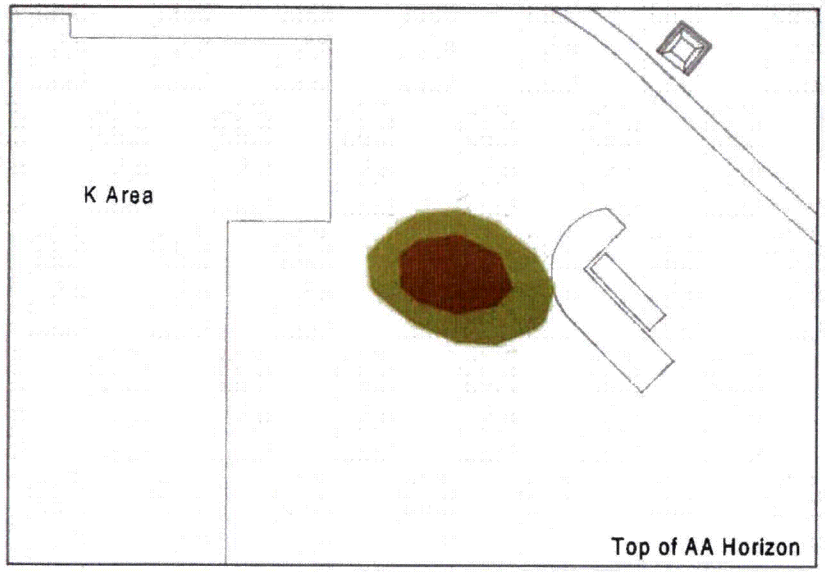

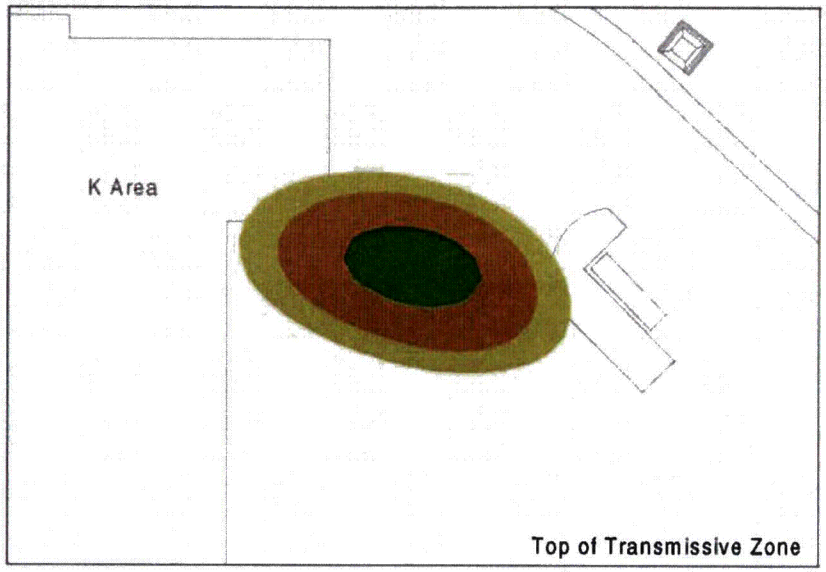

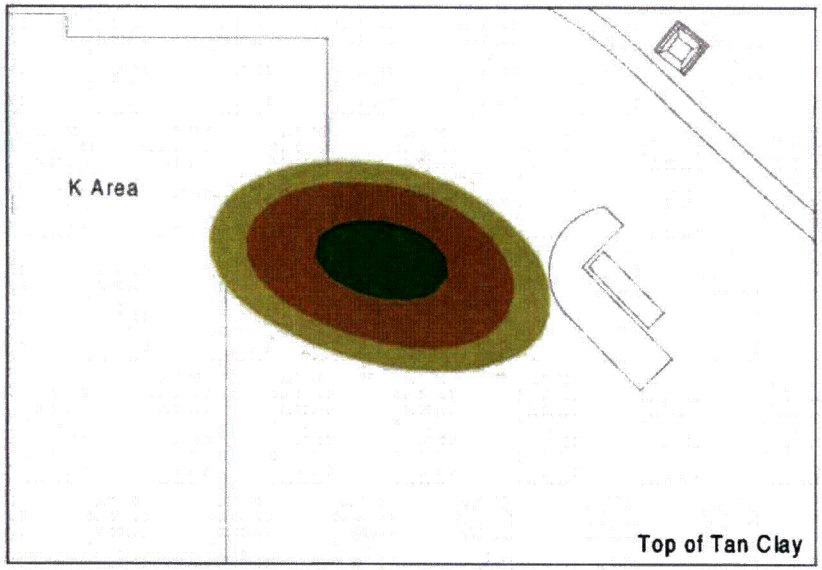

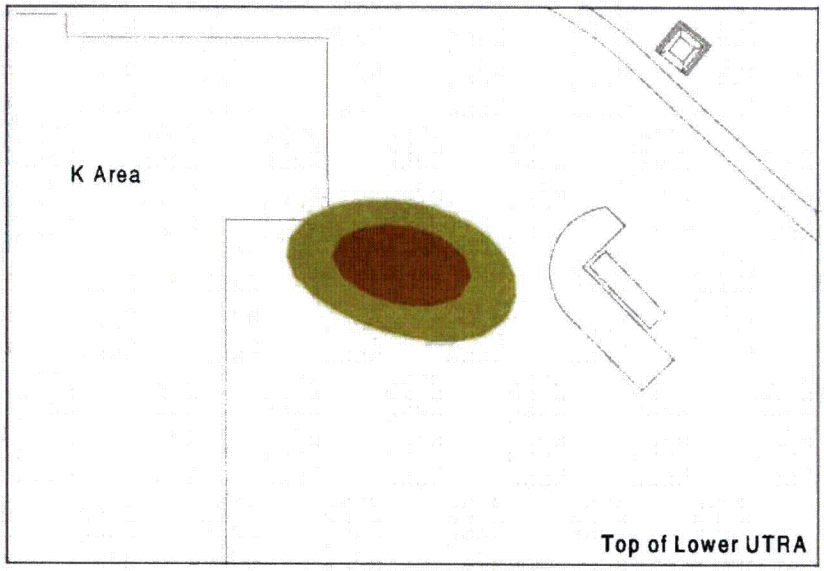

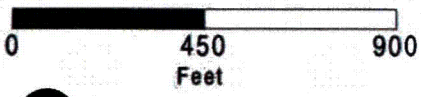

Legend

Concentration contour (ug/L)

- 1 ug/L
- 2 ug/L
- 5 ug/L
- 10 ug/L
- >15 ug/L

Areal maps of model predicted future TCE concentrations after three years based on currently observed concentration levels and inactive source

HSI GEOTRANS
A TETRA TECH COMPANY

CHECKED:	JJB	FIGURE:
DRAFTED:		5-15
FILE:	fig5-15.SRF	
DATE:		

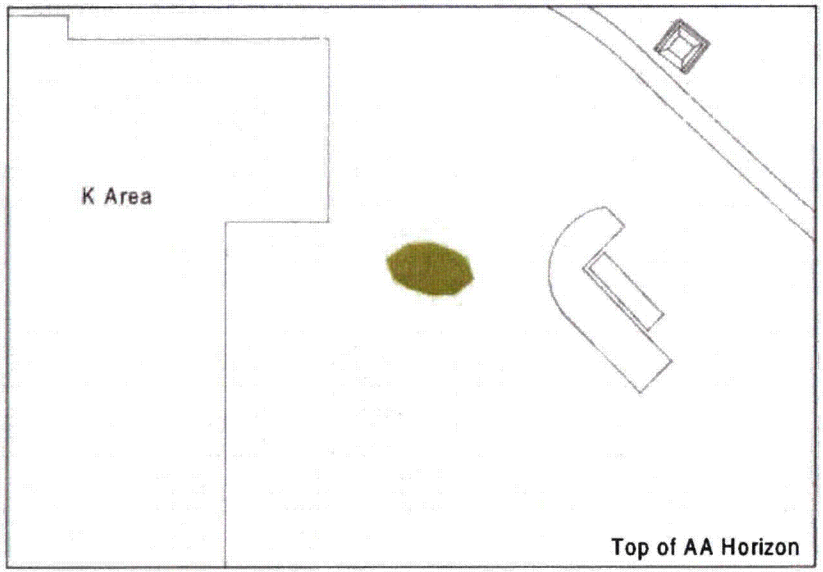

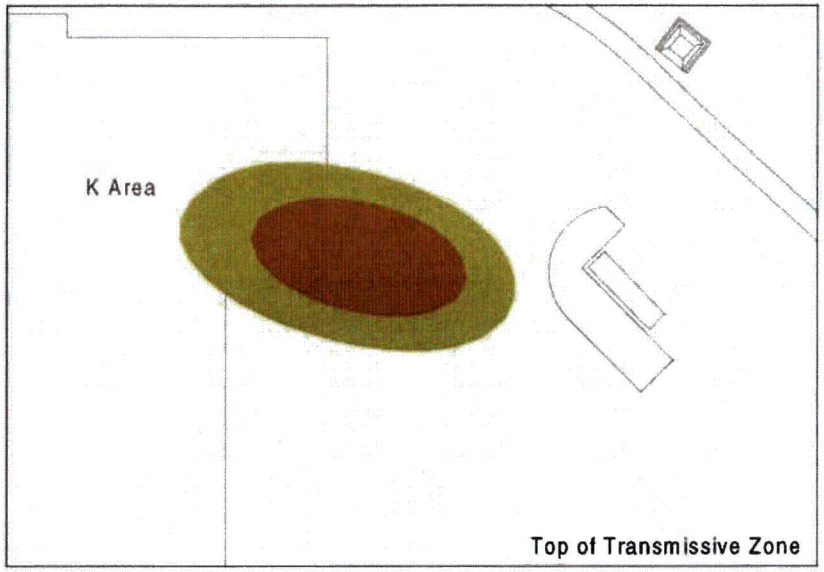

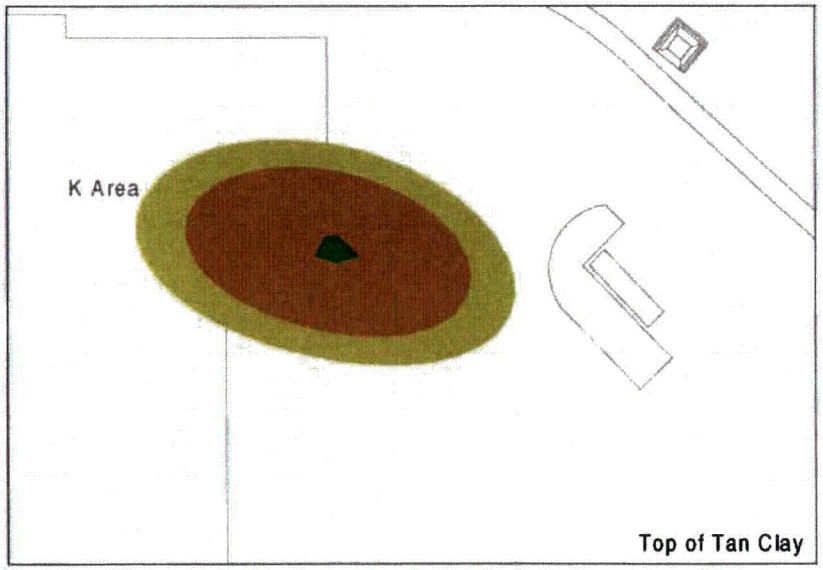

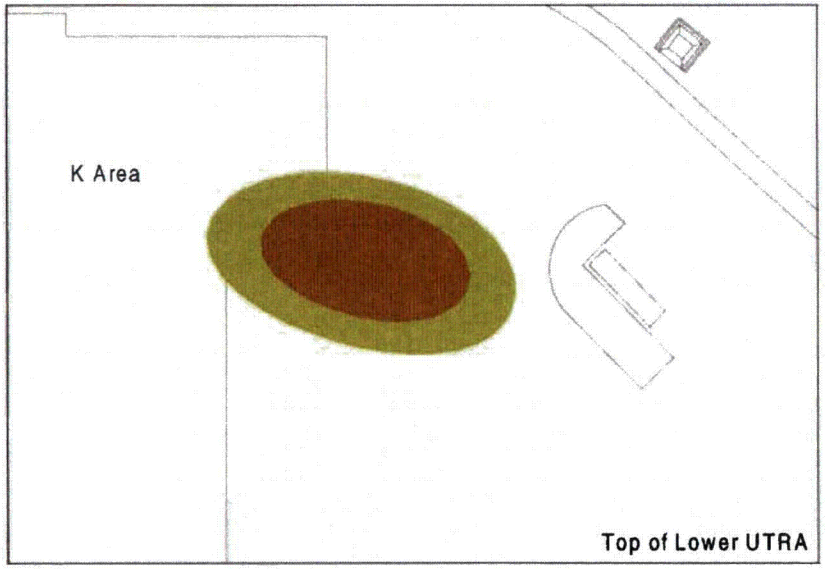

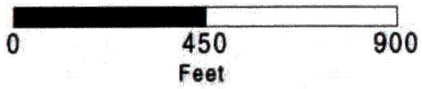

Legend

Concentration contour (ug/L)

- 1 ug/L
- 2 ug/L
- 5 ug/L
- 10 ug/L
- >15 ug/L

Areal maps of model predicted future TCE concentrations after five years based on currently observed concentration levels and inactive source

HSI GEOTRANS
A TETRA TECH COMPANY

CHECKED:	JJB	FIGURE:
DRAFTED:		5-16
FILE:	fig5-16.SRF	
DATE:		

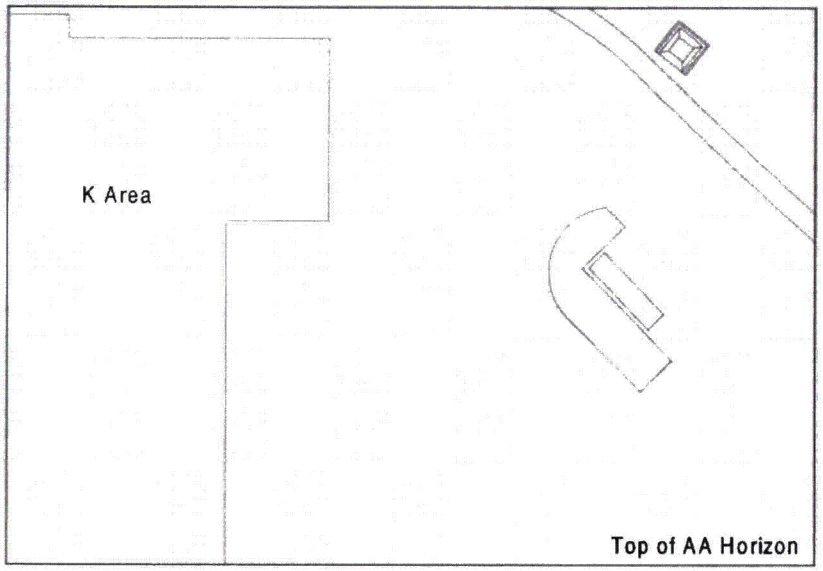

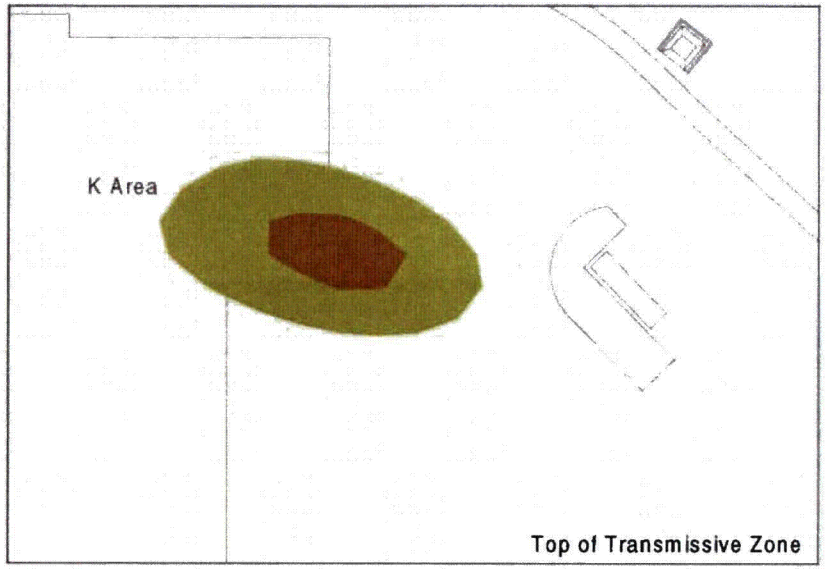

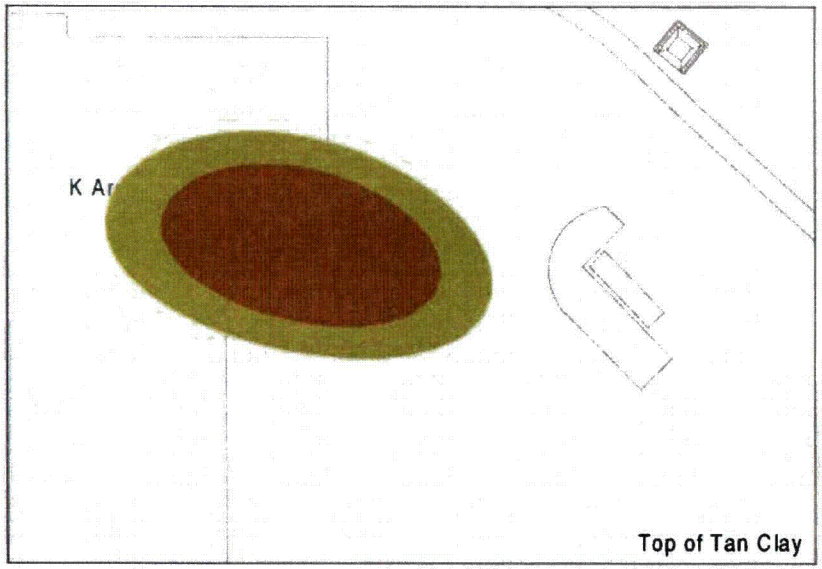

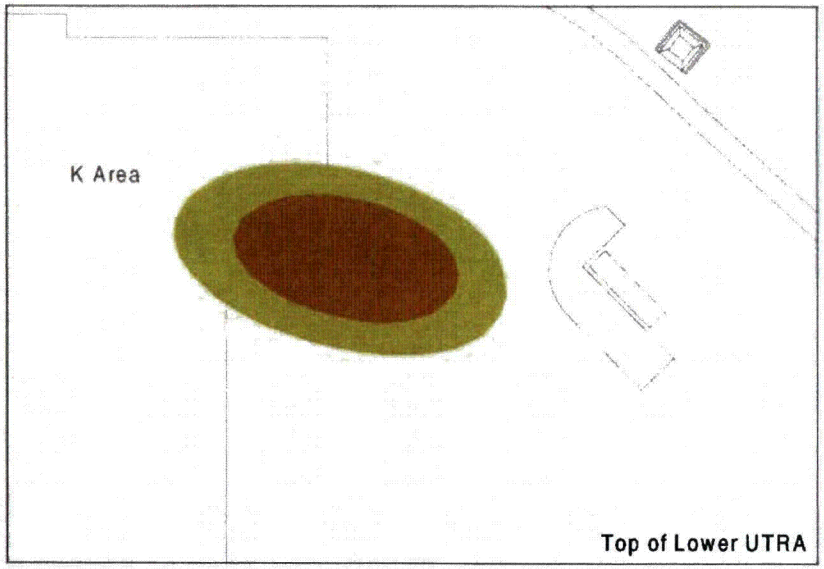

N

Legend

Concentration contour (ug/L)

1 ug/L
2 ug/L
5 ug/L
10 ug/L
>15 ug/L

0 450 900
Feet

Areal maps of model predicted future TCE concentrations after six years based on currently observed concentration levels and inactive source

HSI GEOTRANS
A TETRA TECH COMPANY

CHECKED:	JJB	FIGURE:
DRAFTED:		5-17
FILE:	fig5-17.SRF	
DATE:		

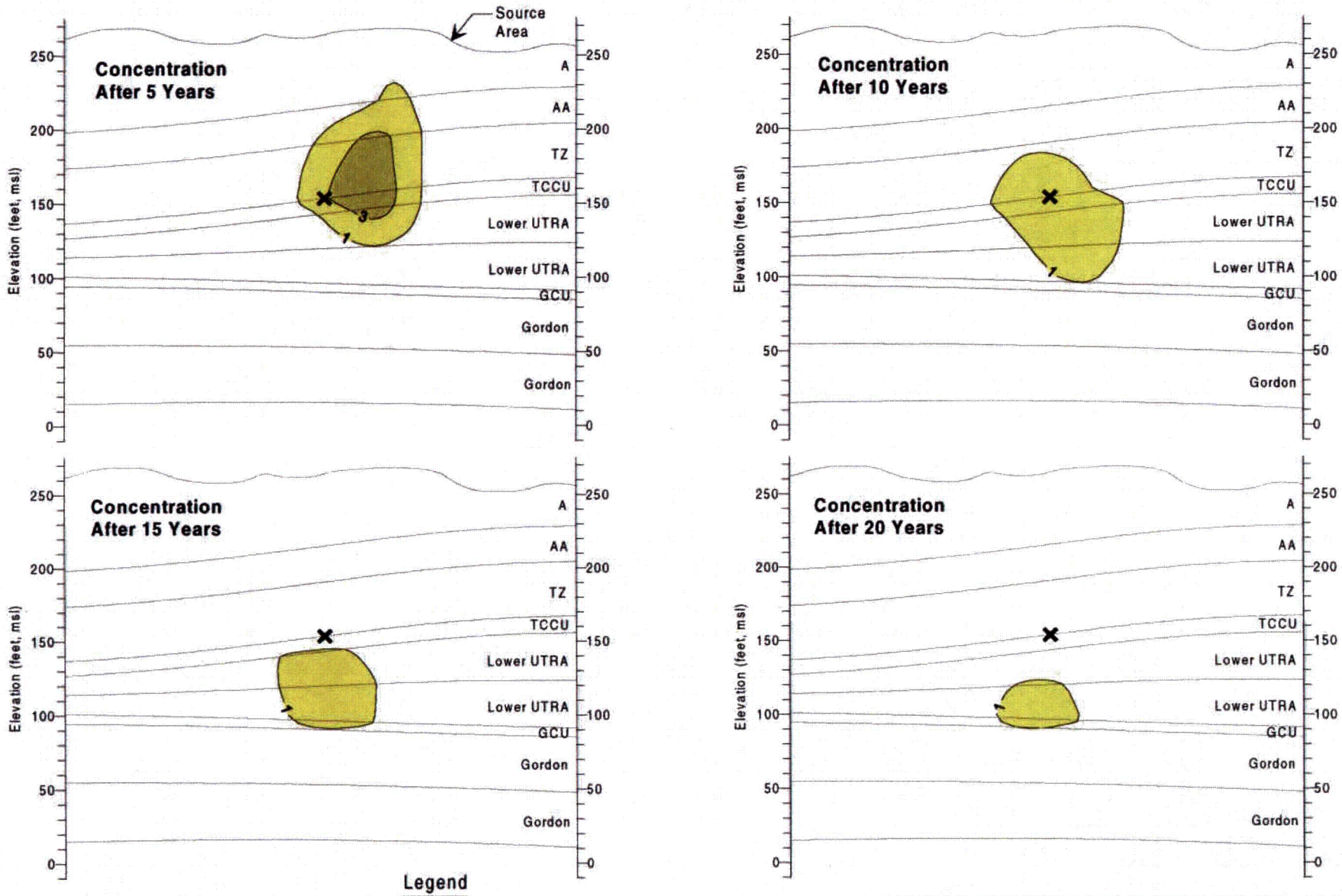

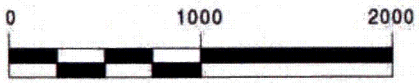

Horizontal Scale in Feet
(Vertical Exaggeration x10)

Legend

- 1-3 ppb
- 3-5 ppb
- 5-10 ppb
- >10 ppb
- ✖ Proposed Compliance Location

Note:
Section shown along the 69th row of nodes.

Vertical cross-sectional view of model predicted future TCE concentrations based on currently observed concentration levels and inactive source

HSI GEOTRANS
A TETRA TECH COMPANY

CHECKED:		FIGURE:
DRAFTED:	GWC	5-18
FILE:	fig5-18.srf	
DATE:	May 1998	

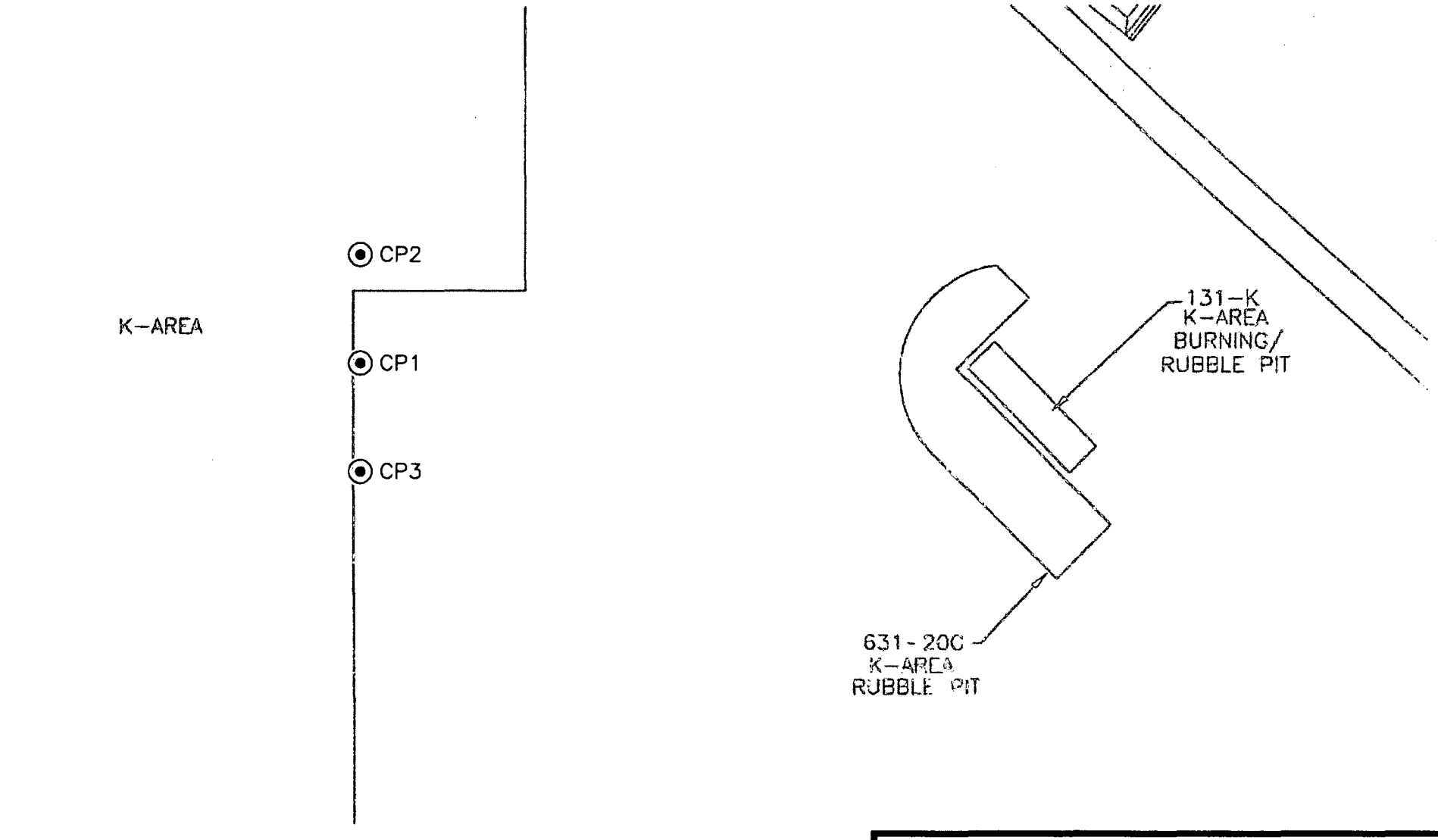

LEGEND

COMPLIANCE WELL CLUSTER LOCATION

0 200 400

SCALE IN FEET

TITLE: LOCATION OF COMPLIANCE BOUNDARY WELL LOCATIONS BASED ON TRANSPORT MODELING RESULTS

LOCATION: Savannah River Site, Aiken, South Carolina

HSI GEOTRANS
A TETRA TECH COMPANY

CHECKED:	DKB
DRAFTED:	CMP
FILE:	1014014A.DWG
DATE:	5-5-98

FIGURE: 5-19

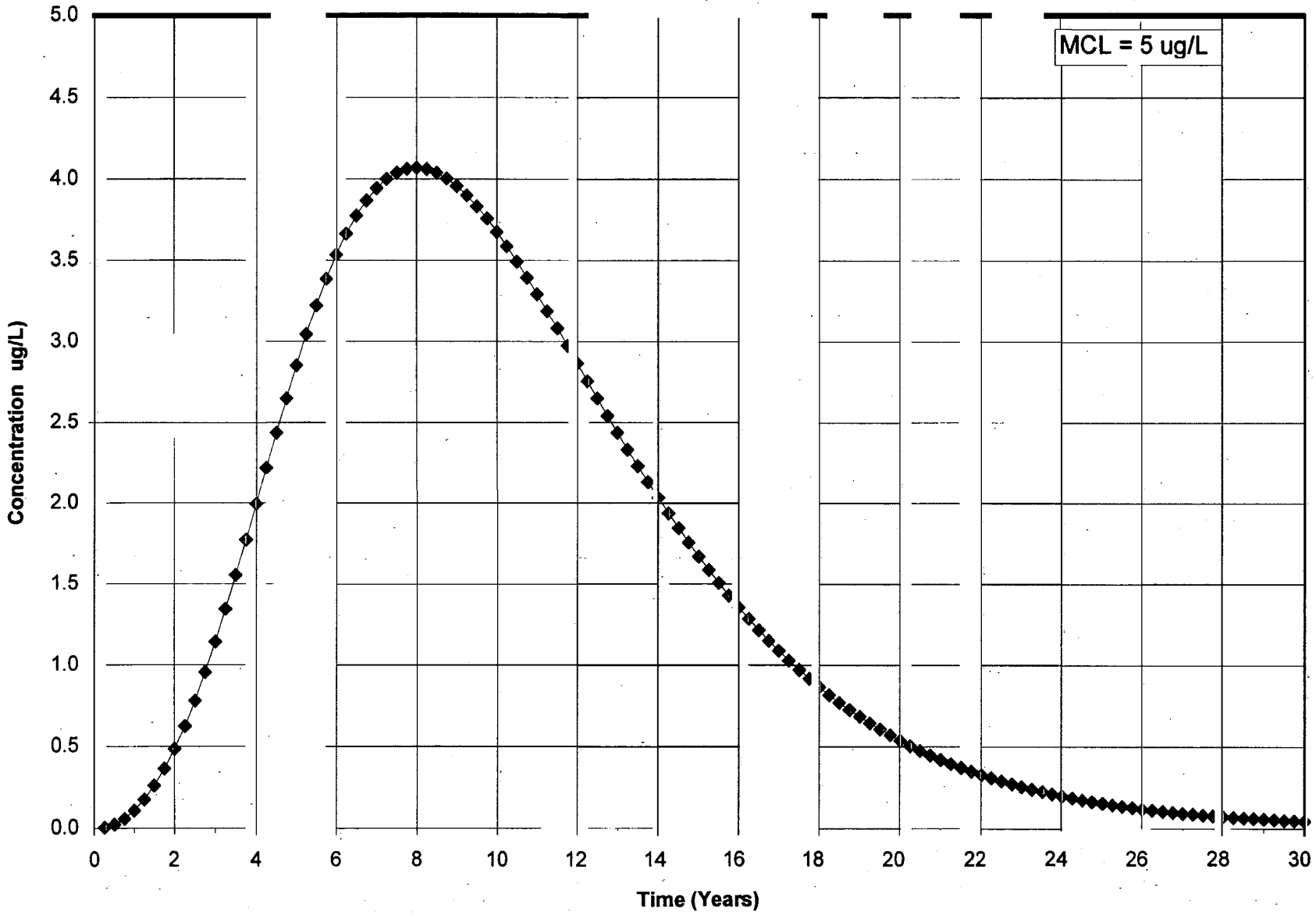

Figure 5-20. Model simulated PCE concentrations versus time along the plume centerline at the compliance boundary.

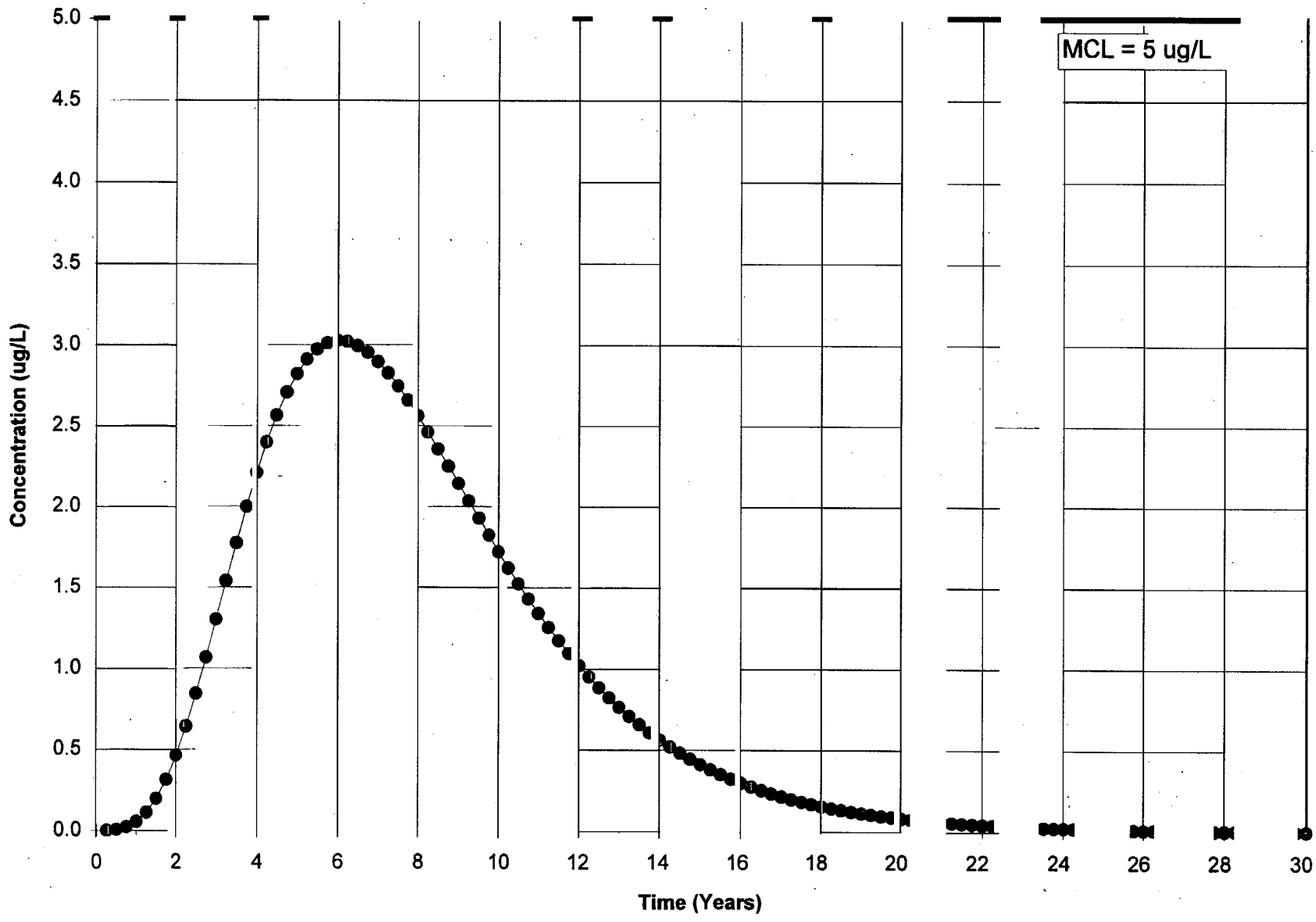

Figure 5-21. Model simulated TCE concentrations versus time along the plume centerline at the compliance boundary.

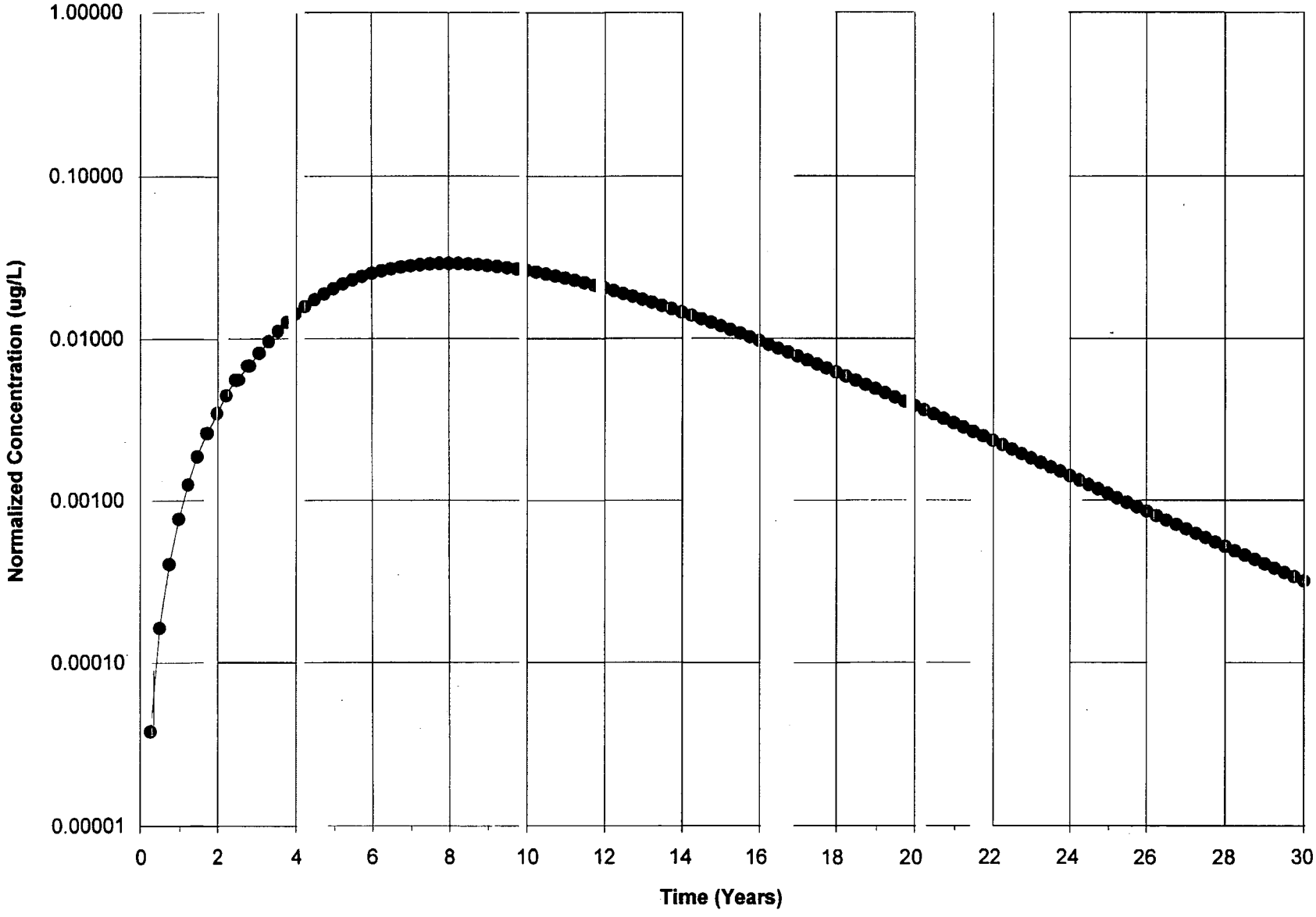

Figure 5-22. Model simulated normalized concentrations versus time along the plume centerline at the compliance boundary.

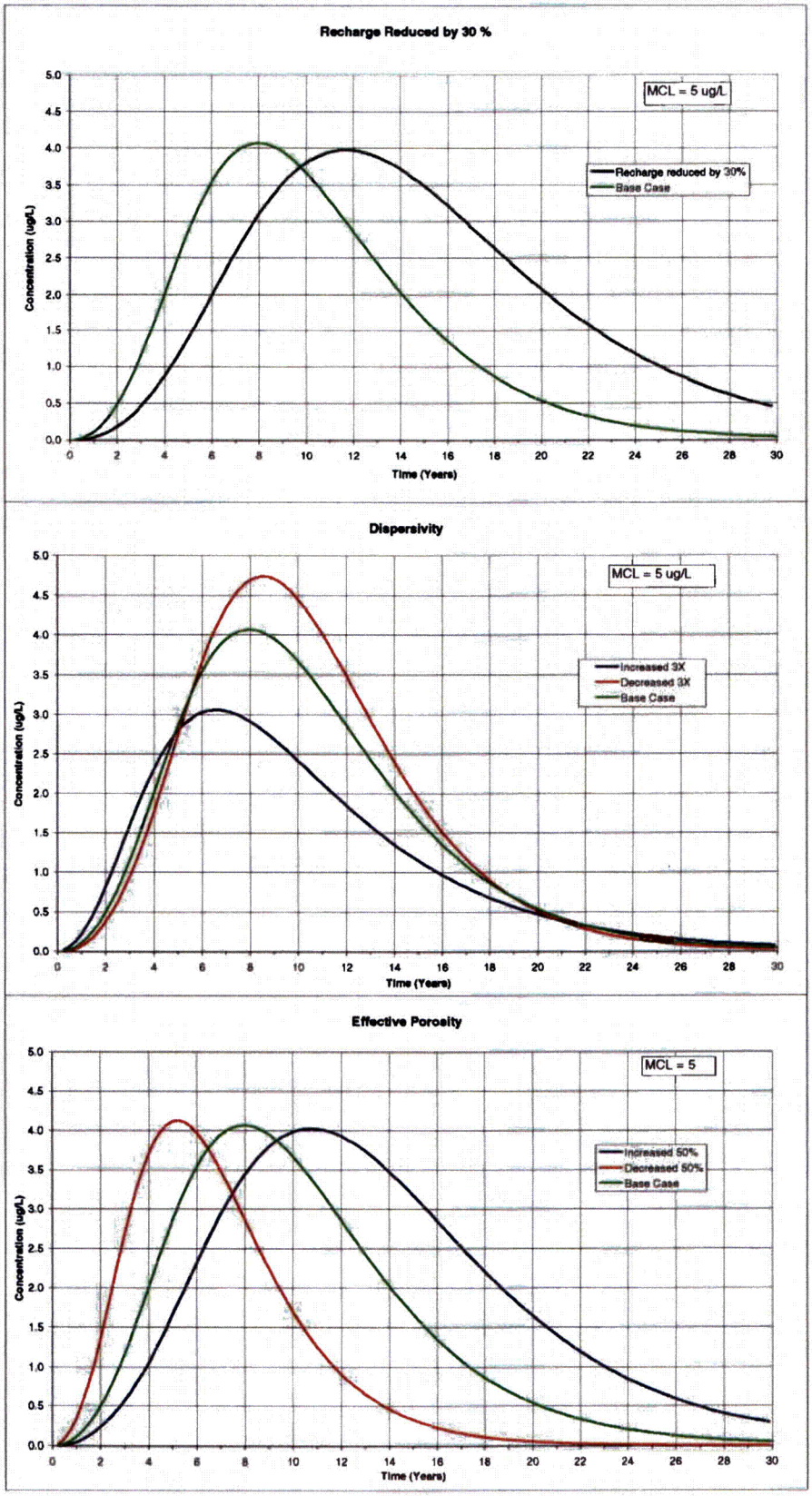

Figure 5-23. Results of sensitivity analysis for PCE at compliance point.

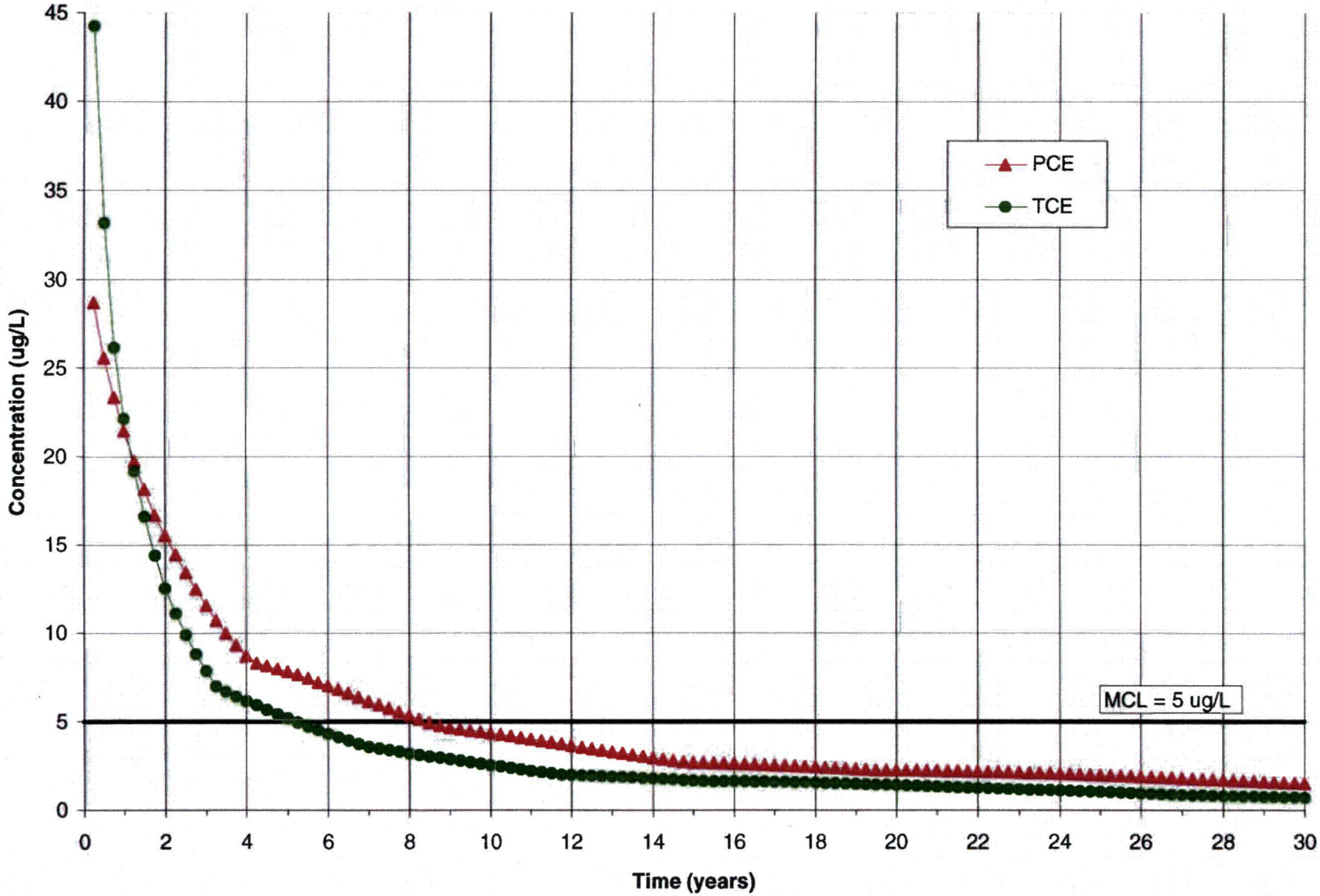

Figure 6-1. Estimate of natural attenuation restoration time based on plots of maximum model predicted concentrations at various times for PCE and TCE.

)

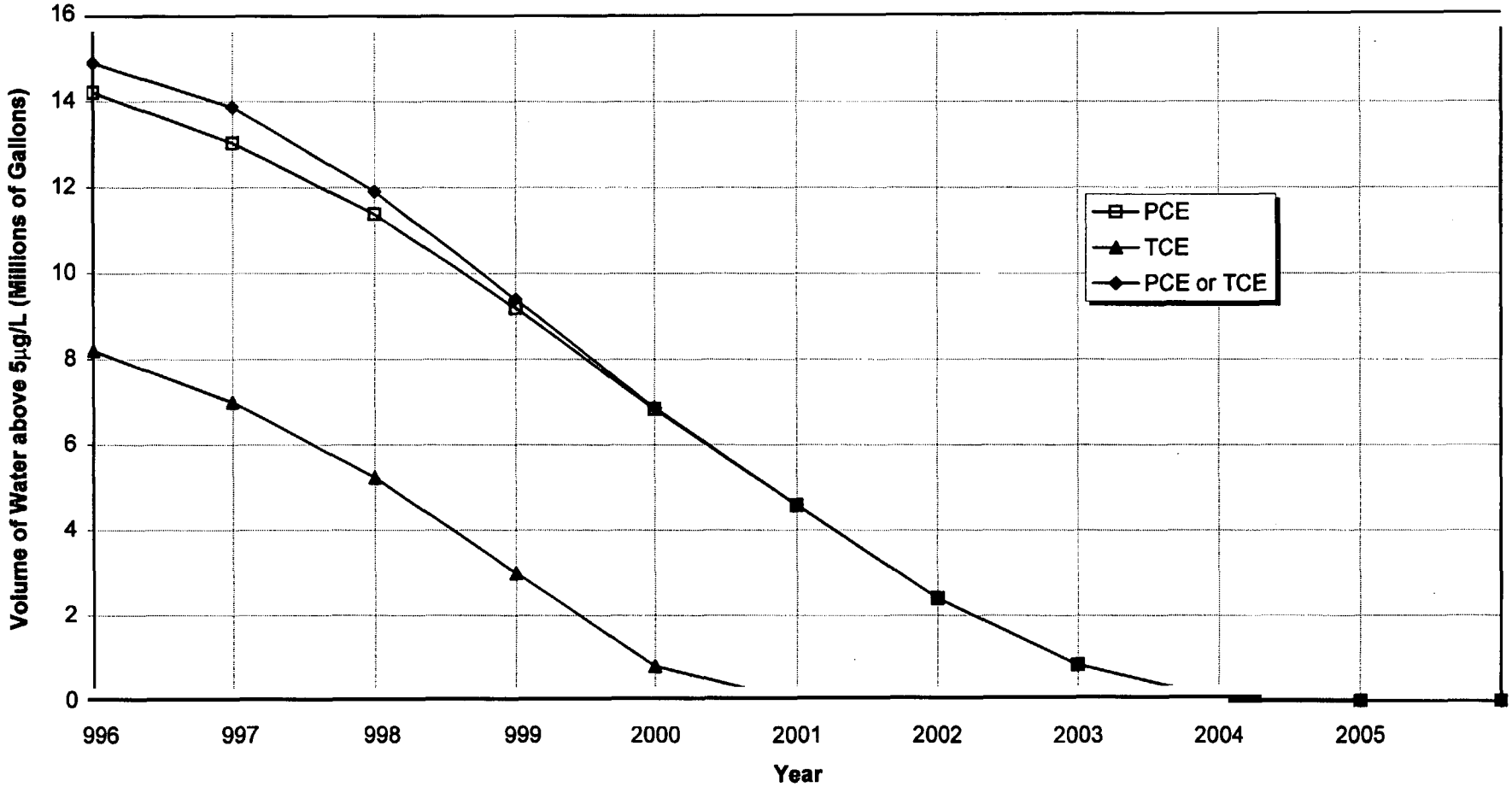

Figure 6.2 Volume of water with a concentration of 5 µg/L or more for PCE and TCE.

Table 4-1. Calibrated groundwater flow model and transport parameter values.

Model Parameter	Parameter Value		
Areal recharge rate	10 to17 in/yr		
Bulk density	1.6 g/mL		
Dispersivity			
Longitudinal	30 ft		
Horizontal transverse	5 ft		
Vertical transverse	0.1 ft		
Hydrostratigraphic Unit	**Horizontal Conductivity**	**Vertical Conductivity**	**Effective Porosity**
Upper zone of UTRA	1-10 ft/day	0.1-1.0 ft/day	0.20
Tan Clay	0.01 ft/day	0.001 ft/day	0.10
Lower zone of UTRA	7 ft/day	0.7 ft/day	0.20
Gordon confining unit	0.007 ft/day	0.0007 ft/day	0.10
Gordon Aquifer	38 ft/day	3.8 ft/day	0.20
Soil-Water Distribution Coefficient (K_d)			
PCE	0.038 mL/g		
TCE	0.013 mL/g		
Decay Constant (day^{-1})			
PCE	0 day^{-1}		
TCE	0 day^{-1}		

Table 5-1. Flow model calibration statistics.

Name	Average Observed Water Level (ft. MSL)	Simulated Water Level (FACT)	Residual
K301P	204.90	206.60	-1.70
KAB 1	204.97	206.20	-1.23
KAB 3	202.97	204.90	-1.93
KAB 4	202.04	204.00	-1.96
KAC 1	219.81	217.00	2.81
KAC 2	222.24	217.40	4.84
KAC 3	222.57	217.50	5.07
KAC 4	218.58	216.80	1.78
KAC 5	222.51	217.40	5.11
KAC 6	222.47	217.20	5.27
KAC 7	219.58	217.10	2.48
KAC 8	221.18	217.00	4.18
KAC 9	220.84	217.00	3.84
KCB 1	203.96	204.80	-0.84
KCB 2	202.25	204.10	-1.85
KCB 3	201.71	202.90	-1.19
KCB 4	204.00	203.70	0.30
KCB 5	200.43	202.60	-2.17
KCB 6	200.97	202.90	-1.93
KCB 7	205.33	206.00	-0.67
KDB 1	208.20	208.10	0.10
KDB 2	206.79	207.50	-0.71
KDB 3	207.58	208.10	-0.52
KDB 4	206.28	207.30	-1.02
KDB 5	204.98	206.80	-1.82
KDT 1D	208.10	207.90	0.20
KRB 15	204.74	203.90	0.84
KRB 19D	203.70	202.80	0.90
KRP 1	218.52	217.40	1.12
KRP 2	219.42	218.40	1.02
KRP 3	219.47	219.20	0.27
KRP 4	218.57	218.10	0.47
KRP 5	216.03	215.70	0.33
KRP 6	217.44	216.40	1.04
KRP 7	215.38	214.40	0.98
KSB 1	203.80	206.00	-2.20
KSB 2	203.54	205.70	-2.16
KSB 5C	204.88	206.40	-1.52
KSB 5D	204.54	206.60	-2.06
KSM 1D	208.15	207.70	0.45
KSS 1D	174.43	179.10	-4.67
KSS 2D	164.78	169.70	-4.92
KSS 3D	163.95	168.50	-4.55
P-25B	177.95	179.10	-1.15
P-25C	194.56	193.50	1.06

Mean Residual:	0.04
Mean Standard Deviation:	2.50
Residual Sum of Squares:	274

Table 5-2. Simulated versus observed volumetric flux (cfs) along stream gage target locations.

	Simulated Results	Total Measured Baseflow Value	30% of Total Measured Flow
Indian Grave Branch Stations			
Station 1 to 2:	0.36 cfs	2.6 cfs	0.78 cfs
Station 2 to 3:	0.63 cfs	2.5 cfs	0.75 cfs
Total (Station 1 to 3):	0.99 cfs	5.1 cfs	1.53 cfs
Pen Branch Stations			
Station 9 to 10:	0.17 cfs	0.06 cfs	0.02 cfs
Station 10 to 11:	0.36 cfs	0.90 cfs	0.27 cfs
Total (Station 9 to 11):	0.53 cfs	0.96 cfs	0.29 cfs
Total (Pen Branch and Indian Grave Branch):	1.52 cfs		1.82 cfs

Table 5-3. Results of flow model sensitivity analysis.

Calibrated flow model	Mean Residual:	0.04
	Mean Standard Deviation:	2.50
	Residual Sum of Squares:	274

Sensitivity Run

Increased K_v in Tan Clay (Layer 7) to 0.01 ft/d	Mean Residual:	7.44
	Mean Standard Deviation:	4.52
	Residual Sum of Squares:	3315
Decreased K_v in Tan Clay (Layer 7) to 0.0001 ft/d	Mean Residual:	-8.88
	Mean Standard Deviation:	4.46
	Residual Sum of Squares:	4328
Increased K_h in A Horizon (Layer 10) to 5 ft/d	Mean Residual:	0.35
	Mean Standard Deviation:	2.70
	Residual Sum of Squares:	320
Decreased K_h in A Horizon (Layer 10) to 0.2 ft/d	Mean Residual:	0.24
	Mean Standard Deviation:	2.40
	Residual Sum of Squares:	250
Increased K_h in AA Horizon (Layer 9) to 30 ft/d	Mean Residual:	3.46
	Mean Standard Deviation:	3.18
	Residual Sum of Squares:	962
Decreased K_h in AA Horizon (Layer 9) to 1.2 ft/d	Mean Residual:	-1.39
	Mean Standard Deviation:	2.43
	Residual Sum of Squares:	339
Increased K_h in TZ (Layer 8) to 50 ft/d	Mean Residual:	12.81
	Mean Standard Deviation:	4.20
	Residual Sum of Squares:	5796
Decreased K_h in TZ (Layer 8) to 2 ft/d	Mean Residual:	-10.76
	Mean Standard Deviation:	4.62
	Residual Sum of Squares:	6011
Increased recharge globally by 30%	Mean Residual:	-4.96
	Mean Standard Deviation:	2.50
	Residual Sum of Squares:	1353
Decreased recharge globally by 30%	Mean Residual:	5.34
	Mean Standard Deviation:	3.03
	Residual Sum of Squares:	1647
Increased stream conductance by 10 times	Mean Residual:	-3.67
	Mean Standard Deviation:	4.43
	Residual Sum of Squares:	1438
Decreased stream conductance by 10 times	Mean Residual:	0.41
	Mean Standard Deviation:	2.96
	Residual Sum of Squares:	385

Table 5-4. Summary of sensitivity simulations performed with the solute transport model.

Parameter Varied	Time of Peak Concentration (yrs)	Peak Concentration (µg/L)
(Calibrated Model)	8	4.1
Reduce Recharge 30%	11.5	4.0
Increase Dispersivity	6.5	3.1
Decrease Dispersivity	9	4.7
Increase Effective Porosity	11	4.0
Decrease Effective Porosity	5	4.2

Sec 2.3 Ref 14

United States Department of Energy

Savannah River Site

Groundwater Flow and Contaminant Transport Modeling in Support of the RRSB Operable Unit (U)

INTERA Incorporated, Austin, TX

WSRC-RP-2002-4081
Revision 1
March 2003

Prepared by:
Westinghouse Savannah River Company, LLC
Savannah River Site
Aiken, South Carolina 29808

PREPARED FOR THE U.S. DEPARTMENT OF ENERGY UNDER CONTRACT DE-AC09-96SR18500

DISCLAIMER

This report was prepared by Westinghouse Savannah River Company, LLC (WSRC) for the United States Department of Energy under Contract No. DE-AC00-9-96SR18500 and is an account of work performed under that contract. Reference herein to any specific commercial product, process, or services by trademark, name, manufacturer or otherwise does not necessarily constitute or imply endorsement, recommendation, or favoring of same by WSRC or by the United States Government or any agency thereof.

Printed in the United States of America

Prepared for

U.S. Department of Energy

by

Westinghouse Savannah River Company

Aiken, South Carolina

EXECUTIVE SUMMARY

This document describes the development of groundwater flow and transport models at the R-Area Reactor Seepage Basins (RRSB) Operable Unit (OU). These models were developed to: 1) support the Corrective Measures Study/Feasibility Study (CMS/FS) remedial alternative evaluations, 2) determine the potential for previously identified contaminant migration constituents of concern (CMCOC) to break through to the water table above maximum concentration limits (MCL), and 3) determine the potential benefit of using a Groundwater Mixing Zone (GWMZ) as the remedy for Sr^{90} in the groundwater.

The RRSB are located to the north of the R-Area Reactor and consist of six unlined basins. These basins were excavated between 1957 and 1958 for the disposal of low-level radioactive purge water discharged from the R-Reactor disassembly building. The discharge water primarily contained Cs^{137}, Sr^{90}, and tritium. Discharge to the basins was discontinued by 1964 and the basins were backfilled. Various treatments were used to limit vegetative growth until the existing asphalt cover was installed over the entire RRSB area in 1996.

The results from soil borings and gamma-probe testing, conducted in 1996 and 1998, indicated that contaminant mass was adsorbed to the unsaturated-zone soils beneath the seepage basins. Spatial distributions of the constituent mass within the unsaturated zone were developed and termed a potential threat source mass (PTSM). The RFI/RI/BRA identified Am^{241}, C^{14}, $Pu^{239/240}$, and Sr^{90} as CMCOCs. Sr^{90} was identified as a constituent of concern (COC) because sampling of the shallow groundwater aquifer showed concentrations of Sr^{90} above the 8 pCi/L MCL.

Remedial Alternatives

The RRSB is currently covered with an 11-acre asphalt cover, which reduces the infiltration of water into the subsurface. To support the CMS/FS, groundwater flow and transport modeling was conducted for a suite of remedial alternatives. These alternatives had cover footprints equal to the existing 11-acre cover or a proposed 15-acre cover. The remedial alternative simulations developed are summarized as follows:

1. **Existing Asphalt Cover**: Assumed the existing asphalt cover was maintained throughout the duration of the simulation.

2. **Failed Asphalt Cover (No Action case)**: Assumed that the current asphalt cover catastrophically failed at the present time and the infiltration through the cover increased to one half of the background recharge rate.

3. **$1x10^{-5}$ cm/s Soil Cover with the existing cover footprint**: Assumed the existing asphalt cover was replaced with a soil-cover system with an average hydraulic conductivity of $1x10^{-5}$ cm/s and the same footprint as the existing cover.

4. **$1x10^{-5}$ cm/s Soil Cover with the 15-acre cover footprint**: Assumed the existing asphalt cover was replaced with a soil-cover system with an average hydraulic conductivity of $1x10^{-5}$ cm/s with a 15-acre cover footprint.

5. **Concrete Cover with the 15-acre cover footprint**: Assumed the existing asphalt cover was replaced with a concrete-cover system with a 15-acre cover footprint.

6. **Reinforced asphalt Cover with the 15-acre cover footprint**: Assumed the existing asphalt cover was replaced with a commercial modified-asphalt cover system (Reinforced Asphalt) with a 15-acre cover footprint.

7. **Enhanced Existing Asphalt Cover**: Assumed a sealant was placed on the existing asphalt cover that decreased the infiltration capacity through the cover. (This remedial alternative was only considered in the unsaturated-zone modeling and was not carried forward into the saturated-zone modeling.)

The groundwater flow and contaminant transport modeling was divided into two phases. Transport of CMCOCs within the unsaturated zone was modeled in the first phase. The second phase coupled the unsaturated-zone transport results for Sr^{90} to the saturated-zone flow and transport models.

Historical water levels within the shallow groundwater aquifer at the RRSB have shown periods of significant change in the water-level elevations; therefore, each unsaturated-zone simulation was modeled with both an assumed "high" and "low" water-table elevation. Thus the sensitivity of the concentrations calculated at the water-table surface to the location of the water table was incorporated into the unsaturated-zone modeling. In addition, the lack of observed C^{14} within the shallow groundwater aquifer indicates that the retardation of C^{14} is higher than expected within the unsaturated zone. Therefore, the magnitude of the distribution coefficient (K_d) for C^{14} is unknown at this time. To investigate the possible range in the sorption for C^{14}, simulations were conducted with K_d values of 6, 55, and 500 mL/g.

CMCOC Breakthrough at the Water Table

The concentration breakthrough curves were developed based on an unsaturated-zone flow and transport analysis. Estimates of the infiltration rate through the PTSM were developed for each of the remedial alternatives. Using the developed source mass distributions and the estimated infiltration rates, transient concentration profiles (breakthrough curves) were generated for each CMCOC at the water-table surface for each remedial alternative.

The CMCOC concentrations calculated at the water-table surface were then converted to a groundwater concentration for comparison to the corresponding MCL. This conversion was based on a simple mixing volume in which the concentrations at the water table were mixed with the larger saturated-zone groundwater volume. The results of these calculations demonstrated that most of the CMCOC concentrations decreased to below the MCL once mixed. However, some of the CMCOC concentrations still exceeded the MCL over time, especially for the higher infiltration rate cases. The unsaturated-zone transport simulations demonstrated that the

magnitude of the concentrations calculated at the water-table surface were directly proportional to the infiltration rate through the basin cover.

Saturated Groundwater Flow and Sr^{90} Transport Modeling

Saturated-zone groundwater flow and contaminant transport simulations were conducted to determine if the development of a GWMZ for Sr^{90}, the only groundwater COC that was detected in monitoring wells above its MCL, would be appropriate. The model domain for the saturated-zone modeling was centered on the RRSB area and was bounded on the east by Joyce Branch and Pond A, on the west by Mill Creek, on the south by no flow boundaries and by constant head boundaries to the southwest and north. Vertically, the domain extended to the top of the Gordon Confining Unit, and thus included the entire Upper Three Runs Aquifer (UTRA).

As stated previously, water-level elevations within the shallow groundwater aquifer have varied over time. Therefore, for the calibration of the saturated-zone groundwater flow model, an average water level was calculated for each observation well. These average values were based on the full historical range of data and were used as the calibration targets during the development of the calibrated steady-state flow field based on the existing asphalt cover.

A concentration distribution of the present Sr^{90} mass within the shallow groundwater aquifer was developed based on observed Sr^{90} groundwater concentrations. This distribution was initialized within the transport model as the starting concentrations within the groundwater. The transient Sr^{90} concentrations, calculated from the unsaturated-zone transport modeling, were incorporated into the saturated-zone transport model as the Sr^{90} concentration in the recharge entering the ground surface. The time-stepping of the saturated-zone transport model was designed such that the detailed transient nature of the concentration to the water table could be accurately incorporated into the saturated zone through the simulation time of 400 years.

The remedial alternatives were simulated by changing the areal footprint of the basin cover and the infiltration rate (recharge rate) through the cover, as applicable. A new steady-state flow field was developed for each remedial alternative based on modifications to the calibrated flow field. The flow field for each remedial alternative was then used for the applicable transient Sr^{90} transport model. The remedial alternative transport simulations also included the effects of sorption and radioactive decay.

The results for the remedial alternative simulations are very similar. For example, the maximum Sr^{90} concentrations within the "transmissive zone" (TZ) unit of the UTRA are similar for all of the remedial alternative simulations. Flow within the saturated zone is predominantly vertical within the upper portions of the UTRA; indicating that Sr^{90} will not discharge to surface water bodies. As a result of the significant vertical flow component, Sr^{90} concentrations greater than 8 pCi/L are simulated to reach just below the TZ into the top of the TCCZ within the UTRA. These results suggest that development of a GWMZ application for Sr^{90} would be appropriate.

TABLE OF CONTENTS

EXECUTIVE SUMMARY ES-1

LIST OF TABLES iii

LIST OF FIGURES iv

ACRONYMS AND ABBREVIATIONS x

1.0 INTRODUCTION 1-1
- 1.1 Process History and Unit Description 1-2
- 1.2 Hydrogeological Conceptual Model 1-3
  - 1.2.1 Geological Setting 1-4
  - 1.2.2 Hydrostratigraphy 1-4
- 1.3 Summary of Approach 1-7
- 1.4 Remedial Alternatives 1-8
- 1.5 Review of Historical Water Levels 1-9

2.0 UNSATURATED-ZONE MODEL 2-1
- 2.1 Source Term Development 2-1
- 2.2 Selection of the Computer Code 2-1
- 2.3 Assignment of Model Parameters 2-2
- 2.4 Assumptions 2-5
- 2.5 Results 2-5
  - 2.5.1 Basin 2-6
  - 2.5.2 Water-table Elevation 2-6
  - 2.5.3 Cover Configuration 2-7
  - 2.5.4 Distribution Coefficient 2-7
  - 2.5.5 Summary 2-8
- 2.6 Estimated Saturated-Zone Concentrations 2-8
- 2.7 Conclusions 2-13

3.0 SATURATED-ZONE FLOW MODEL 3-1
- 3.1 Selection of the Computer Code 3-1
- 3.2 Assignment of Boundary Conditions 3-1
- 3.3 Assignment of Flow Model Parameters 3-5
- 3.4 Assumptions 3-6
- 3.5 Discretization of the Model Domain 3-6
- 3.6 Flow Model Calibration Results 3-7
- 3.7 Particle Track Analysis 3-8
- 3.8 Sensitivity Analysis 3-9
- 3.9 Remedial Alternative Flow Fields 3-13

4.0 SATURATED-ZONE TRANSPORT MODEL 4-1

4.1 Selection of the Computer Code 4-1
4.2 Assignment of Transport Parameters 4-1
4.3 Source/Mass Loading 4-2
4.3 Assumptions 4-3
4.5 Results 4-3
4.6 Transport Model Sensitivity Analysis 4-4
4.6.1 Longitudinal Dispersivity 4-5
4.6.2 Distribution Coefficient (K_d) 4-5
4.6.3 Porosity 4-6
4.7 Results of the Remedial Alternative Simulations 4-6
4.7.1 Failed Asphalt Cover (No Action) 4-6
4.7.2 $1x10^{-5}$ cm/s Soil Cover with Existing Cover Footprint 4-7
4.7.3 $1x10^{-5}$ cm/s Soil Cover with the 15-acre Cover Footprint 4-7
4.7.4 Concrete Cover with the 15-acre Cover Footprint 4-7
4.7.5 Reinforced Asphalt Cover with the 15-acre Cover Footprint 4-8
4.7.6 Summary of Remedial Alternative Simuluations 4-8

5.0 MODEL LIMITATIONS AND UNCERTAINTIES 5-1

6.0 SUMMARY AND CONCLUSIONS 6-1

7.0 REFERENCES 7-1

LIST OF TABLES

Table 1-1 Lithostratigraphic and Hydrostratigraphic Units at the RRSB (WSRC, 2001a) 1-5
Table 1-2 Modeled Hydrostratigraphic Units 1-6
Table 1-3 Listing of Remedial Alternative Simulations 1-8
Table 2-1 Basecase Radionuclide Parameters 2-4
Table 2-2 Maximum Saturated-Zone Groundwater Concentrations (pCi/L) 2-10
Table 2-3 MCL or RBA Values for Each Radionuclide 2-12
Table 3-1 Calibration Targets and Residuals 3-2
Table 3-2 Initial Hydraulic Conductivity Values for the Groundwater Flow Model 3-6
Table 3-3 Vertical Layers in the Saturated-Zone Flow and Transport Models 3-7
Table 3-4 Calibrated Hydraulic Conductivity Values 3-8
Table 3-5 Parameter Values Used in the Flow Model Sensitivity Analysis 3-10
Table 3-6 Flow Model Sensitivity Analysis Results 3-11
Table 4-1 Summary of Transport Parameters for the Saturated-Zone Model 4-1
Table 4-2 Summary of Sr^{90} Activity Distribution for the Saturated-Zone Transport Simulations 4-10

LIST OF FIGURES

Figure 1-1 Location of the R-Area in relation to the SRS boundary. 1-11
Figure 1-2 Location of R-Reactor Building, R-Reactor Seepage Basins, and surface water features. 1-12
Figure 1-3 Location of the process sewer line (red lines), an abandoned sanitary sewer line (yellow lines), and the discharge lagoon. 1-13
Figure 1-4 R-Reactor Seepage Basins. 1-14
Figure 1-5 Location of RPC-1 and P-20 well clusters. 1-15
Figure 1-6 Extent of Sr^{90} contamination, as defined by the MCL of 8 pCi/L, within the RRSB OU shallow groundwater aquifer. 1-16
Figure 1-7 Time series of Sr^{90} concentrations in selected monitoring wells for the RRSB OU. 1-17
Figure 1-8 Time series of water-level elevations in selected monitoring wells for the RRSB OU. 1-18
Figure 1-9 Original HCM for the RRSB OU. 1-19
Figure 1-10 Modified HCM for the RRSB OU. 1-20
Figure 1-11 Location of the existing 11-acre cover (white outline) and the proposed 15-acre cover (yellow fill). 1-21
Figure 2-1 Source-term soil concentrations (pCi/g) for Basins 1, 3, and 6. 2-14
Figure 2-2 Comparison of HYDRUS and MT3DMS Sr^{90} transport results for Basin 1 and a high water table elevation. 2-15
Figure 2-3 Generalized conceptual models for Basins 1, 3, and 6. 2-16
Figure 2-4 Photographs showing the surface condition of the existing asphalt cover located over the RRSB. 2-17
Figure 2-5a Unsaturated-zone contaminant concentrations (pCi/L) for Basin 1 with a high water table. 2-18
Figure 2-5b Unsaturated-zone contaminant concentrations (pCi/L) for Basin 1 with a high water table. 2-19
Figure 2-6a Unsaturated-zone contaminant concentrations (pCi/L) for Basin 3 with a high water table. 2-20
Figure 2-6b Unsaturated-zone contaminant concentrations (pCi/L) for Basin 3 with a high water table. 2-21
Figure 2-7 Unsaturated-zone contaminant concentrations (pCi/L) for Basin 6 with a high water table. 2-22
Figure 2-8a Unsaturated-zone contaminant concentrations (pCi/L) for Basin 1 with a low water table. 2-23
Figure 2-8b Unsaturated-zone contaminant concentrations (pCi/L) for Basin 1 with a low water table. 2-24
Figure 2-9a Unsaturated-zone contaminant concentrations (pCi/L) for Basin 3 with a low water table. 2-25
Figure 2-9b Unsaturated-zone contaminant concentrations (pCi/L) for Basin 3 with a low water table. 2-26
Figure 2-10 Unsaturated-zone contaminant concentrations (pCi/L) for Basin 6 with a low water table. 2-27

Figure 2-11 Conceptual model for the calculation of the maximum saturated-zone groundwater concentrations. 2-28
Figure 2-12a Saturated-zone contaminant concentrations (pCi/L) for Basin 1 with a high water table. 2-29
Figure 2-12b Saturated-zone contaminant concentrations (pCi/L) for Basin 1 with a high water table. 2-30
Figure 2-13a Saturated-zone contaminant concentrations (pCi/L) for Basin 3 with a high water table. 2-31
Figure 2-13b Saturated-zone contaminant concentrations (pCi/L) for Basin 3 with a high water table. 2-32
Figure 2-14 Saturated-zone contaminant concentrations (pCi/L) for Basin 6 with a high water table. 2-33
Figure 2-15a Saturated-zone contaminant concentrations (pCi/L) for Basin 1 with a low water table. 2-34
Figure 2-15b Saturated-zone contaminant concentrations (pCi/L) for Basin 1 with a low water table. 2-35
Figure 2-16a Saturated-zone contaminant concentrations (pCi/L) for Basin 3 with a low water table. 2-36
Figure 2-16b Saturated-zone contaminant concentrations (pCi/L) for Basin 3 with a low water table. 2-37
Figure 2-17 Saturated-zone contaminant concentrations (pCi/L) for Basin 6 with a low water table. 2-38
Figure 3-1 Model domain for the saturated-zone flow and transport models. 3-14
Figure 3-2a Lateral boundary conditions for the saturated-zone flow model. 3-15
Figure 3-2b Lateral boundary conditions for the saturated-zone flow model. 3-16
Figure 3-3 Average interpolated water-table surface for the "undifferentiated", "A", and "AA" soil horizons. 3-17
Figure 3-4 Average interpolated potentiometric surface for the TZ. 3-18
Figure 3-5 Average interpolated potentiometric surface for the MAZ. 3-19
Figure 3-6 Average interpolated potentiometric surface for the LAZ. 3-20
Figure 3-7 Model recharge to the uppermost saturated cells for the saturated-zone flow model for the condition of the existing asphalt cap. 3-21
Figure 3-8 Lateral model grid for the saturated-zone flow and transport models showing cross-section locations. 3-22
Figure 3-9 Oblique view of cross sections through the model grid for the saturated-zone flow and transport models. 3-23
Figure 3-10 Water-table surface (combined "A" and "AA" soil horizons) for the calibrated saturated-zone flow model using the existing asphalt cover. 3-24
Figure 3-11 TZ potentiometric surface for the calibrated saturated-zone flow model. 3-25
Figure 3-12 MAZ potentiometric surface for the calibrated saturated-zone flow model. 3-26
Figure 3-13 LAZ potentiometric surface for the calibrated saturated-zone flow model. 3-27

Figure 3-14 Computed heads versus observed heads and residual versus observed heads for the calibrated saturated-zone flow model. 3-28
Figure 3-15 Hydraulic conductivity zones in the "A" and "AA" horizons. 3-29
Figure 3-16 Hydraulic conductivity zones in the TZ, TCCZ, and MAZ. 3-30
Figure 3-17 Lateral migration of particles for the calibrated saturated-zone flow model. 3-31
Figure 3-18 Lateral migration of particles released from each of the six seepage basins. 3-32
Figure 3-19 Particle pathlines along cross sections created for selected particles released from each of the six seepage basins. 3-33
Figure 3-20 Sensitivity of root mean squared error. 3-34
Figure 3-21 Changes in downward flow from "A" horizon. 3-35
Figure 3-22 Changes in downward flow from "AA" horizon. 3-36
Figure 3-23 Changes in downward flow from TZ. 3-37
Figure 3-24 Changes in downward flow from TCCZ. 3-38
Figure 3-25 Changes in downward flow from MAZ. 3-39
Figure 3-26 Changes in downward flow from TCLC. 3-40
Figure 3-27 Changes in baseflows to Joyce Branch. 3-41
Figure 3-28 Changes in baseflows to Mill Creek. 3-42
Figure 3-29 Changes in baseflows to the R-Effluent Canal and Pond A. 3-43
Figure 3-30 Water-table surface for the Failed Asphalt Cover flow field (recharge = 7.5 in/yr). 3-44
Figure 3-31 Water-table surface for the $1x10^{-5}$ cm/s Soil Cover flow field with the existing asphalt cover footprint (recharge = 6.2 in/yr). 3-45
Figure 3-32 Water-table surface for the $1x10^{-5}$ cm/s Soil Cover flow field with the 15-acre cover footprint (recharge = 6.2 in/yr). 3-46
Figure 3-33 Water-table surface for Concrete Cover flow field with the 15-acre cover footprint (recharge = 3.0 in/yr). 3-47
Figure 3-34 Water-table surface for Reinforced Asphalt Cover flow field with the 15-acre cover footprint (recharge = 1.0 in/yr). 3-48
Figure 4-1 Location of source loading grid cells for the saturated-zone transport model. 4-11
Figure 4-2 Sr^{90} saturated-zone initial concentration (pCi/L) map. 4-12
Figure 4-3 Plan view of model grid showing the location of three cross-sectional lines. 4-13
Figure 4-4 Existing Asphalt Cover simulation Sr^{90} breakthrough curves for the three observation locations within the TZ. 4-14
Figure 4-5 Plan view of Sr^{90} concentrations (pCi/L) within the "A" horizon for the Existing Asphalt Cover. 4-15
Figure 4-6 Existing Asphalt Cover: Cross-sectional views of Sr^{90} concentrations (pCi/L) along A-A' at 20, 50, 100, 200, 300, and 400 years. 4-16
Figure 4-7 Existing Asphalt Cover: Cross-sectional views of Sr^{90} concentrations (pCi/L) along B-B' at 20, 50, 100, 200, 300, and 400 years. 4-17
Figure 4-8 Existing Asphalt Cover: Cross-sectional views of Sr^{90} concentrations (pCi/L) along C-C' at 20, 50, 100, 200, 300, and 400 years. 4-18

Figure 4-9 Existing Asphalt Cover: Plan view showing the maximum lateral extent of Sr^{90} concentrations greater than the 8 pCi/L MCL within the TZ. 4-19
Figure 4-10a Sensitivity analysis Sr^{90} concentration curves for observation location #1 within the TZ. 4-20
Figure 4-10b Sensitivity analysis Sr^{90} concentration curves for observation location #2 within the TZ. 4-21
Figure 4-10c Sensitivity analysis Sr^{90} concentration curves for observation location #3 within the TZ. 4-22
Figure 4-10d Sensitivity analysis Sr^{90} concentration curves for the selected observation locations within the TZ (K_d = 0.6 mL/g). 4-23
Figure 4-11 Sensitivity results for a longitudinal dipsersivity of 10 ft. A-A' cross-sectional views of Sr^{90} concentrations (pCi/L) at 20, 50,100, 200, 300, and 400 years. 4-24
Figure 4-12 Sensitivity results for a longitudinal dipsersivity of 10 ft. B-B' cross-sectional views of Sr^{90} concentrations (pCi/L) at 20, 50, 100, 200, 300, and 400 years. 4-25
Figure 4-13 Sensitivity results for a longitudinal dipsersivity of 10 ft. C-C' cross-sectional views of Sr^{90} concentrations (pCi/L) at 20, 50, 100, 200, 300, and 400 years. 4-26
Figure 4-14 Sensitivity results for a longitudinal dipsersivity of 40 ft. A-A' cross-sectional views of Sr^{90} (pCi/L) concentrations at 20, 50, 100, 200, 300, and 400 years. 4-27
Figure 4-15 Sensitivity results for a longitudinal dipsersivity of 40 ft. B-B' cross-sectional views of Sr^{90} (pCi/L) concentrations at 20, 50, 100, 200, 300, and 400 years. 4-28
Figure 4-16 Sensitivity results for a longitudinal dipsersivity of 40 ft. C-C' cross-sectional views of Sr^{90} (pCi/L) concentrations at 20, 50, 100, 200, 300, and 400 years. 4-29
Figure 4-17 Sensitivity results for a sorption coefficient of 0.6 mL/g. A-A' cross-sectional views of Sr^{90} (pCi/L) concentrations at 20, 50, 100, 200, 300, and 400 years. 4-30
Figure 4-18 Sensitivity results for a sorption coefficient of 0.6 mL/g. B-B' cross-sectional views of Sr^{90} (pCi/L) concentrations at 20, 50, 100, 200, 300, and 400 years. 4-31
Figure 4-19 Sensitivity results for a sorption coefficient of 0.6 mL/g. C-C' cross-sectional views of Sr^{90} (pCi/L) concentrations at 20, 50, 100, 200, 300, and 400 years. 4-32
Figure 4-20 Sensitivity results for a sorption coefficient of 60 mL/g. A-A' cross-sectional views of Sr^{90} (pCi/L) concentrations at 20, 50, 100, 200, 300, and 400 years. 4-33
Figure 4-21 Sensitivity results for a sorption coefficient of 60 mL/g. B-B' cross-sectional views of Sr^{90} (pCi/L) concentrations at 20, 50, 100, 200, 300, and 400 years. 4-34

Figure 4-22 Sensitivity results for a sorption coefficient of 60 mL/g. C-C' cross-sectional views of Sr^{90} (pCi/L) concentrations at 20, 50, 100, 200, 300, and 400 years. 4-35
Figure 4-23 Sensitivity results for a porosity of 0.20. A-A' cross-sectional views of Sr^{90} concentrations (pCi/L) at 20, 50,100, 200, 300, and 400 years. 4-36
Figure 4-24 Sensitivity results for a porosity of 0.20. B-B' cross-sectional views of Sr^{90} concentrations (pCi/L) at 20, 50, 100, 200, 300, and 400 years. 4-37
Figure 4-25 Sensitivity results for a porosity of 0.20. C-C' cross-sectional views of Sr^{90} concentrations (pCi/L) at 20, 50, 100, 200, 300, and 400 years. 4-38
Figure 4-26 Sensitivity results for a porosity of 0.30. A-A' cross-sectional views of Sr^{90} concentrations (pCi/L) at 20, 50, 100, 200, 300, and 400 years. 4-39
Figure 4-27 Sensitivity results for a porosity of 0.30. B-B' cross-sectional views of Sr^{90} concentrations (pCi/L) at 20, 50,100, 200, 300, and 400 years. 4-40
Figure 4-28 Sensitivity results for a porosity of 0.30. C-C' cross-sectional views of Sr^{90} concentrations (pCi/L) at 20, 50, 100, 200, 300, and 400 years. 4-41
Figure 4-30 Failed Asphalt Cover: Cross-sectional views of Sr^{90} concentrations (pCi/L) along A-A' at 20, 50, 100, 200, 300, and 400 years. 4-43
Figure 4-31 Failed Asphalt Cover: Cross-sectional views of Sr^{90} concentrations (pCi/L) along B-B' at 20, 50, 100, 200, 300, and 400 years. 4-44
Figure 4-32 Failed Asphalt Cover: Cross-sectional views of Sr^{90} concentrations (pCi/L) along C-C' at 20, 50, 100, 200, 300, and 400 years. 4-45
Figure 4-33 Failed Asphalt Cover: Plan view showing the maximum lateral extent of Sr^{90} concentrations greater than the 8 pCi/L MCL within the TZ. 4-46
Figure 4-34 $1x10^{-5}$ cm/s Soil Cover with the Existing Asphalt Cover footprint: Cross-sectional views of Sr^{90} concentrations (pCi/L) along A-A' at 20, 50, 100, 200, 300, and 400 years. 4-47
Figure 4-35 $1x10^{-5}$ cm/s Soil Cover with the Existing Asphalt Cover footprint: Cross-sectional views of Sr^{90} concentrations (pCi/L) along B-B' at 20, 50, 100, 200, 300, and 400 years. 4-48
Figure 4-36 $1x10^{-5}$ cm/s Soil Cover with the Existing Asphalt Cover footprint: Cross-sectional views of Sr^{90} concentrations (pCi/L) along C-C' at 20, 50, 100, 200, 300, and 400 years. 4-49
Figure 4-37 $1x10^{-5}$ cm/s Soil Cover with the Existing Asphalt Cover footprint: Plan view showing the maximum lateral extent of Sr^{90} concentrations greater than the 8 pCi/L MCL within the TZ. 4-50
Figure 4-38 $1x10^{-5}$ cm/s Soil Cover with the 15-acre cover footprint: Cross-sectional views of Sr^{90} concentrations (pCi/L) along A-A' at 20, 50, 100, 200, 300, and 400 years. 4-51
Figure 4-39 $1x10^{-5}$ cm/s Soil Cover with the 15-acre cover footprint: Cross-sectional views of Sr^{90} concentrations (pCi/L) along B-B' at 20, 50, 100, 200, 300, and 400 years. 4-52
Figure 4-40 $1x10^{-5}$ cm/s Soil Cover with the 15-acre cover footprint: Cross-sectional views of Sr^{90} concentrations (pCi/L) along C-C' at 20, 50, 100, 200, 300, and 400 years. 4-53

Figure 4-41 $1x10^{-5}$ cm/s Soil Cover with the 15-acre cover footprint: Plan view showing the maximum lateral extent of Sr^{90} concentrations greater than the 8 pCi/L MCL within the TZ. 4-54
Figure 4-42 Concrete Cover with the 15-acre cover footprint: Cross-sectional views of Sr^{90} concentrations (pCi/L) along A-A' at 20, 50, 100, 200, 300, and 400 years. 4-55
Figure 4-43 Concrete Cover with the 15-acre cover footprint: Cross-sectional views of Sr^{90} concentrations (pCi/L) along B-B' at 20, 50, 100, 200, 300, and 400 years. 4-56
Figure 4-44 Concrete Cover with the 15-acre cover footprint: Cross-sectional views of Sr^{90} concentrations (pCi/L) along C-C' at 20, 50, 100, 200, 300, and 400 years. 4-57
Figure 4-45 Concrete Cover with the 15-acre cover footprint: Plan view showing the maximum lateral extent of Sr^{90} concentrations greater than the 8 pCi/L MCL within the TZ. 4-58
Figure 4-46 Reinforced Asphalt Cover with the 15-acre cover footprint: Cross-sectional views of Sr^{90} concentrations (pCi/L) along A-A' at 20, 50, 100, 200, 300, and 400 years. 4-59
Figure 4-47 Reinforced Asphalt Cover with the 15-acre cover footprint: Cross-sectional views of Sr^{90} concentrations (pCi/L) along B-B' at 20, 50, 100, 200, 300, and 400 years. 4-60
Figure 4-48 Reinforced Asphalt Cover with the 15-acre cover footprint: Cross-sectional views of Sr^{90} concentrations (pCi/L) along C-C' at 20, 50, 100, 200, 300, and 400 years. 4-61
Figure 4-49 Reinforced Asphalt Cover with the 15-acre cover footprint: Plan view showing the maximum lateral extent of Sr^{90} concentrations greater than the 8 pCi/L MCL within the TZ. 4-62
Figure 4-50 Breakout of source loading locations as defined in Table 4-2. 4-63

ACRONYMS AND ABBREVIATIONS

amsl	above mean sea level
BYU	Brigham Young University
CBRP	C-Area/Burning/Rubble Pit
Ci	Curies
cm	centimeters
CMCOC	contaminant migration constituent of concern
CMS/FS	Corrective Measures Study/Feasibility Study
cm/s	centimeters per second
COC	constituent of concern
CPT	cone-penetrometer testing
ft	feet
ft/day	feet per day
GAU	Gordon Aquifer Unit
GCU	Gordon Confining Unit
gm	gram
g/cm^3	grams per cubic centimeter
g/L	gram per liter
GMS	Groundwater Modeling System
GWMZ	Groundwater Mixing Zone
HCM	hydrogeological conceptual model
HELP	Hydrologic Evaluation of Landfill Performance
HYDRUS	model for movement of water, heat and solutes in variably-saturated media (code)
in	inches
in/yr	inches per year
K_d	distribution coefficient
LAZ	lower aquifer zone
L/g	liter per gram
MAZ	middle aquifer zone
MCL	maximum contaminant level
mg/L	milligrams per liter
mL	milliliter
mL/g	milliliter per gram
mL/yr	milliliter per year
MODFLOW	a modular three-dimensional finite-difference groundwater flow model (code)
MODPATH	a particle-tracking model based on MODFLOW flow fields (code)
MT3DMS	a modular three-dimensional, multi-species transport model (code)
ng/L	nanograms per liter
OU	operable unit
pCi	picoCuries
pCi/g	picoCuries per gram
pCi/L	picoCuries per Liter
PTSM	principal threat source material
R	retardation value
RA	remedial alternative

RCRA	Resource Conservation and Recovery Act
RFI/RI/BRA	RCRA Facility Investigation/Remedial Investigation/Baseline Risk Assessment
RBA	Risk Based Activity
RMS	root mean square
RRSB	R-Reactor Area Seepage Basins
SRS	Savannah River Site
TC	tan clay
TCCZ	tan clay confining zone
TCLC	tan clay lower clay
TZ	transmissive zone
UAZ	upper aquifer zone
USDA	U.S. Department of Agriculture
US DOD	U.S. Department of Defense
UTRA	Upper Three Runs Aquifer
WSRC	Westinghouse Savannah River Company

1.0 INTRODUCTION

This report describes a series of groundwater flow and contaminant transport simulations conducted for the R-Reactor Area Seepage Basins (RRSB) Operable Unit (OU) at the Savannah River Site (SRS) near Aiken, South Carolina. This groundwater modeling was performed to: 1) support the Corrective Measures Study/Feasibility Study (CMS/FS) remedial alternative evaluations, 2) determine the potential for previously identified contaminant migration constituents of concern (CMCOCs) to break through to the water table above maximum concentration limits (MCL), and 3) determine the potential benefit of using a Groundwater Mixing Zone (GWMZ) as the remedy for Sr^{90} in the groundwater.

Historical monitoring data over the past 40 years, as described in the RCRA Facility Investigation/Remedial Investigation Report with Baseline Risk Assessment for the R-Reactor Seepage Basins/108-4R Overflow Basin Operable Unit (RFI/RI/BRA report) (WSRC, 2001a), has identified Am^{241}, C^{14}, $Pu^{239/240}$, and Sr^{90} as CMCOCs currently in the soil. Sr^{90} was also identified as a constituent of concern (COC) because it was detected in the groundwater at concentrations above the 8 pico-Curie per liter (pCi/L) MCL. Therefore, the modeling presented in this report simulated the transport of the CMCOCs within the unsaturated zone beneath the RRSB and the transport of Sr^{90}, the only COC, within the saturated-zone.

At the RRSB OU, characterization of the geologic properties, hydrologic properties, and contaminant extent has been conducted using the following methods:

- surface-soil sampling
- subsurface-soil sampling
- monitoring well installation
- piezometer installation
- groundwater sampling
- aquifer pump testing
- aquifer slug testing
- cone-penetrometer testing (CPT) pushes
- gamma-probe testing
- soil-moisture testing
- geotechnical sampling of confining layers

Information gathered from these investigations was used in the development of the RFI/RI/BRA report (WSRC, 2001a). Based on the groundwater sampling activities, Sr^{90} is the only constituent with significant and persistent observed concentrations in the upper portion of the shallow groundwater aquifer in the immediate vicinity of the RRSB. Some of these concentrations are greater than the 8 pCi/L MCL; however, the contamination has not spread significantly over the last 40 years.

1.1 Process History and Unit Description

A detailed description of the RRSB OU can be found in the RFI/RI/BRA report (WSRC, 2001a). The R-Reactor Area is located in the east-central portion of the SRS, approximately 5.2 miles from the nearest SRS boundary (Figure 1-1). The RRSB unit is located to the north of the R-Reactor building and consists of six unlined seepage basins (Figure 1-2), a process sewer line, and an abandoned sanitary sewer line and discharge lagoon (Figure 1-3). The six basins were excavated in succession between June 1957 and March 1958 to receive low-level radioactive purge water from the R-Reactor disassembly building. The purge water primarily contained Cs^{137}, Sr^{90}, and tritium (WSRC, 2001a).

Basin 1 (Figure 1-4) was constructed for routine reactor operations with most of the wastewater from the R-Reactor discharged to the R-Effluent Canal (see Figure 1-2). In November 1957, a failed calorimeter experiment resulted in the discharge of large volumes of radioactive wastewater to the R-Effluent Canal and to Basin 1 (WSRC, 1999a). Given the large volume of water being discharged, Basins 2 and 3 were subsequently constructed. During the discharge of wastewater to the basins, water was observed within and discharging from the sanitary sewer system. The sanitary sewer lines had been inadvertently breached during the construction of Basin 1. To eliminate discharge from the sanitary sewer system, the water level within Basin 1 was lowered and portions of the sewer system were backfilled with concrete. Basin 4 was subsequently constructed and Basin 1 was deactivated in January 1958. Slow seepage rates from Basins 2, 3, and 4 resulted in the construction of Basins 5 and 6. The R-Reactor was shutdown in 1964 and decontamination activities were conducted. During operation of the RRSB unit, approximately 5 million gallons of wastewater were discharged to the basins (WSRC, 1999a).

Groundwater monitoring at the RRSB has been performed since shortly after the failed calorimeter test in 1957. By 1960, 39 permanent monitoring wells (A and B series) were installed. Since then, numerous additional monitoring wells have been installed and quarterly monitoring of wells has been performed since the late 1980s. A Phase I investigation was conducted during 1995 and 1996 to address known data gaps and uncertainties related to the contaminant sources, release mechanisms, and exposure pathways (WSRC, 2001a). In 1996, the existing asphalt cover was placed over the seepage basins to limit vegetative growth. Based on the results of the Phase I investigation, a Phase II investigation was conducted in 1997 to gather additional data and to determine the extent of the required remedial efforts (WSRC, 2001a). Several smaller characterization activities were carried out subsequent to the Phase II investigation (WSRC, 2001a). These included aquifer-pumping tests in the RPC-1 and P-20 wells clusters (Figure 1-5), soil moisture and resistivity logging, and additional groundwater sampling to determine the extent of radiological contamination.

Investigation activities within the R-Reactor Area have shown that to date, the extent of the groundwater contamination from all radiological constituents has not extended significantly beyond the boundaries of the RRSB and Sr^{90} is the predominant constituent present within the shallow groundwater aquifer beneath the RRSB OU. Figure 1-6 presents the extent of the Sr^{90} contamination above the 8 pCi/L MCL within the shallow groundwater aquifer, as interpreted from monitoring well data and CPT data. Based on soil data and process history, Basins 1

through 3 received the most contamination. Although soil contamination also exists in Basins 4, 5, and 6, monitoring well data near these basins show no groundwater contamination.

Between 1998 and 2000, the water-table elevations within the RRSB OU dropped (WSRC, 2001a). As a result, the water levels in numerous wells dropped below the screened interval, resulting in fewer sampling points and incomplete coverage of the shallow water-table aquifer within the immediate vicinity of the RRSB. Therefore, for the initialization of Sr^{90} within the groundwater for the transport modeling activities described in this report, WSRC derived a Sr^{90} plume configuration which honors both the observed historical groundwater data and soil data extrapolated to groundwater for Basins 1 through 3 (see Section 4.3).

Figure 1-7 presents a series of plots which illustrate the transient nature of the Sr^{90} concentrations in fourteen monitoring wells located within the upper units of the shallow groundwater system. Of the remaining monitoring wells located within the shallow groundwater system, none showed persistent detections of Sr^{90}. In the monitoring wells sampled during the 1992 to 1995 timeframe, a distinct rise and fall in the Sr^{90} concentration is observed. This change in concentration appears to correspond to a broader rise and fall of the water-table elevation, as observed in the corresponding transient water level plots presented in Figure 1-8.

1.2 Hydrogeological Conceptual Model

A hydrogeological conceptual model (HCM) is a simplified representation of a groundwater flow system. Figure 1-9 presents the HCM for the RRSB OU as defined at the start of the modeling task. Figure 1-9 shows the various hydrostratigraphic layers, the shallow groundwater aquifer, the assumed groundwater flow directions and discharge location, and the contaminant source areas. For the initial RRSB OU HCM, it was assumed that:

- the shallow water table is located in "A" and "AA" horizons;
- the vertical head gradients between the "A"/"AA" horizon and the transmissive zone are large;
- under the seepage basins, groundwater flow is primarily vertically downward;
- relatively low hydraulic conductivity in the "A" and "AA" horizons results in slow percolation to the transmissive zone;
- the tan clay confining zone is an effective confining layer.

This HCM suggested that the flow within the transmissive zone was predominantly horizontal with flow discharging into the local surface water bodies, such as the Old R-Turnout Canal. However, as a result of the saturated-zone groundwater flow modeling presented in Section 3.0, modification to the HCM was required.

Figure 1-10 presents the revised HCM. The main modification in the HCM is the result of strong vertical flow and transport through the transmissive zone and tan clay confining zone and into

the lower aquifer zone. Also, the flow through the seepage basins is predominantly vertical through the transmissive zone with no contaminated groundwater observed to discharge to the local surface water bodies.

The surface topographic relief in the area of the seepage basins drops approximately 20 feet (ft) and predominantly trends from Basin 1 at the south towards Basin 5 in the north (WSRC, 2001a). The western edge of the basin area slopes towards the west. Surface water drainage from the RRSB that flows towards the north and west flows into Mill Creek. The surface water that flows towards the east enters into the R-Effluent Canal and Pond A (see Figure 1-2).

1.2.1 Geological Setting

The SRS is located on the Aiken Plateau within the Upper Atlantic Coastal Plain Province (Aadland and Bledsoe, 1990). The Aiken Plateau is highly dissected by several drainage features. The plateau is characterized as having steep-sided valleys and broad interfluvial areas. The plateau is considered to be well drained; however, several depressions or poorly-drained areas (Carolina Bays) exist as a result of primary depositional processes or secondary dissolution processes.

The Atlantic Coastal Plain is underlain by a wedge of sediments which increase in thickness down dip in a southeasterly direction from the SRS towards the Atlantic Ocean. The sediments mainly consist of unconsolidated interbedded sands, silts, and clays; but some gravel and carbonate deposits are also present. The unconsolidated sediments lie on a southeast-dipping crystalline basement. Although some clay stratigraphic units at the SRS are laterally extensive, most vary in thickness and typically are not extensive. These irregular clay units yield an intricate system of aquifers intermingled with discontinuous aquitards which vary greatly in overall vertical connectivity.

The coastal plain sediments of Tertiary and Quaternary age occur surficially in places within the SRS boundaries (Fallaw, 1991). The coastal plain sediment wedge and the surficial alluvial sediments overlie Paleozoic crystalline and metamorphic rocks associated with the Appalachian Orogeny.

The sedimentary formations encountered in the vicinity of the RRSB OU are of the Eocene and Micoene epochs of Tertiary age (WSRC, 2001a). The formations from oldest to youngest are the Congaree, Warley Hill, Dry Branch, Tobacco Road and the Upland/Altamaha (Table 1-1). The corresponding hydrostratigraphic units included within the RRSB OU groundwater flow and transport models are also listed in Table 1-1.

1.2.2 Hydrostratigraphy

A detailed description of the hydrostratigraphic units relevant to the RRSB can be found in the RFI/RI/BRA report (WSRC, 2001a) and in WSRC (1999a). Table 1-2 shows the hydrostratigraphic units of interest for the groundwater modeling activities. These units are, from the deepest to shallowest, the Gordon Aquifer Unit (GAU), the Gordon Confining Unit (GCU) and the Upper Three Runs Aquifer (UTRA). The UTRA is comprised of three units

termed, from deepest to shallowest, the lower aquifer zone (LAZ), the tan clay (TC), and the "upper" aquifer zone (UAZ). At the RRSB area, the UAZ can be further subdivided. From the deepest to shallowest, the UAZ is comprised of the transmissive zone (TZ), "AA", "A", and "undifferentiated" soil horizons.

Borehole data related to the GAU and the GCU are limited to the P-20 well cluster (see Figure 1-5) within the R-Reactor Area (WSRC, 2001a). Based on these data and other SRS data, the GAU consists of loose sand and clayey sand which is moderately to poorly graded and medium to coarse grained (WSRC, 1999a). At the P-20 well cluster, the GCU is approximately eight-feet thick and consists of interbedded silty and clayey sand, sandy clay, and clay. Based on the results of pumping tests conducted in the R-Reactor Area (WSRC, 2000a), the GCU is a competent confining unit between the GAU and the overlying UTRA with no pressure responses observed across the GCU during pumping.

Table 1-1 Lithostratigraphic and Hydrostratigraphic Units at the RRSB (WSRC, 2001a)

<table>
<tr><th>Epoch</th><th colspan="3">Lithostratigraphic Unit</th><th colspan="4">Hydrostratigraphic Unit</th></tr>
<tr><td>Miocene</td><td colspan="3">Upland unit/Altamaha FM.</td><td rowspan="2">Upper Three Runs Aquifer</td><td rowspan="4">Upper Aquifer Zone</td><td>U. Surface Soil</td><td rowspan="9">Floridian Aquifer system</td></tr>
<tr><td rowspan="8">Eocene</td><td rowspan="4">Barnwell Gp.</td><td colspan="2">Tobacco Road Fm.</td><td>"A Horizon"</td></tr>
<tr><td rowspan="3">Dry Branch Fm.</td><td>Twiggs Clay</td><td>"AA Horizon"</td></tr>
<tr><td>Griffins Ldg. Mbr.</td><td>Transmissive Zone</td></tr>
<tr><td>Clinchfield Sand</td><td colspan="2">Tan Clay</td></tr>
<tr><td colspan="3">Santee Formation</td><td colspan="2">Lower Aquifer Zone</td></tr>
<tr><td colspan="3">Warley Hill Formation</td><td colspan="3">Gordon Confining Unit</td></tr>
<tr><td colspan="3">Congaree Formation</td><td colspan="3" rowspan="2">Gordon Aquifer</td></tr>
<tr><td rowspan="2">Paleocene</td><td colspan="3" rowspan="2">Fourmile Branch Formation</td></tr>
<tr><td colspan="3">Meyers Branch Confining System</td></tr>
<tr><td colspan="3">Snapp Formation</td></tr>
</table>

The LAZ of the UTRA is approximately 67-ft thick within the R-Reactor Area and consists of interbedded clayey sands, sands, and carbonates (WSRC, 2001a). The carbonates are present in both consolidated and unconsolidated forms and have lower measured hydraulic conductivities than the clayey sands and sands. The LAZ is overlain by the TC which is up to 31 ft in thickness in the R-Reactor Area and consists of clay with interbedded sands, silty sands, clayey sands, and sandy clays (WSRC, 1999a). Based on site-specific borehole information, the TC has been further subdivided into three layers. The upper portion of the TC is a fine-grained unit termed

the tan clay confining zone (TCCZ). The middle layer within the TC is a relatively high permeable sand unit that is mappable across the RRSB site and other areas at SRS. This sandy zone is termed the middle aquifer zone (MAZ). The portion of the TC beneath the MAZ is a finer-grained unit and is termed the tan clay lower clay (TCLC) unit. Based on the pumping tests conducted in the R-Reactor Area (WSRC, 2000a), the TC is considered a confining unit between the LAZ and the overlying TZ of the UAZ with a slight response in the TZ due to pumping in the LAZ, and vice versa.

Table 1-2 Modeled Hydrostratigraphic Units

Hydrostratigraphic Units		
Upper Three Runs Aquifer (UTRA)	Upper Aquifer Zone (UAZ)	"undifferentiated" soil horizon
		"A" horizon
		"AA" horizon
		transmissive zone (TZ)
	tan clay (TC)	tan clay confining zone (TCCZ)
		middle aquifer zone (MAZ)
		tan clay lower clay (TCLC)
	lower aquifer zone (LAZ)	
Gordon Confining Unit (GCU)		
Gordon Aquifer (GAU)		

The UAZ is the water table aquifer at the RRSB and ranges from 104 to 136 ft in thickness. The TZ is the lowermost unit of the UAZ and consists of relatively high hydraulic-conductivity silty sands and sands of up to 42 ft in thickness (WSRC, 2001a). The TZ is overlain by the "AA" horizon, which consists of silty and clayey sands with a range in thickness of 16 to 70 ft (WSRC, 2001a). The upper two units of the UAZ are the "A" horizon and the "undifferentiated" surface soil. These units are comprised of fine-grained materials of low hydraulic conductivity and are considered typical of confining units at the SRS (WSRC, 2001a). The upper surface of the "undifferentiated" surface soil is defined by the topography within the R-Reactor Area.

Between 1998 and 2000, the water-table elevations within the RRSB area dropped significantly. In 1999, a soil moisture and resistivity investigation was conducted to determine whether the shallow groundwater aquifer beneath the RRSB is in direct hydraulic communication with the TZ of the UAZ or is the result of a perched water table (WSRC, 1999b). The results of this investigation demonstrated that the shallow groundwater aquifer is in direct hydraulic communication with the TZ; however, given the low hydraulic conductivity of the upper portion of the UAZ, the infiltration from precipitation events is relatively slow (WSRC, 1999b).

1.3 Summary of Approach

To fulfill the objectives of this modeling task, a set of numerical groundwater flow and contaminant transport models was developed for the RRSB OU. Most of the contaminant mass within the subsurface is currently adsorbed to the soil within the unsaturated zone. Therefore, transport simulations were required to encompass both the unsaturated and saturated regions of the subsurface. The modeling for the RRSB used different numerical models for the unsaturated and the saturated zones. Simulations for both the unsaturated and saturated zone models were developed to investigate the impact of various basin cover remedial alternatives on the breakthrough of the CMCOCs at the water table and the transport of Sr^{90} within the saturated zone.

The following briefly outlines the approach taken in this task to complete the required modeling activities:

1. Developed a source term (concentration and distribution) for the CMCOCs within the subsurface soils and for the COC within the groundwater.

2. Developed an unsaturated-zone flow and transport model to calculate the concentration flux of the individual CMCOCs at the water-table surface.

3. Converted the concentration flux for the CMCOCs to a maximum groundwater concentration within an assumed aquifer mixing volume for comparison to corresponding MCLs.

4. Developed saturated-zone flow and transport models to determine the transport of Sr^{90} within the groundwater aquifer, using the contaminant flux from the unsaturated-zone modeling as an additional source term.

Steps 2 through 4 were then repeated to investigate the impact of six basin cover remedial alternatives on the future migration of the contaminants within the unsaturated zone, including the existing asphalt cover. A seventh remedial alternative was included in the unsaturated-zone analyses but was not extended to the saturated-zone analyses.

The groundwater flow and contaminant transport modeling for the saturated zone was conducted using the U.S. Department of Defense (U.S. DOD) Groundwater Modeling System (GMS) (BYU, 1999). The numerical codes MODFLOW (McDonald and Harbaugh, 1998), and MT3DMS (Zheng and Wang, 1999) were used within the GMS modeling platform for the groundwater flow and contaminant transport simulations, respectively.

The groundwater flow and contaminant transport within the unsaturated zone was initially modeled using the numerical code HYDRUS (USDA, 1998). As a result of numerical instability and mass balance errors for some of the simulations, the unsaturated-zone simulations presented in this report were conducted using the GMS modeling platform and the MODFLOW/MT3DMS numerical codes (see Section 2.2).

1.4 Remedial Alternatives

The groundwater flow and contaminant transport modeling included development of remedial alternative simulations to predict contaminant migration within the unsaturated zone and the saturated groundwater aquifers at the RRSB OU. The remedial alternative simulations are listed below in Table 1-3. The Enhanced Asphalt Cover remedial alternative only investigated the transport within the unsaturated zone and was not carried forward into the saturated zone transport simulations. For each of the remedial alternatives, it was assumed that the simulated basin cover was in place at the start of the simulation and was maintained under constant conditions for the simulation timeframe of 400 years. Two cover footprints were utilized in the simulations. These were the existing 11-acre cover footprint and a proposed 15-acre cover footprint. Figure 1-11 shows the outline of the existing 11-acre cover along with the additional coverage areas for the proposed 15-acre cover.

Table 1-3 Listing of Remedial Alternative Simulations

Remedial Alternative	Description
Existing Asphalt Cover	Assume the existing asphalt cover is maintained in its current condition
Failed Asphalt Cover (No Action Case)	Assume the existing asphalt cover fails at the present time
$1x10^{-5}$ cm/s Soil Cover with existing cover footprint	Assume the existing asphalt cover is replaced with a soil cover with an average hydraulic conductivity of $1x10^{-5}$ cm/s with a footprint identical to that of the existing cover
$1x10^{-5}$ cm/s Soil Cover with 15-acre cover footprint	Assume the existing asphalt cover is replaced with a soil cover with an average hydraulic conductivity of $1x10^{-5}$ cm/s with the 15-acre footprint
Concrete Cover with 15-acre cover footprint	Assume the existing asphalt cover is replaced with a six-inch thick layer of concrete with the 15-acre footprint
Reinforced Asphalt Cover with 15-acre cover footprint	Assume the existing asphalt cover is replaced with a four-inch thick layer of the reinforced asphalt (i.e. MatCon™) with the 15-acre footprint
Enhanced Asphalt Cover	Assume existing asphalt cover is sealed, thereby increasing the runoff percentage (Unsaturated-Zone Only)

The first remedial alternative assumes that the Existing Asphalt Cover will be maintained under the current conditions for the duration of the simulation. The infiltration rate through the existing asphalt cover is estimated to be 0.45 inches per year (in/yr) (see Section 2.3). This infiltration rate will be maintained throughout the simulation timeframe.

The second alternative is the Failed Asphalt Cover and is considered the No-Action alternative, which assumes that the condition of the existing asphalt cover deteriorated at the present time such that the runoff percentage decreased from 97% to 50%. This decrease in runoff would result in increased infiltration and recharge to the water table. Therefore, a recharge value of 7.5 in/yr (see Section 2.3) was used in the simulations for the failed asphalt cover.

The third and fourth remedial alternatives assume the construction and maintenance of RCRA-type soil covers, placed with a uniform hydraulic conductivity of $1x10^{-5}$cm/s with the existing cover footprint and the 15-acre cover footprint, respectively. To date, no site-specific design activities have been undertaken with respect to a soil cover at the RRSB OU to determine the hydraulic properties of a soil cover and its impact on the groundwater system. Therefore, the results from a similar and relevant analysis were used for the RRSB OU. A calculation was performed to predict the percent reduction in average yearly infiltration through the C-Area Burning/Rubble Pit (CBRP) following the installation of an interim action soil cover system (Bell, 2001). Average yearly infiltration through the pre- and post-cover CBRP was estimated using the U.S. Environmental Protection Agency/US Army Corps of Engineers computer model, Hydrologic Evaluation of Landfill Performance (HELP) Version 3.01. The HELP simulations investigated the percent reduction in infiltration and the assumed infiltration rate through the soil cover based on a range of average hydraulic conductivity values. These simulations indicated an infiltration rate of 6.2 in/yr for an average hydraulic conductivity value of $1x10^{-5}$ cm/s (Bell, 2001).

The fifth remedial alternative assumes the existing asphalt cover is replaced with a six-inch thick layer of concrete with the 15-acre footprint. The infiltration rate through the concrete is assumed to be 3.0 in/yr. The sixth remedial alternative assumes that the existing asphalt cover is replaced with a four-inch thick layer of a reinforced asphalt material (i.e. commercial product MatCon™) with the 15-acre footprint. The infiltration rate through the reinforced asphalt cover is assumed to be 1.0 in/yr.

The seventh remedial alternative assumes that a sealant would be applied to the existing asphalt cover, thereby increasing the runoff and decreasing infiltration through the cover. It is assumed that the sealant would increase the assumed runoff percentage from 97% to 99% and reduce the infiltration rate through the cover to 0.15 in/yr.

1.5 Review of Historical Water Levels

The hydrographs presented in Figure 1-8 show that the water levels at the RRSB have historically fluctuated. This modeling task also investigated two issues related to the water-table elevation in the immediate vicinity of the existing asphalt cover. These issues were 1) the potential for the water-table surface to intersect the principle threat source material (PTSM) and 2) the potential impact of the presence of the asphalt cover on the location of the water table.

Based on the observed groundwater elevations and Sr^{90} concentrations, there is evidence that, at times, the water table has risen and intersected the PTSM. The water level in monitoring well RSE1A (see Figure 1-8), located next to Basin 1, was consistently greater than 290 ft above mean sea level (amsl) from approximately 1992 to 1994. This elevated water table resulted in the Sr^{90} source mass being in direct contact with the saturated zone (see Section 2.3). Therefore, it is assumed that as the water-table elevation increases to the maximum elevations observed, the groundwater comes into contact with either more contaminant percolation water within the unsaturated zone or with contaminant mass adsorbed onto the soil matrix. In either case, more mass is available for direct dissolution into the groundwater. As the water-table elevation

decreases, a corresponding decrease in the Sr^{90} concentration would be expected. This decrease is probably a result of dilution within the saturated zone and sorption from the groundwater back onto the soil matrix as the water table drops.

The seepage basins are located on a topographic high (mound) which results in a groundwater divide through the seepage basins. The existing asphalt cover was installed in 1996. Water-level measurements were reviewed to see if a noticeable change in the water levels could be correlated to the installation of the asphalt cover. As shown in Figure 1-8, the water-level measurement data for the wells located nearest the basins, are limited from 1995 to the present. Therefore, insufficient data exist to properly define the effect of the asphalt cover on the water-table elevation. The saturated groundwater flow modeling (presented in Section 3.0) developed several steady-state flow fields for the evaluation of the various remedial alternatives. Potentiometric surfaces (water-table elevations) were developed for each basin cover considered. The results of these simulations (see Section 3.9) demonstrate that as the magnitude of the groundwater recharge through the basin cover is changed, an impact on the configuration of the water-table surface is observed. Based on this observation from the model results, it is assumed that the existing asphalt cover reduces the infiltration in the vicinity of the seepage basins. Therefore, the current location of the water-table surface would be expected to be at a higher elevation without the presence of the existing asphalt cover. However, insufficient data are available to determine whether the existing asphalt cover would provide a sufficient reduction in infiltration to prevent the overall water-table surface from rising into the contaminant source location during periods of high precipitation.

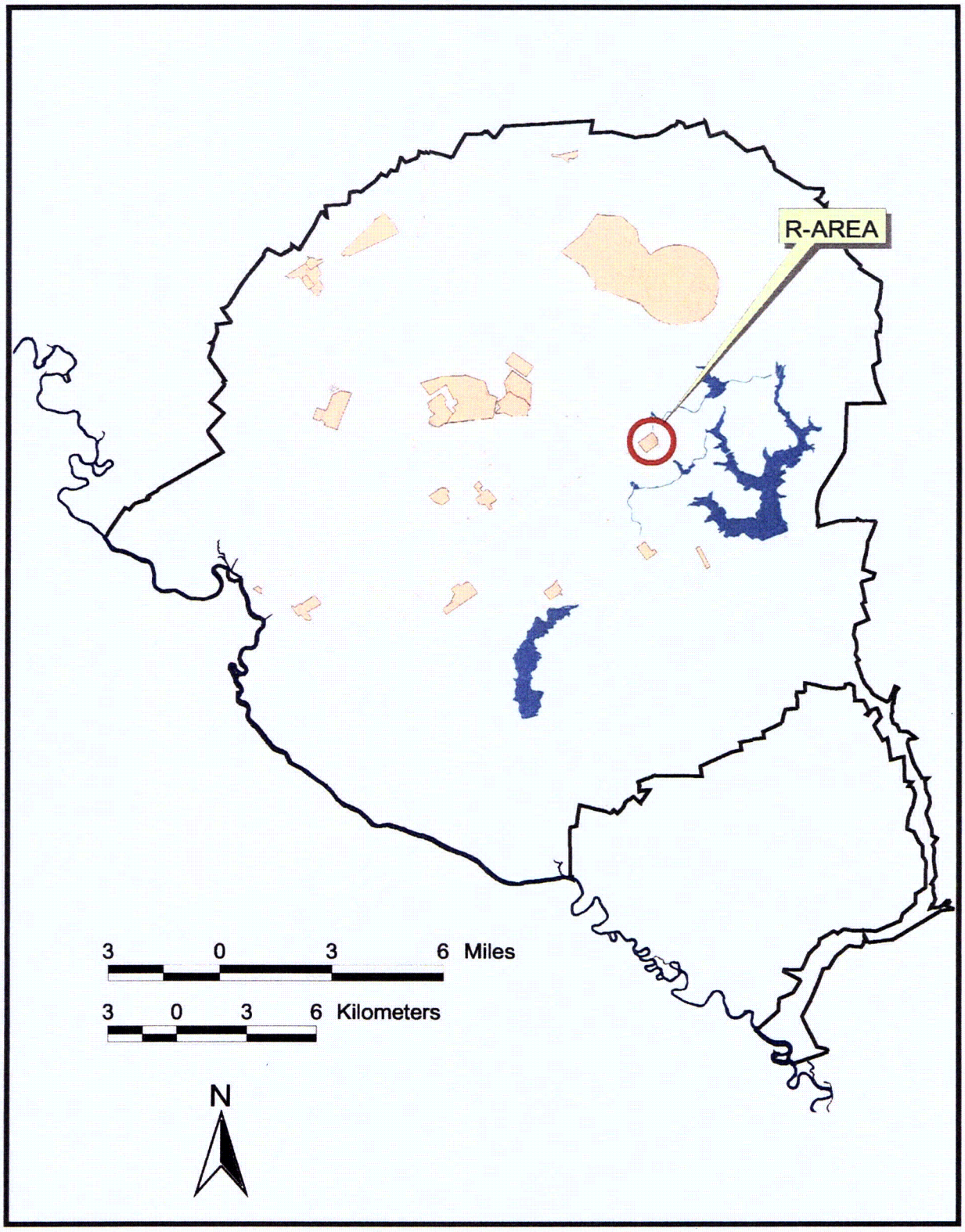

Figure 1-1. Location of the R-Area in relation to the SRS boundary.

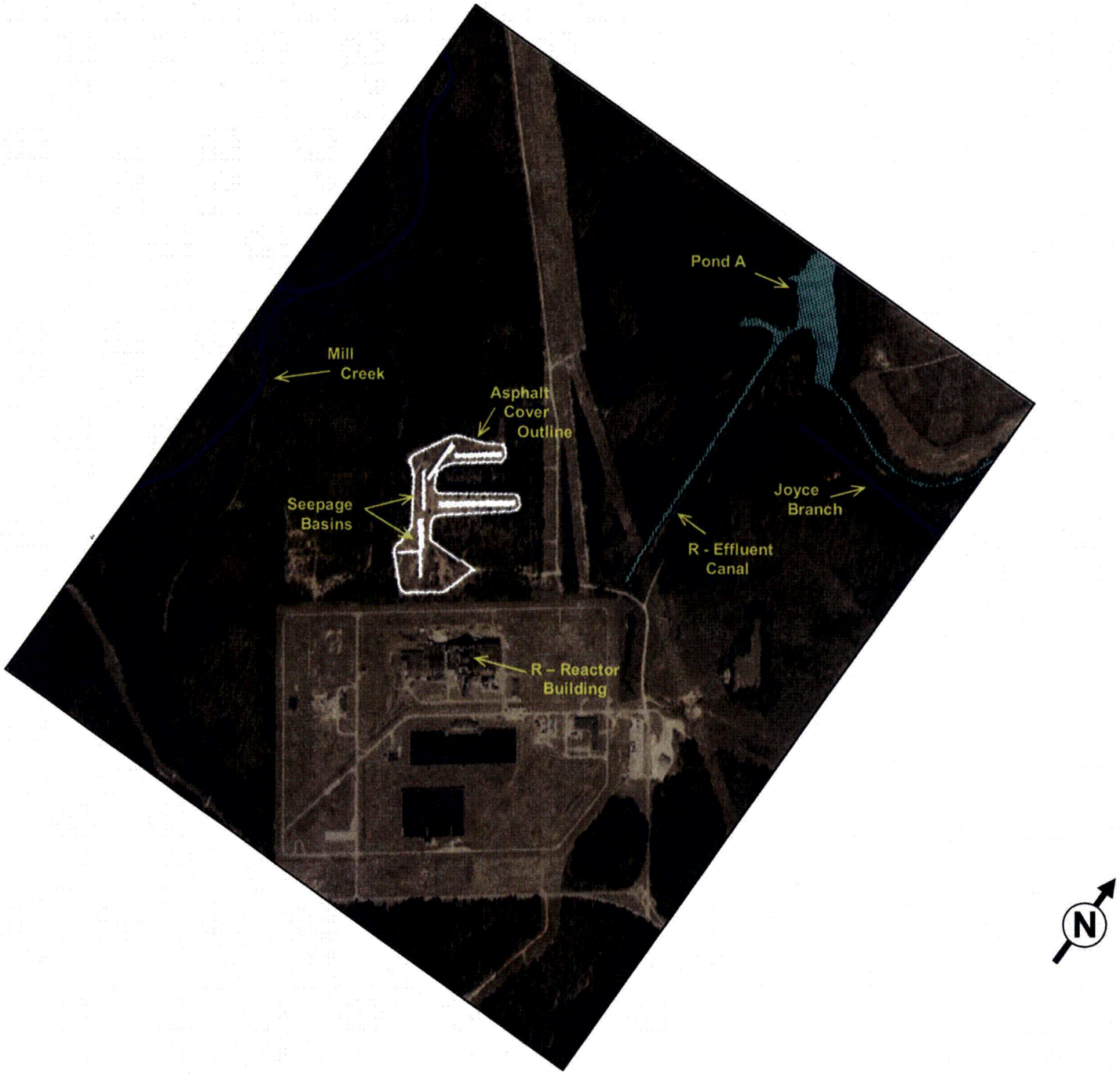

Figure 1-2. Location of R-Reactor Building, R-Reactor Seepage Basins, and surface water features.

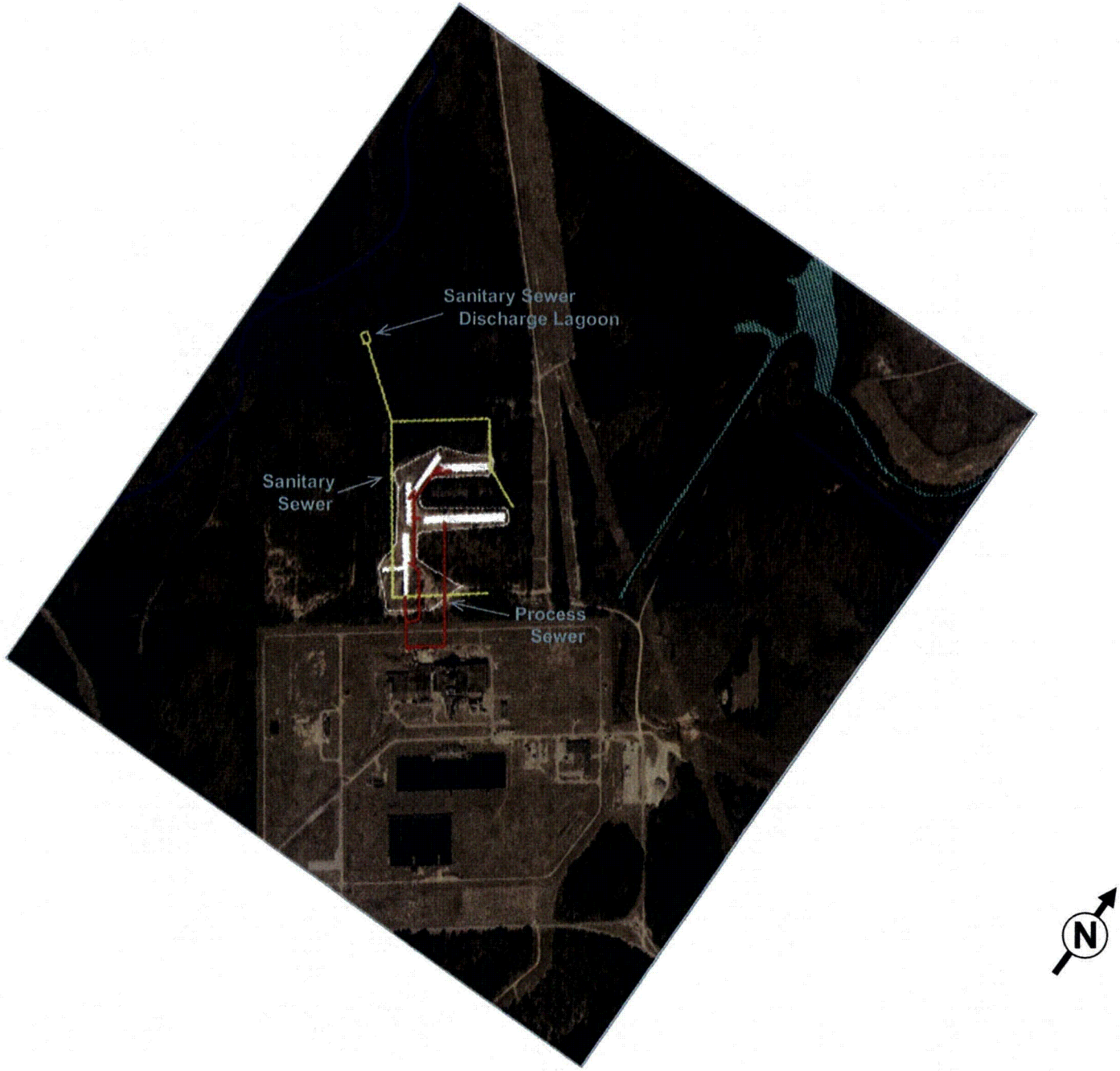

Figure 1-3. Location of the process sewer line (red lines), an abandoned sanitary sewer line (yellow lines), and the discharge lagoon.

Figure 1-4. R-Reactor Seepage Basins.

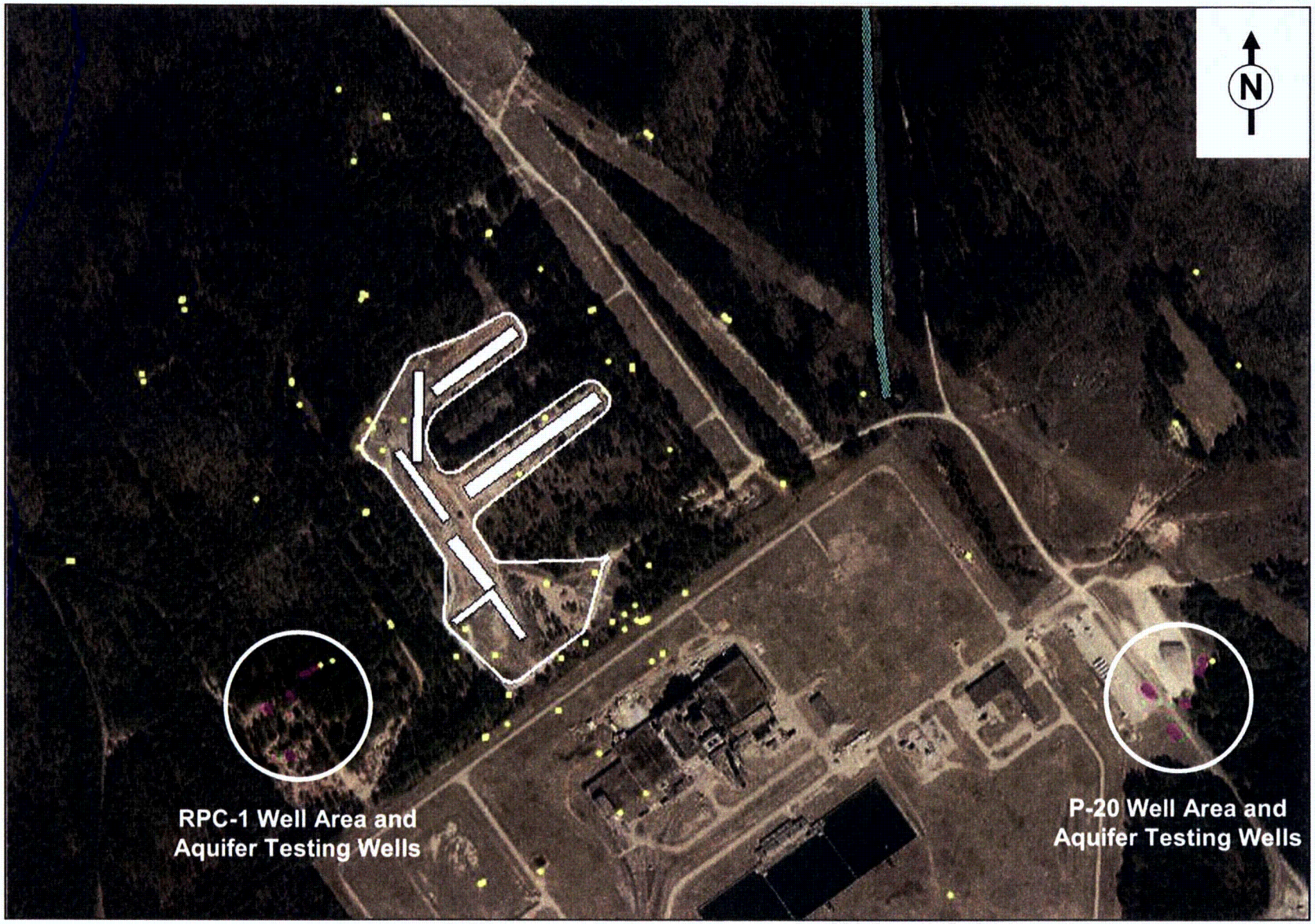

Figure 1-5. Location of RPC-1 and P-20 well clusters.

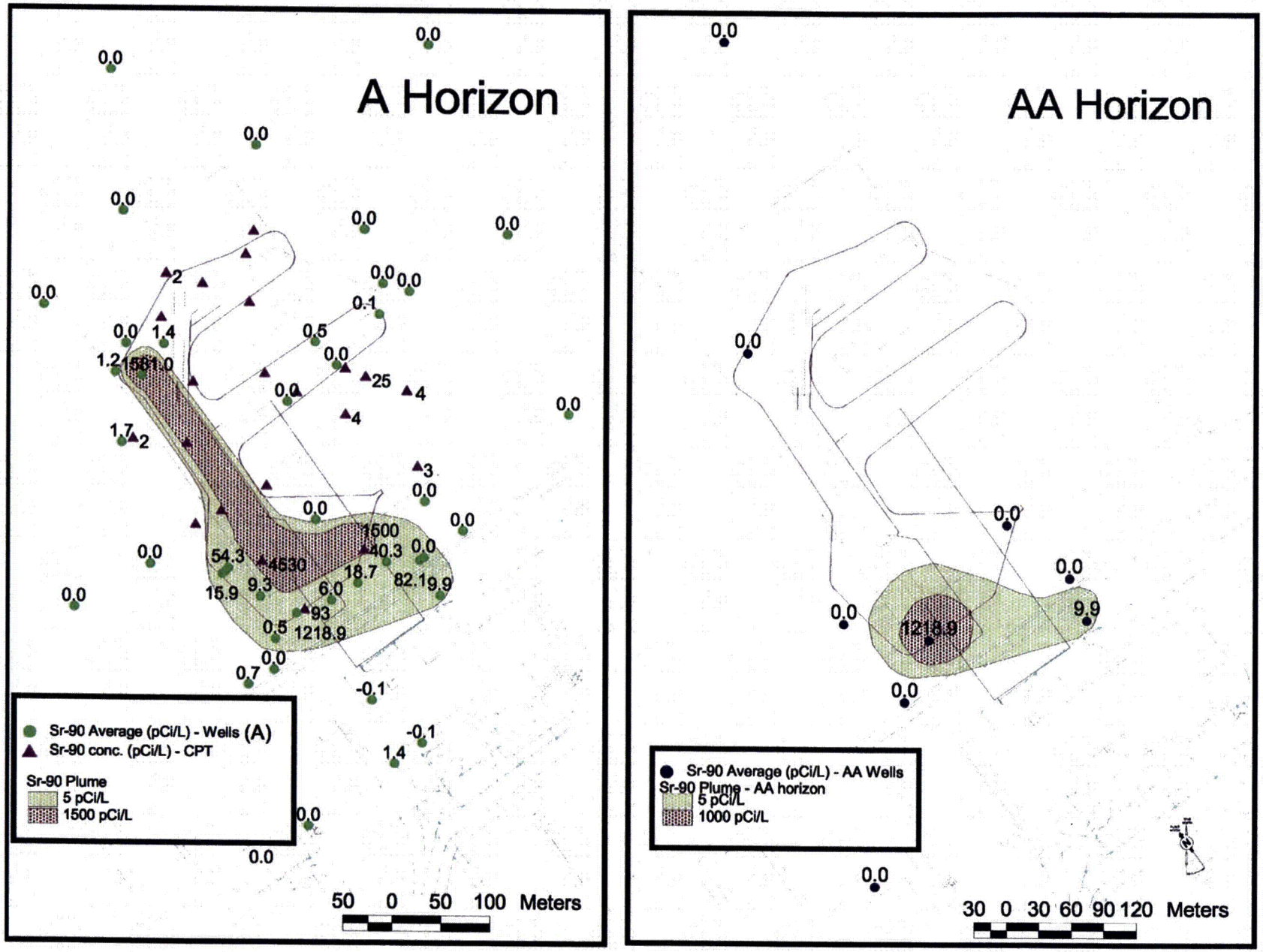

Figure 1-6. Extent of Sr^{90} contamination, as defined by the MCL of 8 pCi/L, within the RRSB OU shallow groundwater aquifer.

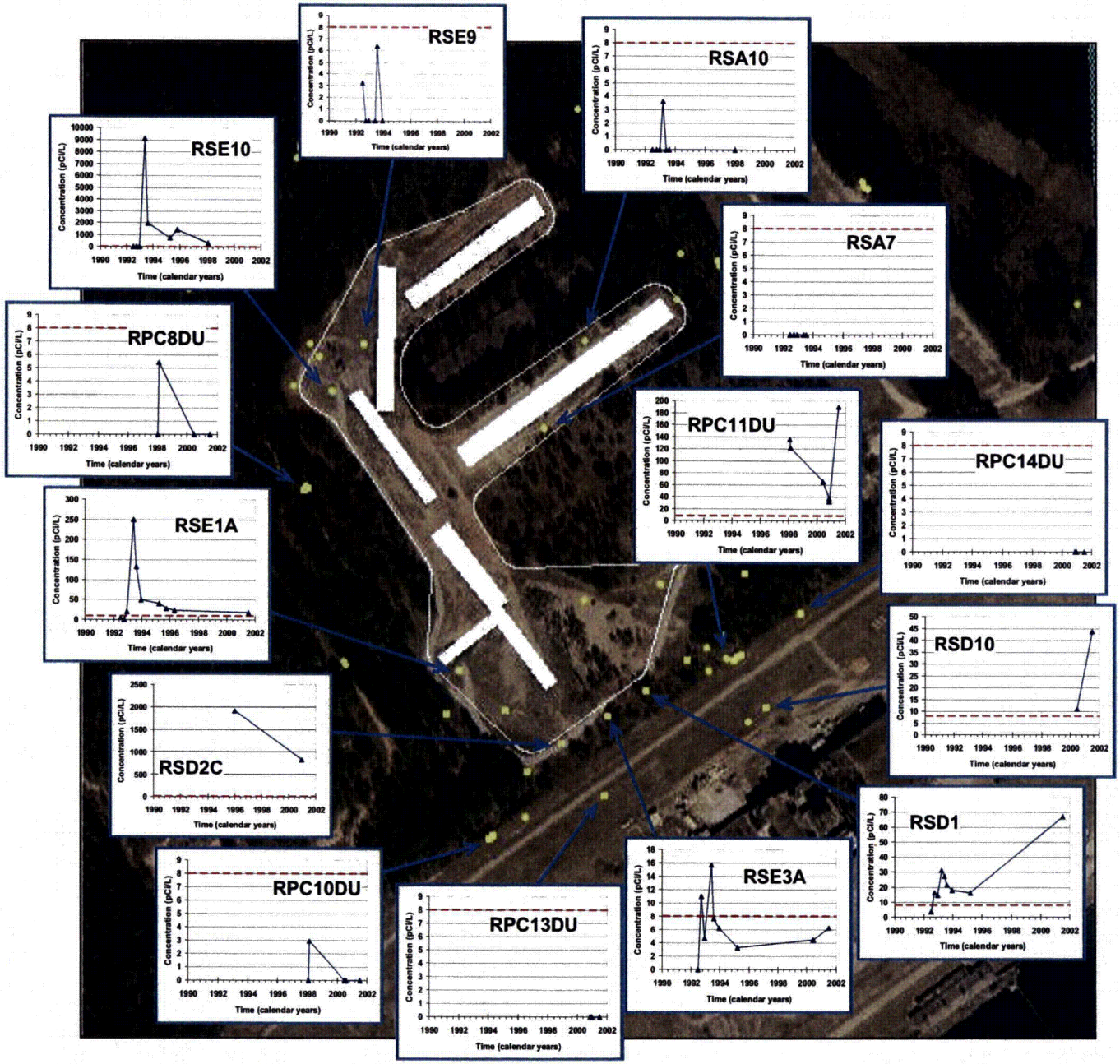

Figure 1-7. Time series of Sr^{90} concentrations in selected monitoring wells for the RRSB OU.

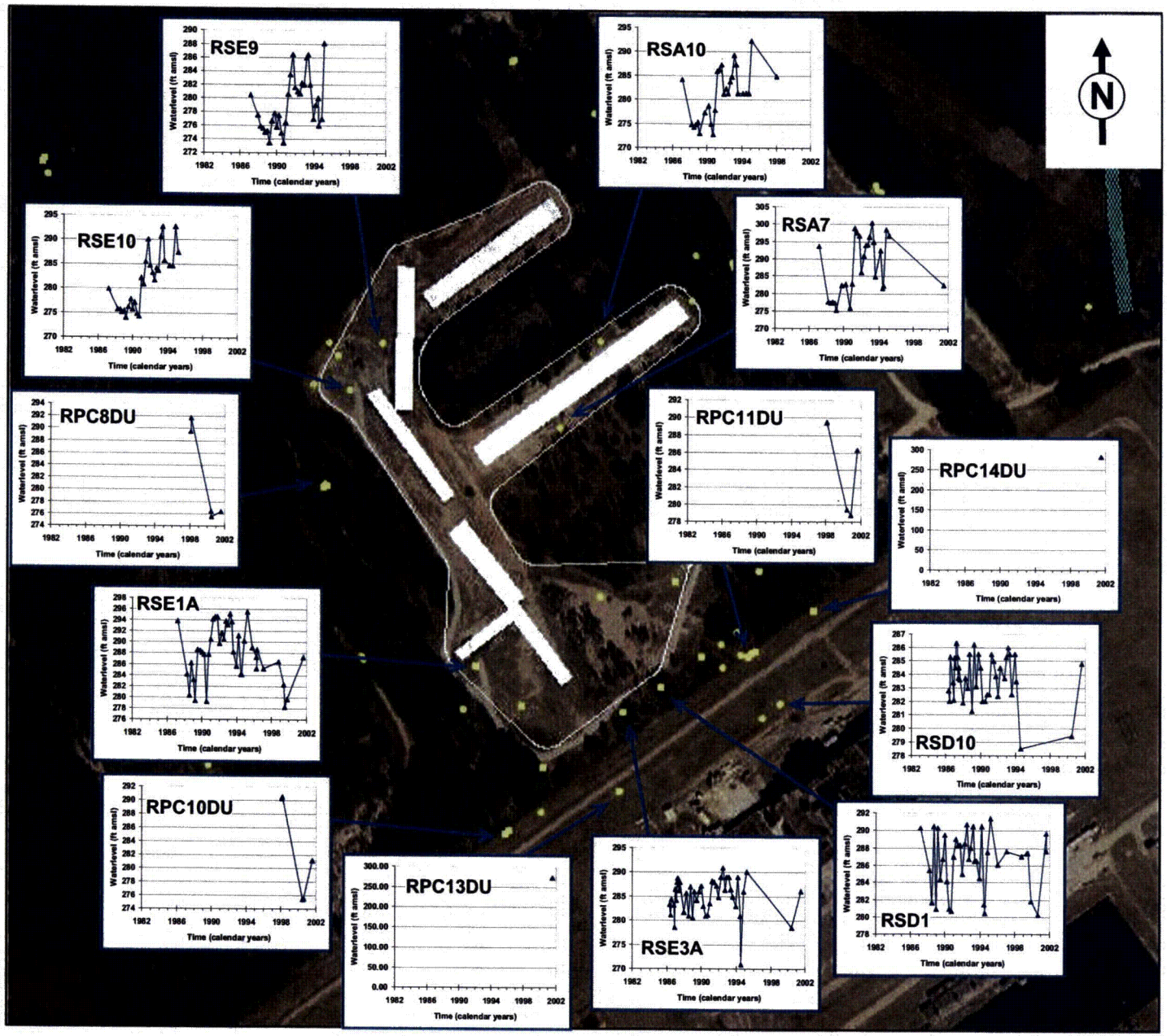

Figure 1-8. Time series of water-level elevations in selected monitoring wells for the RRSB OU.

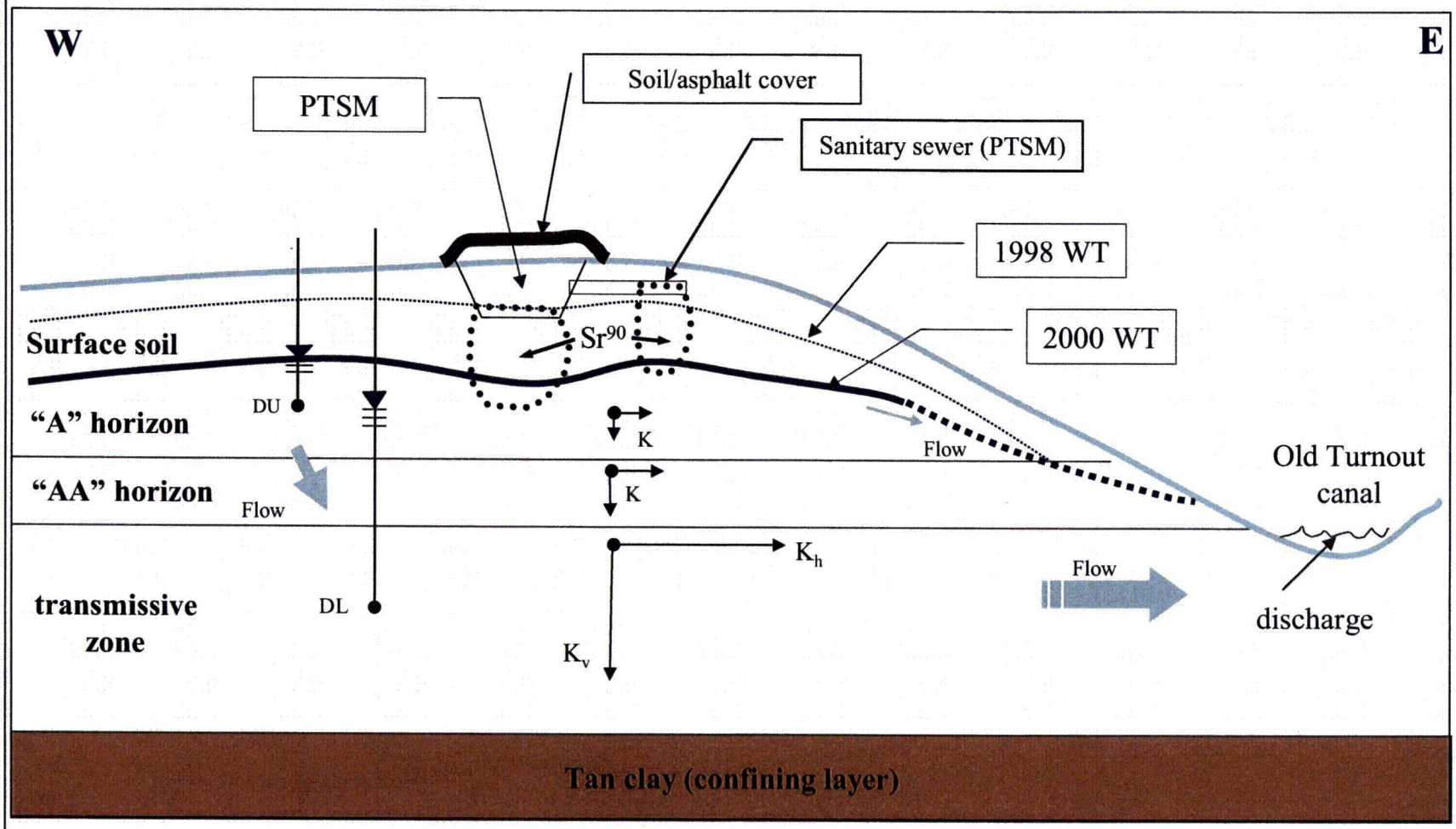

DU – upper monitoring zone
DL – lower monitoring zone
K – hydraulic conductivity
K_h – horizontal hydraulic conductivity
K_v – vertical hydraulic conductivity
WT – water table

Figure 1-9. Original HCM for the RRSB OU.

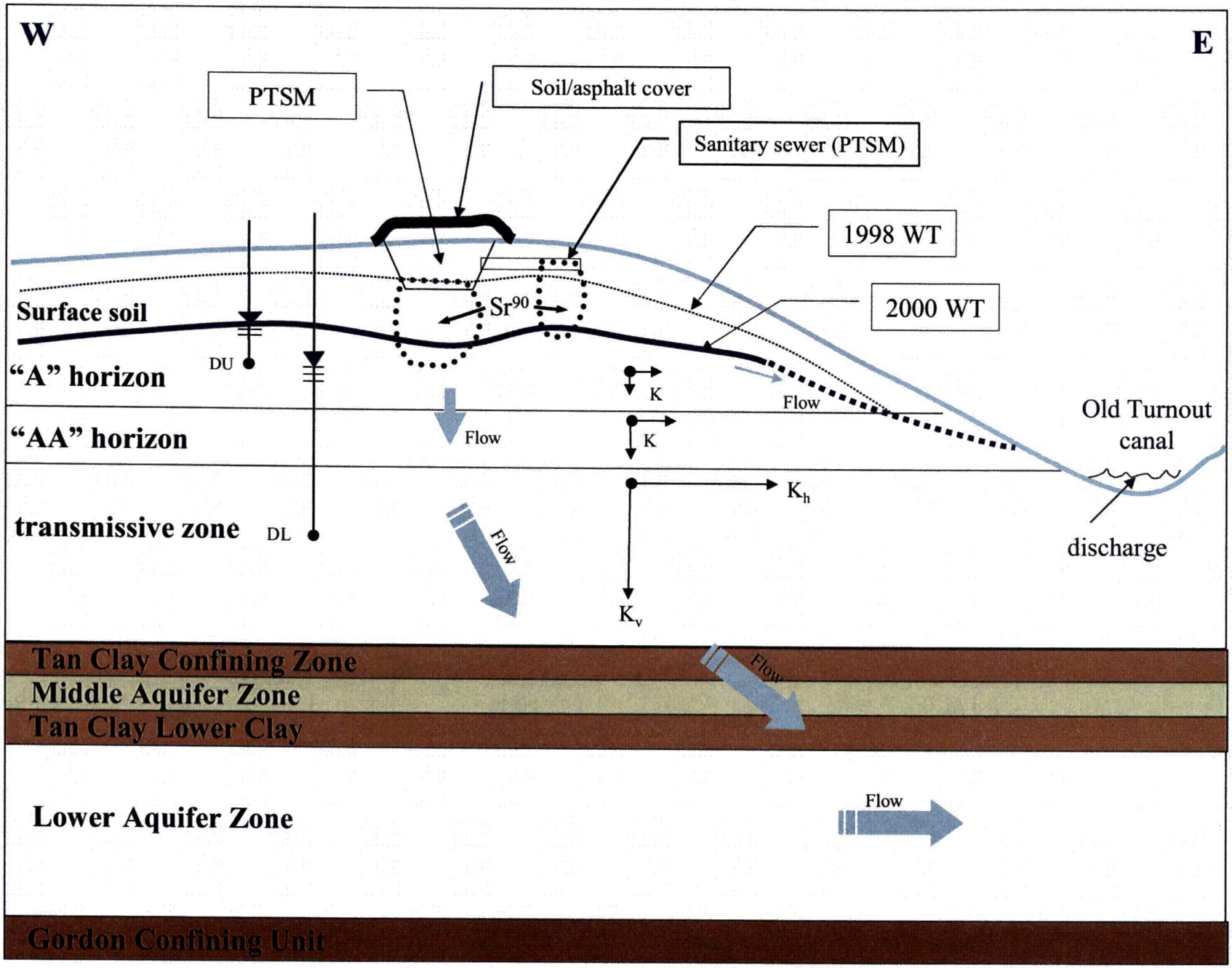

Figure 1-10. Modified HCM for the RRSB OU.

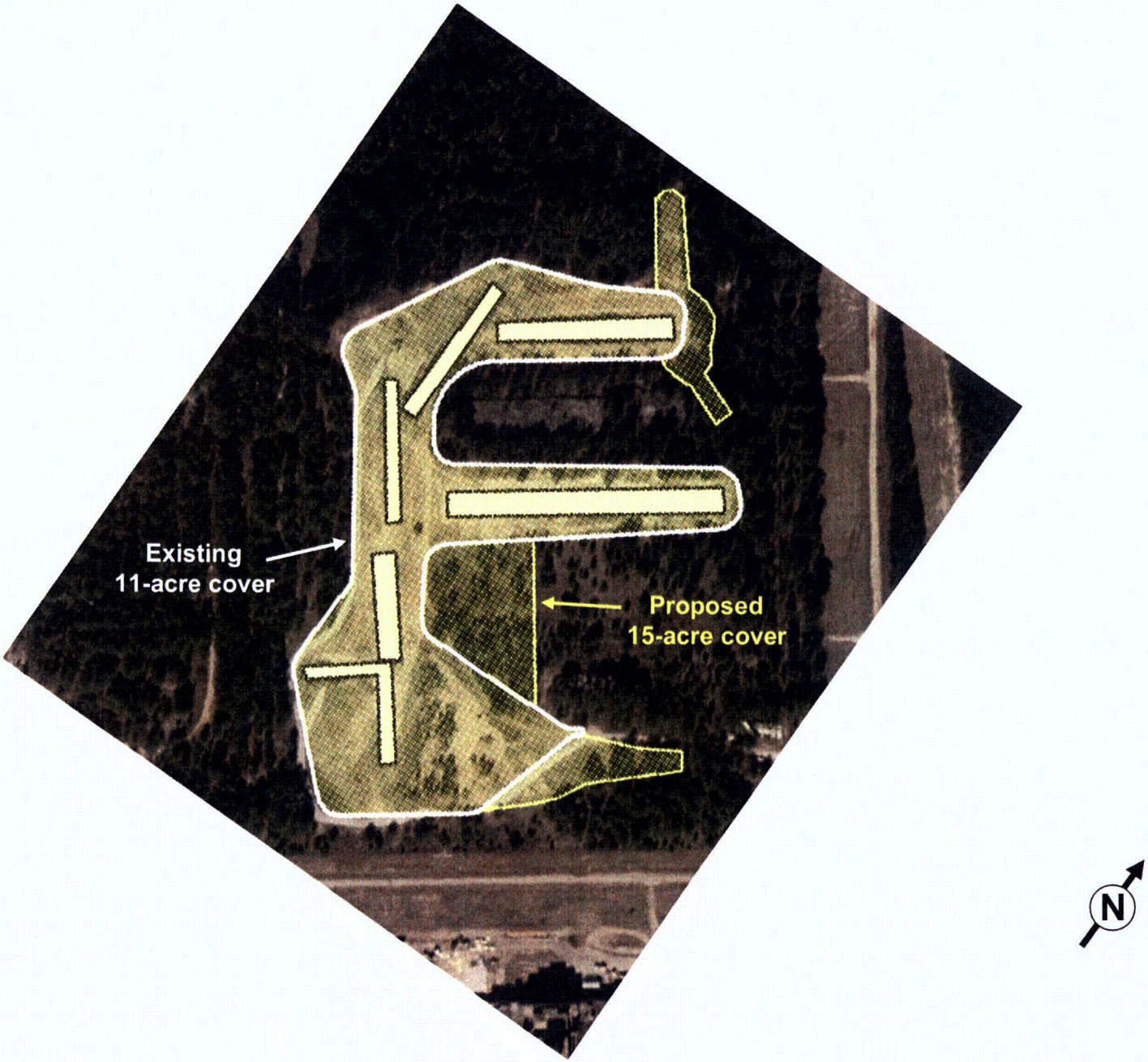

Figure 1-11. Location of the existing 11-acre cover (white outline) and the proposed 15-acre cover (yellow fill).

2.0 UNSATURATED-ZONE MODEL

Unsaturated-zone simulations were conducted to determine the potential for the identified CMCOCs to break through to the water table above the MCLs based on a suite of infiltration rates and contaminant transport sorption coefficient parameters. For each simulation, the transient contaminant concentration (pCi/L) for each CMCOC was calculated at the water-table surface. These transient concentration profiles were then used to calculate the maximum expected saturated-zone concentrations directly beneath the basin footprints within the "A" horizon.

2.1 Source Term Development

Results from soil-boring analyses and gamma-probe investigations conducted in 1996 and 1998 (WSRC, 1999b) indicate that the majority of the contaminant mass is adsorbed to the subsurface soil. The site characterization activities at the RRSB were reviewed and distributions of the CMCOCs beneath the basins were developed (WSRC, 2001d). The calculated vertical distributions (soil concentration) of Am^{241}, C^{14}, $Pu^{239/240}$, and Sr^{90} beneath Basins 1, 3, and 6 are presented in Figure 2-1.

The source characterization data are limited to Basins 1, 3, and 6; therefore, no source terms were developed for Basins 2, 4, and 5. Figure 2-1 indicates that for each constituent, except C^{14}, Basin 1 contains the highest soil concentrations and Basin 6 contains the lowest soil concentrations, with no C^{14} present in Basin 6. This distribution coincides with the unit history and previous investigations which indicate that Basin 1 received a larger percentage of contaminated discharge water and thus more contaminant mass than the other basins (WSRC, 2001a).

2.2 Selection of the Computer Code

The unsaturated-zone modeling conducted for the first version of this document (WSRC, 2002) was performed using the numerical simulator HYDRUS, version 6.0 (USDA, 1998). HYDRUS was developed by the U.S. Salinity Laboratory of the U.S. Department of Agriculture (USDA) to simulate one-dimensional flow and transport of heat and multiple solutes in a variably-saturated heterogeneous soil column. The solutes of interest can degrade in a variety of ways, including first-order radioactive decay. The HYDRUS numerical code was selected based on the ability of the code to incorporate vertical contaminant soil profiles and heterogeneity. The HYDRUS model developed for the RRSB was specified as a one-dimensional, unit-area, vertical flow tube with a constant infiltration rate. The water table was specified as the lower pressure boundary condition. Additional simulations conducted with HYDRUS subsequent to the development of the initial report (WSRC, 2002) showed mass balance instabilities with the HYDRUS transport solution for higher infiltration rate simulations. The instability was related to the transport solution only, with no mass-balance errors in the unsaturated-zone flow solution. Therefore, the HYDRUS code was not utilized in the development of the unsaturated-zone flow and transport

simulations for this revision of the report. To maintain consistency, all of the unsaturated-zone models presented in this report were developed with the new numerical flow and transport code.

Based on the groundwater flow results from the HYDRUS code, a steady-state flow field was established within the first year, with the groundwater flux through the model equal to that of the applied recharge. The moisture content within the model ranged from 0.386 at the ground surface to a saturated value of 0.400 at the water table. The results in the HYDRUS groundwater flow models demonstrated that the unsaturated zone was effectively saturated and could be simulated with a numerical code which solves for the groundwater flow and transport within saturated media. The revised unsaturated-zone groundwater flow and transport modeling was conducted using the numerical codes MODFLOW and MT3DMS, respectively, contained within the GMS modeling platform. The GMS interface allows development of a generic or non-model specific conceptual model. Once the conceptual model is developed and parameterized, GMS creates the specific files necessary to run MODFLOW/MT3DMS. The results generated by MODFLOW/MT3DMS are then processed by GMS for visual presentation and calculation of various mass budget summaries.

A comparison of the HYDRUS and MODFLOW/MT3DMS results for selected simulations is presented in Figure 2-2. A detailed description of the contaminant transport models developed using HYDRUS is presented in the initial version of this report (WSRC, 2002). The development of the MODFLOW/MT3DMS models used in generating the data presented in Figure 2-2 is described below in this report section. The transient concentration curves demonstrate that for the lower infiltration rates, the HYDRUS and MODFLOW/MT3DMS simulations mirror each other with the overall MODFLOW/MT3DMS concentrations being slightly less than the HYDRUS simulations. For the higher infiltration rate scenarios, the MODFLOW/MT3DMS simulations mirror those of HYDRUS at early times but then deviate significantly at later times. As stated previously, there were mass balance errors within HYDRUS simulations for the higher infiltration rate scenarios. These errors lead to the creation of mass at later simulation times. The transient concentration curves for infiltration rates greater than 1.0 in/yr all trend to the same concentration values and declining slope as a results of the mass balance errors. The MODFLOW/MT3DMS simulations properly conserved mass for all scenarios.

2.3 Assignment of Model Parameters

The unsaturated-zone model was discretized into a series of thin elements of unit area from the estimated land surface to the estimated top of the water table. Each element was assigned a uniform length (thickness) of 2.0 inches. One model was developed for each of the three simulated basins (Basins 1, 3, and 6). Using the source terms listed in Figure 2-1, the contaminant mass was initialized within the models. Figure 2-3 presents a generalized conceptual model of the mass distribution for Basins 1, 3, and 6. This conceptual model shows the vertical thickness over which the mass was distributed and the locations of the assumed water-table elevations. As stated previously, water-table elevations decreased from 1998 to 2000. Therefore, to incorporate the uncertainty in the depth to water, two water-level elevations were investigated for the unsaturated-zone modeling. These "high" and "low" water-table elevations

for Basins 1, 3, and 6 are shown in Figure 2-3. Historically, the water-table elevation has been shown to come into direct contact with the PTSM source area. However, the high water-table elevations presented in Figure 2-3 are based on the water levels during the 1996-1998 timeframe in which the soil-sampling activities were performed. To have an unsaturated-zone transport pathway present between the bottom of the source area and the surface of the water table, the high water-table elevation within the model was set at one foot below the bottom of the source area (WSRC, 2001b). The low water-table elevation was set based on data from 2001, which reflect the greatest depth to water measured in the vicinity of the basins. The distance between the bottom of the source and the low water table ranged from 10 to 15 ft (Figure 2-3).

A detailed description of the initial vadose-zone models developed with HYDRUS was presented in the initial version of this report (WSRC, 2002). The current flow models developed using MODFLOW were configured such that the groundwater flux through the model was equal to the recharge rate through the selected cover. This was accomplished by inserting an injection well (source) within the upper model cell to simulate the recharge into the model and an extraction well (sink) at the base of the model to capture the flow at the water table. By configuring these wells, the groundwater flux through the model was maintained at the appropriate value.

The unsaturated-zone transport modeling included the relevant parameters that define the retardation of the CMCOCs as a result of radioactive decay and sorption of the contaminants to the subsurface sediments. Radioactive decay is presented as the half life (years) and the sorption potential is defined with the K_d. The K_d describes the partitioning of contaminant mass between the soil materials (sorbed phase) and water (aqueous phase). The following equation defines the K_d (L/g):

$$K_d = C_{soil} / C_{aq}$$

where C_{soil} is the concentration of the contaminant sorbed to the soil materials (pCi/g) and C_{aq} is the contaminant concentration in the aqueous phase (pCi/L). The K_d is used in the contaminant transport equations to define how migration of the contaminant is retarded due to its sorption to soil particles.

The retardation (R) of each constituent is defined by the following equation as:

$$R = 1 + (\rho_b * K_d / \varphi).$$

where ρ_b is the bulk density of the soil (g/L) and φ is the effective aquifer porosity. The higher the K_d, and thus higher retardation, the more sorption of mass to the soil particles and the slower the migration of the contaminant mass.

As contaminated water flows through uncontaminated soil, an equilibrium reaction occurs whereby mass is transferred from the aqueous phase to the sorbed phase, based on the K_d parameter. The partitioning of mass based on the K_d retards the movement of the contaminants; however, contaminant mass may transfer from the sorbed phase to the aqueous phase to maintain the required distribution between the sorbed and aqueous phases.

The unsaturated-zone transport simulations assumed an effective porosity of 0.25 and a bulk density of 1.69 grams/cubic centimeter (g/cm^3), respectively (WSRC, 1999c). A single K_d was assumed for each constituent for all hydrostratigraphic units (WSRC, 1999c). The half-life, K_d values, and calculated retardation values for each constituent are presented in Table 2-1. To initialize the source mass within the unsaturated-zone models, the contaminant activity (pCi/g of soil) was converted to a mass (mg/g of soil) based on the specific activity values listed in Table 2-1. Because the soil concentrations could not be directly input into MT3DMS, the soil concentrations (mg/g of soil) were then converted to aqueous concentrations (mg/L) using the assumed K_d values listed in Table 2-1. These aqueous concentrations were initialized within the model as the starting aqueous concentrations. The MT3DMS code subsequently determines the amount of sorbed contaminant mass, based on the K_d values listed in Table 2-1.

Table 2-1 Basecase Radionuclide Parameters

Radionuclide	Specific Activity (pCi/g)	Half-life (years)	K_d (mL/g)	Retardation Factor
Am^{241}	3.44×10^{12}	432	100	677
C^{14}	4.46×10^{12}	5730	6	41.5
$Pu^{239/240}$	6.14×10^{10}	24100	250	1691
Sr^{90}	1.42×10^{14}	28.1	6	41.5

Table 2-1 indicates that, conceptually, C^{14} should migrate to the water table relatively quickly because of its expected low retardation. However, during the 1996-1998 sampling events, approximately 40 years after placement, C^{14} was detected sorbed to the soil. The chemical species of the C^{14} source is unknown at this time as is the K_d for this constituent. Therefore, to incorporate the uncertainty of the C^{14} sorption potential, two additional K_d values for C^{14} have been selected for simulation (55 and 500 mL/g).

The current K_d value assumed for Sr^{90} is 6 mL/g (WSRC, 1999c). To investigate the effects of a higher K_d on transport, an additional simulation was developed where the K_d value for Sr^{90} was increased by a factor of 10 to 60 mL/g. This results in an increase in the retardation factor from 41.5 to 407.

The long-term average recharge to the water-table aquifers within the SRS was estimated to be 15 inches per year (in/yr) (WSRC, 2001c). The presence of the existing asphalt cover over the source areas decreases the amount of water available to the subsurface directly through the basins and thus decreases the amount of water infiltrating through the PTSM source area. Several saturated permeability tests conducted on the as-built asphalt cover (WSRC, 2001e) yielded an average saturated hydraulic conductivity of approximately 1×10^{-5} cm/s. For the unsaturated-zone modeling, the presence of the asphalt cover was not directly incorporated into the model as a discrete layer of a known hydraulic conductivity. Rather, the impact of the asphalt cover was indirectly incorporated within the model as an assumed percent reduction of infiltration into the underlying soils.

From pavement construction design specifications, it is estimated that 95% of the precipitation that falls on standard asphalt surfaces runs off (Caltrans, 2001). The current asphalt cover is in good physical condition with no noticeable cracks or obvious direct pathways for water to infiltrate to the subsurface (Figure 2-4). Also, the surface of the asphalt cover slopes in various directions based on the surface topography and, thereby, increases the amount of runoff. Therefore, for this task, the existing asphalt cover was assumed to create a 97% reduction in the background infiltration (15 in/yr), due to increased runoff and evaporation, which yields an infiltration rate of 0.45 in/yr through the asphalt cover.

The transport within the unsaturated-zone model was assumed to be one-dimensional, which neglects any effects of transverse dispersivity on the movement of the constituent. Given the uncertainty in the longitudinal dispersivity for the unsaturated-zone transport simulations, an average value of 20 cm (7.9 in) was assumed, which is approximately 10% of the average transport distance for the high- and low-water table elevations.

2.4 Assumptions

The development of the unsaturated-zone flow and transport simulations was based on a set of assumptions. These assumptions include:

- The soil column is effectively saturated such that the numerical simulators MODFLOW and MT3DMS are applicable.
- The source term calculated from limited soil samples and gamma-probe testing correctly defines the mass distribution beneath Basins 1, 3, and 6.
- The K_d for each constituent is the same for each hydrostratigraphic unit.
- The high water-table elevation was set to one foot beneath the lower elevation of the PTSM in each basin.
- Radioactive decay of each CMCOC was incorporated within the unsaturated-zone transport model.

2.5 Results

The unsaturated-zone simulations were designed to investigate the impact of various remedial actions on the CMCOC concentrations calculated at the water-table surface. In addition, selected simulations were coupled with the saturated-zone contaminant transport simulations described in Section 4.0. Each unsaturated-zone simulation was based on a change in either the infiltration rate through the PTSM and/or the K_d value for Sr^{90} and C^{14} from the basecase simulation (Existing Asphalt Cover). The infiltration rates simulated ranged from a low of 0.15 in/yr for the Enhanced Asphalt Cover to a high of 15 in/yr for areas of potential contamination located outside of the cover footprint (No Cover).

Each simulation generated multiple transient concentration curves at the water-table interface. The simulated aqueous concentrations from the unsaturated-zone models were in units of mg/L. These concentrations were subsequently converted to units of pCi/L for presentation. Figures 2-5a through 2-10 present the results of the unsaturated-zone modeling. Figures 2-5a through 2-7 present the results for the high water table simulations. Figures 2-8a through 2-10 present the results for the low water table simulations. The results for the unsaturated-zone modeling simulations are described below by comparison of the results by basin, water-table elevation, cover configuration, and K_d value (for Sr^{90} and C^{14}).

2.5.1 Basin

Figures 2-5a through 2-7 show the results for Basins 1, 3, and 6, assuming a high water-table elevation. Each figure presents the results by CMCOC and infiltration rate through the cover. The No Cover (15 in/yr) simulation will be used for comparison of the basin results. The results from Basin 1, Figure 2-5a, shows a maximum Sr^{90} (K_d = 6 mL/g) concentration of approximately 200,000 pCi/L occurring at a simulation time of 30 years, with the concentration decreasing after the peak. For Basins 3 and 6, Figures 2-6a and 2-7, respectively, the peak Sr^{90} concentrations for the No Cover case are approximately 100,000 and 30,000 pCi/L, respectively. The effect of a short half life is seen in the decreasing Sr^{90} concentrations at later times. For Am^{241} and $Pu^{239/240}$, the concentrations are continually increasing and the peak concentration is not obtained prior to the end of the 400 year simulation time frame. As with the Sr^{90}, the maximum Am^{241} and $Pu^{239/240}$ concentrations for the No Cover simulation are highest for Basin 1, less for Basin 3 and lowest for Basin 6. Also, the rise in the breakthrough curves is delayed for Basins 3 and 6. The C^{14} concentration breakthrough for the No Cover simulation is presented in Figures 2-5b and 2-6b for Basins 1 and 3, respectively. The peak concentration is higher in Basin 3 (10,000 pCi/L) than in Basin 1 (400 pCi/L).

The simulation results between the basins are as expected given the historical loading to the basins and the observed soil concentrations (Figure 2-1) used to initialize the models. The maximum concentrations for Sr^{90}, Am^{241} and $Pu^{239/240}$ are highest in Basin 1 and lowest in Basin 6. The maximum concentrations for C^{14} are higher in Basin 3 than in Basin 1.

2.5.2 Water-table Elevation

Figures 2-5a and 2-5b show the concentration flux curves for Basin 1 assuming a high water-table elevation, as compared to the low water-table elevation simulations presented in Figures 2-8a and 2-8b. For Basin 1, the lower water-table elevation is nine feet lower than the high water table, thereby increasing the transport distance to the water table and decreasing the activity flux over time. Comparing the Sr^{90} (K_d = 6 mL/g) No Cover simulations for Basin 1, the peak concentration for the low water table is decreased by approximately one order of magnitude and delayed by a factor of three in the arrival of the peak concentration. The Sr^{90} concentration curves for the other remedial alternatives (Figure 2-5a and 2-8a) show that for the lower infiltration rates, the peak Sr^{90} concentrations are greatly reduced and the time to peak breakthrough is delayed significantly. These changes in peak concentration are a result of the short half-life for $Sr^{90}$and the additional transport distance to the water table. Similar behavior is observed for the maximum Am^{241} and $Pu^{239/240}$ concentrations between the high and low water

tables under Basin 1. The breakthrough of the peak concentrations for C^{14} are delayed similarly to the other CMCOCs but the magnitude of the peak concentrations has not decreased significantly because of the long half-life of C^{14} and the resulting lack of activity reduction due to decay.

The transient concentration curves for the high and low water tables for the Basin 3 and 6 simulations are presented in Figures 2-6a through 2-7 and Figures 2-9a through 2-10. These results are similar to those as described for Basin 1 with the additional transport distance decreasing the peak concentrations and delaying the overall breakthrough of the CMCOCs.

2.5.3 Cover Configuration

Figures 2-5a shows the impact of the seven cover types on the calculated Sr^{90} concentration flux at the water-table surface for Basin 1 with a high water-table elevation. The only difference in the model configurations for these simulations is the magnitude of the infiltration rate through the PTSM. These infiltration rates vary from 15 in/yr for the No Cover case to 0.15 in/yr for the Enhanced Asphalt Cover scenario.

Except for C^{14}, the overall magnitude of the concentrations observed at the water-table surface for each simulation is directly proportional to the assumed infiltration rate. The peak Sr^{90} (K_d = 6.0 mL/g) concentration decreases from a high of approximately 200,000 pCi/L for the No Cover case to a low of approximately 200 pCi/L for the Enhanced Asphalt Cover. In general, this relationship between the concentration magnitude calculated at the water-table surface and the infiltration rate is observed for all basins, water-table elevations, and K_d values. For the C^{14} simulations, the peak concentrations observed during the simulation time frame, particularly for the K_d = 6.0 mL/g case, are similar with only a time delay in the arrival of the peak.

2.5.4 Distribution Coefficient

The assumed initial K_d values for both Sr^{90} and C^{14} was 6 mL/g. As discussed in Sections 1.4 and 2.3 above, additional simulations were conducted to determine the impact of increasing the Sr^{90} and C^{14} K_d values. The Sr^{90} K_d was increased by one order of magnitude from 6 to 60 mL/g. This increase results in a corresponding increase in the retardation from 41.5 to 407. Figure 2-5a presents the results for the Sr^{90} K_d values of 6 mL/g and 60 mL/g for Basin 1 and high water-table elevation. The results for Sr^{90} No Cover scenario demonstrate that the order of magnitude increase in the K_d decreases the peak concentration by almost three orders of magnitude, from approximately 200,000 pCi/L to 400 pCi/L. For the low water table simulation (Figure 2-8a), the decrease in peak Sr^{90} concentration is approximately six orders of magnitude for the No Cover scenario. For the remaining basins, the reduction in the maximum Sr^{90} concentration is at least two orders of magnitude for the high water table and at least seven orders of magnitude for the low water-table simulations. For C^{14}, three K_d values (6, 55 and 500 mL/g) were simulated to determine the possible range in concentration to the water-table surface, given the uncertainty in the chemical species for C^{14}. These three K_d values correspond to a retardation factor of 41.5, 373, and 3381, respectively. The results for Basin 1 and a high water-table elevation are shown in Figure 2-5b. These results indicate that as the K_d value is increased, the magnitude of the concentrations calculated at the water-table surface decreases, given the increased retardation.

The Existing Asphalt Cover transient concentration curves for the two higher C^{14} K_d values do not effectively breakthrough to the water table within 400 years. Similar results are observed at the low water table for Basin 1 and both the high and low water table for Basin 3.

2.5.5 Summary

The results from the unsaturated-zone transport simulations show that the transient concentrations to the water table for each CMCOC are highly dependent on the magnitude of the infiltration rate (basin cover), the location of the water table with respect to the PTSM, and the magnitude of the retardation. In general, the higher the infiltration rate through the PTSM, the greater the concentrations at the water-table surface. Also, the extra transport distance between the high and low water-table elevations resulted in a significant decrease in the CMCOC concentrations for most of the basin cover scenarios. Overall, these simulations show that the presence of the Existing Asphalt Cover causes a significant reduction in the infiltration through the PTSM and thus the migration of radionuclides to the water table.

2.6 Estimated Saturated-Zone Concentrations

The unsaturated-zone transport simulations presented above calculated the transient CMCOC concentrations in the water infiltrating through the PTSM within the unsaturated zone. These concentrations were subsequently converted into maximum groundwater concentrations in the saturated aquifer directly beneath the seepage basins for comparison to the MCL or the risk based activity (RBA) criteria.

To calculate these concentrations, a volume of the saturated "A" horizon was required for mixing the unsaturated-zone leachate mass with the saturated-zone groundwater. The conceptual model for how the groundwater concentrations were calculated is presented in Figure 2-11. At each simulation time step, a volume of contaminated water from the unsaturated zone enters the top of the mixing cell and, assuming vertical flow only, an equal volume of water exits through the bottom of the mixing cell. The water entering the mixing cell is assumed to instantaneously mix with the water within the mixing cell. The contaminant mass is then partitioned between the sorbed and the aqueous phases depending on the K_d of the individual radionuclides. The aqueous phase concentration is then calculated based on the amount of mass in the aqueous phase during each time step. The water exiting the bottom of the mixing cell is assumed to have a concentration equal to that of the previous time step.

The mixing cell area perpendicular to flow was assumed to have a unit area and a depth equal to the thickness of the "A" horizon (50 ft), where most of the saturated-zone contamination is found. The following equations were utilized to calculate the mass in the mixing volume (Mb), the concentration in the mixing volume (Cb), the concentration in the water flowing out of the mixing cell per time step (Cout), and the mass leaving the mixing cell per time step (Mout).

$$Min_i = Qin * Cin_i$$

$$Mb_i = Mb_{i-1} + Min_i - Mout_{i-1}$$

$$Mbaq_i = Mb_i / (K_d * (Msoil / Vbaq)) + 1)$$

$$Cb_i = Mbaq_i / Vbaq$$

$$Cout_i = Cb_i$$

$$Mout_i = Cout_{i-1} * Qout$$

$$Qout = Qin$$

Where Qin is the flow rate into the mixing cell (mL/yr), Cin is the concentration (activity flux) into the mixing cell (pCi/L), Min is the mass entering the mixing cell (pCi), Mout is the mass leaving the mixing cell (pCi), Mbaq is the aqueous phase mass in the mixing cell (pCi), Msoil is the mass of soil within the mixing cell (gm), and Vbaq is the volume of water within the mixing cell (mL). The subscripts *i* and *i-1* refer to the simulation time steps, with *i* being the current and *i-1* being the previous time step. The necessary conversion factors were applied during the calculations to maintain consistent units.

Figures 2-12a through 2-17 show the calculated maximum saturated-zone groundwater concentrations for all the corresponding unsaturated-zone concentration plots presented in Figures 2-5a through 2-10. Because of the relatively large size of the mixing cell and the high K_d values, the saturated-zone groundwater concentrations are lower, as expected, than those presented in the unsaturated-zone transport results. Calculation of the groundwater concentrations accounted for sorption of the radionuclides to the aquifer materials; however, the impact of radioactive decay, once in the saturated zone, was not incorporated. This can be seen in the concentration curves that reach an asymptotic value over time. Therefore, the maximum concentrations are considered to be conservative in that they are higher than expected.

Table 2-2 presents the maximum groundwater concentrations for each radionuclide from each unsaturated-zone simulation. Because of the relatively large size of the mixing cell and the high K_d values, the calculated saturated-zone groundwater concentrations are lower, as expected, than those presented in the unsaturated-zone transport results. A value of $1x10^{-5}$ pCi/L was chosen as the minimum value at which the concentrations were noted in Table 2-2. The 't' columns in Table 2-2 present the simulation time at which the maximum concentration was reached. A time of 400 years indicates that the concentrations were still increasing at the end of the simulation timeframe. The black/solid filled cells show the concentrations that are above the MCL or the RBA, if a MCL is not available (WSRC, 2001a). The MCL or RBA values for each radionuclide are listed in Table 2-3.

The following summarizes the results presented in Table 2-2:

1) Existing Asphalt Cover: For the Existing Asphalt Cover, no CMCOC exceeded its MCL or RBA. However, a Sr^{90} (K_d = 6.0 mL/g) maximum concentration of 6.3 pCi/L is only slightly lower than the 8 pCi/L MCL for Basin 1 at a high water-table elevation.

Table 2-2 Maximum Saturated-Zone Groundwater Concentrations (pCi/L)

Basin	Watertable Elevation	Cover Scenario	Infiltration Rate (in/yr)	Maximum Saturated-Zone Concentrations (pCi/L), Time (years) to Maximum Concentration and K_d (mL/g)											
				Sr^{90} (K_d = 6)	t	Sr^{90} (K_d = 60)	t	C^{14} (K_d = 6)	t	C^{14} (K_d = 55)	t	Am^{241} (K_d = 100)	t	$Pu^{239/240}$ (K_d = 250)	t
1	H	Enhanced Asphalt Cover	0.15	7.4×10^{-1}	400	1.6×10^{-5}	400	3.5×10^{-4}	400			1.8×10^{-4}	400		
		Existing Asphalt Cover	0.45	6.3	398	4.2×10^{-4}	400	1.2×10^{-1}	400			4.1×10^{-3}	400		
		Reinforced Asphalt Cover	1.0	55.9	354	5.5×10^{-3}	400	4.5	400			4.2×10^{-2}	400	3.3×10^{-5}	400
		Concrete Cover	3.0	1,448	230	1.4×10^{-1}	386	48.7	400	1.2×10^{-4}	400	6.2×10^{-1}	400	1.6×10^{-3}	400
		1×10^{-5} cm/s Soil Cover	6.2	6,903	150	9.7×10^{-1}	396	55	268	5.0×10^{-2}	400	2.7	400	1.0×10^{-2}	400
		No Action / Failed Cover	7.5	9,500	132	1.8	388	55	222	1.5×10^{-1}	400	4.4	400	1.6×10^{-2}	400
		No Cover	15.0	22,527	80	17.9	316	56	110	2.2	400	54.9	400	6.3×10^{-2}	400
	L	Enhanced Asphalt Cover	0.15												
		Existing Asphalt Cover	0.45												
		Reinforced Asphalt Cover	1.0	1.7×10^{-4}	400			2.6×10^{-5}	400						
		Concrete Cover	3.0	4.3	400			4.6	400						
		1×10^{-5} cm/s Soil Cover	6.2	238	284			47.5	400						
		No Action / Failed Cover	7.5	531	250			51	394						
		No Cover	15.0	4,471	148	6.8×10^{-4}	400	52	196	1.4×10^{-3}	400	1.0×10^{-3}	400		
3	H	Enhanced Asphalt Cover	0.15	1.7×10^{-2}	400			1.8×10^{-2}	400						
		Existing Asphalt Cover	0.45	3.8×10^{-1}	400			2.4	400						
		Reinforced Asphalt Cover	1.0	7.8	398	1.5×10^{-5}	400	75.0	400			1.2×10^{-4}	400		
		Concrete Cover	3.0	443	254	3.0×10^{-3}	400	1,210	400	6.7×10^{-3}	400	6.8×10^{-3}	400	2.3×10^{-5}	400
		1×10^{-5} cm/s Soil Cover	6.2	2,805	166	6.3×10^{-2}	400	1,544	306	9.0×10^{-1}	400	6.0×10^{-2}	400	1.0×10^{-3}	400
		No Action / Failed Cover	7.5	4,571	146	1.5×10^{-1}	400	1,547	252	2.5	400	9.8×10^{-2}	400	2.3×10^{-3}	400
		No Cover	15.0	11,094	86	3.4	358	1,569	126	42.6	400	4.1×10^{-1}	400	2.2×10^{-2}	400
	L	Enhanced Asphalt Cover	0.15												
		Existing Asphalt Cover	0.45												
		Reinforced Asphalt Cover	1.0												
		Concrete Cover	3.0	7.5×10^{-2}	400			8.5	400						
		1×10^{-5} cm/s Soil Cover	6.2	22.4	354			846	400						
		No Action / Failed Cover	7.5	65.3	310			1,246	400						
		No Cover	15.0	1,098	184			1,437	246	9.4×10^{-5}	400				

Table 2-2 (continued)

Basin	Watertable Elevation	Cover Scenario	Infiltration Rate (in/yr)	Maximum Saturated-Zone Concentrations (pCi/L), Time (years) to Maximum Concentration and K_d (mL/g)											
				Sr^{90} (K_d = 6)	t	Sr^{90} (K_d = 60)	t	C^{14} (K_d = 6)	t	C^{14} (K_d = 55)	t	Am^{241} (K_d = 100)	t	$Pu^{239/240}$ (K_d = 250)	t
6	H	Enhanced Asphalt Cover	0.15	$6.9x10^{-2}$	400										
		Existing Asphalt Cover	0.45	$7.9x10^{-1}$	400	$3.5x10^{-5}$	400								
		Reinforced Asphalt Cover	1.0	10.4	354	$4.8x10^{-4}$	400								
		Concrete Cover	3.0	289	216	$1.3x10^{-2}$	400					$1.3x10^{-5}$	400		
		$1x10^{-5}$ cm/s Soil Cover	6.2	1,239	138	$1.3x10^{-1}$	400					$4.6x10^{-4}$	400		
		No Action / Failed Cover	7.5	1,655	122	$2.6x10^{-1}$	400					$1.0x10^{-3}$	400		
		No Cover	15.0	3,583	72	3.6	308					$1.8x10^{-2}$	400	$2.7x10^{-4}$	400
	L	Enhanced Asphalt Cover	0.15		400										
		Existing Asphalt Cover	0.45		400										
		Reinforced Asphalt Cover	1.0		400										
		Concrete Cover	3.0	$1.1x10^{-1}$	400										
		$1x10^{-5}$ cm/s Soil Cover	6.2	14.1	318										
		No Action / Failed Cover	7.5	35.9	278										
		No Cover	15.0	419	164										

Notes:
1. No C^{14} in Basin 6
2. No C^{14} above $1x10^{-5}$ pCi/L for a K_d of 500 mL/g
3. Black filled cells show concentrations higher than the MCL or the RBA
4. Maximum concentrations below $1x10^{-5}$ pCi/L were not included in table

Table 2-3 MCL or RBA Values for Each Radionuclide

Radionuclide	MCL (pCi/L)	RBA (pCi/L)
Am^{241}		0.145
C^{14}	2000	
$Pu^{239/240}$		0.151
Sr^{90}	8	

2) Failed Asphalt Cover (No Action Case): Two CMCOCs exceeded their respective MCLs for this remedial alternative. The Sr^{90} (K_d = 6.0 mL/g) concentrations for all three basins and both water-table elevations exceeded the MCL, with concentrations ranging from 35.9 to 9,500 pCi/L. The Am^{241} concentration for the high water-table elevation in Basin 1 also exceeded the RBA with a value of 4.4 pCi/L.

3) $1x10^{-5}$ cm/s Soil Cover: Two of the CMCOCs exceeded their respective MCLs for this remedial alternative. The Sr^{90} concentrations for all three basins and both water-table elevations exceeded the MCL, with concentrations ranging from 14.1 to 6,903 pCi/L. The Am^{241} concentration for the high water-table elevation in Basin 1 also exceeded the RBA with a value of 2.7 pCi/L.

4) Concrete Cover: Two of the CMCOCs exceeded their respective MCLs for this remedial alternative. The Sr^{90} (K_d = 6.0 mL/g) concentrations for all three basins at the high water-table elevation and exceeded the MCL, with concentrations ranging from 289 to 1,448 pCi/L. The Am^{241} concentration for the high water-table elevation in Basin 1 also exceeded the RBA with a value of 0.62 pCi/L.

5) Reinforced Asphalt Cover: Only the Sr^{90} (K_d = 6.0 mL/g) concentrations for Basins 1 and 6 at the high water-table elevation exceeded the MCL, with values of 55.9 and 10.4 pCi/L, respectively.

6) No Cover: The maximum Sr^{90} concentrations for the basecase K_d value of 6.0 mL/g exceeded the MCL for all three basins and both water-table elevations, with values ranging from 419 to 22,527 pCi/L. The maximum Sr^{90} concentrations for the increased K_d value of 60.0 mL/g only exceeded the MCL for Basin 1 and the high water-table elevation with a value of 17.9 pCi/L. The Am^{241} concentration for the high water-table elevation in Basins 1 and 3 also exceeded the RBA, with values of 54.9 and 0.41 pCi/L, respectively.

7) The maximum saturated-zone concentrations calculated for C^{14}, based on all three K_d values, and $Pu^{239/240}$ do not exceed the MCL or RBA for any combination of basin, water-table elevation, or basin cover configuration.

Overall, the maximum groundwater concentrations are highly dependent on the assumptions made in the calculations. These assumptions included a vertical mixing thickness of 50 ft. If this thickness is decreased, then the mixing volume and subsequent amount of dilution would

decrease, resulting in higher concentrations. However, the effects of radioactive decay are not included in these calculations; therefore, these calculations tend to yield higher concentrations than would be observed in the field, given radioactive decay.

2.7 Conclusions

The source terms developed for this task distributed the CMCOC contaminant activity among the basins based on the historical source loading to the basins. The unsaturated-zone modeling incorporated these source terms to determine the transient concentrations of the CMCOCs at the water-table surface, based on the assumption of vertical flow within the unsaturated zone beneath the basins. The unsaturated-zone models were developed to be representative of various remedial alternatives in support of the CMS/FS. The resulting unsaturated-zone concentrations were subsequently converted to maximum saturated-zone concentrations located directly beneath the basins, for comparison against the MCL standards or the RBA criteria.

The modeling results and subsequent saturated-zone concentration calculations predict that Am^{241} will exceed its RBA criteria for only a few selected remedial alternatives and only for the higher infiltration cases under high water-table elevations. Given the expected decrease in concentration as a result of a lower water-table elevation and the exclusion of radioactive decay and dispersive forces in the concentration calculation, it is not expected that Am^{241} will actually exceed its RBA within the saturated zone beneath the seepage basins.

The uncertainty in the magnitude of the retardation potential for C^{14} was investigated by varying the K_d value over two orders of magnitude. These results predict that C^{14} will not exceed its MCL, but approaches the MCL of 2000 pCi/L for the higher infiltration rate scenarios through Basin 3, which has the largest C^{14} source term.

The results indicate that Sr^{90} (K_d = 6 mL/g) will exceed its MCL value in the saturated aquifer located directly beneath the basins for all of the remedial alternatives evaluated, except for the Enhanced Asphalt Cover and the Existing Asphalt Cover. These two alternatives incorporate the lowest infiltration rates. The predicted Sr^{90} concentrations within the groundwater are expected to decrease through time given radioactive decay and dispersive processes as the Sr^{90} is transported further into the saturated zone. However, in order to quantify the concentrations and the transport of Sr^{90} within the saturated zone, additional detailed groundwater flow and transport modeling is required. This detailed modeling was conducted and is presented in Sections 3.0 and 4.0.

Basin 1					Basin 3					Basin 6					
Elevation (ft amsl)	Am^{241}	C^{14}	$Pu^{238/239}$	Sr^{90}	Elevation (ft amsl)	Am^{241}	C^{14}	$Pu^{238/239}$	Sr^{90}	Elevation (ft amsl)	Am^{241}	C^{14}	$Pu^{238/239}$	Sr^{90}	Elevation (ft amsl)
302					302					302					302
301					301		15			301					301
300					300		15			300					300
299					299		15			299					299
298	61		2.6		298		15			298	0.09		0.09		298
297	61		2.6		297		15			297	1.1		1.1		297
296	17116	8.5	73	4940	296	0.04	175	0.03	3025	296	1.1		1.1	54	296
295	1716	8.5	73	4940	295	1.8	175	1.2	3025	295	1.1		1.1	54	295
294	1716		73	4940	294	1.8	32	1.2	3025	294	0.06		0.06	1300	294
293	25		1.1	4940	293	1.8	32	1.2	3025	293	0.06		0.06	1300	293
292	25		1.1	60	292	1.8		1.2	23	292	0.06		0.06	5.7	292
291	25		1.1	60	291	1.8		1.2	23	291				5.7	291
290	25		1.1	60	290	1.8		1.2	23	290				5.7	290
289					289	0.06		0.4		289					289
288					288					288					288

Note: Soil Concentrations in pCi/gram of soil

Figure 2-1. Source-term soil concentrations (pCi/g) for Basins 1, 3, and 6.

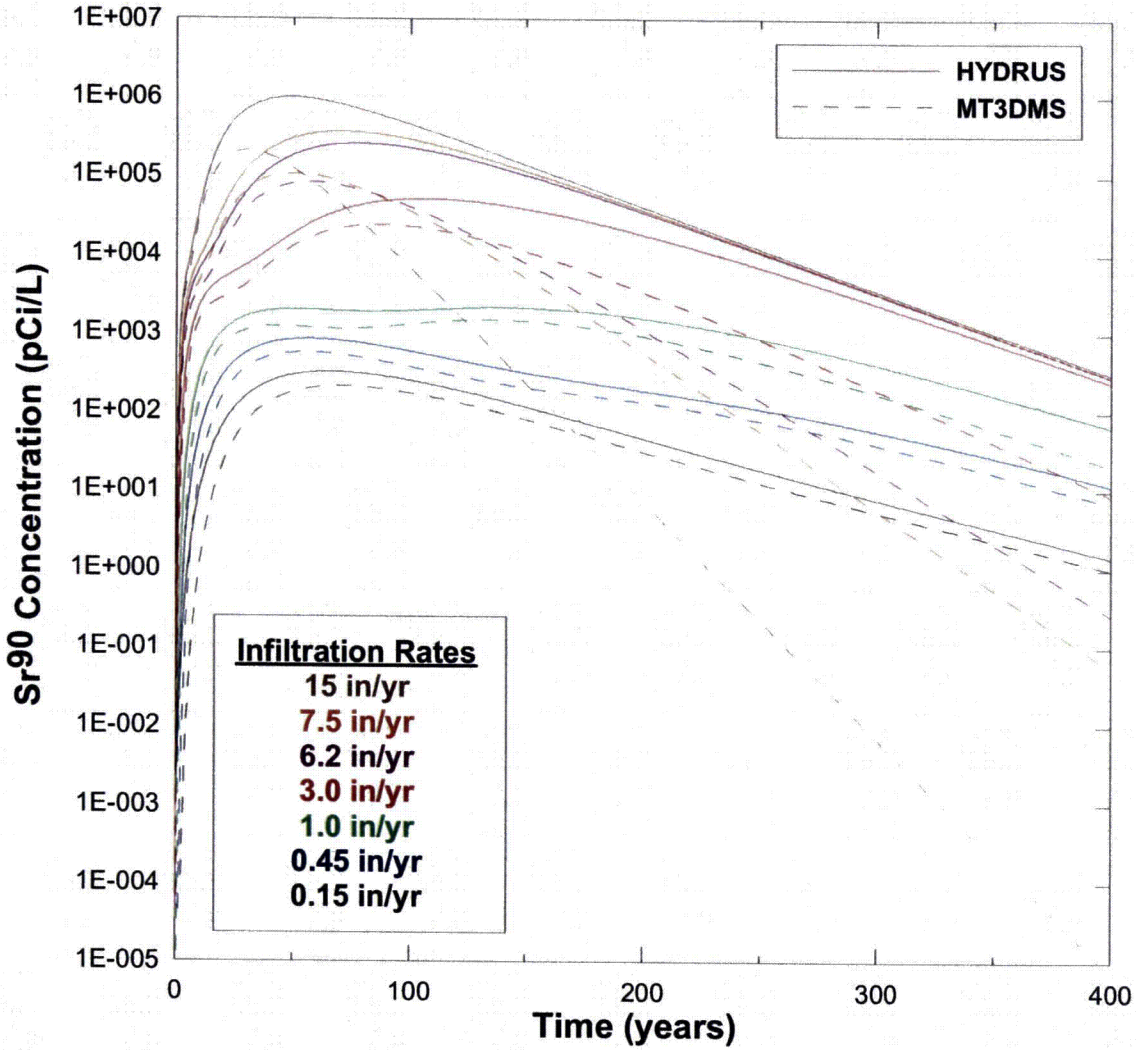

Figure 2-2. Comparison of HYDRUS and MT3DMS Sr^{90} transport results for Basin 1and a high water table elevation.

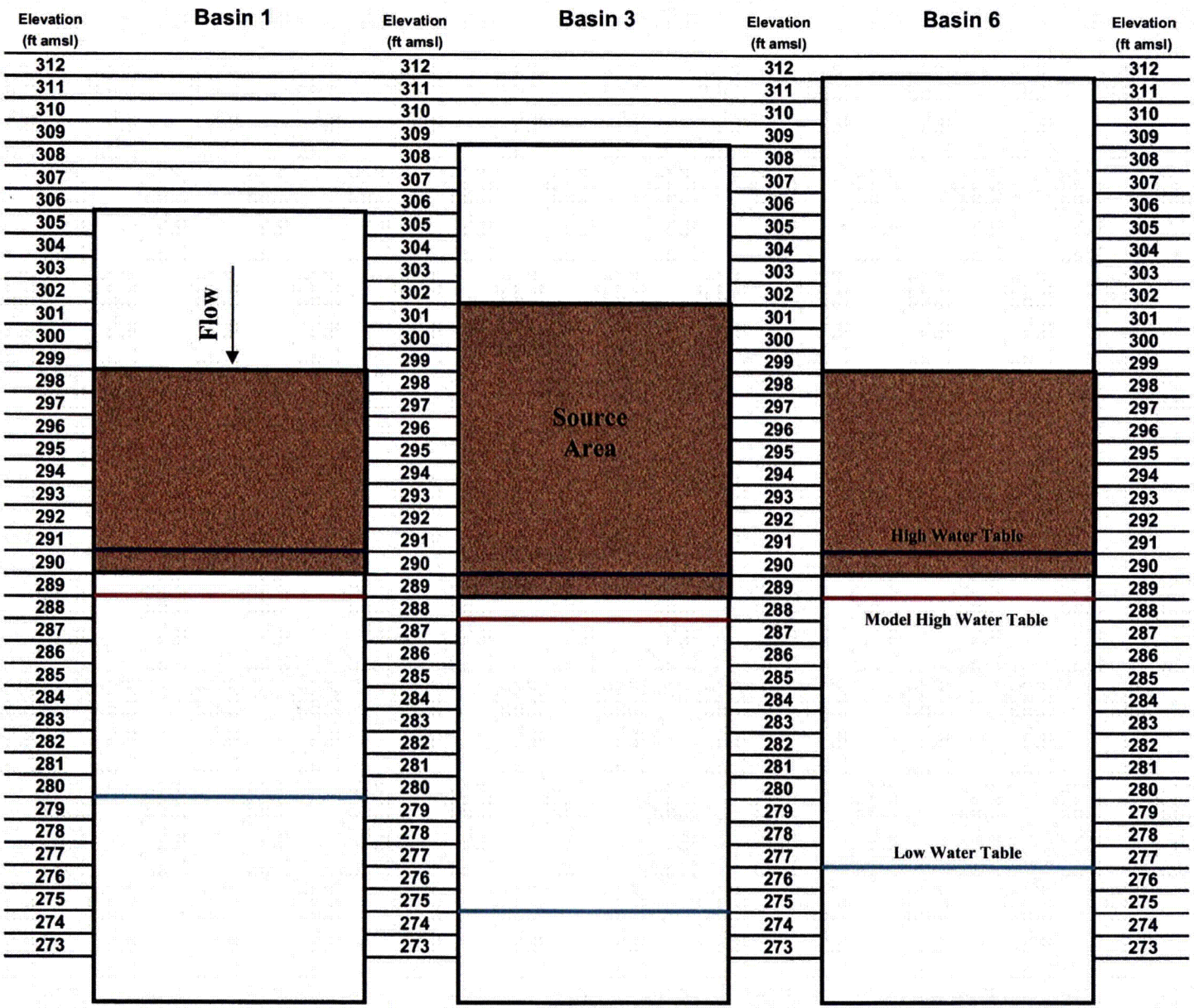

Figure 2-3. Generalized conceptual models for Basins 1, 3, and 6.

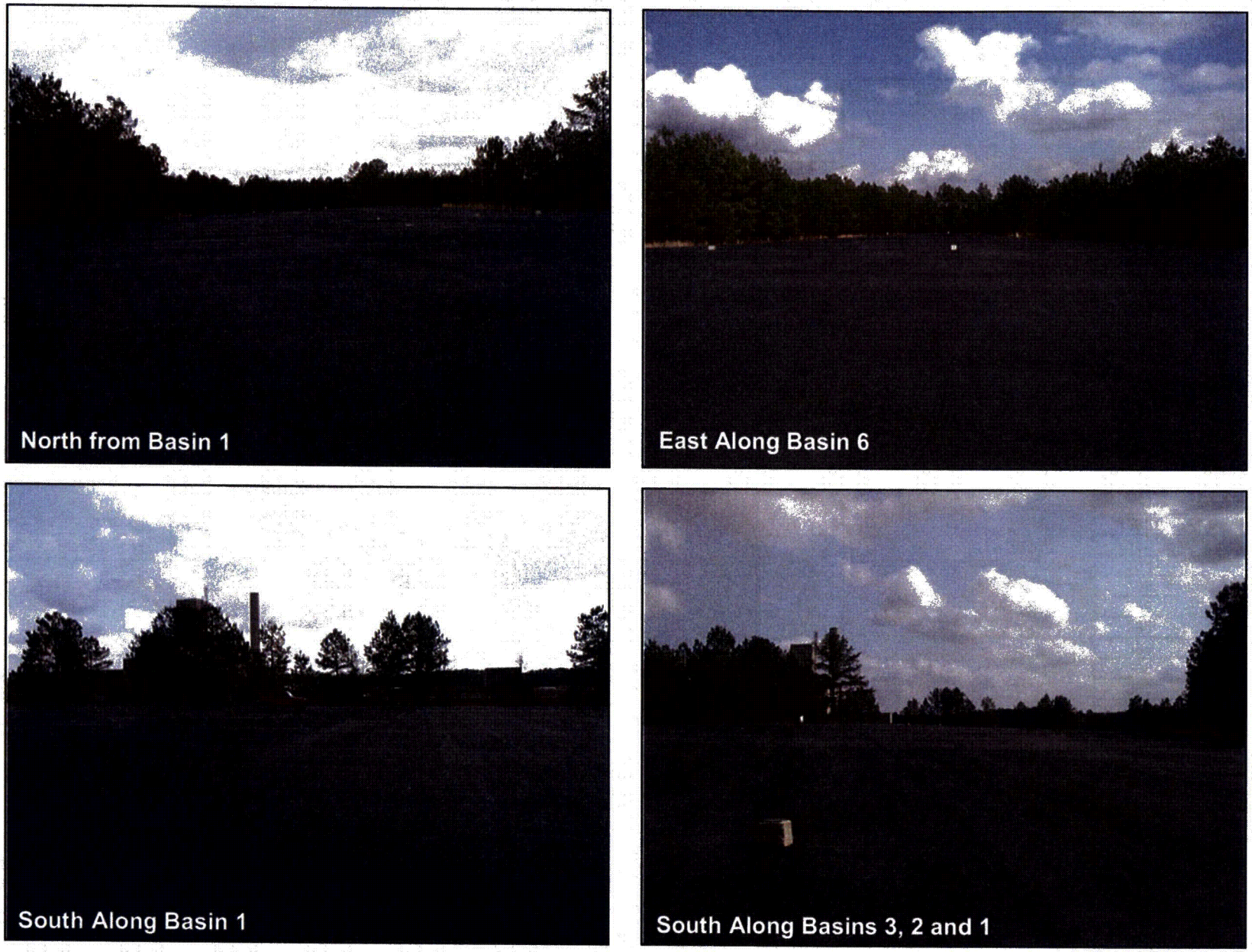

Figure 2-4. Photographs showing the surface condition of the existing asphalt cover located over the RRSB.

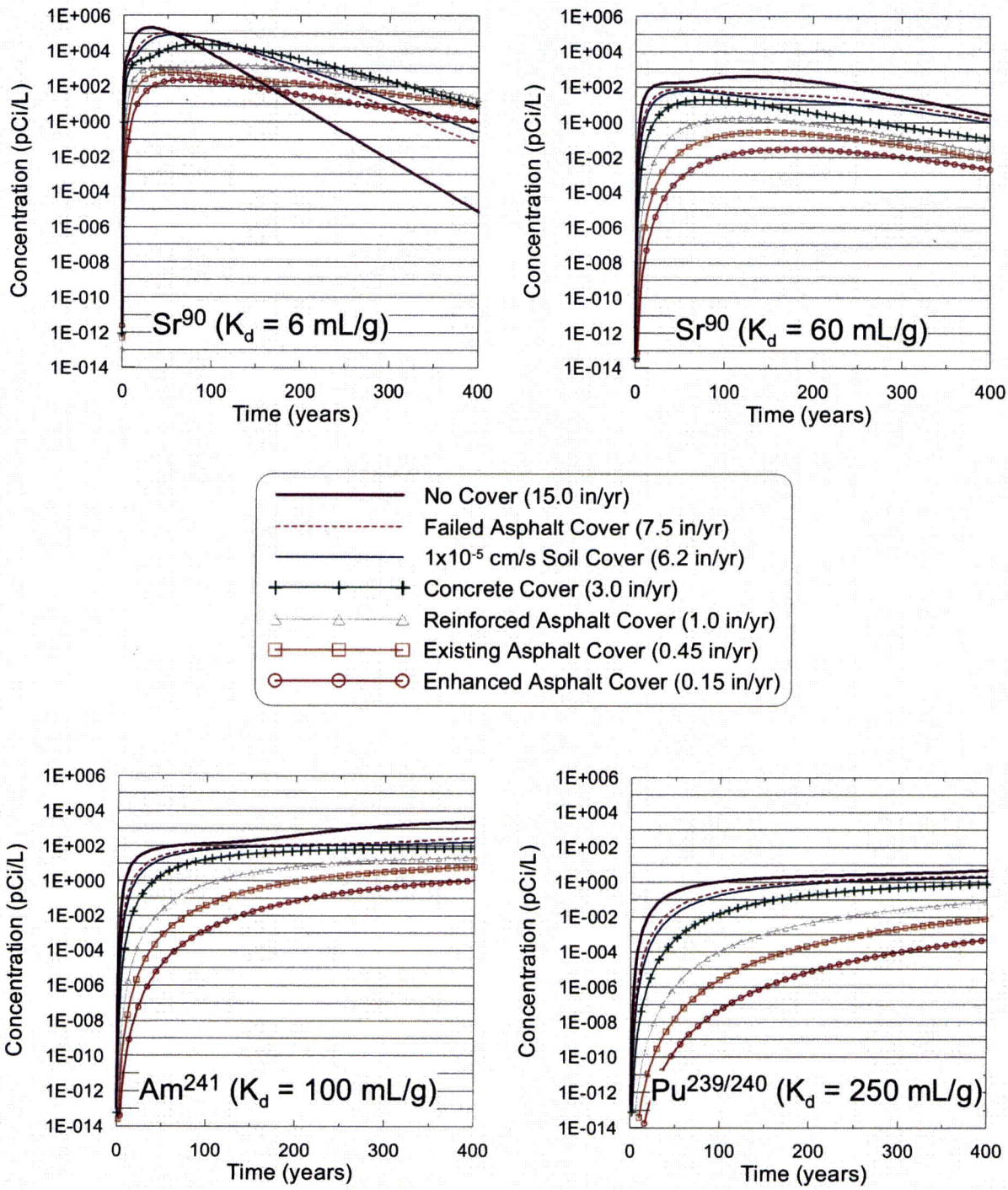

Figure 2-5a. Unsaturated-zone contaminant concentrations (pCi/L) for Basin 1 with a high water table.

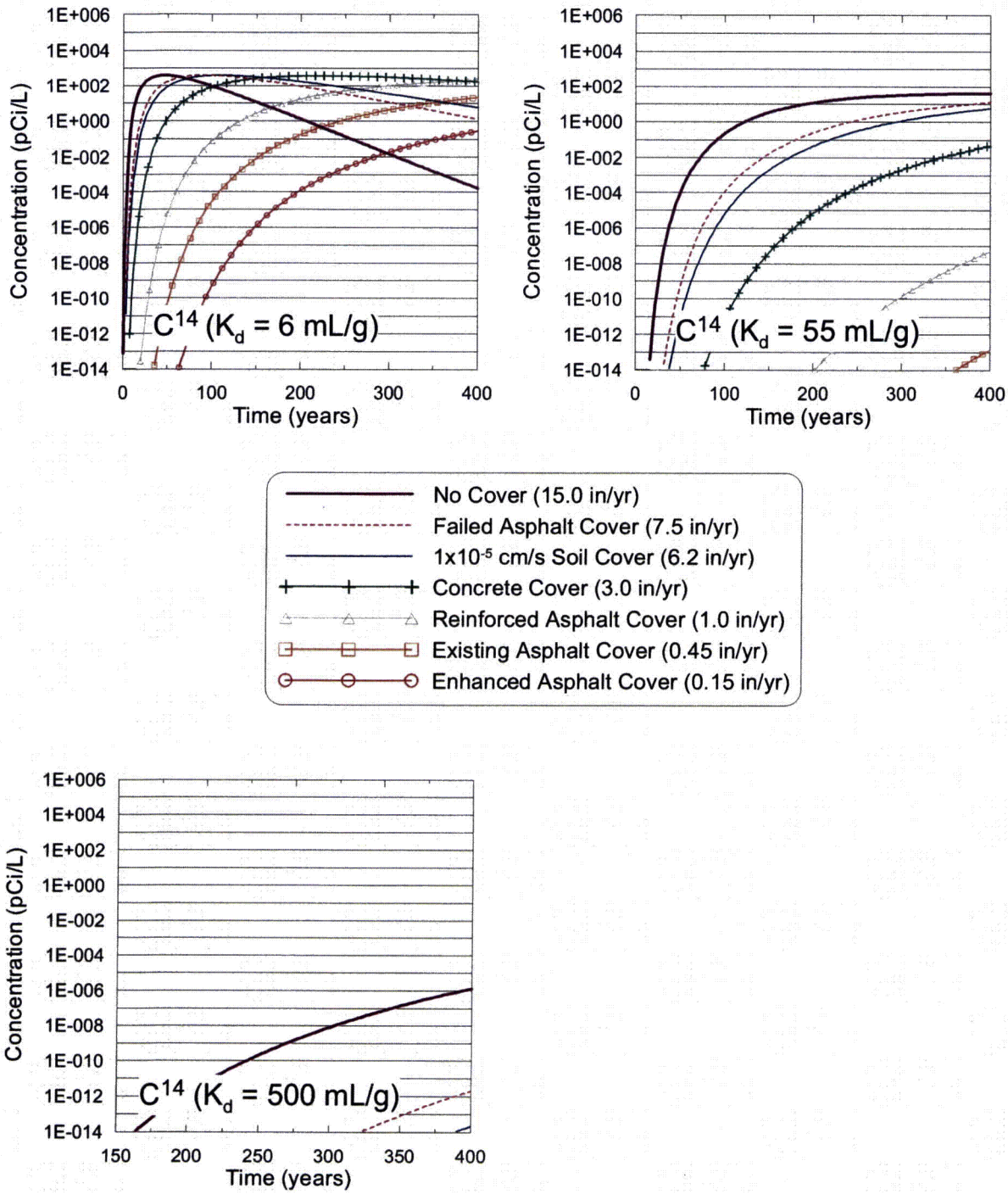

Figure 2-5b. Unsaturated-zone contaminant concentrations (pCi/L) for Basin 1 with a high water table.

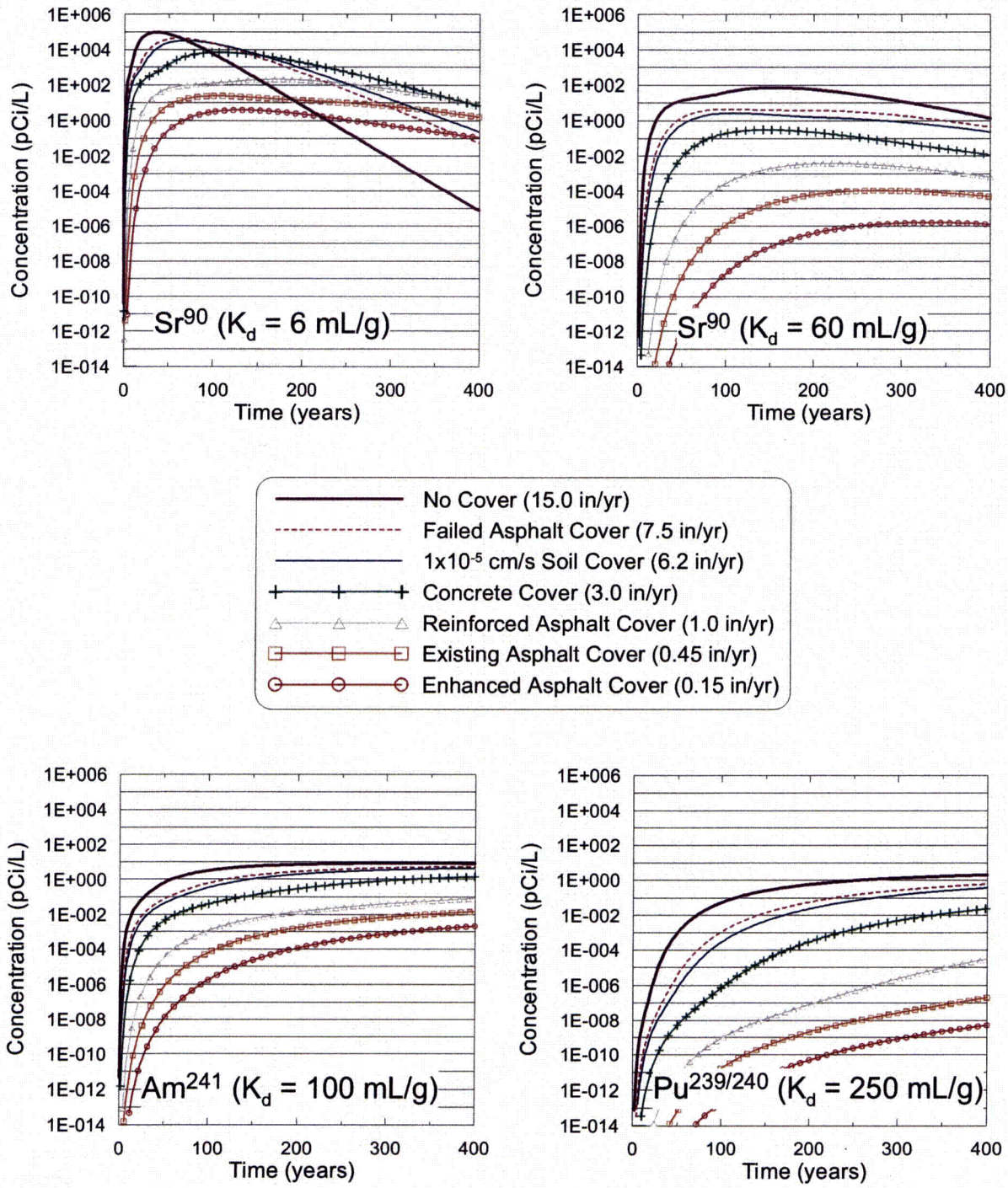

Figure 2-6a. Unsaturated-zone contaminant concentrations (pCi/L) for Basin 3 with a high water table.

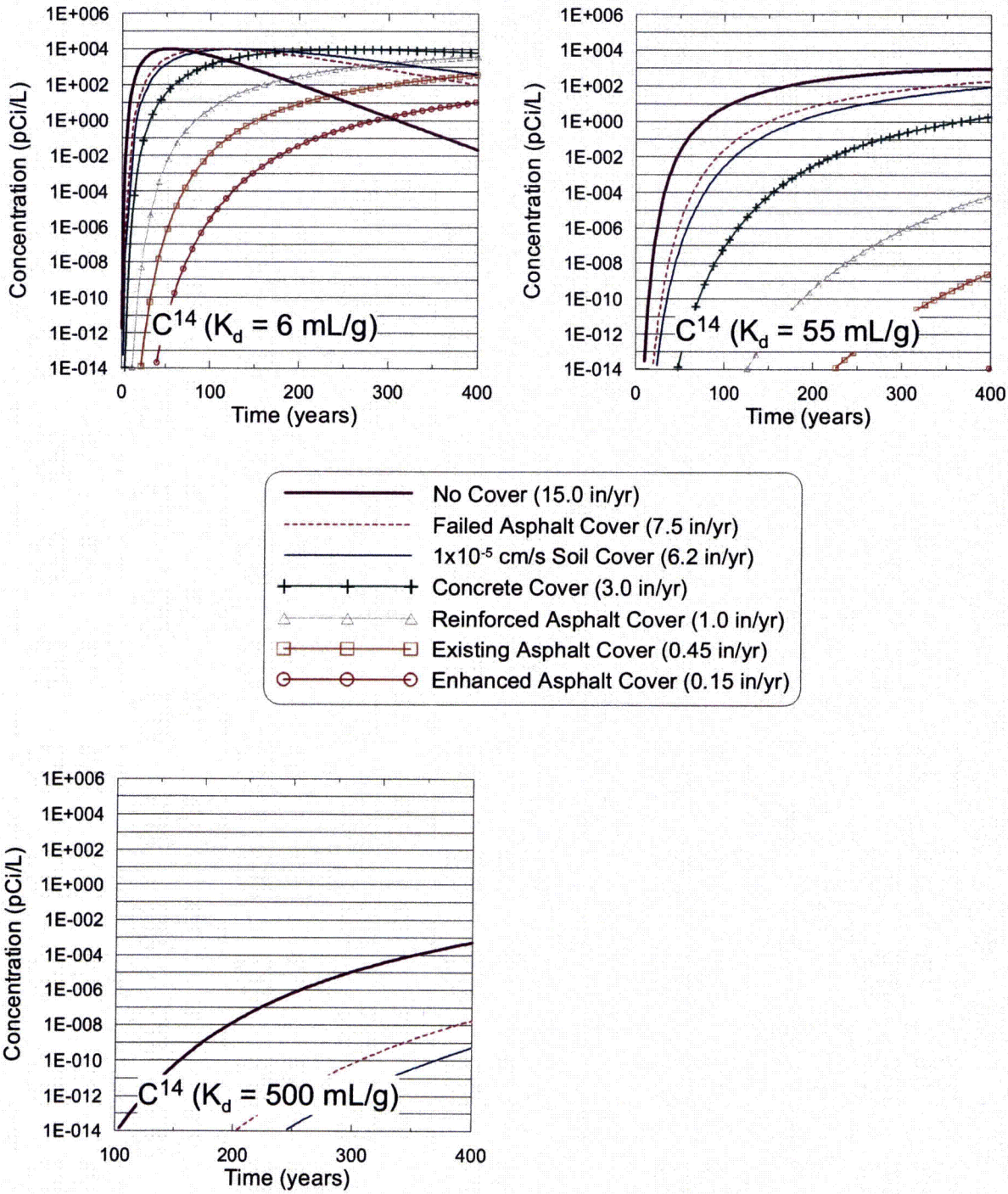

Figure 2-6b. Unsaturated-zone contaminant concentrations (pCi/L) for Basin 3 with a high water table.

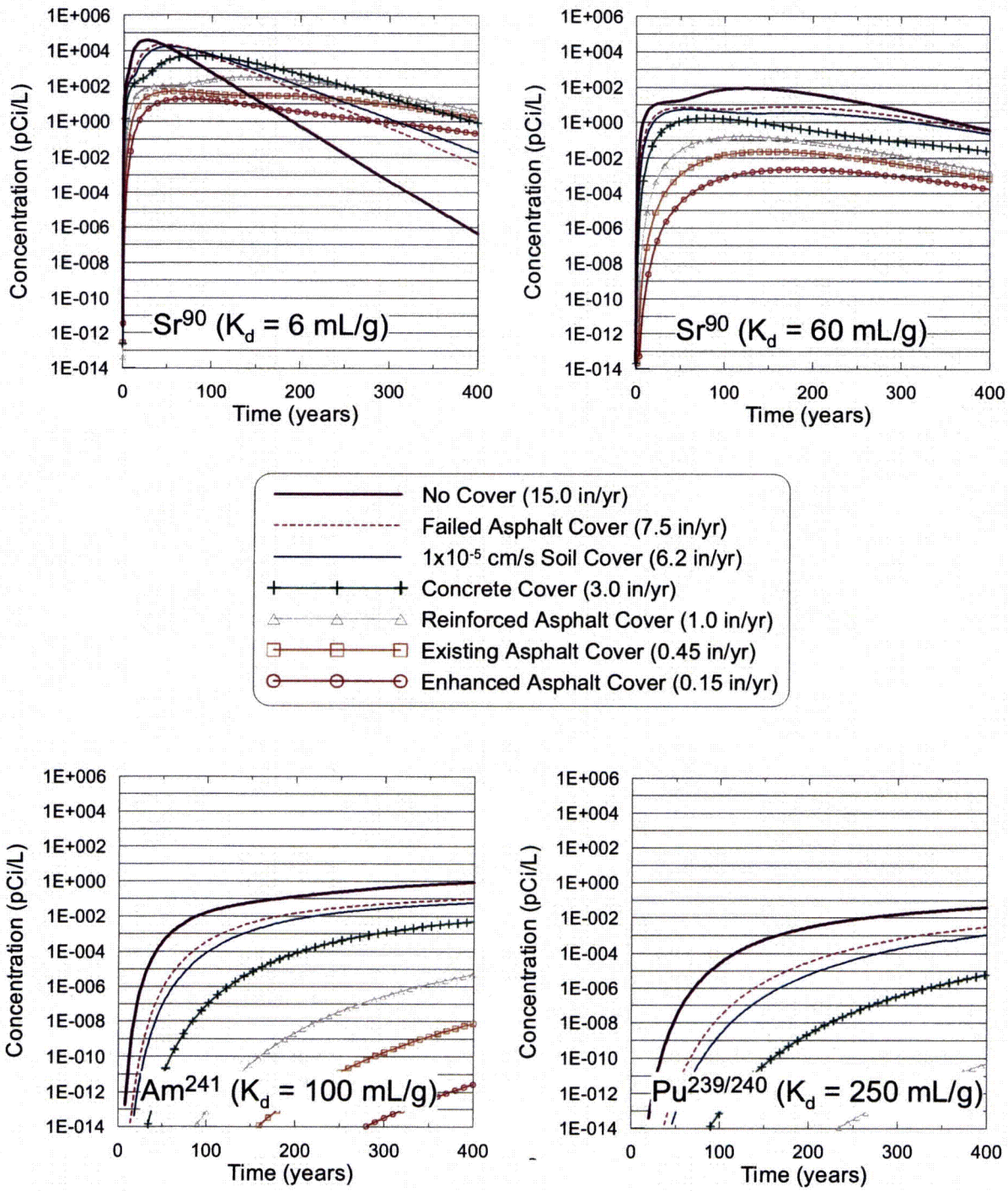

Figure 2-7. Unsaturated-zone contaminant concentrations (pCi/L) for Basin 6 with a high water table.

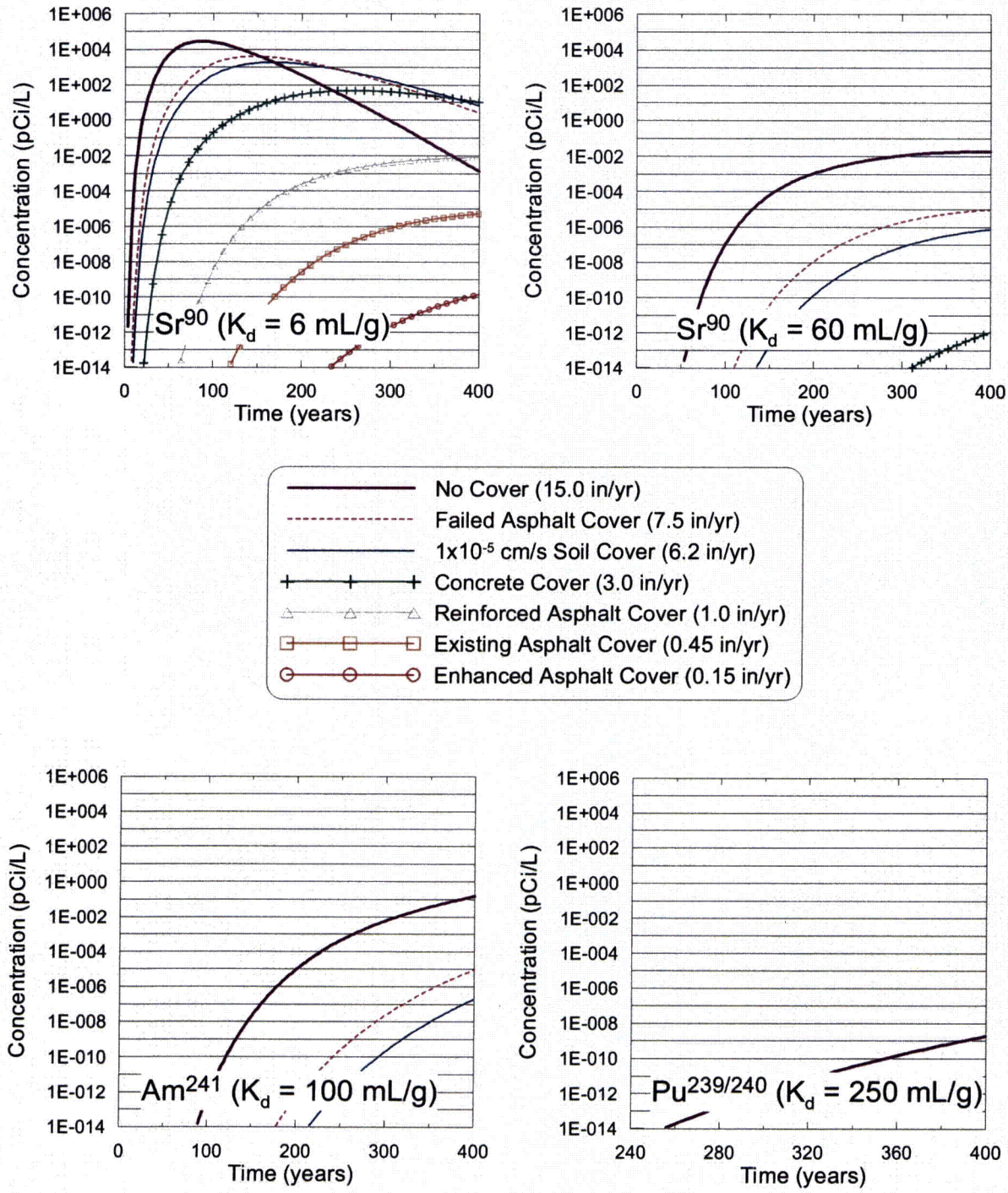

Figure 2-8a. Unsaturated-zone contaminant concentrations (pCi/L) for Basin 1 with a low water table.

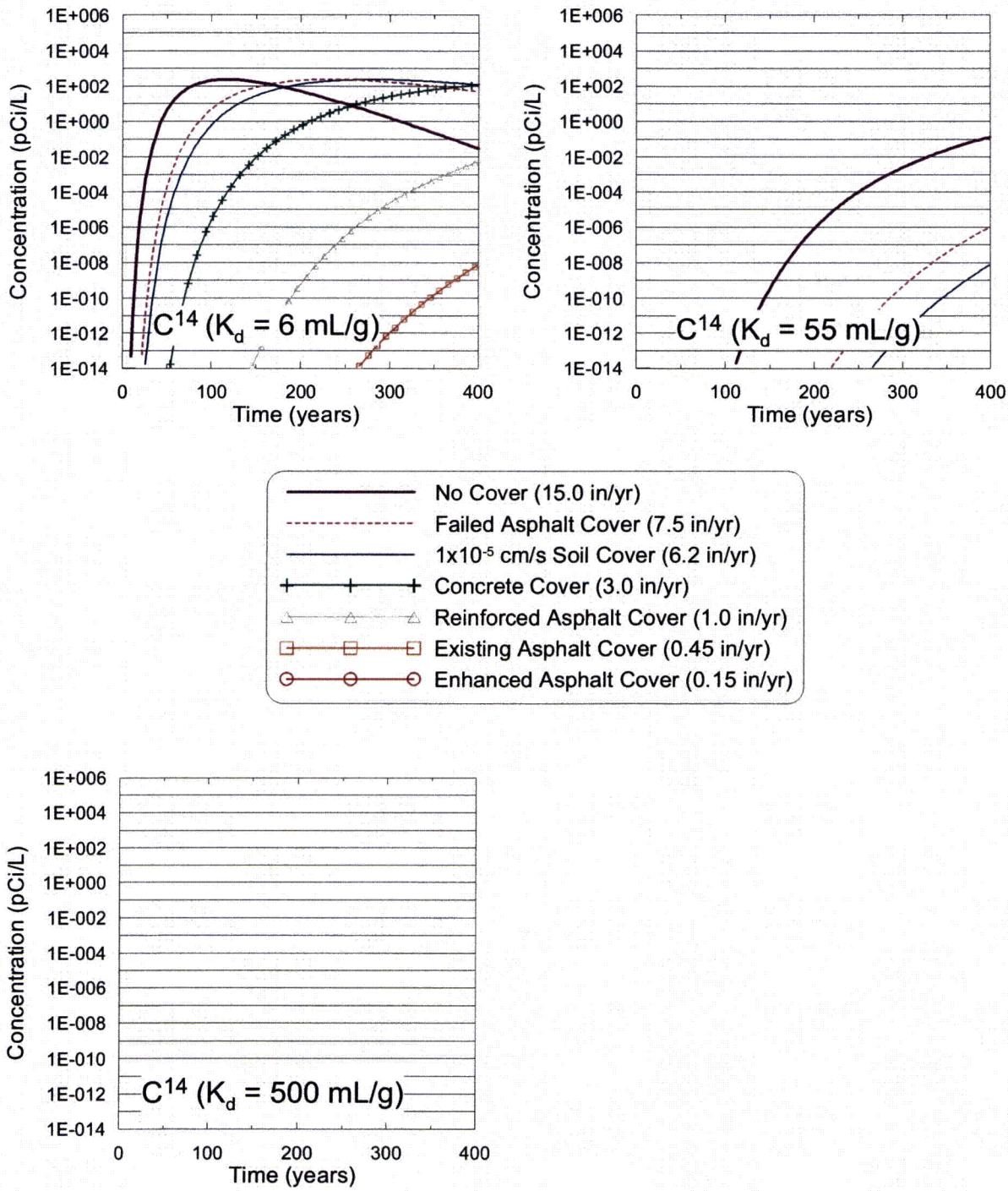

Figure 2-8b. Unsaturated-zone contaminant concentrations (pCi/L) for Basin 1 with a low water table.

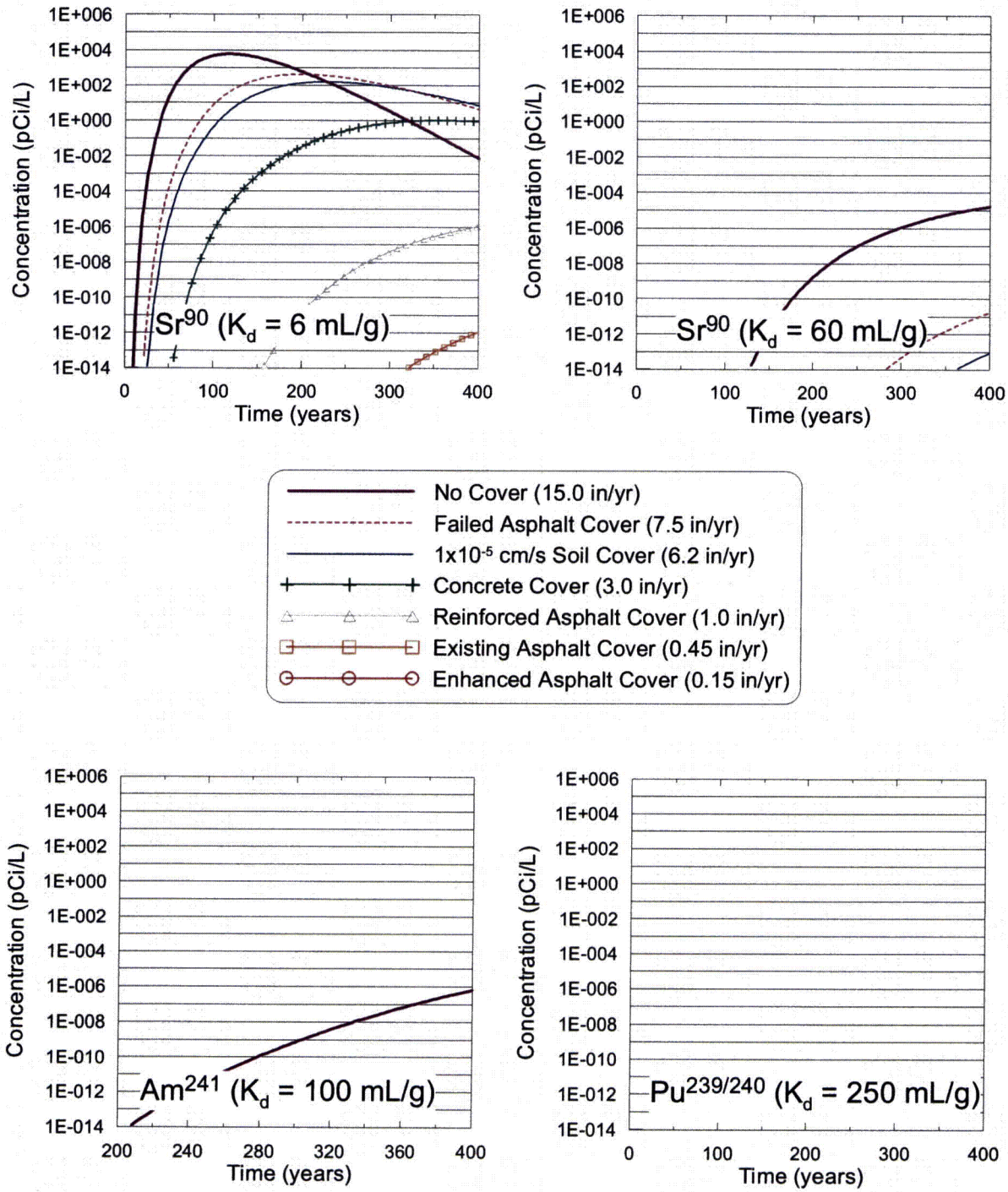

Figure 2-9a. Unsaturated-zone contaminant concentrations (pCi/L) for Basin 3 with a low water table.

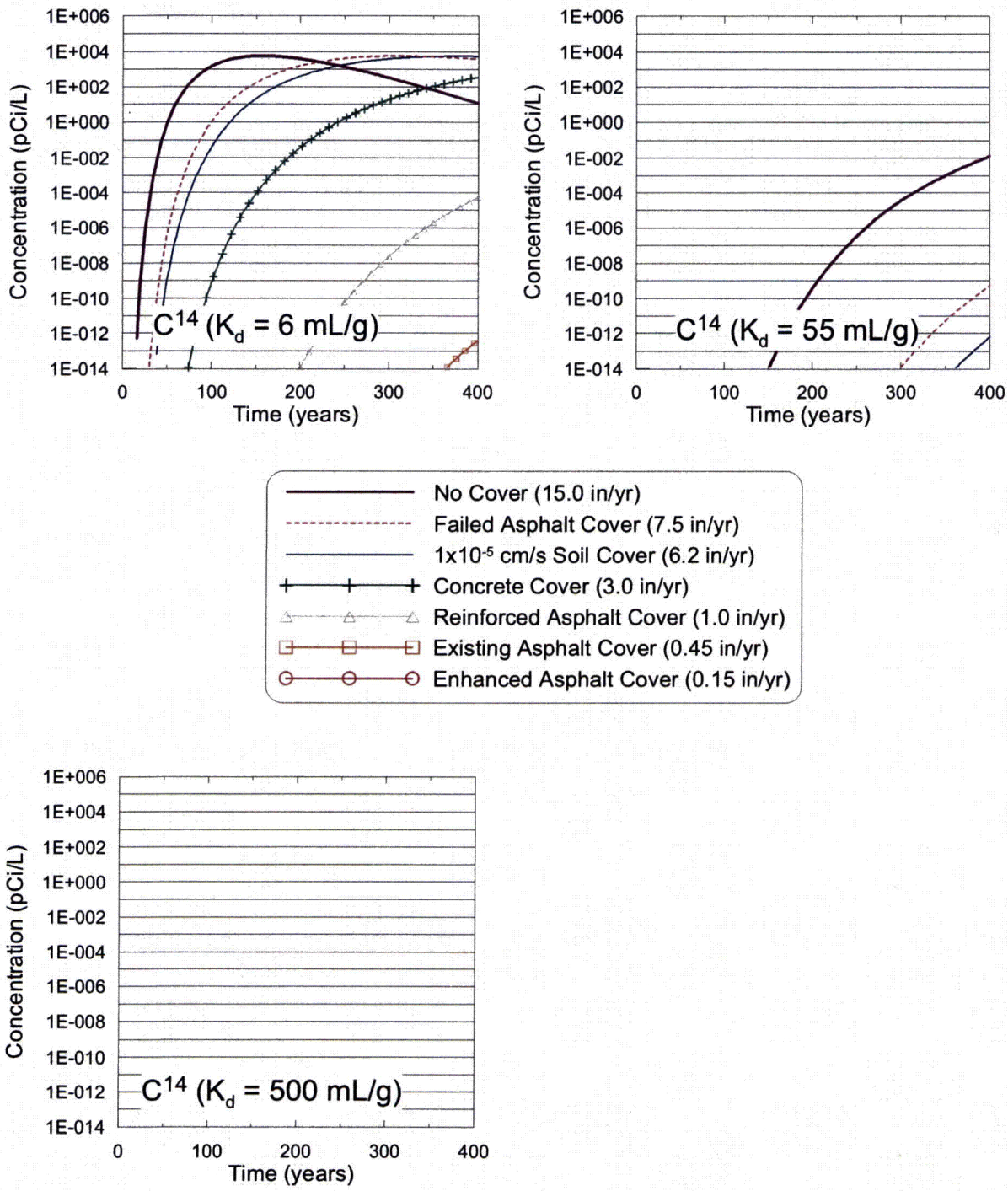

Figure 2-9b. Unsaturated-zone contaminant concentrations (pCi/L) for Basin 3 with a low water table.

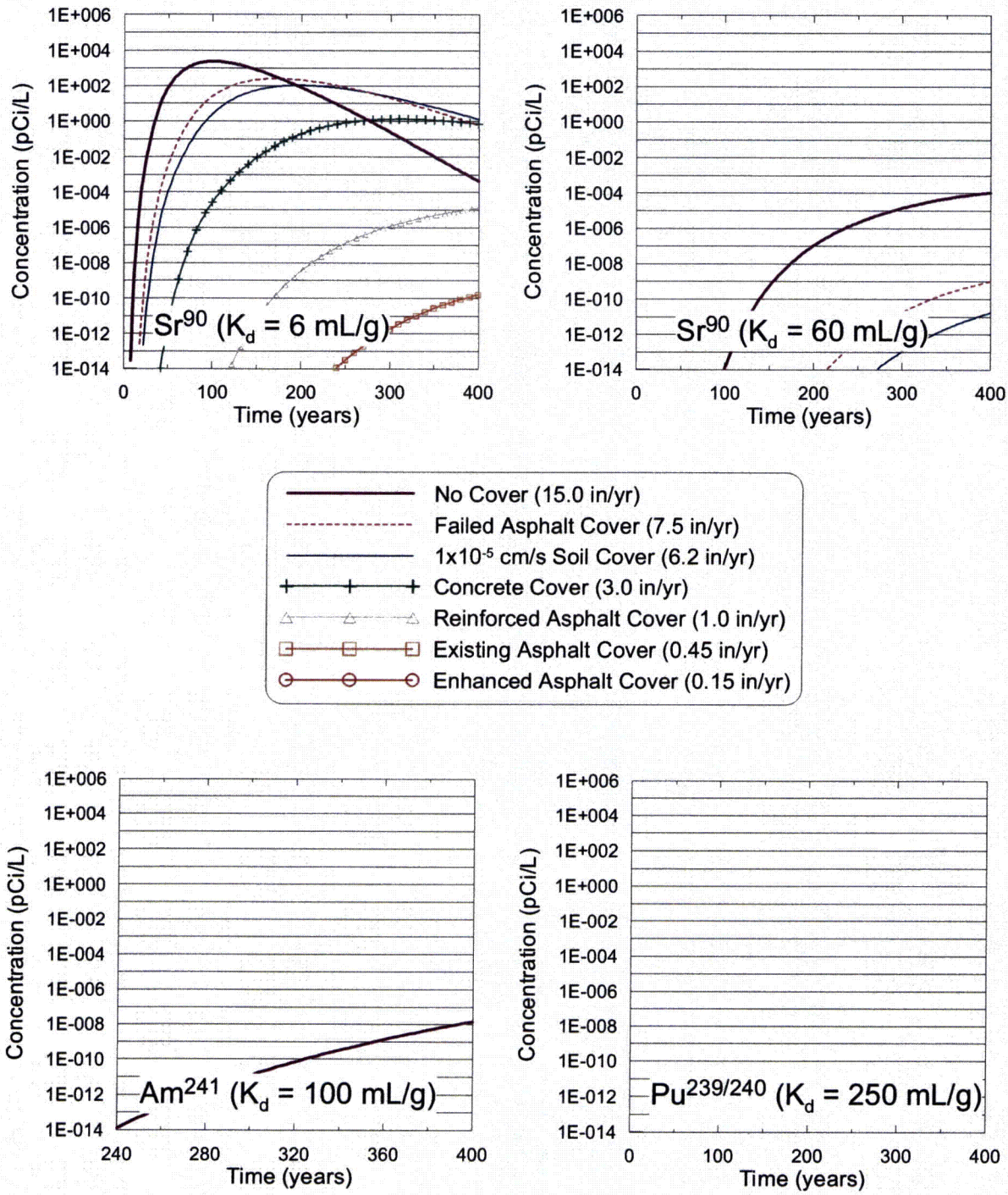

Figure 2-10. Unsaturated-zone contaminant concentrations (pCi/L) for Basin 6 with a low water table.

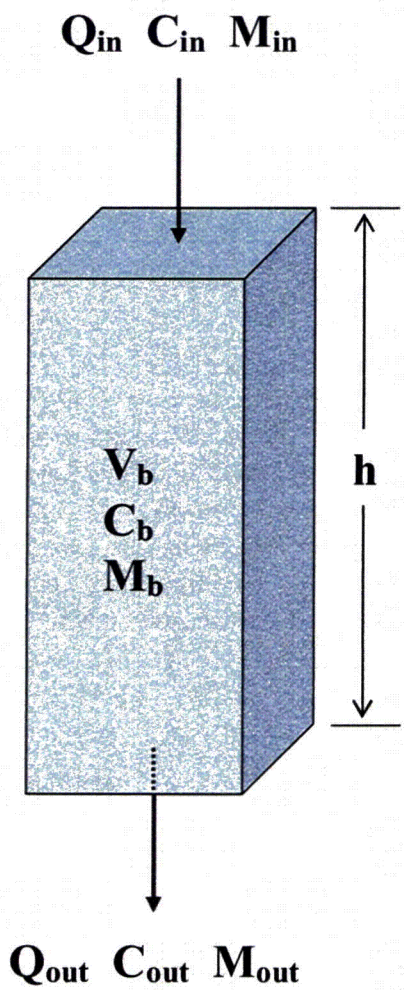

Figure 2-11. Conceptual model for the calculation of the maximum saturated-zone groundwater concentrations.

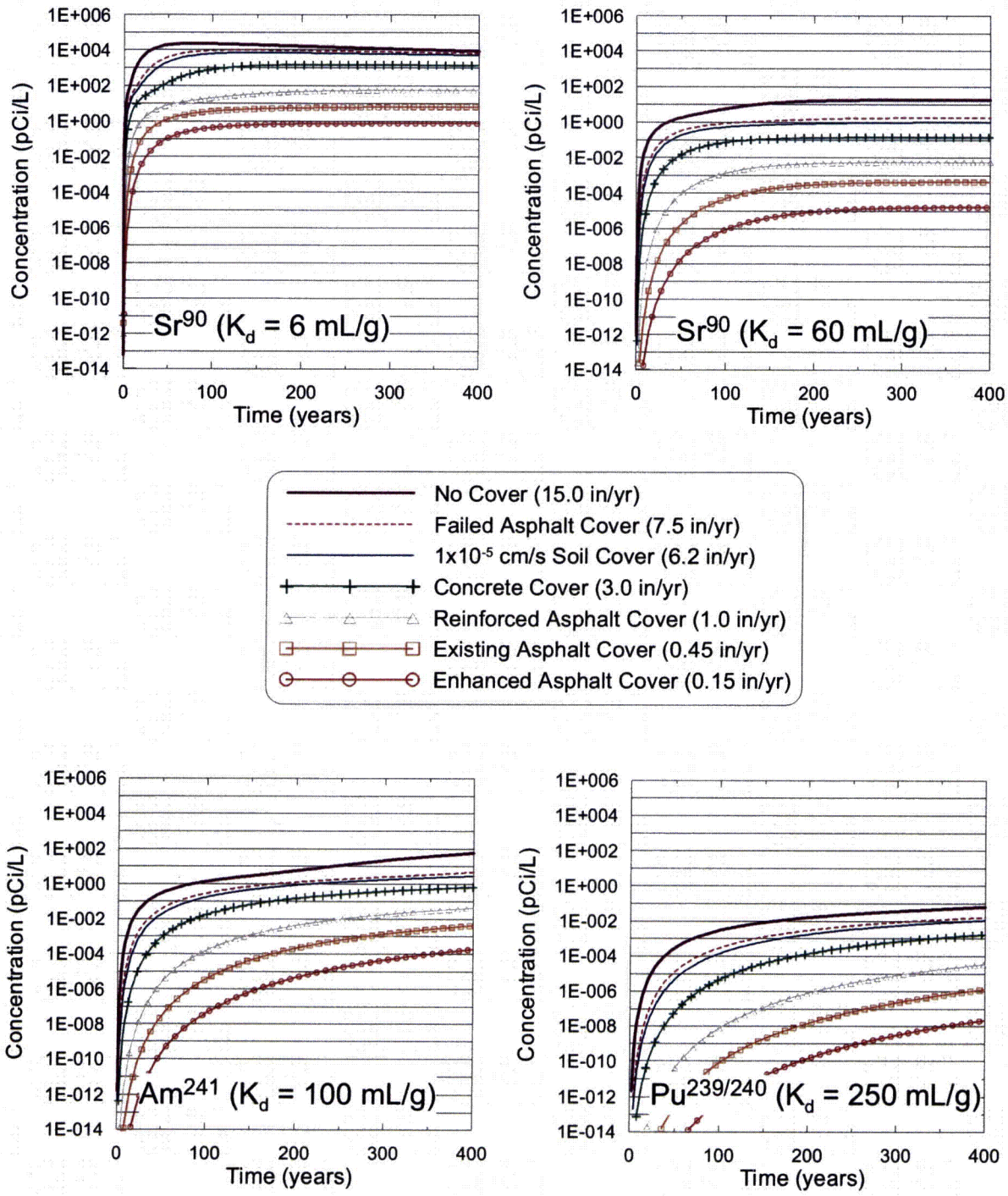

Figure 2-12a. Saturated-zone contaminant concentrations (pCi/L) for Basin 1 with a high water table.

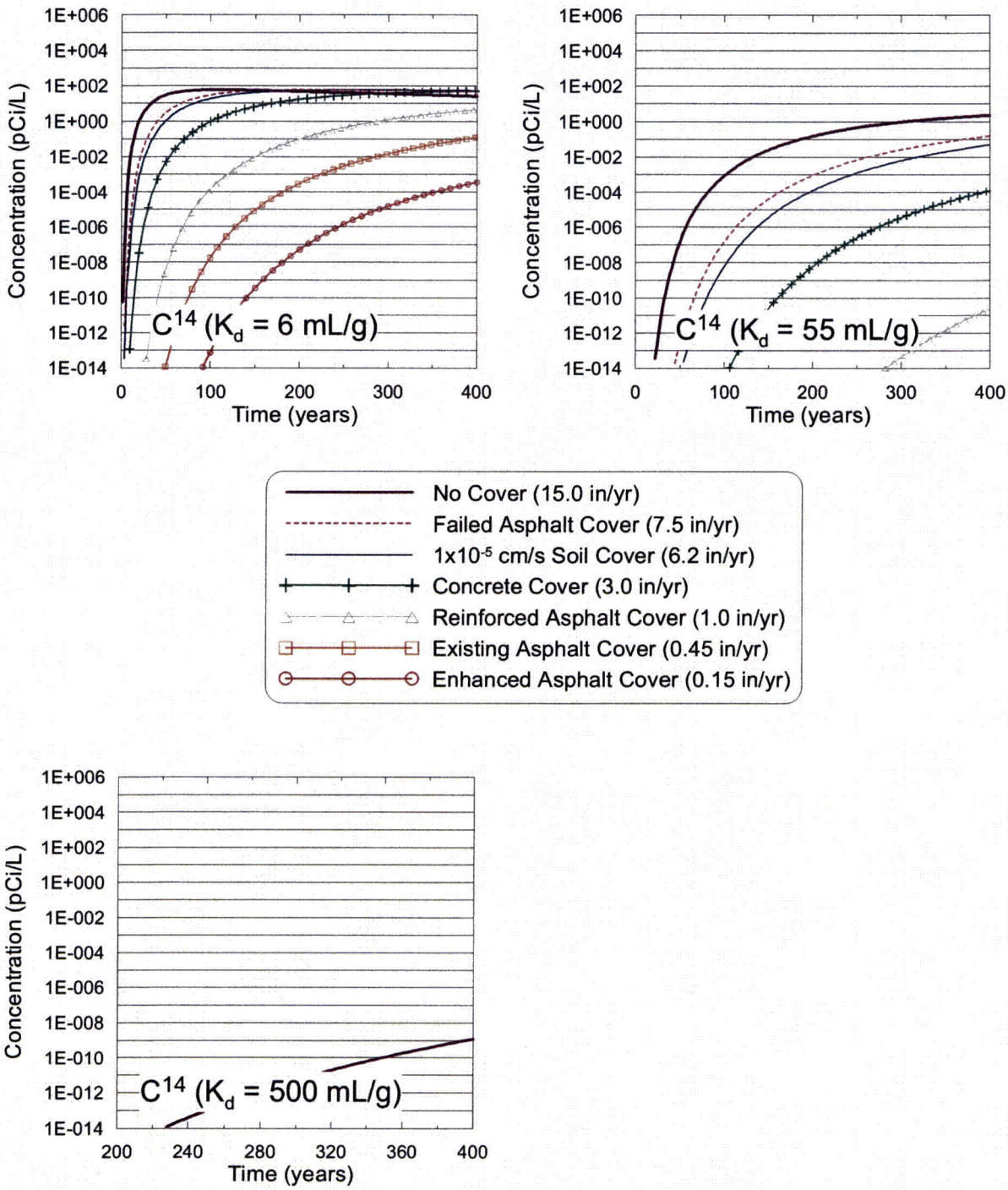

Figure 2-12b. Saturated-zone contaminant concentrations (pCi/L) for Basin 1 with a high water table.

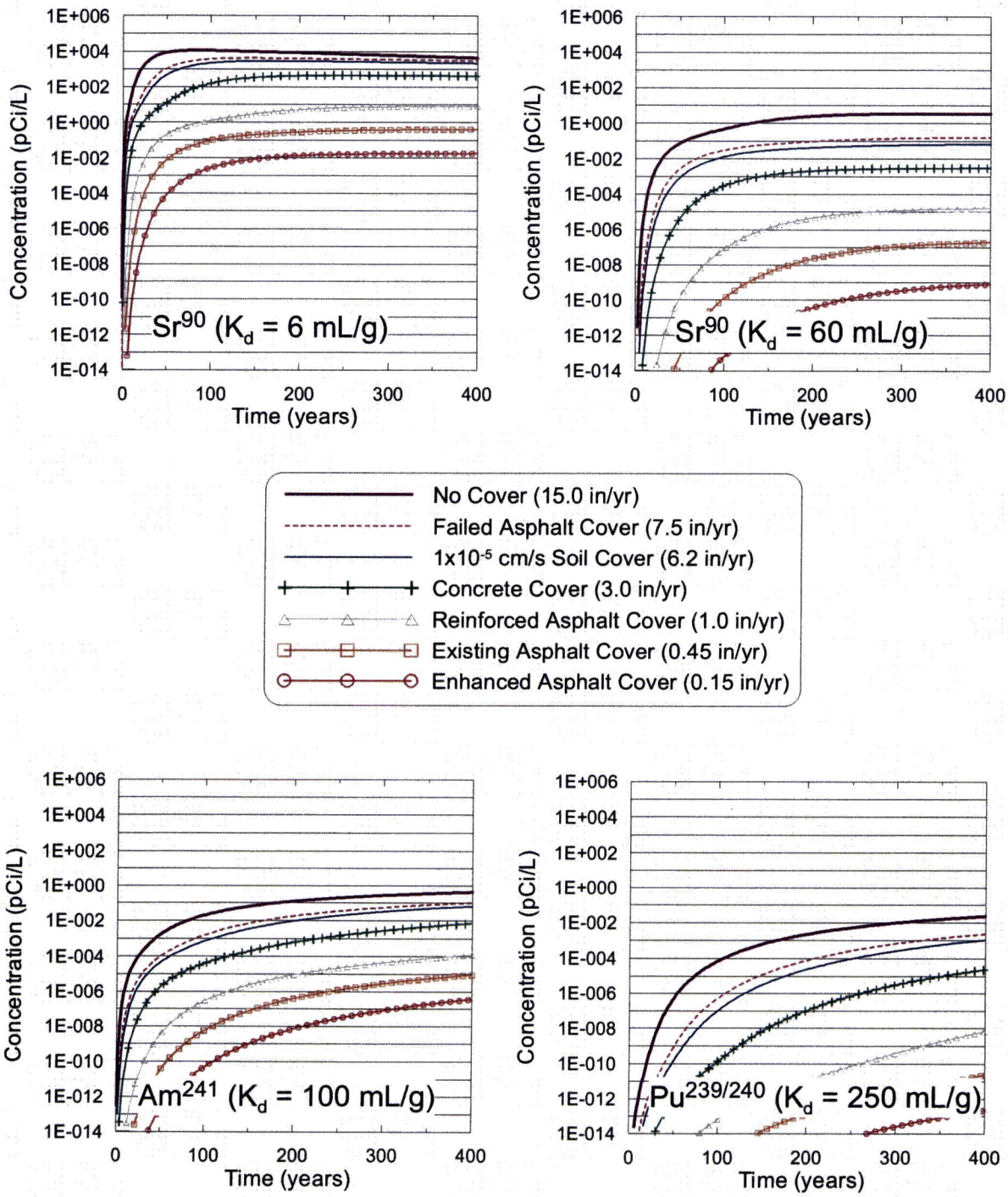

Figure 2-13a. Saturated-zone contaminant concentrations (pCi/L) for Basin 3 with a high water table.

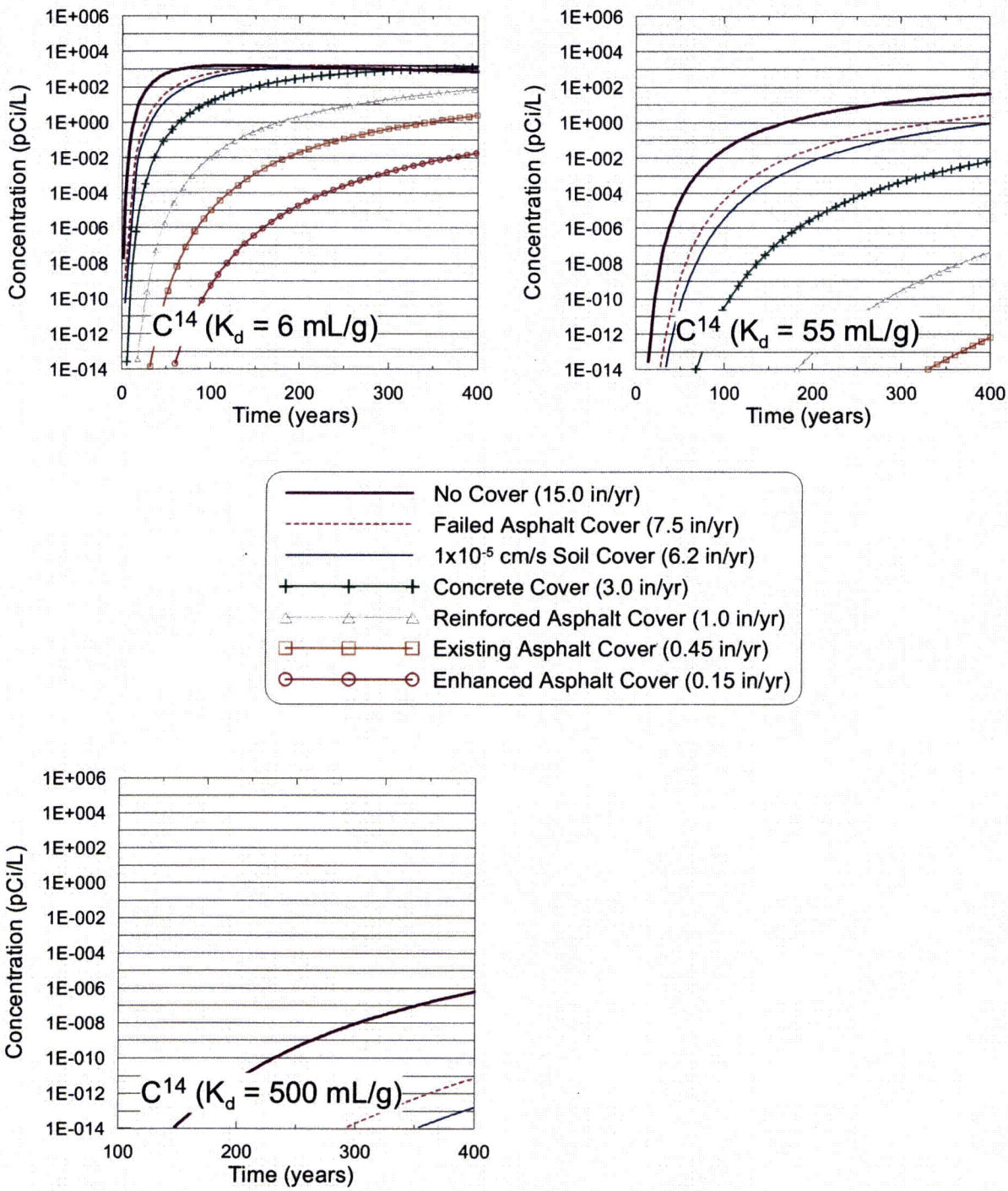

Figure 2-13b. Saturated-zone contaminant concentrations (pCi/L) for Basin 3 with a high water table.

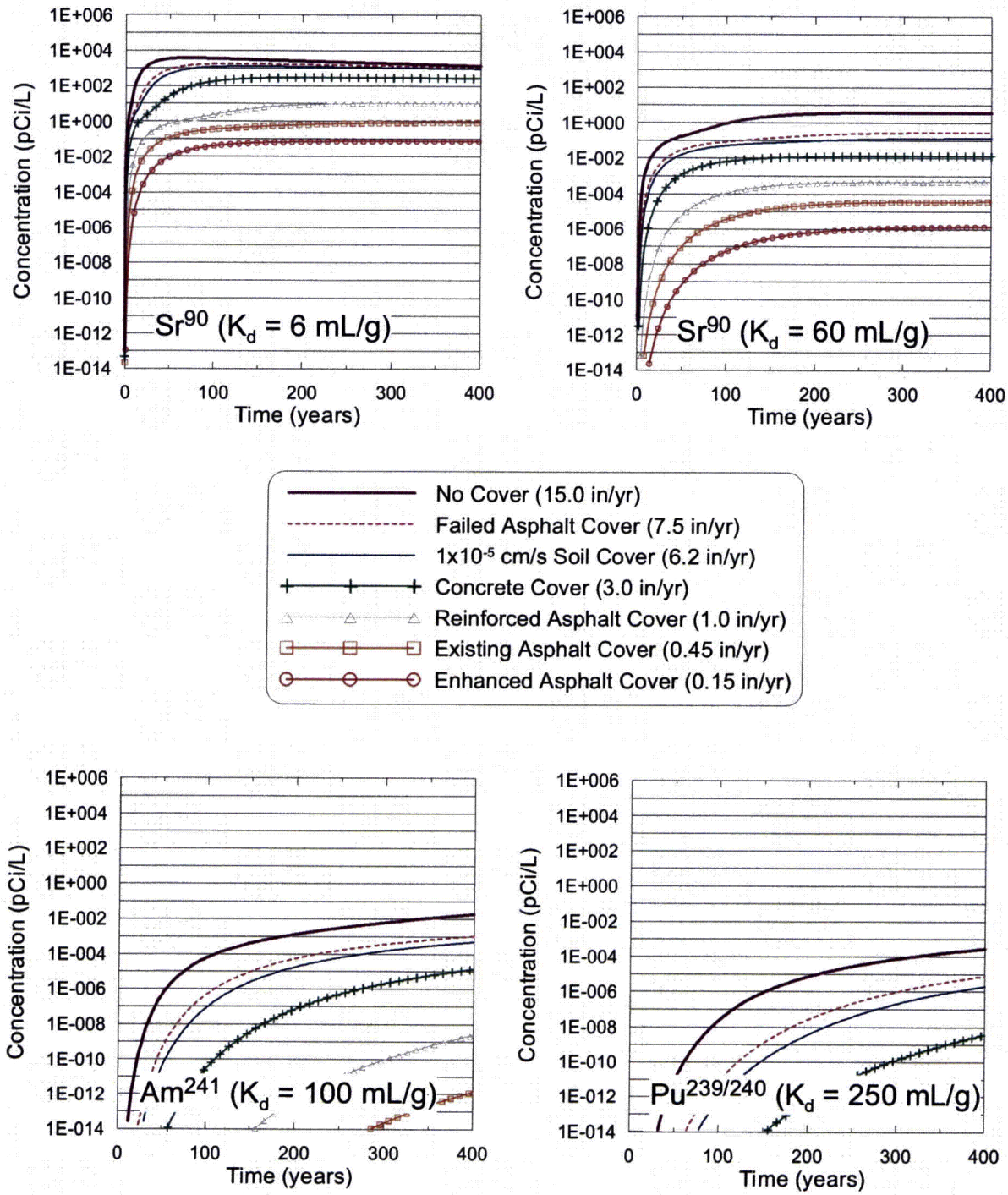

Figure 2-14. Saturated-zone contaminant concentrations (pCi/L) for Basin 6 with a high water table.

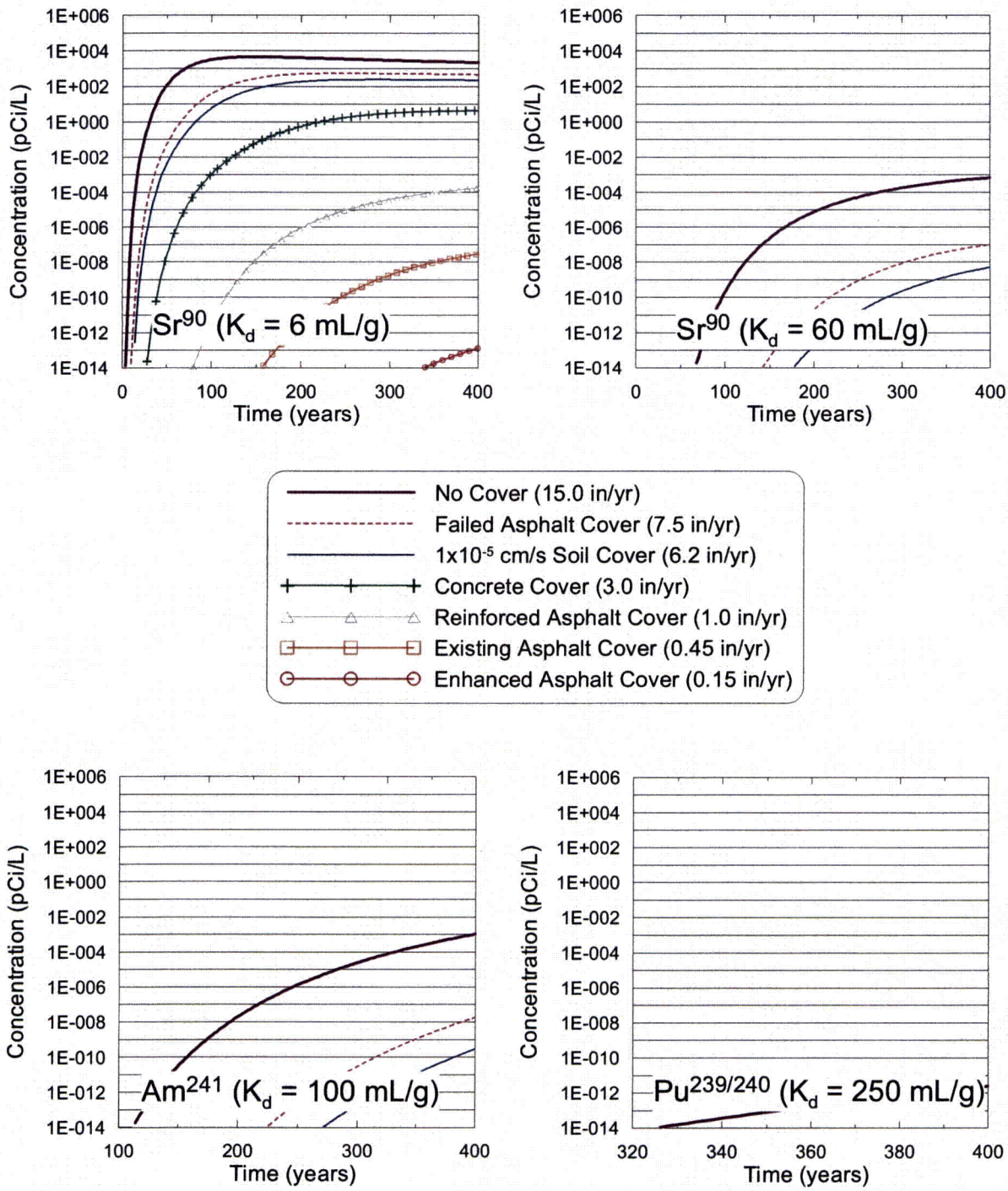

Figure 2-15a. Saturated-zone contaminant concentrations (pCi/L) for Basin 1 with a low water table.

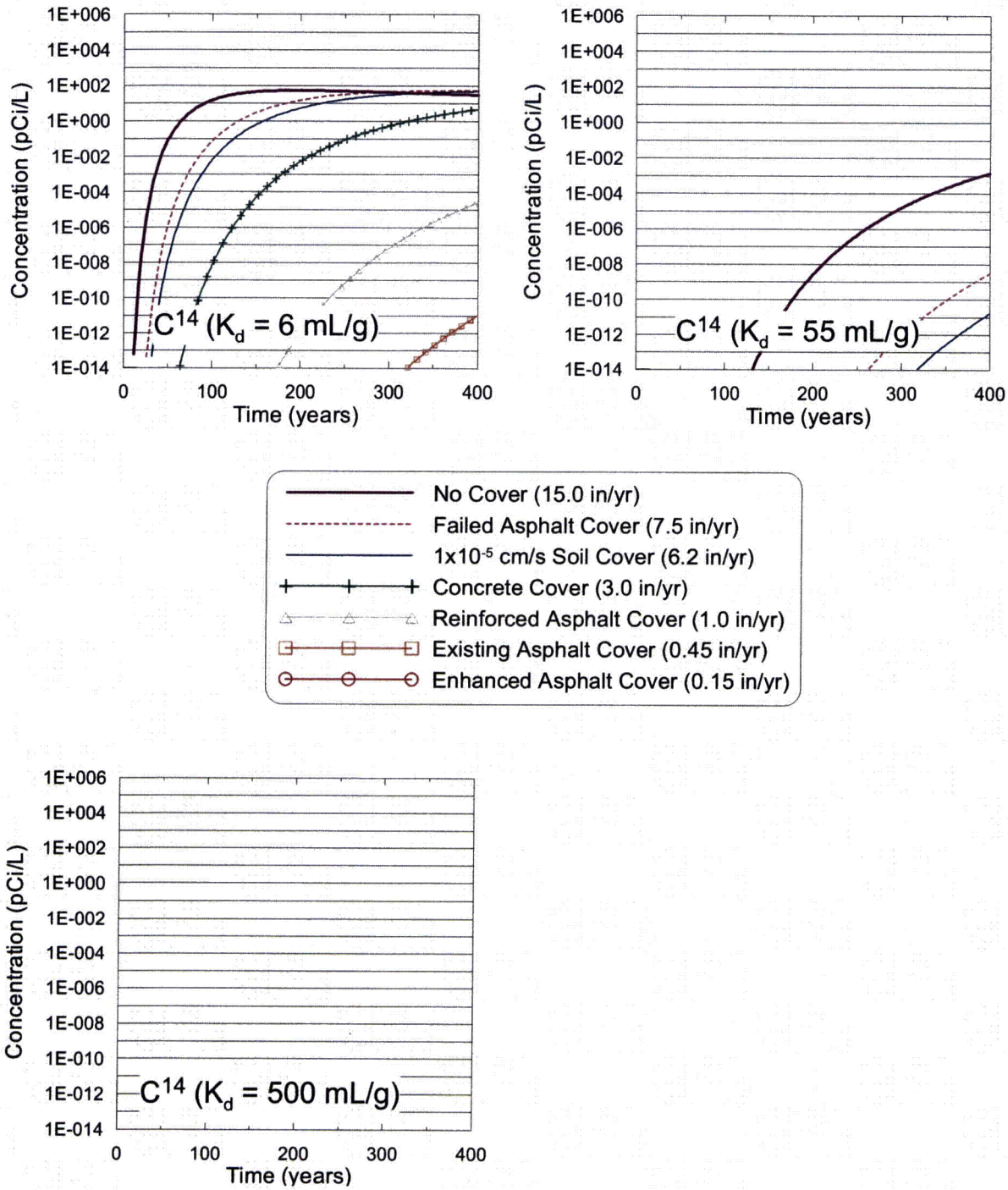

Figure 2-15b. Saturated-zone contaminant concentrations (pCi/L) for Basin 1 with a low water table.

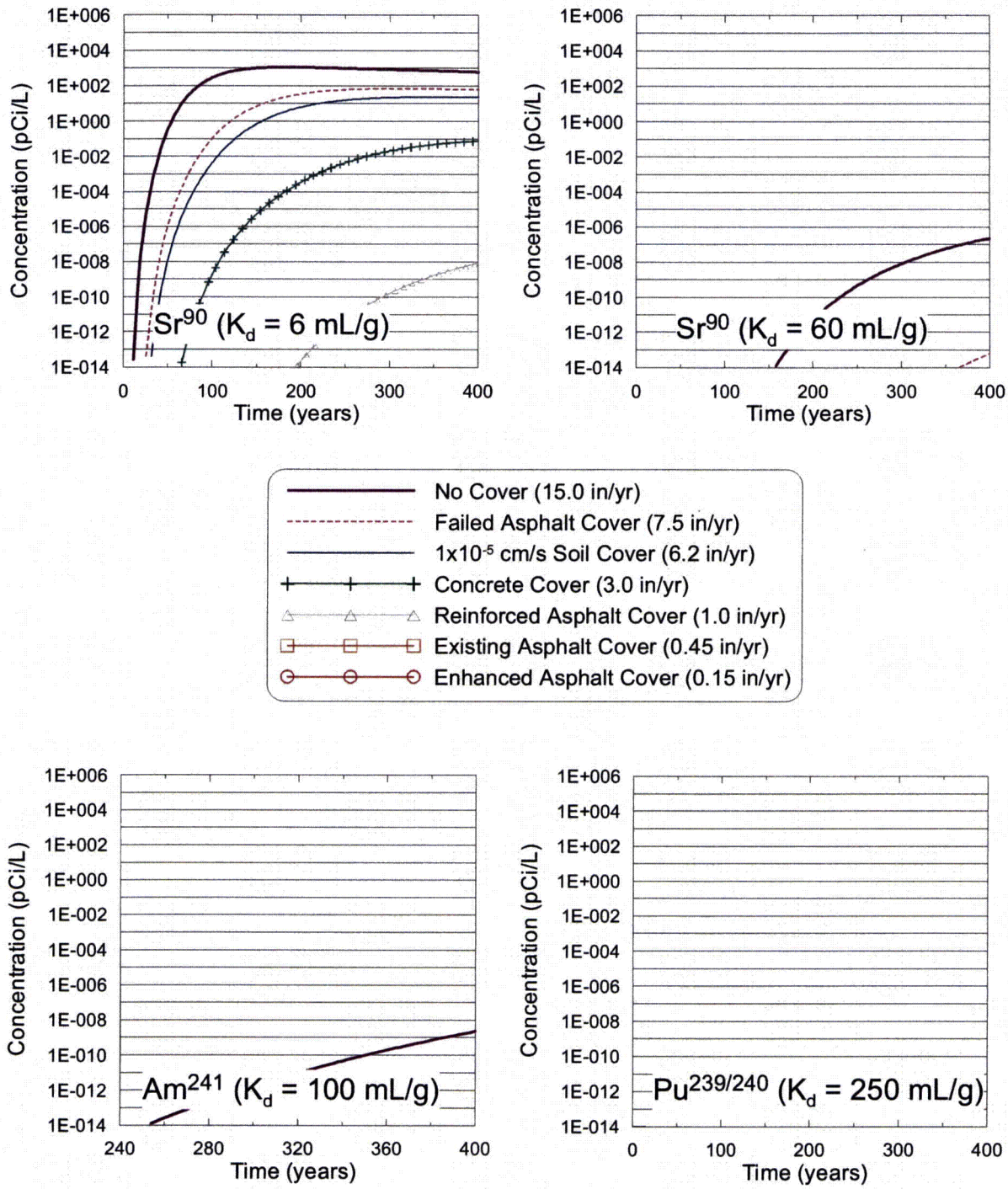

Figure 2-16a. Saturated-zone contaminant concentrations (pCi/L) for Basin 3 with a low water table.

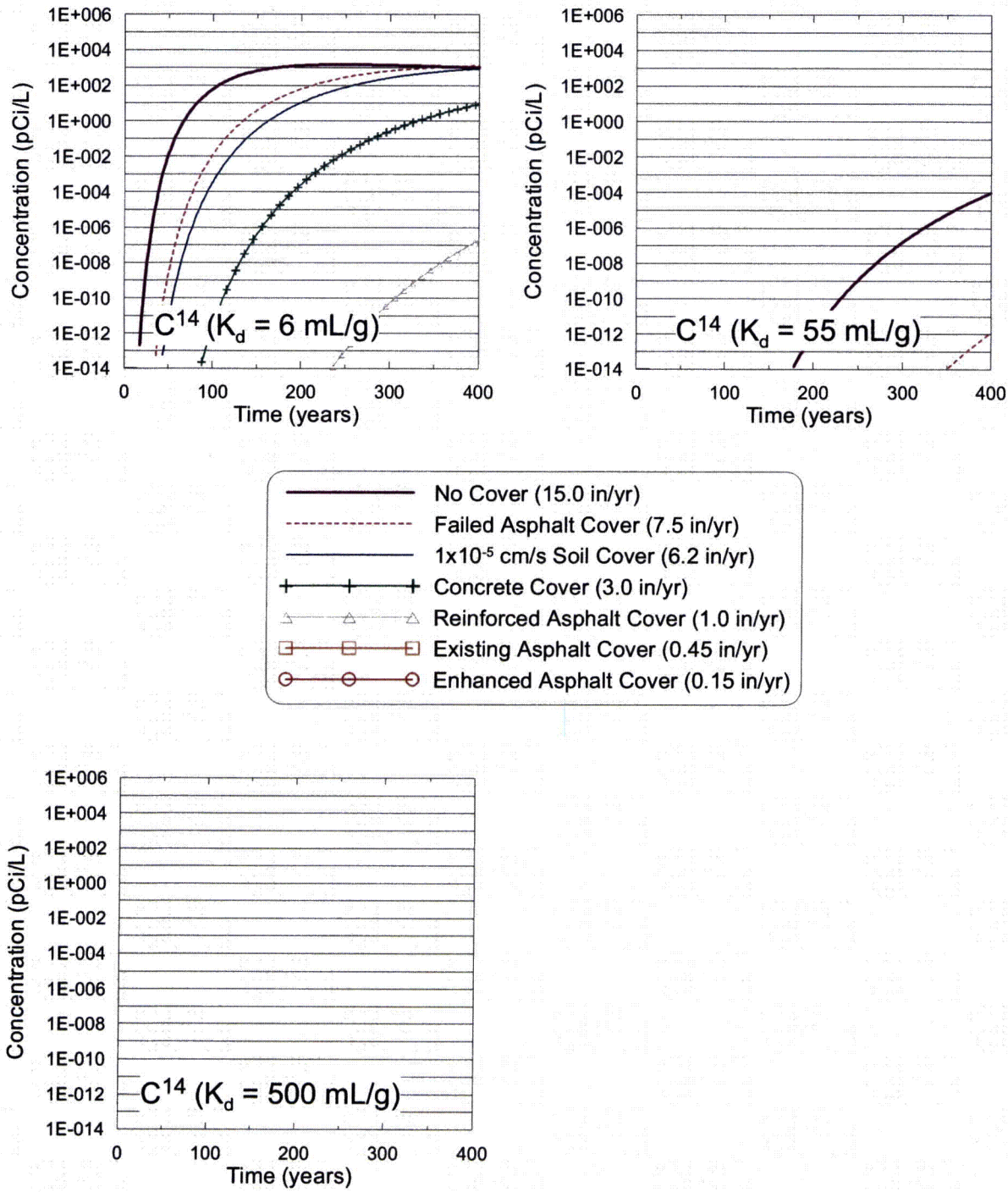

Figure 2-16b. Saturated-zone contaminant concentrations (pCi/L) for Basin 3 with a low water table.

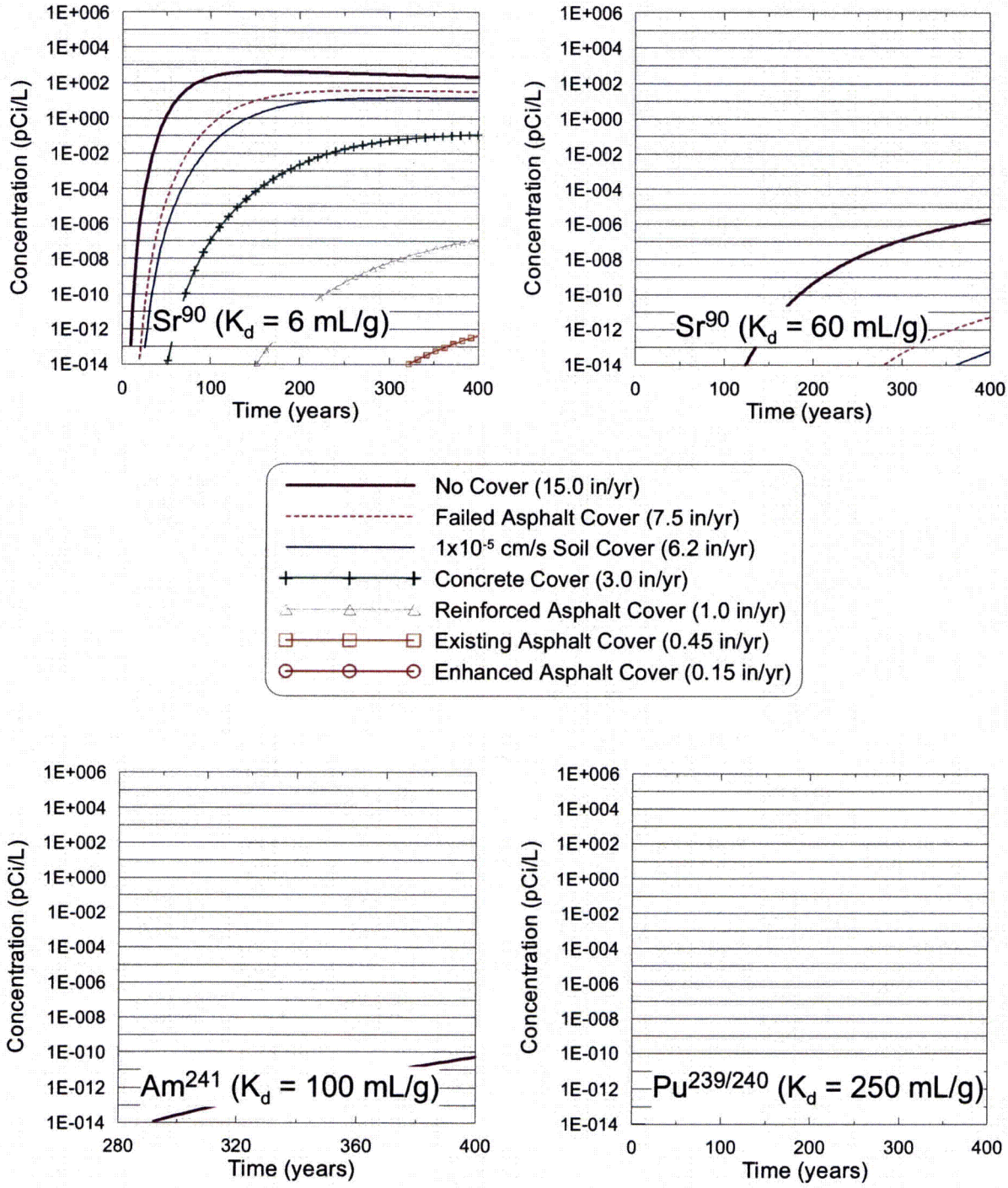

Figure 2-17. Saturated-zone contaminant concentrations (pCi/L) for Basin 6 with a low water table.

3.0 SATURATED-ZONE FLOW MODEL

Saturated-zone groundwater flow modeling was conducted to support the CMS/FS. The groundwater flow beneath the RRSB and in the surrounding region was simulated for the existing asphalt cover conditions and for five remedial alternatives. An initial saturated-zone flow model was developed and calibrated based on the existing conditions. Specific model parameters, such as cover area and recharge through the cover, were modified to simulate the remedial alternatives.

3.1 Selection of the Computer Code

The saturated-zone groundwater flow modeling was conducted using the numerical code MODFLOW contained within the GMS modeling platform. The GMS interface allows development of a generic, or non-model specific, conceptual model. Once the conceptual model is developed and parameterized, GMS creates the specific files necessary to run MODFLOW. The resulting flow field generated by MODFLOW is then processed by GMS for visual presentation of the results, calculation of various calibration parameters, and flow budget summaries.

3.2 Assignment of Boundary Conditions

The model domain for the groundwater flow model is shown in Figure 3-1. The domain is roughly bounded by Mill Creek to the west and Upper Joyce Branch and Pond A to the east. The northern and southern boundaries are formed by lines connecting Pond A and Mill Creek and Joyce Branch and Mill Creek. To develop the groundwater flow field, boundary conditions, which will control the flow of groundwater in and out of the model domain, must be specified. In the RRSB flow model, constant-head, general-head, head-dependent (drains), and no-flow boundary conditions were used (Figure 3-2).

As shown in Figure 1-8, the water levels within RRSB OU wells can vary significantly over time. Therefore, to develop the calibrated groundwater flow model for the existing asphalt cover, an average water level was calculated for each monitoring well (Table 3-1). These average water levels were then contoured to develop a potentiometric surface for each hydrostratigraphic layer (Figures 3-3 through 3-6). These surfaces were used to specify the constant-head boundary conditions along the lateral boundaries of the model domain. These constant-head boundary conditions allow flow to occur either out of or into the model domain to maintain the head value along the boundary.

The southern boundary of the model within the "A" and "AA" horizon is comprised of general-head and no-flow boundary conditions. The location of the southern boundary was defined by a flow line derived from the groundwater flow modeling presented in WSRC (1999c) and the centerline of a tritium plume located along the southeastern edge of the model. This tritium

Table 3-1 Calibration Targets and Residuals

Well Names	SRS Eastings	SRS Northings	Ground Surface Elevation (ft)	Screened Interval Elevations		Aquifer Designation from Model	Average Water Table Elevation (ft)	No. of Observation Years	Simulated Head (ft)	Residual (ft)
				Top (ft)	Bottom (ft)					
RDB1D	74844.5	57097.3	290.50	285.50	265.50	A	286.08	12	NC	*
RDB2D	74782.2	56879.8	290.70	285.70	265.70	A	285.44	12	NC	*
RDB3D	74899.0	56881.9	290.80	285.80	265.80	A	283.06	12	NC	*
RPC10DU	74540.1	57380.3	292.45	287.45	272.48	A	281.42	4	NC	*
RPC11DU	75250.0	57380.4	291.21	286.21	271.22	A	284.09	3	NC	*
RPC1PW	74187.6	57938.3	305.06	285.56	270.56	A	273.06	1	NC	*
RPC1PZ	74171.4	57936.9	305.29	285.27	270.23	A	273.00	1	NC	*
RSD1	75035.1	57440.8	298.70	287.70	267.90	A	287.26	15	NC	*
RSD3	74702.3	57451.6	298.70	289.10	269.30	A	287.28	15	NC	*
RSD4	75154.6	57441.4	299.60	290.60	270.60	A	289.23	13	NC	*
RSD5	75207.0	57439.9	299.60	289.60	269.60	A	288.30	13	NC	*
RSD6	75256.6	57441.3	300.10	290.10	270.10	A	287.82	13	NC	*
RSD7	75178.4	57394.3	291.30	287.30	267.30	A	285.80	14	NC	*
RSD8	75229.6	57394.0	291.30	287.30	267.30	A	286.21	14	NC	*
RSE1A	74712.7	57734.5	302.30	294.80	274.80	A	287.84	15	NC	*
RSE1B	74698.1	57731.4	301.70	295.70	275.70	A	290.05	9	NC	*
RSE3A	74931.2	57445.8	299.20	288.00	268.20	A	285.69	14	NC	*
RSP1D	74426.8	56879.4	291.80	289.70	274.70	A	287.43	3	NC	*
RSP3D	76333.3	56881.8	284.30	281.20	261.20	A	275.40	3	NC	*
RPC7DU	74720.2	58803.8	299.82	277.82	240.82	A	271.14	4	271.7409	0.60
RSP5D	76277.5	58773.9	293.80	282.90	262.80	A	273.66	5	274.1291	0.47
RPC2D	76123.4	58087.9	292.29	279.39	259.39	A	270.67	5	275.0446	4.37
RPC1D	74215.6	57931.3	304.96	284.46	264.46	A	275.56	5	275.9543	0.39
RSC5	75484.9	58901.2	302.30	278.30	258.30	A	272.52	13	276.8879	4.37
RPC5DU	75610.6	58820.5	302.30	277.30	262.30	A	271.58	4	276.9101	5.33
RPC9DU	74507.7	57898.4	301.34	283.34	268.34	A	277.27	4	277.4641	0.19
RSA9	75616.2	58123.8	309.70	284.50	264.60	A	283.85	12	277.5846	-6.26
RPC3DU	75745.0	58126.2	306.19	287.19	272.23	A	280.94	4	277.6663	-3.27
RSC7	75686.2	58200.1	306.40	283.40	263.40	A	281.14	13	277.6754	-3.46
RSE12	74842.3	58318.2	304.10	269.10	259.10	A	277.61	4	277.8006	0.19
RPC4DU	75741.9	58382.5	299.86	284.86	269.86	A	281.21	4	278.039	-3.17

Table 3-1 (continued)

Well Names	SRS Eastings	SRS Northings	Ground Surface Elevation (ft)	Screened Interval Elevations		Aquifer Designation from Model	Average Water Table Elevation (ft)	No. of Observation Years	Simulated Head (ft)	Residual (ft)
				Top (ft)	Bottom (ft)					
RSE11	74787.7	58357.6	302.10	272.10	262.10	A	283.77	8	278.2825	-5.49
RSC6	75686.1	58607.1	300.70	287.70	267.70	A	285.24	15	278.3994	-6.84
RPC6DU	75119.7	58901.4	298.78	283.78	268.96	A	278.04	4	278.5074	0.47
RSC4	75097.8	58900.3	298.60	288.60	268.60	A	279.50	14	278.5221	-0.98
RSE7	74783.7	58481.5	300.90	286.30	266.50	A	280.49	15	279.3211	-1.16
RCP1D	74223.5	56967.9	294.80	281.30	261.30	A	280.61	8	279.3221	-1.29
RSE19	74791.2	58318.4	302.50	282.50	262.50	A	281.66	8	279.8973	-1.76
RSE2	74743.5	57594.9	300.70	289.50	269.70	A	286.31	13	281.0349	-5.27
RPC13DU	74814.0	57305.0		264.40	249.30	A	273.98	1	281.0475	7.07
RPC8DU	74664.7	58279.1	301.00	288.00	273.00	A	280.06	4	281.1004	1.04
RSE10	74848.3	58420.7	303.20	290.50	270.70	A	282.39	9	281.153	-1.24
RSA10	75389.3	58172.8	309.70	288.70	268.80	A	282.38	10	281.1935	-1.19
RSE9	74971.1	58463.3	304.20	286.70	266.70	A	280.05	10	281.2778	1.23
RSE18	74839.5	58247.2	305.10	288.10	268.10	A	279.89	8	281.3071	1.41
RSE8	74869.4	58538.8	300.20	291.00	271.20	A	284.32	14	281.4438	-2.88
RSP4D	75939.8	57479.7	298.20	285.20	265.20	A	278.75	5	282.3994	3.65
RSA7	75195.9	58065.7	310.50	289.50	269.60	A	288.05	10	282.5414	-5.51
RSE4A	75101.1	57528.4	302.60	270.60	260.60	A	287.20	9	283.5367	-3.67
RSB7	75044.3	57692.8	307.20	292.60	272.70	A	285.69	12	285.1377	-0.55
RPC14DU	75429.0	57374.0		271.90	256.90	A	282.37	1	285.2805	2.91
RSD9	75185.9	57245.6	290.70	271.70	251.70	A	283.82	13	285.7376	1.91
RCP12DU	77084.4	58264.1	271.04	262.04	247.04	A/AA	266.6	1	267.0171	0.42
RSC10	75470.0	59542.7	293.50	275.50	255.50	A/AA	270.97	12	272.3852	1.41
RSC9	74565.3	59241.2	299.60	271.60	251.60	A/AA	271.34	9	272.4932	1.15
RSP7D	74294.9	59123.1	302.50	278.40	258.50	A/AA	271.70	5	273.1192	1.42
RSP6D	75363.2	59311.0	297.90	276.00	255.90	A/AA	268.71	5	273.2022	4.49
RSC2	74378.6	58543.0	299.90	281.90	261.90	A/AA	277.48	12	274.5101	-2.97
RSE24	74638.9	57370.4	291.60	257.60	237.60	A/AA	279.51	12	277.4739	-2.03
RPC11DM	75267.0	57380.0		243.40	233.40	A/AA	276.63	1	280.3353	3.71
RPC18DM	74572.5	59272.4	300.00	254.00	244.00	AA	268.02	1	271.1561	3.14

Table 3-1 (continued)

Well Names	SRS Eastings	SRS Northings	Ground Surface Elevation (ft)	Screened Interval Elevations		Aquifer Designation from Model	Average Water Table Elevation (ft)	No. of Observation Years	Simulated Head (ft)	Residual (ft)
				Top (ft)	Bottom (ft)					
RSF1	74869.4	58505.3	300.80	238.80	228.80	AA	277.57	12	271.9864	-5.58
RSF2	74628.6	57670.4	300.30	235.30	224.80	AA	277.97	12	273.9135	-4.05
RSF3	75206.7	57621.4	304.80	239.80	229.80	AA	279.30	12	276.1154	-3.18
RBP1D	77581.2	57216.4	303.21	253.31	243.31	AA/TZ	256.45	4	261.3263	4.88
RPC16DM	73712.1	58753.0	289.01	254.01	244.01	AA/TZ	273.18	1	272.7103	-0.47
RPC2PR	74150.3	57942.8	305.90	270.90	230.90	AA/TZ	273.18	1	272.935	-0.25
RSC3	74699.7	58724.7	299.60	278.60	258.60	AA/TZ	275.64	12	273.1861	-2.45
RBP2D	77510.3	56862.0	303.27	253.37	243.37	TZ	257.56	5	258.7432	1.19
RBP3D	77205.7	56829.1	307.68	258.68	248.68	TZ	260.61	5	261.4339	0.82
RPC19DL	75553.3	59363.2	301.90	206.90	196.90	TZ	266.19	1	268.9089	2.72
RPC5DL	75604.7	58817.2	302.34	197.34	187.34	TZ	268.28	4	269.8583	1.58
RPC4DL	75752.4	58382.0	299.40	189.40	179.42	TZ	267.73	4	269.9997	2.27
RPC3DL	75747.1	58136.5	305.88	191.23	181.24	TZ	268.13	4	270.256	2.12
RPC8DL	74671.7	58276.9	301.15	214.15	204.15	TZ	274.48	4	271.3428	-3.13
RPC11DL	75240.1	57380.0	291.20	190.20	180.20	TZ	272.84	4	271.688	-1.15
RPC9DL	74507.9	57908.3	301.37	226.37	216.37	TZ	274.68	4	272.3008	-2.38
RPC1TR	73976.1	57918.9	309.00	260.00	240.00	TZ	273.61	1	272.5179	-1.09
RPC10DL	74551.5	57380.2	292.46	210.46	200.48	TZ	275.94	4	272.6942	-3.24
RPC16DL	73707.2	58758.4	288.86	217.86	207.86	TZ/TCCZ	267.69	1	270.1756	2.49
RCP12DL	77095.9	58279.1	270.63	191.63	181.63	TCCZ/MAZ	261.41	1	262.6989	1.29
RPC18DL	74581.6	59274.1	299.83	214.83	204.83	TCCZ/MAZ	267.70	1	268.1079	0.41
RPC6DL	75117.5	58914.0	298.60	188.60	178.61	MAZ	269.82	4	268.2071	-1.61
RPC17DL	74304.7	59145.5	302.67	196.67	186.67	MAZ/TCLC	265.26	1	265.7374	0.48
RPC2CL	76120.7	58077.2	292.35	107.35	97.25	LAZ	247.04	5	247.4816	0.44
RPC19C	75551.7	59369.8	301.90	157.90	147.90	LAZ	253.97	1	252.8055	-1.16
RPC1CU	74292.8	57939.0	303.54	147.24	137.24	LAZ	260.70	3	255.8899	-4.81
RPC1CL	74261.9	57923.2	304.28	113.28	103.33	LAZ	255.26	5	255.9324	0.67
RPC3PZ	73940.6	57736.6	306.42	186.42	176.42	LAZ	255.67	1	256.5304	0.86

Note: The values of NC in the Simulated Heads column represent observation wells where GMS did not calculate a simulated head value because the observation well depths were located above the calibrated water-table elevation and where thus considered 'dry'.

plume is not discussed in this report because it is part of the R-Area Groundwater Operable Unit. Initial simulations assumed no-flow boundary conditions along the entire southern boundary. However, specification of general-head boundary conditions was required near the seepage basins to obtain a better flow field calibration. The general-head boundary conditions are similar to the constant-head boundary conditions but they provide some control on the rate at which water can enter or exit the boundary based on an assigned hydraulic conductance.

To approximate flow into and out of the surface water bodies (Mill Creek, Joyce Branch, Pond A and the R-Effluent canal), head-dependent boundary conditions, called drains, were specified. The drain boundary condition allows for the discharge of groundwater out of the model domain if the head along the boundary is greater than a preset elevation (i.e. ground surface or creek bed elevation). For Mill Creek, it was assumed that groundwater discharged into the creek from the "A" and "AA" horizons, as well as from the TZ. Therefore, drains formed the western model boundary along Mill Creek for layers 1 through 10. For the Mill Creek drains, a conductance of 5,000 ft/day•stream length was selected. Similarly, drains were used to simulate Joyce Branch within the model layers and boundaries. Because of topographic effects, drains for Joyce Branch were only contained in the "AA" horizon and the TZ. For the Joyce Branch drains, a conductance of 5,000 ft/day•stream length was also assumed. Groundwater discharge to the R-Effluent canal and Pond A was modeled using drains in the "A" horizon. A conductance of 15,000 ft^2/day was assigned to the drains used to approximate Pond A, with 5,000 ft/day•stream length assigned as the conductance to the R-Effluent canal drains. For all the drains, elevations were assigned based on surveyed elevations.

3.3 Assignment of Flow Model Parameters

Based on the hydrogeological conceptual model, the groundwater flow model consists of seven hydrostratigraphic units. Figure 3-1 shows the relative thicknesses of the seven hydrostratigraphic layers and the surface topography. The contacts between the hydrostratigraphic layers were developed based on stratigraphic elevation data obtained from various monitoring wells and CPT logs.

As discussed in Section 2.0, the average recharge at the SRS was assumed to be 15 in/yr. This net recharge was applied as a constant areal source to the uppermost saturated cell throughout the flow model, with the exception of the basin cover footprint. For the calibrated flow field, which is based on the Existing Asphalt Cover, a recharge of 0.45 in/yr was applied for the basin cover footprint (Figure 3-7).

Table 3-2 lists the initial horizontal and vertical hydraulic conductivity values assigned to each of the hydrostratigraphic units within the flow model. A single value of conductivity was assigned to each unit at the initiation of the simulation activities. These hydraulic conductivity values were selected based on a review of the observed range in hydraulic conductivity values across the SRS and at the R-Reactor Area (WSRC, 2000a; WSRC, 2000b; WSRC 2001a).